**UNIVERSITY OF SOUTHAMPTON**

FACULTY OF ENGINEERING AND THE ENVIRONMENT

Institute of Sound and Vibration Research

# Fatigue Life for non-Gaussian Random Excitations

by

**Frédéric Kihm**

Thesis for the degree of Doctor of Philosophy

December 2017

**UNIVERSITY OF SOUTHAMPTON**

# ABSTRACT

FACULTY OF ENGINEERING AND THE ENVIRONMENT
Institute of Sound and Vibration Research

Thesis for the degree of Doctor of Philosophy

**FATIGUE LIFE FOR NON-GAUSSIAN RANDOM EXCITATIONS**

Frédéric Kihm

This thesis presents several developments in analysing the fatigue life of mechanical components subjected to various kinds of random excitations and the subsequent mechanical vibration. Typically components must be designed in such a way that they can withstand the effects of the exposure to environmental conditions without being damaged. Their design must be verified using laboratory testing or by Finite Element (FE) calculations. Often, design and testing are performed on the basis of specifications taken from internal, national or international standards, with the implicit assumption that if the equipment survived the particular environment it would also survive the vibrations it will see in service.

Previous work in the area has developed computer-based models to predict the fatigue damage witnessed by components under random loads, but most of these are limited to only stationary Gaussian random excitations. A few have concentrated on non-Gaussian responses, not excitation, resulting from some non-linearities in the structure being activated.

This thesis describes the development of original statistical analysis methods with the ability to determine extreme responses and fatigue life estimates for linear structures when subjected to non-Gaussian random excitations. The emphasis is mainly on two sources of non-Gaussian random excitations namely clipped random excitations and random excitations with a high kurtosis value. Fatigue damage from specific sine-on-random excitations is also studied. In all cases, theoretical formulations were derived to obtain fatigue life estimates without the need for long time domain realisations. Such a statistical approach is particularly suited for simulating the fatigue damage induced during a random test on a shaker system.

One of the main benefits of being able to assess the fatigue life in the case of a structure subjected to a leptokurtic random excitation is to create an accelerated test definition. The idea is to associate a specific kurtosis value to a given Power Spectral Density (PSD) in order to reduce the exposure duration, while encompassing the same fatigue damage potential as the original stationary and Gaussian random test. In practice, the engineer will be able to simulate the effects of the kurtosis control capability of some commercial vibration control systems on the fatigue damage experienced by in the device under test. This process will be achieved using a FE-based fatigue analysis tool, where the user specifies the excitation PSD, the kurtosis value and an FE results file representing the frequency response function linking the excitation and the stress response at each node or element of the FE model of the test article. The stress response PSD with the associated response kurtosis are obtained and the statistical rainflow histogram is extracted. Fatigue life estimates are then derived by associating the statistical rainflow histogram with the material fatigue curve.

The theoretical formulations derived are applied to examples coming from numerical simulations. The estimate of the probability density functions obtained for the response stress

and fatigue life correlate well with the results obtained from time domain simulated data, showing the robustness and the accuracy of the theoretical expressions.

# Table of Contents

# List of Tables

# List of Figures

# DECLARATION OF AUTHORSHIP

I, Frédéric Kihm declare that this thesis and the work presented in it are my own and has been generated by me as the result of my own original research.

Fatigue Life for non-Gaussian Random Excitations .....

I confirm that:

1. This work was done wholly or mainly while in candidature for a research degree at this University;
2. Where any part of this thesis has previously been submitted for a degree or any other qualification at this University or any other institution, this has been clearly stated;
3. Where I have consulted the published work of others, this is always clearly attributed;
4. Where I have quoted from the work of others, the source is always given. With the exception of such quotations, this thesis is entirely my own work;
5. I have acknowledged all main sources of help;
6. Where the thesis is based on work done by myself jointly with others, I have made clear exactly what was done by others and what I have contributed myself;
7. Parts of this work have been published and presented at conferences as:

   F. Kihm, A. Halfpenny and N. S. Ferguson, "Fatigue Life from Sine-on-random Excitations," *Procedia Engineering*, vol. 101, pp. 235-242, 2015.

   F. Kihm, S. Rizzi and N. Ferguson, "Understanding how kurtosis is transferred from input acceleration to stress response and its influence on fatigue life," in *11th International Conference RASD*, Pisa, 2013.

   F. Kihm and D. Delaux, "Vibration fatigue and simulation of damage on shaker table tests: the influence of clipping the random drive signal," *Procedia Engineering*, vol. 66, pp. 549-564, 2013.

   F. Kihm and S. A. Rizzi, " The Effect of Drive Signal Limiting on High Cycle Fatigue Life Analysis," in *International Conference on Vibration and Vibro-acoustics*, Harbin, China, 2014.

   F. Kihm, N. Ferguson and J. Antoni, "Fatigue life from kurtosis controlled excitations," in *6th Fatigue Design conference*, Senlis, France, 2015 Procedia Engineering, Volume 133, 2015, Pages 698-713

   F. Kihm, A. Halfpenny and K. Munson, "Synthesis of Accelerated and More Realistic Vibration Endurance Tests Using Kurtosis," in SAE Technical Paper 016-01-0275, 2016.

Signed: .....

Date: December 2017

# Acknowledgements

I am most sincerely grateful to my supervisor Dr Neil Ferguson for his guidance, his advice and his patience with me throughout the five years it took me to pursue this PhD thesis. I am also grateful to my review committee, Professor White, Dr Renno and Dr Blumensath for their comments and suggestions during the various reviews.

I am thankful to my employer HBM Prenscia who sponsored this PhD. Special thanks to my colleague Andrew Halfpenny, who has always been a professional mentor to me and whose advice is extremely inspirational.

I would also like to express gratitude to Steve Rizzi (NASA, Langley Research Center) and David Delaux (Valeo) for the enlightening discussions and their collaboration. I am also grateful to Jérôme Antoni (INSA Lyon) for his decisive technical help. I also wish to thank Turan Dirlik for his support and suggestions.

Last but not least, I must acknowledge my wife, Sabrina, and children Eva, Emilio and Alessio who have supported me throughout this demanding period in my life.

# Definitions and Abbreviations

## Abbreviations

| | |
|---|---|
| CDF | Cumulative Density Function |
| CLT | Central Limit Theorem |
| DFT | Discrete Fourier Transform |
| FE | Finite Element |
| FEA | Finite Element Analysis |
| FFT | Fast Fourier Transform |
| FRF | Frequency Response Function |
| IDFT | Inverse Discrete Fourier Transform |
| i.i.d | independent and identically distributed |
| JPDF | Joint Probability Density Function |
| LC | Level Crossing (histogram) |
| LTI | Linear Time Invariant |
| PSD | Power Spectral Density |
| PDF | Probability Density Function |
| RMS | Root Mean Square |
| SOR | Sine-on-Random |
| TWR | Time Waveform Replication |

## List of symbols

| | |
|---|---|
| $a(t)$ | Modulating function |
| $a_k$ | Fourier coefficients of the periodic modulating function |
| $b$ | Basquin exponent |
| $c_i$ | Coefficients of the polynomial transform equation |
| $c_{x,r}$ | The $r^{th}$ cumulant of a random variable $x$ |
| $g(.)$ | Monotonically increasing polynomial function |
| $\tilde{h}_3, \tilde{h}_4$ | Coefficients of Winterstein's second order model |
| $h_i, h(\tau)$ | Impulse Response Function (IRF) of a linear system |
| $l_i$ | Impulse Response Function (IRF) of a colouring filter |
| $m_r$ | The r$^{th}$ order spectral moment |
| $p_R$ | Probability density function for the material strength |
| $p_x$ | Probability density function for the instantaneous values of the random signal $x(t)$ |
| $p_{x_p}$ | The peak probability density function for the signal $x(t)$ |
| $p_{X_m}$ | the PDF of the largest peak value out of $N_pT$ peaks |
| $p_{xy}$ | Joint probability density of two random variables $x$ and $y$ |
| $r_b$ | Proportion of the burst deviation in a period of the modulation function |
| $t$ | Time |
| $\{x_k(t)\}$ | A random process made of an ensemble of sample function $x_k(t)$ |
| $x_k(t)$ | Sample function of a random process $\{x_k(t)\}$ |
| $x_{th}$ | Clipping level for the signal $x(t)$ |
| $x(t)$ | Stationary Gaussian signal |
| $y(t)$ | Non-Gaussian signal obtained by transformation of $x(t)$ (PDF transform, amplitude modulation, adding harmonic tones) |
| $z(t)$ | Response signal of a linear system excited by $y(t)$ |

| | |
|---|---|
| $A$ | amplitude of the bursts in the modulation function |
| $B$ | offset of the modulation function |
| $C$ | Basquin coefficient |
| $CF$ | Crest factor |
| $C_{x,r}$ | The $r^{th}$ standardised cumulant of a random variable *x* |
| $\mathcal{C}_{xx}(t, t+\tau)$ | The covariance function of *x*(*t*) at instants $t$ and $t+\tau$ |
| $D$ | Fatigue damage |
| $E[\quad]$ | Expectation operator |
| $G_{xx}(f)$ | One-sided PSD of *x*(*t*) |
| $G_{xy}(f)$ | One-sided CSD of *x*(*t*) and *y*(*t*) |
| $H$, $H(f)$ | Frequency Response Function (FRF) of a linear system |
| K | Scale coefficient of Winterstein's second order model |
| $L(f)$ | Frequency Response Function (FRF) of a colouring filter |
| $L_h$ | Linear system |
| $M'_{x,r}$ | The $r^{th}$ raw statistical moment of a random variable *x* |
| $M_{x,r}$ | The $r^{th}$ central statistical moment of a random variable *x* |
| $N_0{}^+$ | Expected number of zero crossings per unit time with a positive slope |
| $N_f$ | Number of rainflow cycles to failure |
| $N_\beta{}^+$ | Expected number of crossings of the level $\beta$ per unit time with a positive slope |
| $N_p$ | Number of expected peaks per unit time |
| $N_{p,x\geq x_0}$ | The mean number of peaks greater than $x_0$ per unit time |
| $P_f$ | Probability of failure |
| $P_{x_p}$ | the Cumulative Distribution Function (CDF) of the peaks |
| $P_{X_m}$ | CDF of the maximum peak |
| $R$ | Material strength |
| $R_a(p)$ | Correlation function of the Fourier coefficients $a_k$ of the periodic modulation function |
| $R_{xx}(\tau)$ | Autocorrelation function of *x*(*t*) |
| $R_{xy}(\tau)$ | Cross-correlation function of *x*(*t*) and *y*(*t*) |
| $R_{xx}^{\alpha}(\tau)$ | Cyclic autocorrelation function of *x*(*t*) |
| $S_m$ | Mean stress |
| $S_R$ | Stress range |
| $S_{xx}(f)$ | Two-sided PSD of *x*(*t*) |
| $S_{xy}(f)$ | Two-sided CSD of *x*(*t*) and *y*(*t*) |
| $S_{xx}^{\alpha}(f)$ | Cyclic spectrum of *x*(*t*) |
| $T_f$ | Time to failure |
| $T_s$ | Service life |
| $T_t$ | Test duration |
| $T$ | Period of the modulation function |
| $T_0$ | Length of a burst in the modulation function |
| $T_{r,x\geq x_0}$ | Return period such that on average, there is one peak equal to or higher than a given threshold $x_0$ |
| $\overline{X_m}$ | Average value of the largest peak |

| | |
|---|---|
| $\alpha$ | Cyclic frequency |
| $\gamma$ | Irregularity factor |
| $\delta(\tau)$ | Kronecker delta function |
| $\varepsilon$ | Euler constant |
| $\kappa_x$ | Kurtosis value of signal $x(t)$ |
| $\kappa_w$ | Kurtosis associated with a white noise |
| $\lambda_x$ | Skewness value of signal $x(t)$ |
| $\mu_x$ | Mean value of signal $x(t)$ |
| $\rho$ | Correlation coefficient |
| $\sigma_x$ | Root Mean Square (RMS) value of signal $x(t)$ |
| $\tau_p$ | Average time interval between two successive maxima |
| $\tau_{\mathrm{p},,x\geq x_0}$ | Average time interval between two successive maxima above the level $x_0$ |
| $\varphi$ | Phase of the modulation function |
| $\varphi_x$ | First characteristic function of the random variable $x$ |
| $\Psi_x$ | Second characteristic function of the random variable $x$ |

# 1 Introduction

In all industrial sectors such as Automotive, Aerospace, Energy, etc. components are designed to withstand the real operational conditions to which they will be subjected during their service life. A fatigue resistant design may reduce warranty costs and unnecessary maintenance. A reliable design will also increase safety and will invariably yield a better corporate reputation.

Fatigue life estimates require a good knowledge of the material's resistance to fatigue and the level of stress in the material. This research work concentrates on the latter. When the external load is random, it cannot be considered deterministic since random loads cannot be described by an explicit mathematical relationship. In this case a statistical approach needs to be adopted to estimate the distributions of peaks and stress cycles that can possibly lead to static or fatigue failures.

This first chapter is a global introduction to the subject of environmental test and vibration induced fatigue. It also explains the motivations that led to this work, the aims and objectives of this thesis and underlines the questions considered and the original contributions that have been obtained in answering them.

## 1.1 Introduction to environmental testing

### 1.1.1 The need for environmental testing

Environmental testing is a form of vibration testing, where a test article is subjected to vibration of a specified form and amplitude for a period of time, in order to assess its operational integrity. Shaker tests are typically performed to qualify the endurance of a product.

An example vibration test is illustrated in Figure 1.

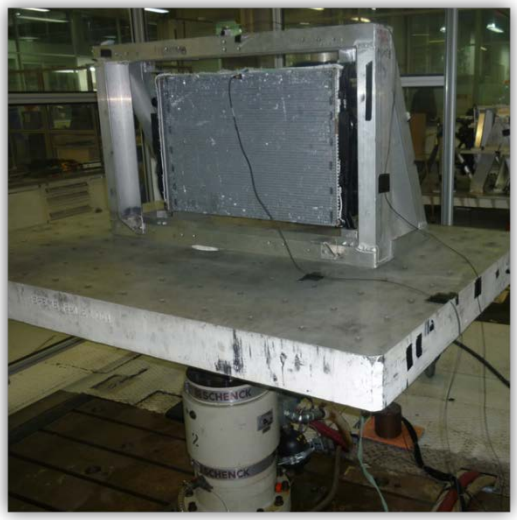

**Figure 1: Example vibration test of an automotive radiator on a shaker (image courtesy of Valeo)**

The objective of product testing is to check that the test article is qualified for its expected service life. In order to replicate the same failure mechanism as in real conditions, the test specification must be representative of the service loads. In practice, vibration test requirements are often specified by industry standards such as STANAG 4370 [1], MIL STD 810 [2], DEF STAN [3], RTCA DO 160G [4], GAM EG-13 [5] etc. or synthesized from measurements under real operational conditions using a test tailoring approach [6, 7]. The test profile must incorporate at least the same damage content, which the original data would produce, but will also require considerably shorter test times than the true service life.

### 1.1.2 Random vibration tests

Often, long term operational loads are stochastic in nature, with a given distribution of energy across various frequencies. For random vibration tests, the input excitation is typically defined as a vibration profile called Power Spectral Density (PSD). An example PSD is illustrated in Figure 2.

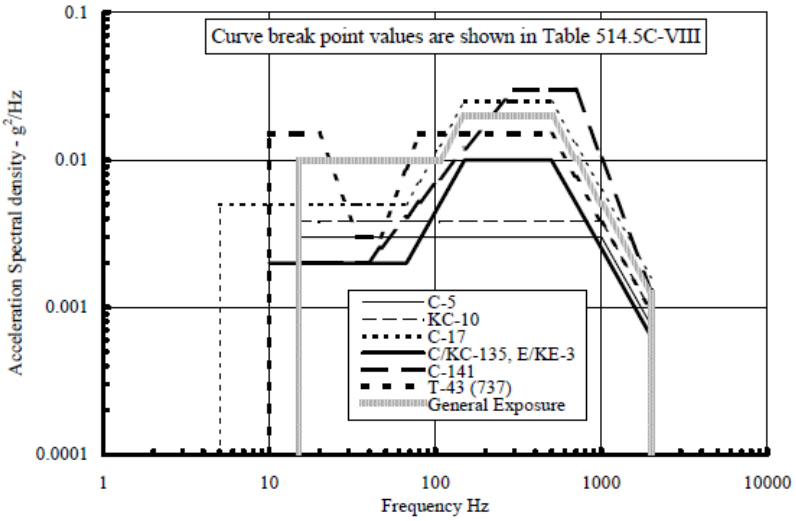


FIGURE 514.5C-6. Jet aircraft cargo vibration exposure.

**Figure 2: Example profiles for an acceleration PSD from the military standard MIL STD 810 [2]**

From the PSD profile, an excitation signal is generated to drive the shaker or excitation system [8]. The reproduced signal is meant to be random stationary and Gaussian. A process is said to be stationary if its statistics are not affected by a shift in the time origin. A random process is qualified as Gaussian if its values are distributed according to a normal distribution.

### 1.1.3 Random vibration tests with sigma clipping

In the laboratory, however, the controller typically limits the drive signal to prevent high amplitude peaks from damaging shaker components [9, 10]. The high amplitude peaks are truncated at a given level, typically described as a number, which is a product of the root mean square of the excitation signal (RMS, but also denoted $\sigma$, hence the name “sigma clipping”). Due to this amplitude limiting, the shaker system can deliver more power without exceeding the amplifier/shaker abort limits since the high amplitude peaks are eliminated.

### 1.1.4 Random vibration tests with kurtosis-control

The various standards for environmental tests require the test laboratories to adopt specific actions when simulating random vibration environments that appear to be non-Gaussian when measured in service. The MIL-STD-810G [2] standard, in method 528, recommends to "carefully examine field measured response probability density information for non-Gaussian behaviour". In this case, it establishes that "specialized shaker control system software is required…to replicate an autospectral density estimate with a non-Gaussian amplitude distribution". The UK Defence Standard 00-35 [3], in part 5, acknowledges that "although the vibration experienced by a road vehicle is of random character, it does not usually conform to a Gaussian distribution of amplitudes". The risk of not considering the non-Gaussian behaviour is clearly stated: "the measured data represent a greater damage potential than Gaussian data because of their higher probability of high amplitudes". The NATO Standard [1] , in STANAG 4370, AECTP 200, describes the vibration environment generated by wheeled and tracked vehicles in this way: "it can be non-stationary resulting in relatively high peak to RMS ratios. It is therefore also non-Gaussian. These properties of non-stationary and non-Gaussian are in contrast to the character of vibration generated in test laboratories. Consequently, special steps may need to be taken to avoid under testing in the laboratory."

Recently, several shaker controllers developed a way to reproduce leptokurtic excitation signals. This is often referred to as "kurtosis control" [8]. The kurtosis is defined as the fourth standardised statistical moment. Values of kurtosis greater than three indicate that a probability density function has heavier tails, i.e. more higher peaks, than a Gaussian distribution. This is why the kurtosis is often used as a metric to describe the "peakedness" or the "impulsiveness" of the data.

The generated signal with a different kurtosis than found in a Gaussian distribution can possess the same PSD and hence overall energy in terms of mean square level, but is more impulsive compared to a stationary Gaussian signal. Figure 3 shows the probability density functions of two standardised excitation signals with zero mean values. The one using a dashed black line corresponds to a Gaussian stationary signal, the one using a red line corresponds to a non-Gaussian signal where the kurtosis is set to 6.0. The horizontal axis represents the acceleration level of the original input time series. Both excitation signals have the same unitary RMS value. The vertical axis represents the probability density plotted on a logarithmic axis.

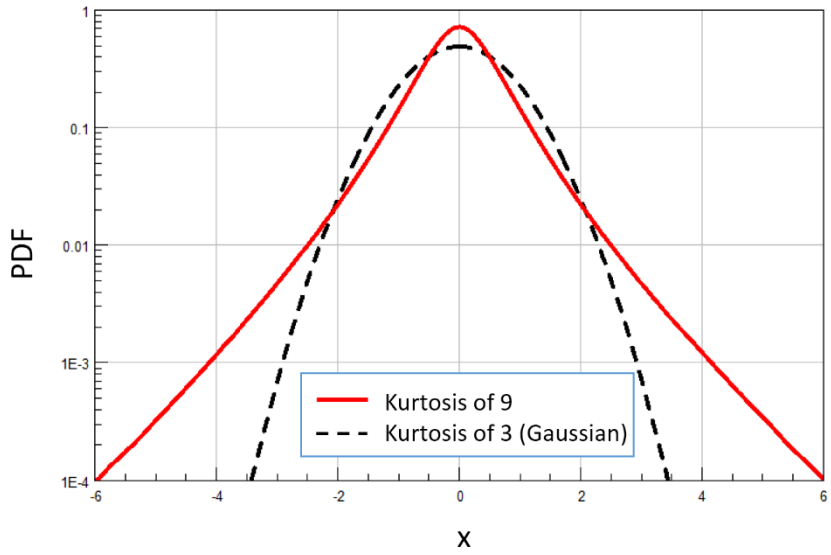


**Figure 3: Example distribution of excitation signals: Gaussian (dashed black) and with high kurtosis (red)**

From Figure 3, it is clear that the signal with high kurtosis exhibits higher amplitude peak levels than the Gaussian one. Tests with high kurtosis values can therefore be more representative of certain real non-Gaussian, impulsive environments [11].

Another application of kurtosis control is the acceleration of a test in order to reduce the time taken for qualification testing. More impulses means higher expected damage on the test article, so that the test duration can be reduced while reproducing the same overall damage [6].

### 1.1.5 Sine-on-random vibration tests

Rotating machinery typically produces non-Gaussian vibration environments. Examples of rotating machines are internal combustion engines, turbines, pumps, electric motors or generators. The generated vibration environment is typically made of harmonic tones from the rotation or firing orders superimposed on background noise.

Such sine-on-random excitations are also considered in several military and civil standards such as MIL STD 810G [2] and RTCA DO 160G [4]. An example test specification for helicopter vibration from MIL STD 810G involving sine-on-random is given in Figure 4, where $f_1$ is the rotor rotating frequency, $f_2 = Nf_1$ the blade passing frequency and $f_3$, $f_4$ its harmonics.

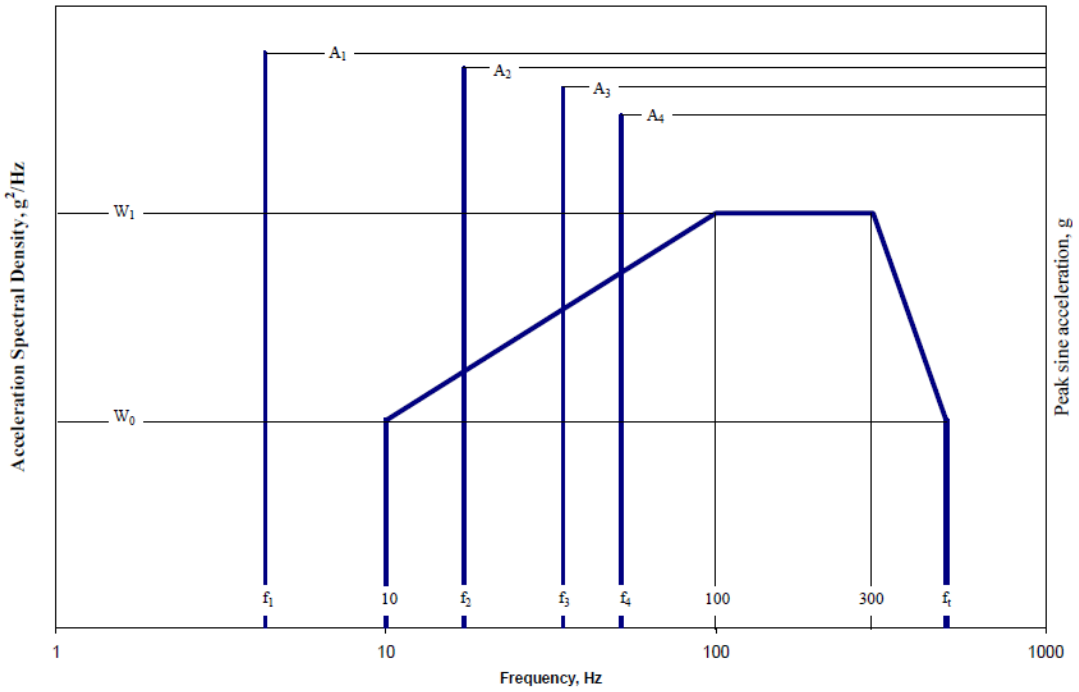


**Figure 4: Example test specification - Helicopter vibrations exposure - MIL STD 810G Figure 514.6C-8 [2]**

## 1.2 Virtual vibration endurance tests

### 1.2.1 The need for virtual vibration tests

Durability simulations based on numerical predictions using, for example, Finite Element Analysis (FEA) can help to optimise the design of a component. It allows sensitivity analysis to be performed in order to select the optimum material, geometry, process, etc. required to fulfil a target in terms of service life. The design often aims to minimise the maximum stresses within the component when loaded, which will subsequently improve the fatigue life.

Durability simulations can also drastically limit the number of prototypes in the design phase. At the qualification stage, if the test article fails during the qualification test, FE-based durability simulations can help investigate why failure has occurred.

Other applications of FEA-based durability simulations include finding out what the margins of a successful test are or checking that a profile for random vibration test is not over-accelerated. In this last case, the excessive loads might introduce a non-linear response such as levels of stress above yield, which alters the load paths and changes the failure mode or creates forms of non-linear damping [12, 13, 14].

### 1.2.2 State of the art of virtual vibration tests

When a linear system is excited by a random stationary and Gaussian signal, the spectral and statistical characteristics of its stress response are known [15, 16, 17, 18, 19, 20, 12, 21]. When the linear system is a mechanical device and the excitation is the acceleration signal produced by a electrodynamic or hydraulic shaker, then the stress response can be derived in terms of both its Power Spectral Density and its Probability Density Function. Statistical methods exist to derive the distribution of peaks and valleys [15, 16, 22, 17, 20, 23, 21, 24, 25] and to approximate the distribution of the rainflow stress ranges [26, 27, 28, 29, 30, 31, 32] for stationary and Gaussian stress responses.

The benefits of such a statistical approach are:

- Increased performance - since there is no need to perform long time domain realisations
- Better accuracy - since the distributions obtained are smooth, with well-defined tails.

It is indeed worth noting that fatigue damage and stress range are linked in a power law, so when considering a distribution of stress cycles, the fatigue damage is governed essentially by the larger cycles in the tail of the distribution. This is where the distributions obtained from generated signals show a significant variability due to the finite duration of a signal realization, leading to larger spread in the estimated damage values. In contrast, the distributions obtained from a statistical approach provide a good estimate of the *mean* number of cycles of various ranges.

The time domain approach can be time consuming and does not encourage an engineering understanding of the problem. This is the main reason why a spectral approach is relevant and preferable.

The current state of the art in virtual vibration endurance testing does not allow one to simulate kurtosis-control tests nor sine-on-random tests nor the effects of clipping the excitation signal. Even for stationary and Gaussian random tests, there is no methodology to take into account the effects of sigma clipping.

## 1.3 Motivations

Engineers from both design and test departments want to estimate the fatigue life of a structure subjected to random vibrations. When the mechanical environment is random, a common way to proceed is to adopt a statistical approach to assess the number of stress peaks in the response at various levels or the stress cycles in various ranges. Current statistical approaches are limited to inputs (excitations) that are random stationary and Gaussian excitations.

The present work is motivated by the need to provide engineers with a solution based on a statistical approach to non-Gaussian excitations found in industrial situations such as:

i. clipped random excitations,
ii. random excitations with high kurtosis.

Note that the fatigue damage due to a sine-on-random excitation was also considered in this thesis, but since the developments in that domain were not very significant the work done can be found in the appendix with a summary of the output in the main content of the thesis.

## 1.4 Aims of the study

The main aim of this thesis is to simulate and predict the fatigue life for non-Gaussian loadings, which are typically applied in environmental tests. The approaches described in this work will be beneficial to Finite Element Analysis (FEA) engineers wanting to estimate the fatigue life under practical non-Gaussian mechanical environments. With a robust way to estimate the fatigue life of a component, a design engineer can perform sensitivity analysis and assess the influence of changing geometry, material, surface finish, etc. in order to optimise its design.

Engineers in test departments will also find benefit in having a robust methodology to derive the expected fatigue life under random excitations. A first application is to make sure the test will be successful before actually running it. In the case of premature failure, the expert can investigate what caused it and establish how to remedy it. In the case of a successful test, it is useful to understand what the margins or limits are for the design.

Finally, for maintenance purposes, a better life prediction leads to optimized inspection planning during the service life of the product.

The findings of this work are hence applicable to improving the time-to-failure estimates for more realistic loadings.

## 1.5 Objectives of the research

The global objective is to extend the existing statistical approach for fatigue analysis under non-Gaussian random loads. This will be achieved by obtaining some intermediate results, such as the statistical distributions of the response stress peaks and rainflow cycles for various non-Gaussian excitations of a linear structure.

The non-Gaussian excitations studied and considered as the main objectives in this thesis are:

i. Clipped random signals: the design engineer needs to understand the influence of limiting the drive signal on the fatigue life of a specimen when simulating a random shaker test. The test engineer would need some guidelines to help decide how clipping should be applied under different test scenarios.
ii. Random signals with high kurtosis: the design engineer needs to understand the influence of the kurtosis parameter on the resulting fatigue life. The test engineer wants to know the relationship between kurtosis and test duration in order to reduce the test duration, while reproducing the same amount of fatigue damage.

These objectives will be answered in various sections in this thesis, which will highlight the relevant background literature (chapter 2), the means to generate non-Gaussian signals (chapter 3), the statistics of the response (chapter 4), the rainflow cycle distribution and finally the fatigue damage estimates (chapter 5). A theoretical formulation will be proposed and applied to examples coming from numerical simulations, demonstrating the benefits and potential for adoption by academics and practical engineers.

In the final concluding chapter, the reader will see how these objectives were met. The original contributions are summarised in the following section.

## 1.6 Contributions presented in the thesis

Based on the well-known and well documented statistical approach for random stationary and Gaussian excitations [15, 16, 22, 17, 20, 23, 21, 24, 25], some extensions are proposed to take into account the fact that the excitation is clipped, or leptokurtic or contains sine tones.

The contributions in the various themes are detailed hereafter.

Influence of sigma clipping on the fatigue life

Sigma clipping was considered as a zero-memory non-linear transformation of a Gaussian signal. The original contributions include:

- The influence of various clipping techniques applied to a stationary Gaussian random signal in terms of statistics (see chapter 3.3, pages 92 to 97).
- Formulations are given for the stress response statistics and for the peak and valley distributions, which are produced after the clipped signal is filtered through a linear system (see chapter 4.3, pages 119 to 124).
- An algorithm was developed and proposed to estimate the fatigue life of a structure based on the excitation PSD, the level of clipping and the dynamic characteristics of the structural configuration (see chapter 5, pages 134 to 159).

Fatigue from kurtosis controlled tests

Various ways to generate a signal from a prescribed PSD and kurtosis value were investigated. The original contributions include:

- Formulation for the stress response statistics and for the peak and valley distributions, after the leptokurtic signal is filtered through a linear system (see chapter 4.4, pages 125 to 131 and chapter 5, pages 134 to 159).
- A new way to generate a signal from a prescribed PSD and kurtosis value has been developed, optimizing the kurtosis transfer rate between the excitation and response (see chapter 3.5, pages 103 to 116 and chapter 4.5, pages 131 to 132).
- An algorithm to estimate the fatigue life of a structure based on the excitation PSD, the kurtosis and the dynamic characteristics of the structural configuration has been produced (see chapter 5, pages 134 to 159).

Fatigue from sine-on-random tests

The derivations of the peak and valley distributions from sine-on-random loadings is mostly based on various papers by S.O. RICE written between 1944 and 1974 in connection with the analysis of electrical noise signals [15, 33, 34] and later adapted to the field of fatigue analysis. The thesis produced original contributions which include:

- The number of expected peaks per unit time (see Appendix C, page 192).
- The distribution of peaks for the case where the random process is broadband (see Appendix C, pages 192 to 193).

Note that the fatigue damage due to a sine-on-random excitation was also considered in this thesis, but since the developments in that domain were not very significant the work done can be found in appendix.

More generally, the basic theories and their extensions have been implemented and extensively tested for robustness, accuracy and applicability.

Table 1.1 helps the reader to find which chapter covers a specific aspect for each of the different types of signal.

**Table 1.1: Sumary table giving the chapters where the various aspects of a specific type of signal are studied**

| Aspect studied / Signal type | Signal generation | Statistics after linear filtering | Distributions of instantaneous values and peaks in the stress response | Rainflow cycle count histogram and fatigue damage estimates |
|---|---|---|---|---|
| Stationary Gaussian random | Chapter 3.2 | Chapter 4.2 | Chapter 2.2.4<br>Chapter 2.2.8 | Chapter 2.6.3<br>Chapter 2.6.4 |
| Sigma clipping | Chapter 3.3 | Chapter 4.3 | Chapter 5.2.2<br>Chapter 5.3.2 | Chapter 5.5.2<br>Chapter 5.6.2 |
| Kurtosis (steady leptokurtic) | Chapter 3.4 | Chapter 4.4 | Chapter 5.2.1<br>Chapter 5.3.1 | Chapter 5.5.1<br>Chapter 5.6.1 |
| Kurtosis (nonstationary leptokurtic) | Chapter 3.5 | Chapter 4.5 | Chapter 5.2.3<br>Chapter 5.3.3 | Chapter 5.5.3<br>Chapter 5.6.3 |
| Sine on random | Appendix C | Appendix C | Appendix C | Appendix C |

## 1.7 Overview of the thesis contents

The thesis topic, “Fatigue life for non-Gaussian random excitations”, will be explored in the following chapters using a combination of theoretical aspects and numerical simulation or physical results.

The present chapter, chapter 1, sets the scene for the background knowledge. The requirements and current practice are discussed such that the motivations and the objectives become clear.

Chapter 2 presents a literature review. Some of the fundamental technical basics of statistics, spectra and fatigue analysis are recalled and summarised. These basics will be used and referenced throughout the thesis.

Chapter 3 introduces ways to generate Gaussian and non-Gaussian random signals. Note that the outcome of chapter 3 will be used only for simulation and validation purposes. The objective of this work is to find a statistical (as opposed to deterministic) approach to some specific non-Gaussian loadings, that does not require realisations of long time domain signals.

Chapter 4 will discuss the statistics of the response of a linear system to Gaussian and various non-Gaussian excitations. The linear system is considered to be a mechanical component and the response is expressed in terms of the stress response. The reader will realise that, for some specific non-Gaussian loadings, it is possible to determine the statistics of the response knowing only some statistics of the excitation and the dynamic characteristics of the linear system, without having to perform simulations with long time histories.

Figure 5 illustrates how chapter 3 and 4 interact. It also introduces the variables that are used throughout this thesis: $x(t)$ is a Gaussian signal, $y(t)$ is a non-Gaussian, transformed version of $x(t)$. When $y(t)$ is used as an input to a linear system, then the response signal is $z(t)$.

Note that $x(t)$ and $y(t)$ are generally considered to be acceleration signals in this thesis, while $z(t)$ is considered to be stress. Acceleration is typically assumed as coming from real in-service measured data.

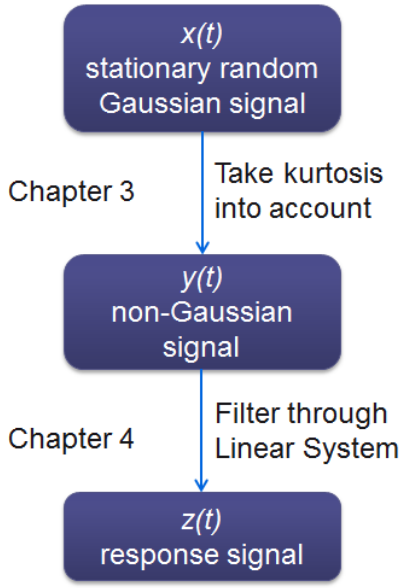


**Figure 5: Some notations used and the order that ideas are considered**

Chapter 5 will use the statistics of the response to derive the distributions of the peaks and valleys and to obtain an approximation for the rainflow cycle distribution. Estimates of the time-to-failure are then possible.

Figure 6 gives a very concise overview of the logic built into the content presented in this thesis. The green boxes are the inputs, the blue ones contain algorithms. Each blue box corresponds to a particular chapter. It is suggested to read through the thesis linearly, but if the interest is in signal generation or input/output statistics, then the reader can start or stop where relevant.

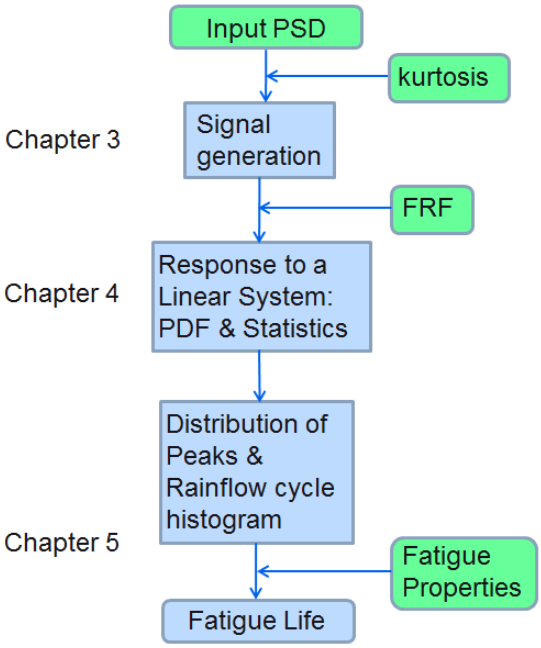


**Figure 6: Outline of the thesis content and its interaction**

The final chapter, chapter 6, will summarise the thesis, highlighting the original contributions, and will suggest areas for future research.

References used in this thesis are given at the end. Some of the derivations, mathematical manipulations, etc., are given in the appendices to ensure clarity in the main body of the text.

# 2 Review of random vibration and fatigue analysis

This chapter presents a brief review of the well-known formulations concerning fatigue analysis from random vibration loadings. It covers the literature on the various subjects that form the basis for this study.

It starts with some definitions linked with random vibrations; reviews the statistics involved, the behaviour of linear systems and the probabilistic peak distributions of the subsequent stress response for mechanical systems. It continues with the modelling of fatigue damage.

The last section introduces the various methods for accelerating an endurance vibration test. It will particularly mention the traditional load amplification endurance tests and introduce a more recent technique called Kurtosis control. There are outstanding questions around the Kurtosis control technique, which will be answered in the rest of this thesis.

## 2.1 Random variables - definitions

### 2.1.1 Random and deterministic variables

Any observed data representing a physical phenomenon can be classified as being either deterministic or nondeterministic [16]. Deterministic data are those that can be described by an explicit mathematical relationship allowing the data to be an explicit function of time or space. In mechanical engineering, random vibration is related to non-deterministic motion, meaning that future behaviour cannot be precisely predicted but its statistical properties can be estimated. Examples of random loads include road surfaces, wind turbulence, wave loading and general vibrations. Structural response to random vibration is usually treated using probabilistic approaches.

### 2.1.2 Random variables – probability fundamentals

The possible outcomes of an experiment represent a set of points called the sample space. A random variable $x(k)$ is a set function defined for points $k$ from the sample space. In the rest of this thesis the index $k$ will be omitted for simplicity in notation.

### 2.1.3 Probability Density Function

A probability density function (PDF) is a function that describes the probability for a random variable to take a given value. The probability for the random variable to fall within a particular range of values is given by the integral of this density function over the range. The probability density function is nonnegative everywhere, and its integral over the entire range of possible values in the sample space is equal to one.

If a random variable $x$ has a probability density function $p(x)$, then the probability that $x$ satisfies $a \leq x \leq b$ is given by:

$$Prob\{a \leq x \leq b\} = \int_a^b p(x)dx \qquad \text{Equation 2.1}$$

The cumulative distribution function (CDF) of $x$, $P(x)$, is defined by the equation:

$$P(x) = \int_{-\infty}^{x} p(u)du \qquad \text{Equation 2.2}$$

Providing $P(x)$ is continuous, the PDF $p(x)$ is obtained as the derivative of the CDF. Thus

$$p(x) = \frac{dP(x)}{dx} \qquad \text{Equation 2.3}$$

### 2.1.4 Expected values

The expected value or mean $\mu_x$ of a random variable $x$ is by definition the integral

$$\mathrm{E}[x] = \int_{-\infty}^{\infty} xp(x)dx = \mu_x \qquad \text{Equation 2.4}$$

where $E[\cdot]$ denotes the expectation operator.

For a random variable $x$ with mean $\mu_x$, the quantity $x - \mu_x$ represents the deviation of the random variable from its mean. Since this deviation can be either positive or negative, the quantity $(x - \mu_x)^2$ is used and its average value $E[(x - \mu_x)^2]$ represents the average square deviation of $x$ around its mean. The variance ${\sigma_x}^2$ of the random variable $x$ is by definition the integral:

$${\sigma_x}^2 = \mathrm{E}[(x - \mu_x)^2] = \int_{-\infty}^{\infty} (x - \mu_x)^2 p(x)dx \qquad \text{Equation 2.5}$$

The positive square root of the variance $\sigma_x = \sqrt{\mathrm{E}[(x - \mu_x)^2]}$ is known as the standard deviation of $x$. Note that $\sigma_x$ represents the root mean square (RMS) value of the variation of the random variable $x$ around its mean $\mu_x$.

### 2.1.5 The Gaussian distribution

A random variable $x$ is qualified as being Gaussian if its values are distributed according to a Gaussian distribution. The Probability Density Function (PDF) of a Gaussian variable is given by:

$$p_x(x) = \frac{1}{\sigma_x\sqrt{2\pi}} . e^{-\frac{1}{2}\frac{(x-\mu_x)^2}{{\sigma_x}^2}} \qquad \text{Equation 2.6}$$

where $\mu_x$ is the mean value and $\sigma_x^2$ the variance of the random variable $x$.

The mean value indicates the value which is at the centre of the distribution. The variance gives the spread of the distribution around the mean value.

Note that the PDF of a centred Gaussian process only depends on its variance. The frequency bandwidth of the process does not have any influence on the shape of the distribution.

The cumulative distribution function (CDF) for a Gaussian distribution is given by:

$$\Phi_x(x) = \int_{-\infty}^{x} p_x(\alpha)d\alpha = \frac{1}{2}\left[1 + \text{erf}\left(\frac{x-\mu_x}{\sigma_x\sqrt{2}}\right)\right] \qquad \text{Equation 2.7}$$

where erf() is the error function, defined as [35]:

$$\text{erf}(x) = \frac{2}{\sqrt{\pi}}\int_{0}^{x} e^{-t^2}dt \qquad \text{Equation 2.8}$$

Figure 7 shows the standardised PDF of a Gaussian function.

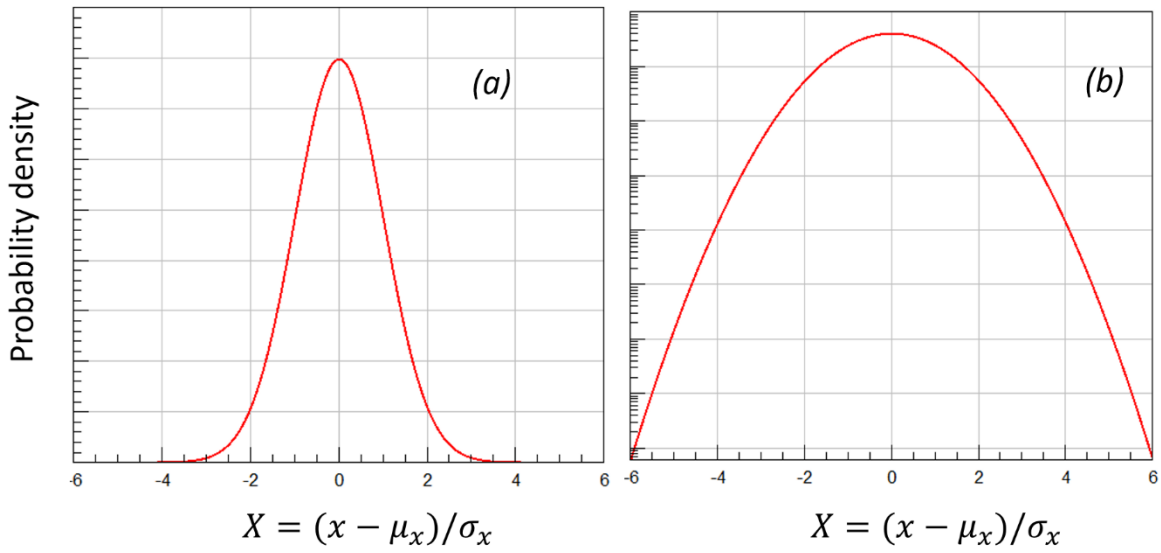


**Figure 7: Standardised Gaussian distribution with linear (a) and logarithmic (b) vertical axis**

About 68% of values drawn from a normal distribution are within one standard deviation $\sigma_x$ away from the mean; about 95% of the values lie within two standard deviations; and about 99.7% are within three standard deviations. More generally, the probability that the random Gaussian variable $x$ lies in the range $\mu_x - n.\sigma_x$ and $\mu_x + n.\sigma_x$ is given by:

$$P(\mu_x - n\sigma_x \leq x \leq \mu_x + n\sigma_x) = \int_{\mu_x - n\sigma_x}^{\mu_x + n\sigma_x} p_x(x)dx = \text{erf}\left(\frac{n}{\sqrt{2}}\right) \qquad \text{Equation 2.9}$$

Using Equation 2.9, Table 2. can be established. It shows the probability that the variable $x$ lies between $\mu_x - n\sigma_x$ and $\mu_x + n\sigma_x$ for various integer values of $n$:

**Table 2.1: Probability table for a Gaussian random variable**

| $n$ | **Probability to lie between** $\mu_x \pm n\sigma_x$ | **Probability to lie outside** $\mu_x \pm n\sigma_x$ |
|---|---|---|
| 1 | 0.68269 | 0.3173 |
| 2 | 0.95449 | 0.0455 |
| 3 | 0.99730 | 0.00269 |
| 4 | 0.99993 | 0.000063 |
| 5 | 0.9999994 | 0.00000057 |

### 2.1.6 Central Limit Theorem

Given $n$ independent continuous random variables $x_i$, let $\boldsymbol{x}$ be their sum $\boldsymbol{x} = x_1 + \cdots + x_n$. Note that the random variables $x_i$ need not to be normally distributed. Then $\boldsymbol{x}$ is a random variable with mean $\boldsymbol{\mu} = \mu_1 + \cdots + \mu_n$ and variance $\boldsymbol{\sigma}^2 = {\sigma_1}^2 + \cdots + {\sigma_n}^2$.

The central limit theorem (CLT) states [36] that the probability density function $p(x)$ of $\boldsymbol{x}$ approaches a normal probability density function with the same mean $\boldsymbol{\mu}$ and variance $\boldsymbol{\sigma}$:

$$p(x) \xrightarrow{n\to\infty} \frac{1}{\boldsymbol{\sigma}\sqrt{2\pi}} e^{-\frac{(x-\boldsymbol{\mu})^2}{2\boldsymbol{\sigma}^2}} \qquad \text{Equation 2.10}$$

In other words, the sum of a large number of independent $n$-dimensional random variables is asymptotically normally distributed [37]. For the exact conditions for the validity of the theorem, the reader is referred to Cramer [37] or Papoulis [36].

### 2.1.7 Joint Gaussian distributions

Consider two random variables $x$ and $y$. The joint probability distribution function $p_{xy}(x, y)$ is defined to be the probability that both random variables simultaneously take on a given set of values $x_0$ and $y_0$.

In particular, the joint probability of two random variables $x$ and $y$ both distributed normally, with zero mean and variances ${\sigma_x}^2$ and ${\sigma_y}^2$ respectively will be:

$$p_{xy}(x,y) = \frac{1}{2\pi\sigma_x\sigma_y\sqrt{1-\rho^2}} exp\left\{-\frac{1}{2(1-\rho^2)}\left(\frac{x^2}{{\sigma_x}^2} + \frac{y^2}{{\sigma_y}^2} - \frac{2\rho xy}{\sigma_x\sigma_y}\right)\right\} \qquad \text{Equation 2.11}$$

where $\rho$ is the correlation coefficient, which lies between -1 and +1. Two random variables $x$ and $y$ whose correlation coefficient is zero are said to be uncorrelated [16].

If $p_{xy}(x, y) = p_x(x)p_y(y)$ then the two random variables $x$ and $y$ are said to be statistically independent [16, 20].

### 2.1.8 Change of variables

The PDF of a random variable $x$ can be transformed to the PDF of a different random variable $y$ using the "PDF transform" [16, 12, 36, 37]:

$$p_y(y) = \frac{p_x(x)}{\left|{dy}/{dx}\right|} \qquad \text{Equation 2.12}$$

when there is a one-to-one monotonic relationship between $x$ and $y$. The monotonic requirement ensures a unique one to one correspondence of one value of $x$ maps to one value of $y$ and vice versa.

The linear transform of a random variable is a particular and simple case of the PDF transform. Let $x$ be a random variable with PDF $p_x$ and $a$ and $b$ two constants, then the random variable $y = ax + b$ has the following PDF:

$$p_y(y) = \frac{1}{|a|} p_x\left(\frac{y-b}{a}\right) \qquad \text{Equation 2.13}$$

This technique will be used extensively throughout this thesis to obtain the PDF after a change of variable.

### 2.1.9 Probability density functions of two random variables

#### *2.1.9.1 PDF of the sum of two independent random variables*

Consider two independent variables $x$ and $y$ with PDF $p_x$ and $p_y$ respectively. The PDF $p_z$ of the variable $z$ defined as $z = x + y$ is [36]:

$$p_z(z) = \int_{-\infty}^{\infty} p_x(z-y)p_y(y)\,dy \qquad \text{Equation 2.14}$$

This expression is the convolution product of both marginal PDFs.

#### *2.1.9.2 PDF of the product of two independent random variables*

Let $x$ and $y$ be independent random variables with PDFs $p_x(x)$ and $p_y(y)$. The PDF of the product of two random variables $z = xy$ is [36]:

$$p_z(z) = \int_{-\infty}^{\infty} \frac{1}{|x|} p_x(x).p_y\left(\frac{z}{x}\right)dx = \int_{-\infty}^{\infty} \frac{1}{|y|} p_x\left(\frac{z}{y}\right).p_y(y)\,dy \qquad \text{Equation 2.15}$$

### 2.1.10 Higher order statistics

The $r^{th}$ raw statistical moment of a probability density function $p(x)$ is defined as:

$$M'_{x,r} = E[x^r] = \int_{-\infty}^{\infty} x^r p(x).dx \qquad \text{Equation 2.16}$$

where $E[\cdot]$ denotes the expectation operator.

The moments about its mean are called central moments $M_{x,r}$

$$M_{x,r} = E[(x - \mu_x)^r] = \int_{-\infty}^{\infty} (x - \mu_x)^r p(x).\, dx \qquad \text{Equation 2.17}$$

The $r^{th}$ standardised moment of a probability distribution is $M_{x,r}/\left(\sqrt{M_{x,2}}\right)^r$ where $M_{x,r}$ is the $r^{th}$ central moment and $M_{x,2}$ is the second central moment, i.e. the variance. The advantage of standardised moments over central moments is that they are scale invariant and they are also dimensionless numbers. Note that the first standardised moment is always zero, by definition of the mean, and the second standardised moment is always one.

The third moment about the mean $M_{x,3}$ is a measure of asymmetry of the process's probability density function. For symmetric distributions such as a Gaussian distributions, $M_{x,3} = 0$. The standardized third moment is called skewness and is calculated as:

$$\lambda_x = \frac{M_{x,3}}{{M_{x,2}}^{3/2}} \qquad \text{Equation 2.18}$$

A zero value indicates that the values are evenly distributed on both sides of the mean, typically implying a symmetric distribution.

The fourth moment about the mean $M_{x,4}$ is related to the degree of flatness of a distribution near its centre. The standardized fourth moment is called kurtosis and is defined as the fourth moment centred about the mean, normalized by the square of the variance:

$$\kappa_x = \frac{M_{x,4}}{{M_{x,2}}^2} \qquad \text{Equation 2.19}$$

The word kurtosis comes from the Greek and means the action of making curved, or making convex. This means that the kurtosis, like the other standardized moments, remains unchanged through multiplication of a constant scalar. In the case of unimodal distributions, the kurtosis is often described as a measure of the "peakedness" of a process.

For a Gaussian distribution, the kurtosis $\kappa$ is 3.0. Values of kurtosis greater than three indicate that a probability density function has heavier tails than found in a Gaussian distribution and are known as leptokurtic. Kurtosis values of less than three are known as platykurtic.

Note that the "coefficient of excess", is defined as: Excess = kurtosis – 3.0 [37]. The classical kurtosis (i.e. 3.0 for a Gaussian distribution) will be used in this thesis.

Kurtosis and skewness are important indicators describing the non-Gaussian features of a unimodal probability distribution. Figure 8 compares the PDF of a standardised Gaussian random variable using a dashed black line with the PDF of a standardised random variable with a nonzero skewness of 1.0 using a red line.

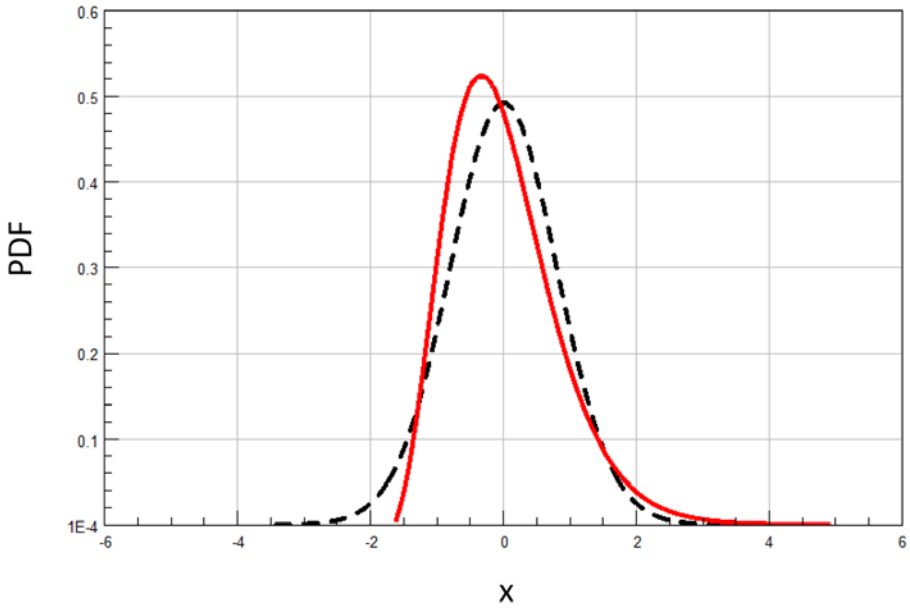


**Figure 8 : Comparison of the PDF of a Gaussian random variable (dashed black) with the PDF of a random variable with positive skewness (red)**

Figure 9 compares the PDF of a standardised Gaussian random variable using a dashed black line with the PDF of a standardised random variable with a kurtosis value of 9.0 using a red line plotted on a logarithmic vertical axis.

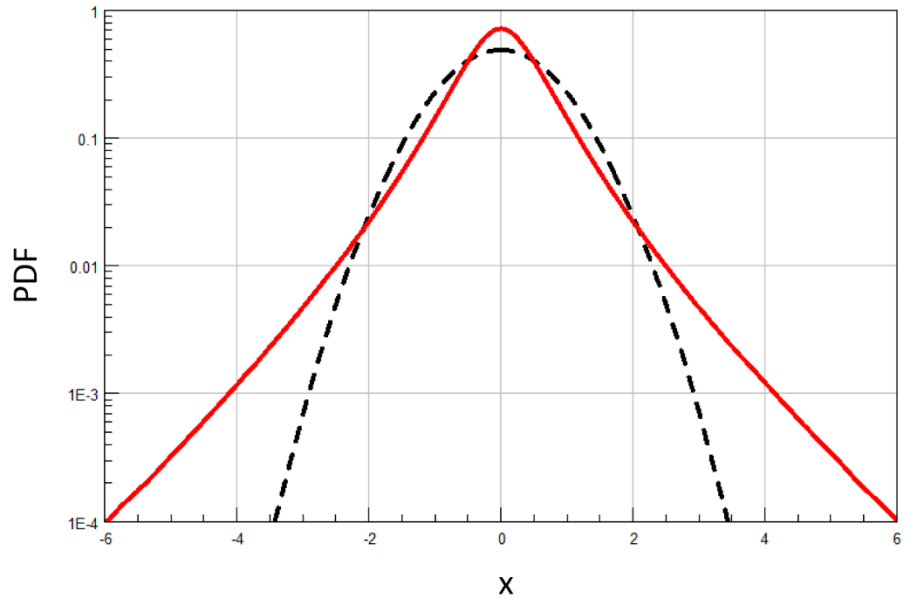


**Figure 9 : Comparison of the PDF of a Gaussian random variable (dashed black) with the PDF of a random variable with a high kurtosis (red)**

In the rest of this thesis, the mean (assumed to be zero) of a signal $x(t)$ will be written $\mu_x$, the variance ${\sigma_x}^2$ and the root mean square (RMS) value $\sigma_x$. The skewness will be assumed to be zero and the kurtosis will be denoted $\kappa_x$.

Note that the higher order statistical moments are rarely used in practice. Generally speaking, the higher the order the more the PDF is considered in detail [18].

### 2.1.11 Characteristic function and cumulants

The cumulants of a probability distribution are a set of quantities that provide an alternative to the moments of the distribution. Cumulants are sometimes also called semi-invariants in the literature [15, 37]. Working with cumulants can have an advantage over using statistical moments, because the cumulants of the sum of statistically independent random variables is the sum of the individual cumulants [18]. This fact will largely be used in this study. For example, in the case of two independent random variables $x$ and $y$, with $r^{th}$ order cumulants $c_{x,r}$ and $c_{y,r}$, the cumulants of their sum $c_{x+y,r}$ is :

$$c_{x+y,r} = c_{x,r} + c_{y,r} \qquad \text{Equation 2.20}$$

The cumulants of a random variable $x$ are defined using the second characteristic function $\Psi_x(v)$, which is the natural logarithm of the first characteristic function $\varphi_x(v)$:

$$\Psi_x(v) = ln\big(\varphi_x(v)\big)$$

The first characteristic function $\varphi_x(v)$ of a random variable $x$ is defined as [36]:

$$\varphi_x(v) = \int_{-\infty}^{+\infty} p_x(u) e^{jvu} du \qquad \text{Equation 2.21}$$

where $j$ is the imaginary number, $p_x$ the probability density function of the variable $x$ and $v$ is a real value representing the transform variable.

Cumulants are defined as the values of the derivative of the second characteristic function $\Psi_x(v)$ at the origin ($v = 0$). The $r^{th}$ order cumulant of the random variable $x$ is denoted $c_{x,r}$ and calculated as [18, 36]:

$$c_{x,r} = (-j)^r \frac{d^r \Psi_x(v)}{dv^r}\bigg|_{v=0}$$

where $j$ is the imaginary number.

The first characteristic function is continuous and its value at the origin ($v = 0$) is 1.0 [36]. Note that the moments of various orders are obtained via the derivative of the first characteristic function at the origin ($v = 0$) [18, 36, 37]. The $r^{th}$ order moment of the random variable $x$ is obtained using:

$$E[x^r] = (-j)^r \frac{d^r \varphi_x(v)}{dv^r}\bigg|_{v=0} \qquad \text{Equation 2.22}$$

The first characteristic function of a centred Gaussian distribution is calculated in Appendix A and obtained as:

$$\varphi_x(\upsilon) = e^{-\frac{1}{2}{\sigma_x}^2\upsilon^2} \qquad \text{Equation 2.23}$$

The second characteristic function is thus expressed as:

$$\Psi_x(\upsilon) = -\frac{1}{2}{\sigma_x}^2\upsilon^2$$

Note that all cumulants above the second order are zero for a Gaussian and centered distribution.

The statistical moments can be recovered from the cumulants using the Leonov and Shiryayev formula [18, 37]. For example, in the case of a random variable with zero mean, Equation 2.24 gives the four first cumulants in function of the first moments:

$$\begin{aligned} c_{x,1} &= M_{x,1} \\ c_{x,2} &= M_{x,2} \\ c_{x,3} &= M_{x,3} \\ c_{x,4} &= M_{x,4} - 3{M_{x,2}}^2 \end{aligned} \qquad \text{Equation 2.24}$$

The $r^{th}$ standardised cumulant is denoted $C_{x,r}$ and is:

$$C_{x,r} = c_{x,r}/\left(\sqrt{c_{x,2}}\right)^r \qquad \text{Equation 2.25}$$

where $c_{x,r}$ is the $r^{th}$ cumulant and $c_{x,2}$ is the second cumulant.

## 2.2 Stationary random processes

### 2.2.1 The concept of a random process

A random process $\{x_k(t)\}$ is an ensemble of real-valued or complex-valued functions that can be characterised through its probability structure. The variable $t$ will be interpreted as time in the rest of this thesis. A random process is also called a stochastic process or a time series. Each particular function $x_k(t)$, where $t$ is variable and $k$ is fixed is called a sample function. A sample function may be thought of as the observed result of a single experiment, where the quantities $x_k(t_1), x_k(t_2), \ldots, x_k(t_N)$ represent $N$ random variables over the index $k$. Figure 10 illustrates an ensemble of sample functions forming a random process.

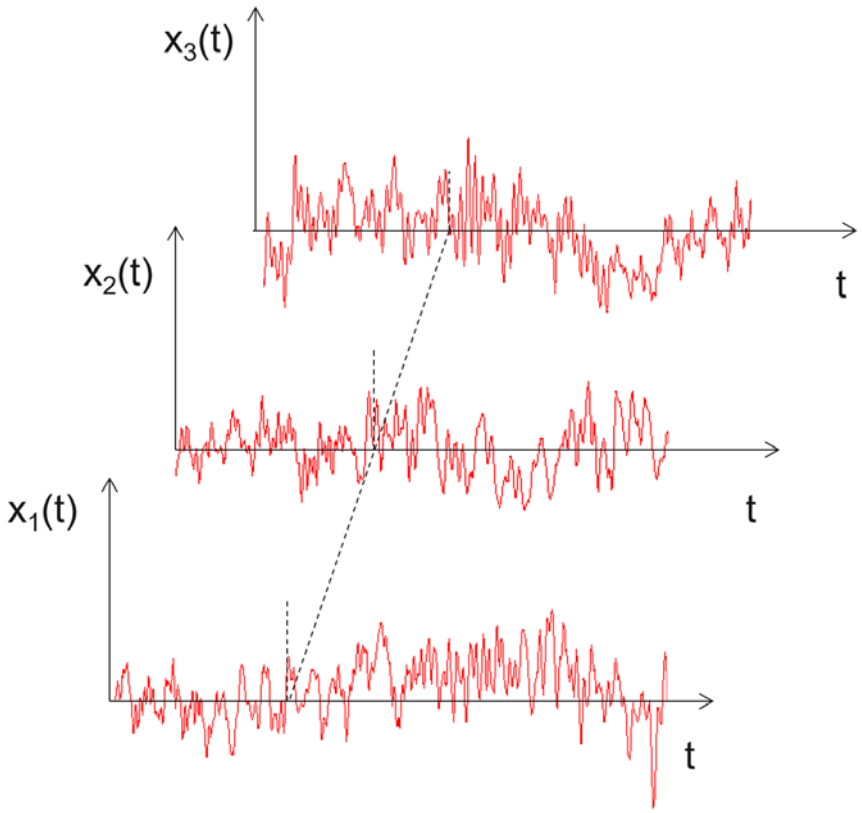


**Figure 10: Ensemble of time histories defining a random process**

One particular sample function $x_k(t)$, would not be suitable for representing the entire random process $\{x_k(t)\}$, unless the random process is ergodic (see section 2.2.3). So, in the general case, the statistics are computed across sample functions, at fixed value of $t$. The first statistical quantities of interest are the ensemble mean values at an arbitrary fixed instant $t$:

$$\mu_x(t) = E[x_k(t)]$$

In general, the mean values are different at different times.

The next statistical quantities of interest are the covariance functions at arbitrary values of $t$ and $t + \tau$, defined as:

$$\mathcal{C}_{xx}(t, t+\tau) = E\left[\left(x_k(t) - \mu_x(t)\right) \cdot \left(x_k(t+\tau) - \mu_x(t+\tau)\right)\right]$$
$$\mathcal{C}_{xy}(t, t+\tau) = E\left[\left(x_k(t) - \mu_x(t)\right) \cdot \left(y_k(t+\tau) - \mu_y(t+\tau)\right)\right] \qquad \text{Equation 2.26}$$

where $y_k(t)$ is a sample function of the random process $\{y_k(t)\}$. Again, in general these quantities are different for each combination of $t$ and $\tau$.

Note that at $\tau = 0$:

$$\mathcal{C}_{xx}(t, t) = E\left[\left(x_k(t) - \mu_x(t)\right)^2\right] = {\sigma_x}^2(t) \qquad \text{Equation 2.27}$$

Therefore the covariance function $\mathcal{C}_{xx}(t,t)$ represents the ordinary variance of $\{x_k(t)\}$ at a fixed value of $t$. Other statistical quantities can be defined over the ensemble that involve fixing three or more times [38] (e.g. $\mathcal{C}_{xxx}(t,t+\tau_1\,,t+\tau_2)$), which permits the probability structure of the random process to be described in finer and finer details.

If the sample functions form a multi-dimensional joint Gaussian distribution at a fixed time, then the sample functions are separately Gaussian at the fixed time considered. The mean values and covariance functions described above provide a complete description of the underlying probability structure.

### 2.2.2 Stationary random process

If the mean values $\mu_x(t)$ and $\mu_y(t)$ and the covariance functions $\mathcal{C}_{xx}(t,t+\tau)$, $\mathcal{C}_{yy}(t,t+\tau)$ and $\mathcal{C}_{xy}(t,t+\tau)$ yield the same results for all fixed values of $t$, then the random processes $\{x_k(t)\}$ and $\{y_k(t)\}$ are said to be weakly stationary. If all possible probability distributions involving $\{x_k(t)\}$ and $\{y_k(t)\}$ are independent of time translation, then the random processes are said to be strongly stationary. Note that for Gaussian random processes, weak stationary implies strong stationary because all possible probability distributions may be derived from the mean values and covariance functions [16].

For a stationary random process, the mean value becomes independent of $t$, that is, for all $t$,

$$\mu_x = E[x_k(t)] \qquad \text{Equation 2.28}$$

The covariance functions of stationary random processes are also independent of $t$, therefore the variance value becomes independent of $t$, that is, for all $t$,

$$\sigma_x{}^2 = \mathrm{E}[(x_k(t)-\mu_x)^2] \qquad \text{Equation 2.29}$$

The autocorrelation function of $\{x_k(t)\}$ and the cross-correlation function of $\{x_k(t)\}$ and $\{y_k(t)\}$ are introduced as:

$$\begin{aligned} R_{xx}(\tau) &= E[x_k(t)x_k(t+\tau)] \\ R_{xy}(\tau) &= E[x_k(t)y_k(t+\tau)] \end{aligned} \qquad \text{Equation 2.30}$$

For nonzero mean values, $R$ is different from $\mathcal{C}$. The covariance functions $\mathcal{C}$ are related to the correlation functions $R$ by the relationships:

$$\begin{aligned} \mathcal{C}_{xx}(\tau) &= R_{xx}(\tau) - \mu_x{}^2 \\ \mathcal{C}_{xy}(\tau) &= R_{xy}(\tau) - \mu_x\mu_y \end{aligned} \qquad \text{Equation 2.31}$$

By definition, two stationary random processes are uncorrelated if $\mathcal{C}_{xy}(\tau)=0$ for all possible lag $\tau$ [36]. In this case, $R_{xy}(\tau)=\mu_x\mu_y$.

A random process $\{x_k(t)\}$ is white noise if its values are uncorrelated i.e. $\mathcal{C}_{xx}(\tau)=0$ for all possible lag $\tau$ and $\tau \neq 0$ [36]. In this case,

$$\mathcal{C}_{xx}(\tau) = {\sigma_x}^2 \delta(\tau) \qquad \text{Equation 2.32}$$

where $\delta(\tau)$ is the Kronecker delta function.

From the stationarity assumption, it follows that the autocorrelation function is an even function of $\tau$,

$$R_{xx}(-\tau) = R_{xx}(\tau) \qquad \text{Equation 2.33}$$

The cross-correlation function satisfies the equation

$$R_{xy}(-\tau) = R_{yx}(\tau) \qquad \text{Equation 2.34}$$

Therefore the correlation properties of stationary random processes need be calculated only for positive values of $\tau$.

When τ=0, by definition, the covariance function corresponds to the variance of the data and the autocorrelation function corresponds to the mean square value.

### 2.2.3 Ergodic random processes

The collection of all realisations of a random process is known as the ensemble of the process. The statistics of a random process are obtained from the averages taken over the ensemble of many different realisations of the process. The mean value of an individual arbitrary sample function $x_k(t)$ computed by a time average is denoted:

$$\mu_x(k) = \lim_{T\to\infty} \frac{1}{T} \int_0^T x_k(t)dt \qquad \text{Equation 2.35}$$

Similarly, the covariance function can be computed by a time average, as in the expression:

$$\mathcal{C}_{xx}(\tau, k) = \lim_{T\to\infty} \frac{1}{T} \int_0^T [x_k(t) - \mu_x(k)][x_k(t+\tau) - \mu_x(k)]dt \qquad \text{Equation 2.36}$$

If these quantities are equal to the ensemble mean value $\mu_x$ and the ensemble covariance function $\mathcal{C}_{xx}(\tau)$, independently of $k$, then the random process $\{x_k(t)\}$ is said to be ergodic.

For a random process to be ergodic, it must first be stationary. An ergodic process is therefore necessarily stationary.

In many practical cases, only one realisation of a process is available. With an ergodic stationary random process, one can effectively take a single sampled time history from the process and safely assume that its time-averaged statistics may be used instead of the ensemble-averaged statistics of the parent process [20].

A random process is considered as weakly ergodic if it is weakly stationary and if the time averages $\mu_x(k)$ and $\mathcal{C}_{xx}(\tau, k)$ are the same for all sample functions $k$. Therefore, often the index

$k$ is no longer needed because the properties of any one sample function will be representative of all other sample functions.

### 2.2.4 Gaussian random processes

A random process $\{x_k(t)\}$ is said to be Gaussian if, for every set of fixed times $\{t_n\}$, the random variables $x_k(t_n)$ follow a multidimensional Gaussian distribution [16].

The instantaneous values of a sample function $x(t)$ of an ergodic Gaussian process are distributed according to a Gaussian distribution (see Equation 2.6 and more details about distributions in Section 2.1.3). The Gaussian probability density function is fully determined by knowledge of the mean value (generally zero in the case of linear mechanical vibration) and the standard deviation. This explains why it is very convenient to consider time histories to be sample functions of an ergodic Gaussian process [22, 18]. The Gaussian assumption is very often loosely made in practice by invoking the Central Limit Theorem [22].

Note that an ergodic random process may have any probability structure and is not necessarily Gaussian. Similarly, a Gaussian process is not necessarily ergodic, nor even stationary.

### 2.2.5 The power spectrum

Random signals are expressed in terms of time histories or Power Spectral Densities (PSD). The PSD is a condensed way of representing random processes. For more details about the definition and use of PSDs, the reader is referred to Newland [20], Bendat & Piersol [16] or Lalanne [22].

The Power Spectral Density (PSD) is defined as :

$$S_{xx}(f) = \lim_{T\to\infty} \frac{E[|X_T(f)|^2]}{T} \qquad \text{Equation 2.37}$$

where $X_T(f)$ is the Fourier transform of a truncated sample function $x_T(t)$ of a random process $x(t)$. The duration of $x_T(t)$ is $T$ seconds.

Furthermore, the PSD can also be obtained from the Fourier transform of the autocorrelation function $R_{xx}(\tau)$, referred to as the Wiener Khinchin theorem [39]:

$$S_{xx}(f) = \int_{-\infty}^{\infty} R_{xx}(\tau) e^{-j2\pi f\tau} d\tau \qquad \text{Equation 2.38}$$

Similarly the two-sided Cross-Power Spectral Density (CSD), denoted $S_{xy}(f)$, is obtained from:

$$S_{xy}(f) = \int_{-\infty}^{\infty} R_{xy}(\tau) e^{-j2\pi f\tau} d\tau \qquad \text{Equation 2.39}$$

From the symmetry properties of the stationary correlation functions given in Equation 2.33 and Equation 2.34, one can demonstrate that:

$$S_{xx}(-f) = S_{xx}{}^{*}(f) = S_{xx}(f)$$
$$S_{xy}(-f) = S_{xy}{}^{*}(f) = S_{yx}(f) \qquad \text{Equation 2.40}$$

where $*$ is the complex conjugate.

Note that $S_{xx}(f)$ and $S_{xy}(f)$ are sometimes called the two-sided spectral densities [39]. The one-sided PSD and CSD are defined by:

$$G_{xx}(f) = 2S_{xx}(f)\ if\ 0 < f < \infty\ otherwise\ zero$$
$$G_{xy}(f) = 2S_{xy}(f)\ if\ 0 < f < \infty\ otherwise\ zero \qquad \text{Equation 2.41}$$

Strictly speaking, only stationary time series can be represented as PSDs [16, 36]. A stationary random process is typically represented as a Power Spectral Density (PSD) showing its spectral content as a function of frequency, i.e. power in each frequency band versus frequency.

Figure 11 shows example PSDs, for narrow and broadband processes with unitary RMS. These two PSDs could represent the dynamic stress response of a system showing respectively one and two resonances.

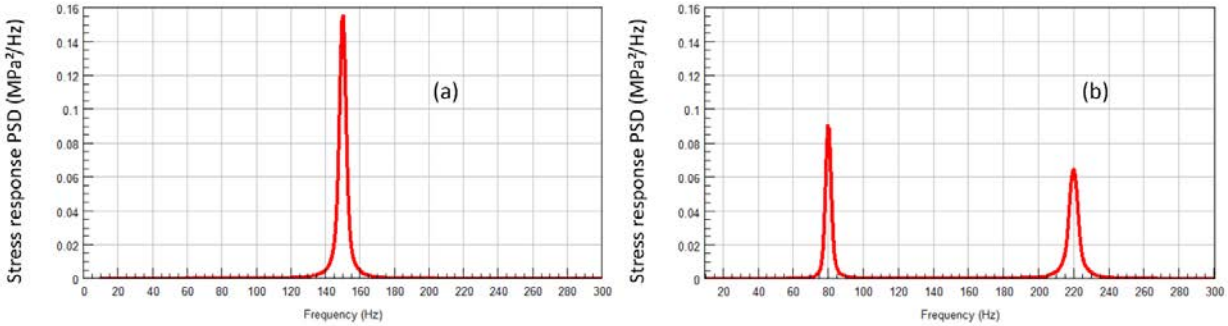


**Figure 11: Example Narrowband and Broadband (bi-modal) PSD with unitary RMS value**

From a PSD, one can generate time series realisations, as will be described in chapter 3. Figure 12 shows 0.2 second extracts of the time series corresponding to the narrow and broadband PSDs given in Figure 11.

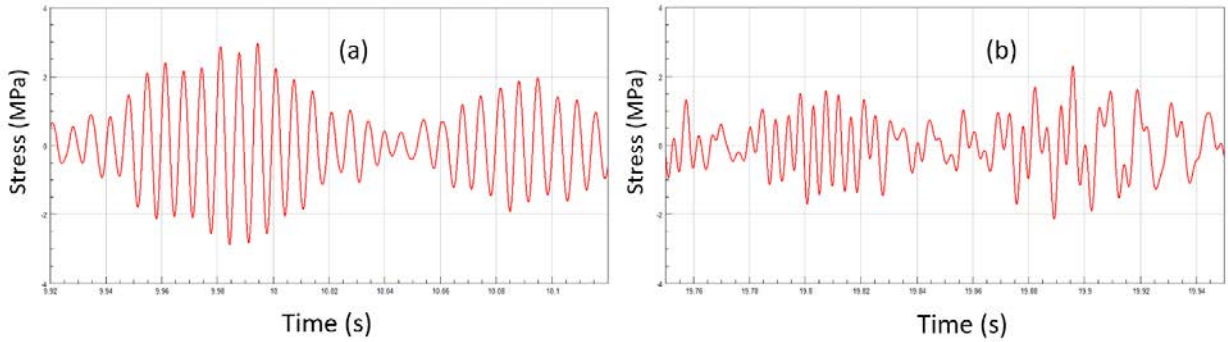


**Figure 12: Example time series corresponding to the PSDs of Figure 11**

The sample time history extracts illustrated in Figure 12 come from the full time series, which are 500 seconds long and sampled at 8192 points per seconds, making a total of over 4 million data points. Figure 12 (a) represents an extract of a narrowband signal, typically corresponding to a spectrum which is confined to a narrow band of frequencies (in the vicinity of a resonant frequency for instance). A narrowband signal typically resembles a sine wave of varying amplitudes and phase [20]. Figure 12 (b) represents an extract of a broad band signal, typically corresponding to a spectrum which covers a broad band of frequencies. A broad band signal is made up of the superposition of the various bands of frequencies.

#### *2.2.5.1 Spectral RMS*

The RMS value $\sigma_x$ is calculated as the square root of the area under the PSD $G_{xx}$, also called the zero order spectral moment of $G_{xx}$:

$$\sigma_x{}^2 = \int_0^\infty G_{xx}(f)df \qquad \text{Equation 2.42}$$

Higher order statistics cannot be calculated from the PSD as it contains only information about the second statistical moment [40].

#### *2.2.5.2 Spectral moments*

The r$^{th}$ order spectral moment $m_r$ of $G_{xx}$ is calculated as:

$$m_r = \int_0^\infty f^r . G_{xx}(f)df \qquad \text{Equation 2.43}$$

Note that the expression used in Equation 2.42 to calculate the mean square value is equivalent to calculating the zero order spectral moment $m_0$.

#### *2.2.5.3 Narrowband and broadband processes*

A narrowband process is a random process whose PSD shows a small frequency spread compared to the centre frequency [16]. Narrowband random processes are typically found when studying the response of lightly damped linear mechanical systems having one predominant mode of response.

A broadband process is a random process whose PSD has significant values over a frequency band which is of the same order of magnitude as the central frequency of the band [22]. Broadband random processes are typically found when studying the random response of a system at frequencies below its first natural resonance (i.e. in the quasi-static regime). Excitations such as jet engine [2], turbulence of supersonic boundary layer [22] or road excitation data [2] can be considered broadband sources.

#### *2.2.5.4 White noise and coloured noise*

In a statistical sense, a time series representing white noise is a sequence of serially uncorrelated random variables with zero mean and finite variance. Strong white noise also has the quality of being independent and identically distributed, which implies no autocorrelation. Such signals are also said to be time independent. In particular, if the time series is normally distributed with zero mean and standard deviation σ, the series is called a Gaussian white noise random signal.

Note that an infinite-bandwidth white noise signal is a purely theoretical construction since the energy of such a theoretical infinite bandwidth white noise would be infinite. The bandwidth of white noise is limited in practice. Therefore, a random signal is considered "white noise" if it is observed to have a flat spectrum over the bandwidth considered [20].

Note that the term ‘white’ generally refers to mean and variance being constant at all frequencies of the bandwidth of interest but in a more general sense, it could also refer to higher order statistics such as skewness, kurtosis, etc. being constant at all frequencies [18].

As opposed to white noise, coloured noise does not vary completely randomly. There is temporal dependency in the input process. In other words, there is a co-variance between the sample values at different time-indexes. Its power spectrum is not constant. Coloured noise can be generated by sending a white noise through a dynamic system, typically a filter. Such a system will be denoted by a colouring filter in this thesis.

### 2.2.6 Level Crossings

From this point forward in the thesis, a random processes will be denoted $x(t)$, omitting its dependence on $k$. Also, unless otherwise stated, ergodic processes are considered from this point forward, such that the behaviour of a sample time history over a long period of time will exhibit the same statistical characteristics as corresponding ensemble averages at various fixed times.

Figure 13 illustrates what is called a level crossing. The expected number of crossings of a given level per unit time can be found by calculating the probability that some data exceeds this level, while its derivative is positive. The processes considered are assumed to be stationary and differentiable.

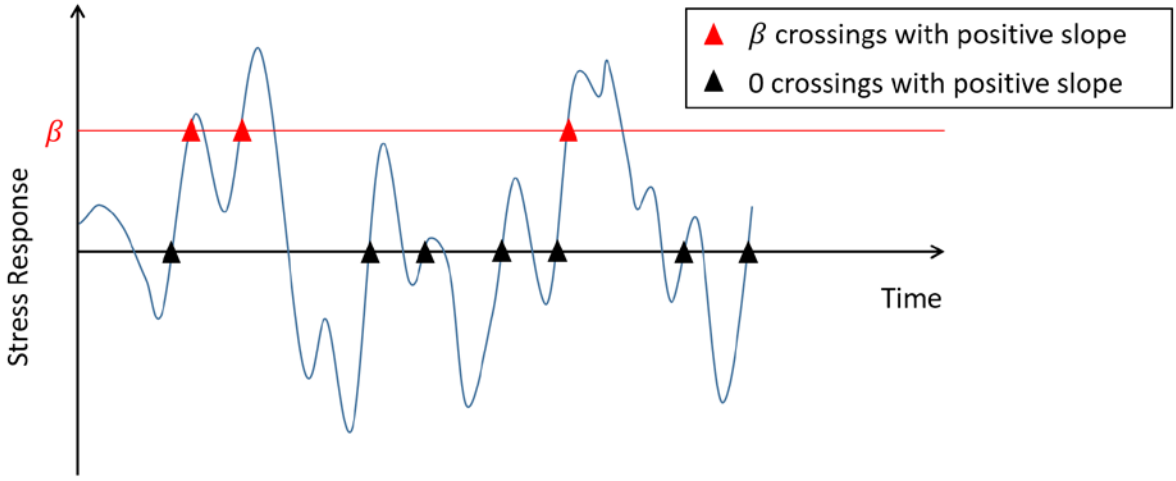


**Figure 13: Level crossings of a time history indicated by triangles for exceeding either a value of $\beta$ (red triangles) or zero (black triangles) with a positive slope**

The expected number of crossings of the level $\beta$ per unit time with a positive slope is written ${N_\beta}^+$ and is given by [16, 20, 15]:

$$ {N_\beta}^+ = \frac{1}{2\pi}\frac{\sigma_{\dot{x}}}{\sigma_x} exp\left(-\frac{\beta^2}{2{\sigma_x}^2}\right) \qquad \text{Equation 2.44} $$

where ${\sigma_{\dot{x}}}^2$ is the variance of the derivative of the process, calculated from the area under the PSD of the derivative as:

$$ {\sigma_{\dot{x}}}^2 = \int_0^\infty f^2 . G_{xx}(f) df \qquad \text{Equation 2.45} $$

${\sigma_{\dot{x}}}^2$ is also typically referred to the second spectral moment of the PSD $G_{xx}$ [13, 22, 41, 42]. The derivations to obtain Equation 2.44 can be found in Appendix A.

The number of zero crossings per unit time ${N_0}^+$ is obtained by setting $\beta = 0$ in Equation 2.44 and is expressed as:

$$ {N_0}^+ = \frac{1}{2\pi}\frac{\sigma_{\dot{x}}}{\sigma_x} \qquad \text{Equation 2.46} $$

Note that ${N_0}^+$ is also sometimes referred to as the apparent frequency [15].

N.B.: By analogy with the statistical moments obtained from a PDF, if the PSD is considered as a distribution of energy across frequencies expressed in Hz, then ${N_0}^+$ is comparable to the standard deviation of the double sided spectrum.

Inserting Equation 2.46 into Equation 2.44, the expected number of crossings of the level $\beta$ per unit time is given by:

$$N_\beta{}^+ = N_0{}^+ exp\left(-\frac{\beta^2}{2\sigma_x{}^2}\right) \qquad \text{Equation 2.47}$$

The formulations in Equation 2.46 and in Equation 2.44 apply to any stationary Gaussian random process, irrespective of its bandwidth.

The level crossing (LC) histogram shows how many times the signal has crossed a given level with a positive slope over a given duration. The expected number of crossings of various levels can be of great interest for ensuring the reliability of a product via analyses such as first passage failure (see section 2.5.2). Figure 14 represents the theoretical LC histogram using dashed black lines is overlaid with the LC histogram (using red lines) of the narrowband and broadband processes given in Figure 11 (a) and Figure 11 (b) respectively.

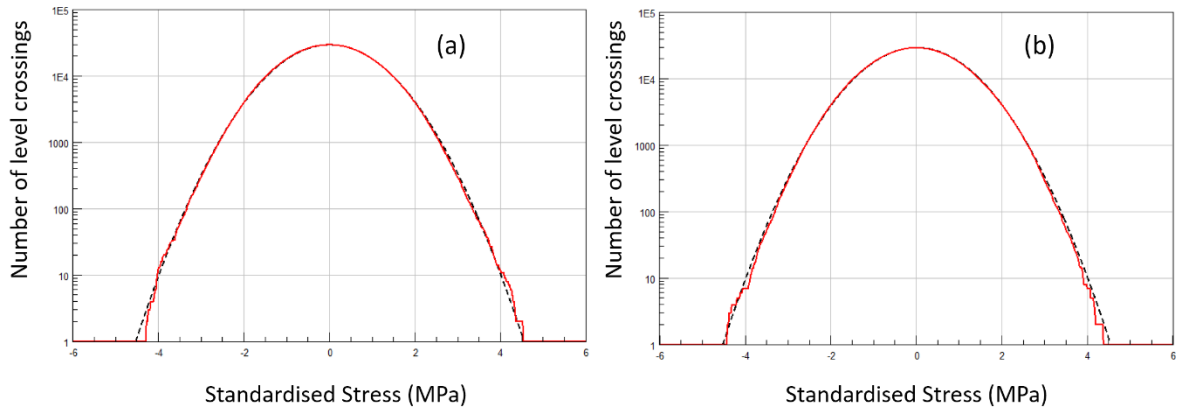


**Figure 14: Theoretical LC histogram (dashed black) versus LC histogram (red) of the numerical simulations of a narrowband process (a) broadband process (b)**

As expected, one can observe that there is a very good match between the theoretical level cross (LC) histogram and the LC histogram obtained from the time domain simulations.

### 2.2.7 Number of peaks

Figure 15 illustrates an example signal with its peaks and valleys.

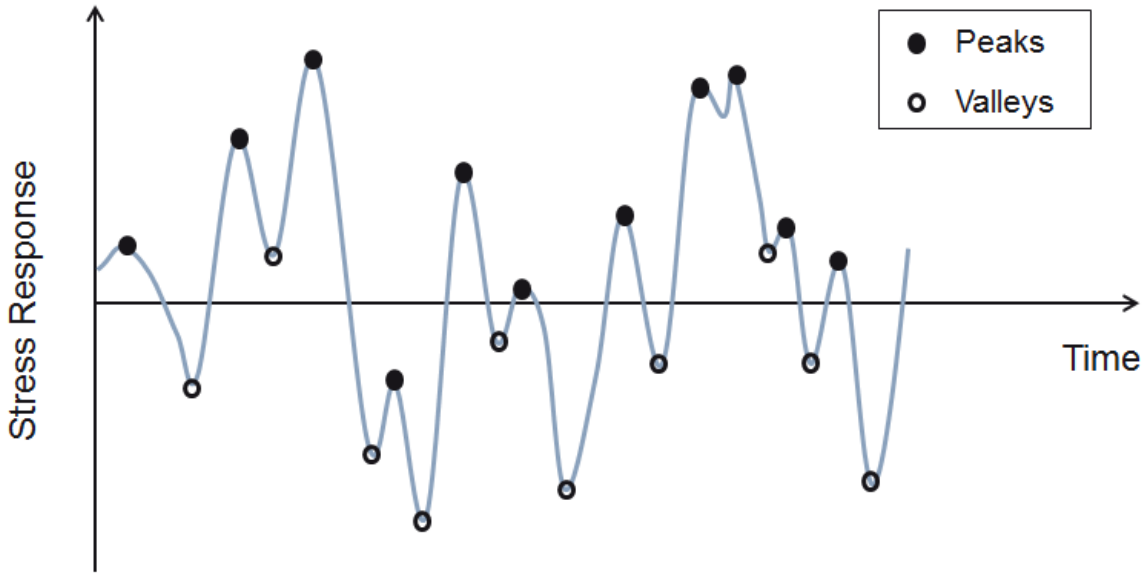


**Figure 15: Peaks and valleys of a signal represented with plain and hollow circles respectively**

The total number of expected peaks per unit time $N_p$ can be derived by stating that a local maximum is obtained when the first derivative of the signal is equal to zero and when the second derivative is negative. In other words, the number of peaks corresponds to the number of zero crossings of $\dot{x}$, the derivative of the process, with a negative slope. $N_p$ is obtained similarly as ${N_0}^+$ (see Equation 2.46) [15, 16, 20]:

$$N_p = \frac{1}{2\pi}\frac{\sigma_{\ddot{x}}}{\sigma_{\dot{x}}} \qquad \text{Equation 2.48}$$

with $\sigma_{\ddot{x}}$ the RMS value of the second derivative of the process calculated from the area under the PSD of the second derivative, also called the fourth spectral moment of the PSD $G_{xx}$ [13, 22, 41, 42]:

$${\sigma_{\ddot{x}}}^2 = \int_0^\infty f^4 . G_{xx}(f) df \qquad \text{Equation 2.49}$$

The average time interval between two successive maxima $\tau_p$ is calculated from the number of peaks per unit time $N_p$, as:

$$\tau_p = 1/N_p$$

### 2.2.8 Distribution of peaks

In this section centred processes (zero-mean) with symmetric marginal distributions are considered, therefore valleys and peaks are simply opposite to each other and all statistics related to the peaks are also valid for the valleys (e.g. number of peaks per second, etc.).

#### *2.2.8.1 PDF of peaks and valleys for a narrowband random process*

For narrowband data, each cycle of the random data leads to a single positive peak and there are therefore $N_0{}^+$ cycles per unit time. The peak probability function $p_{x_p}(x)$ is an extension of the probability of the level crossings. The number of cycles per unit time with peak value exceeding $\beta$ will be $N_\beta{}^+$. Therefore, the proportion of cycles whose peak value exceeds $\beta$ is $N_\beta{}^+/N_0{}^+$.

So, the probability that any peak is greater than $\beta$ can be expressed as:

$$\int_\beta^\infty p_{x_p}(x)dx = \frac{N_\beta{}^+}{N_0{}^+} \qquad \text{Equation 2.50}$$

$p_{x_p}(x)$ is obtained by first inserting Equation 2.44 and Equation 2.46 into Equation 2.50 and then differentiating.

In the case of a Gaussian narrowband random process, the following expression is found:

$$p_{x_p}(x) = \frac{x}{\sigma_x{}^2}.\mathrm{e}^{-\frac{1}{2}\left(\frac{x}{\sigma_x}\right)^2} \qquad \text{Equation 2.51}$$

which is a Rayleigh distribution with scale parameter $\sigma_x$.

Note that the same expression can be obtained using the Rice representation of narrowband noise [15]. The details of the derivation are given in Appendix A.

#### *2.2.8.2 An indicator of bandwidth: the irregularity factor*

In the case of a narrowband process, each zero crossing corresponds to a cycle so the total number of expected peaks per unit time $N_p$ is very similar to the number of zero crossings per unit time with a positive slope $N_0{}^+$. Therefore, one interesting indicator of bandwidth is the rate $N_0{}^+/N_p$, referred to as the irregularity factor $\gamma$.

$$\gamma = \frac{N_0{}^+}{N_p} \qquad \text{Equation 2.52}$$

In the narrowband case, $\gamma$ tends to 1.0 since a zero crossing is typically followed by a peak and there are therefore approximatively an equal number of peaks and zero crossings, as illustrated in Figure 12 (a). Similarly, in the broadband case, $\gamma$ is smaller than 1.0 since a zero crossing may be followed by a number of peaks and there are therefore a larger number of peaks than zero crossings, as illustrated in Figure 12 (b).

The irregularity factor $\gamma$ can be expressed in terms of the spectral moments (see section 2.2.5.2, Equation 2.43):

$$\gamma = \frac{m_2}{\sqrt{m_0 . m_4}} \qquad \text{Equation 2.53}$$

Cartwright and Longuet-Higgins [23] show that $0 < \gamma < 1$, and that $\gamma$ may take values indefinitely near zero or one.

For example, the PSDs shown in Figure 11 (a) and (b) have irregularity factors of 0.99 and 0.82 respectively. Other examples of irregularity factors are given next for some particular cases:

Irregularity factor for a band-limited white noise process:

For a band-limited white noise, whose spectrum is flat and constant between the frequencies $f_1$ and $f_2$ the irregularity factor γ is expressed as:

$$\gamma = \frac{\sqrt{5}}{3} \frac{f_2^3 - f_1^3}{\sqrt{(f_2^5 - f_1^5)(f_2 - f_1)}}$$

Now, writing $f_r = f_2/f_1$, it becomes clear that the irregularity factor γ tends to $\frac{\sqrt{5}}{3}$ as the frequency ratio $f_r$ tends to infinity.

Irregularity factor for a bi-modal process

Consider a bi-modal process, where each mode is assumed to be extremely narrowband. The first mode is centred around $f_1$ Hz and contains an energy value $G_1$. Similarly, the second mode is at $f_2$ Hz and contains an energy value $G_2$. The irregularity factor is expressed as:

$$\gamma = \frac{(f_1^2 G_1 + f_2^2 G_2)}{\sqrt{(G_1 + G_2)(f_1^4 G_1 + f_2^4 G_2)}}$$

Now, writing $f_r = f_2/f_1$ , it becomes clear that the irregularity factor γ tends to 1.0 as $f_r$ tends to zero.

Writing $G_r = G_2/G_1$ , when $f_r$ tends to infinity, then γ tends to $\frac{\sqrt{G_r}}{\sqrt{G_r+1}}$

So, for a bi-modal process γ tends to zero if $f_2 \gg f_1$ and $G_2 \ll G_1$. In this case, the number of peaks between two zero crossings is indeed very large leading to a very small irregularity factor.

Note that if $G_2 = G_1$, the lowest possible irregularity factor is $\frac{1}{\sqrt{2}}$.

### *2.2.8.3 PDF of peaks and valleys for a broadband random process*

Rice [15] stated that a local maximum is obtained when the first derivative of the signal is equal to zero and when the second derivative is negative. Rice [15] showed that in the case of a broadband process, the peak distribution is expressed by Equation 2.54. It is the sum of a Rayleigh distribution, a Gaussian distribution and an interaction term. The irregularity factor $\gamma$

plays the role of a weighting coefficient so that the distribution will tend towards Rayleigh if γ is approaching 1.0 (i.e. narrowband), and towards Gaussian as $\gamma$ reduces close to 0.0 (i.e. broadband).

$$p_{x_p}(x) = \frac{1}{\sigma_x}\left\{\frac{\sqrt{1-\gamma^2}}{\sqrt{2\pi}}.e^{-\frac{x^2}{2.{\sigma_x}^2(1-\gamma^2)}} + \frac{x.\gamma}{2\sigma_x}.e^{-\frac{x^2}{2.{\sigma_x}^2}}.\left(1+\mathrm{erf}\left(\frac{x.\gamma}{\sigma_x\sqrt{2(1-\gamma^2)}}\right)\right)\right\} \quad \text{Equation 2.54}$$

A novel derivation to obtain Equation 2.54 is proposed in this study. Equation 2.54 can indeed be obtained by considering that the value of a peak $x_p$ is the weighted sum of two independent random variables $x_r$ and $x_g$, distributed respectively according to Rayleigh and Gaussian laws. It was found that if the peak $x_p$ is written $x_p = \gamma.x_r + \sqrt{1-\gamma^2}.x_g$, then calculating the PDF of $x_p$ leads to the same expression as Equation 2.54. The derivations are given in Appendix A.

Note that for large positive values of the variable $x$, the distribution of peaks tends asymptotically to :

$$p_{assymp}(x) = \frac{x\gamma}{m_0}e^{\frac{-x^2}{2m_0}} \quad \text{Equation 2.55}$$

which is a Rayleigh distribution multiplied by the irregularity factor.

An example peak distribution is illustrated in Figure 16 for several values of the irregularity factor. The transition from the Rayleigh distribution ($\gamma \to 1$) to the Gaussian distribution ($\gamma \to 0$) can be clearly seen.

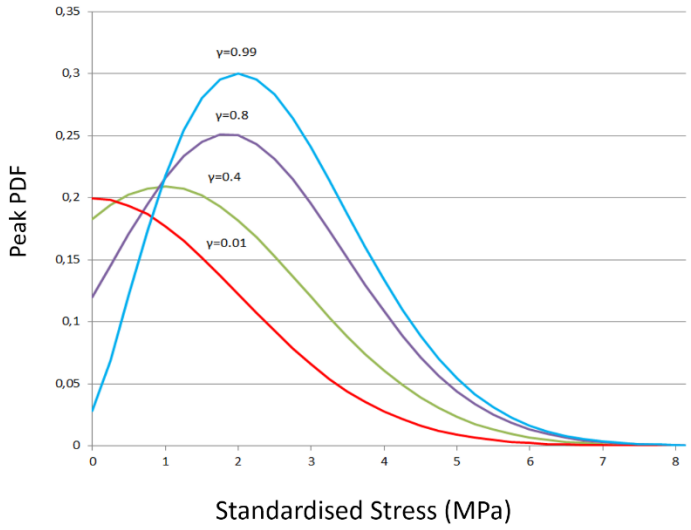


**Figure 16: Example of the peak distributions for the irregularity factor $\gamma$ ranging from 0.01 to 0.99**

Figure 17 shows the peak distributions for the narrowband and broadband signals introduced in Figure 11 and Figure 12. The theoretical peak distributions are represented using dashed black lines and the peak distributions obtained from time series simulations are represented using red lines.

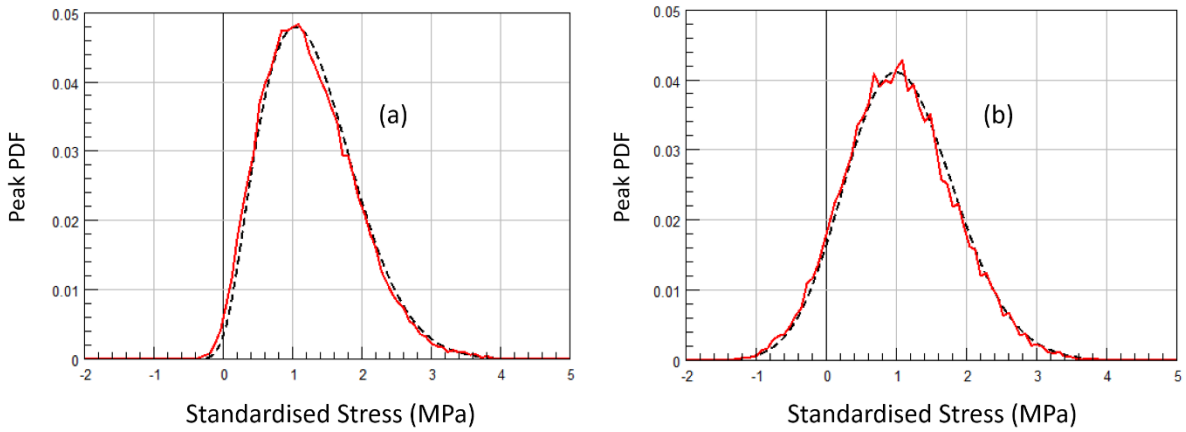


**Figure 17: Theoretical peak PDF (dashed black) versus peak PDF (red) of the numerical simulations of a narrowband (a) and broadband process (b)**

There is again a clear match between theory and simulations. The peak distribution for the narrowband process (Figure 17 (a)) has the shape of a Rayleigh distribution. In the broadband case (Figure 17 (b)) the peak distribution is clearly a mixture between Gaussian and Rayleigh distributions.

The valley distribution function $p_{x_v}$ is obtained from the peak distribution function $p_{x_p}$ using the fact that a centred Gaussian stationary process is symmetric and therefore:

$$p_{x_v}(x) = p_{x_p}(-x) \qquad \text{Equation 2.56}$$

Figure 18 shows the peak and valleys distributions for the narrowband and broadband signals introduced in Figure 11 and Figure 12.

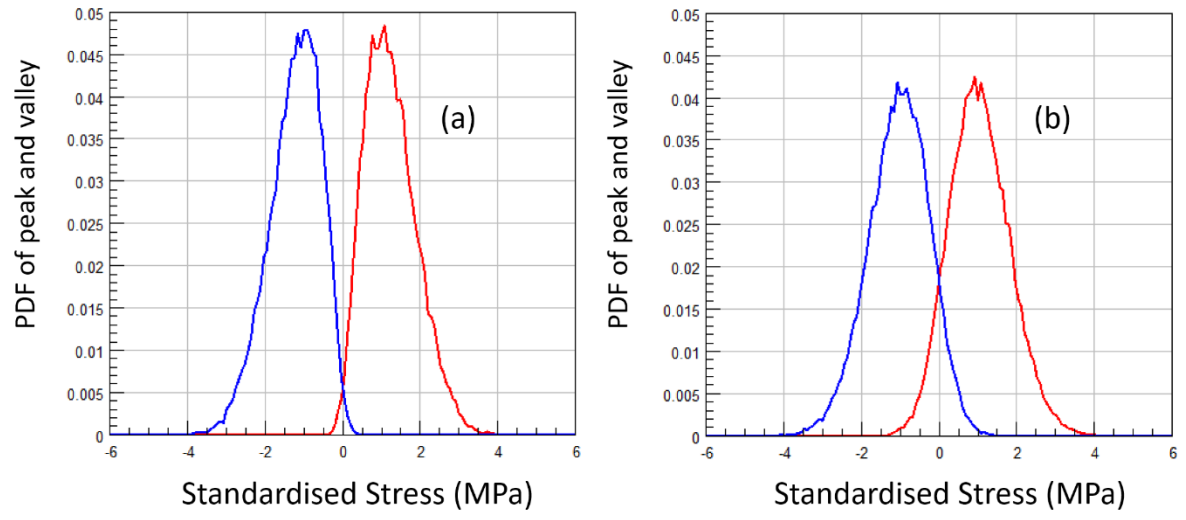


**Figure 18: Peak (in blue) and Valley (in red) distributions for the narrow band (γ=0.99) and broad band γ=(0.85) processes**

Note that the distributions intersect at $x = 0$. This is even more pronounced in the broadband case, meaning that there is a higher probability of finding negative peaks and positive valleys.

The distribution function of the peaks is obtained by integration and given by: [16]

$$P_{x_p}(x) = \frac{1}{2}\left\{1 + \operatorname{erf}\left(\frac{x}{\sigma_x\sqrt{2(1-\gamma^2)}}\right) - \gamma e^{-\frac{x^2}{2.\sigma_x{}^2}}\left(1 + \operatorname{erf}\left(\frac{x\gamma}{\sigma_x\sqrt{2(1-\gamma^2)}}\right)\right)\right\} \quad \text{Equation 2.57}$$

When $x$ is large, the error function tends towards 1.0 and $P_p(s)$ tends towards $1 - \gamma e^{-\frac{s^2}{2.\sigma x^2}}$.

The proportion of peaks with negative values is therefore given as $P_{x_p}(0)$ which is:

$$P_{x_p}(0) = \frac{1-\gamma}{2} \quad \text{Equation 2.58}$$

As displayed in Figure 16, half the peaks have indeed negative values when $\gamma$ is theoretically zero, whereas none have a negative value when $\gamma$ is theoretically one.

The probability that the random variable $x$ exceeds a given threshold $x_0$ is :

$$P(x \geq x_0) = 1 - P_{x_p}(x_0) \quad \text{Equation 2.59}$$

The mean number of peaks greater than a given threshold per unit time is therefore:

$$N_{p,x\geq x_0} = N_p\left(1 - P_{x_p}(x_0)\right) \quad \text{Equation 2.60}$$

The average time interval between two successive maxima above the level $x_0$, denoted by $\tau_{\mathrm{p},,x\geq x_0}$ is equal to the inverse of $T.N_{p,x\geq x_0}$, which represents the mean number of peaks greater than $x_0$ during the exposure time T:

$$\tau_{\mathrm{p},,x\geq x_0} = 1/\left(T.N_{p,x\geq x_0}\right) \quad \text{Equation 2.61}$$

The return period is the time necessary such that on average, there is one peak equal to or higher than a given threshold $x_0$. The return period in seconds $T_{r,x\geq x_0}$ is calculated by rearranging Equation 2.60:

$$T_{r,x\geq x_0}N_p\left(1 - P_{x_p}(x_0)\right) = 1$$

In the case of a narrowband process, this equation can be solved and the return period in seconds $T_{r,x\geq x_0}$ is calculated as:

$$T_{r,x\geq x_0} = \frac{1}{N_p} e^{\frac{{x_0}^2}{2.{\sigma_x}^2}}$$

Note that for a broadband process, an expression for $T_{r,x\geq x_0}$ cannot be obtained using conventional algebra and a numerical approach is needed.

### 2.2.9 Statistics of extreme values

There are a number of research papers involved with finding the distribution for the maximum peak $X_m$ out of $N_pT$ peaks [43, 44, 23, 45]. For a large value of peaks $N_pT$, an asymptotic expression for the mean $\overline{X_m}$ was calculated to be [23]:

$$\overline{X_m} \approx \sigma_x \left( \sqrt{2\, ln(\gamma N_p T)} + \frac{\varepsilon}{\sqrt{2\, ln(\gamma N_p T)}} \right) \qquad \text{Equation 2.62}$$

where $ln(.)$ is the natural logarithm and $\varepsilon$ denotes the Euler constant: $\varepsilon = 0.577215$ ...

Equation 2.62 is valid for an irregularity factor $0 < \gamma \leq 1$. When $\gamma$ approaches zero, the above expression is no longer valid. Fisher & Tippett [43] have shown that the average value of the largest peak out of $N_pT$ peaks in this case is given by:

$$\overline{X_m} \approx \sigma_x \left( \mathrm{m} + \frac{\varepsilon m}{m^2 + 1} \right) \qquad \text{Equation 2.63}$$

where $m$ is the mode of the distribution of maximum peaks $m = \sqrt{ln\left(\frac{(N_pT)^2}{2\pi}\right) - ln\left[ln\left(\frac{(N_pT)^2}{2\pi}\right)\right]}$.

Using the characteristic function of an asymptotic expression for the distribution of maximum peaks, Fisher and Tippett [43] also calculated the statistical moments and found the variance to be:

$$\sigma_{X_m}^2 \approx {\sigma_x}^2 \frac{\pi^2}{6} \frac{m^2}{(m^2+1)^2} \qquad \text{Equation 2.64}$$

Additional details such as the PDF of the largest peak value out of $N_pT$ peaks are found in Appendix A.

Figure 19 illustrates how the average maximum peak increases with the number of peaks from which it is extracted. The value of the maximum peak is displayed for three irregularity factors, showing how the average maximum peak increases as the bandwidth of the spectrum increases. It was calculated using Equation 2.62 and Equation 2.63.

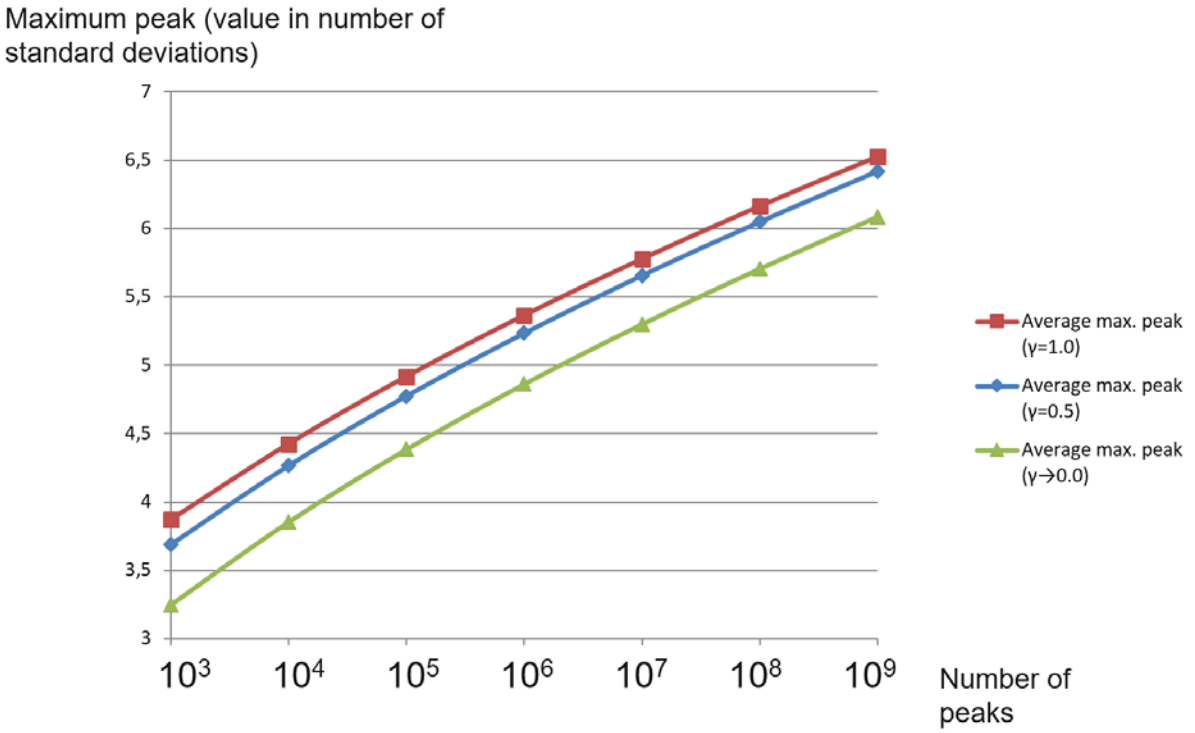


**Figure 19: Evolution of the average maximum peak with the number of peaks and the bandwidth**

Figure 20 illustrates how the standard deviation of the largest peaks decreases with the number of peaks from which it is extracted. It was calculated using Equation 2.64.

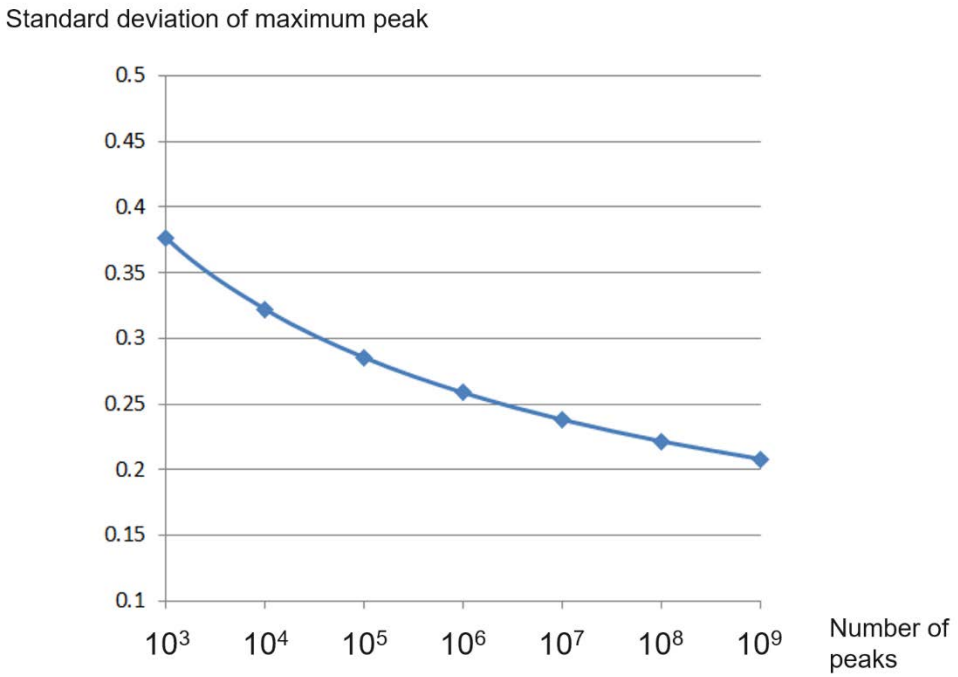


**Figure 20: Standard Deviation of largest peaks**

Figure 21 shows the results of 500 realisations of signals of various lengths (10, 100 and 1000 seconds). The maximum value obtained for each realisation is displayed as a red cross. The distribution of maxima was computed and displayed next to them. Each realisation is sampled

at 4096 points per second. The realisations correspond to a bandlimited white noise between 0 and 100Hz, with unitary RMS, irregularity factor $\gamma = 0.99$ and $N_p \approx 100$ peaks per second.

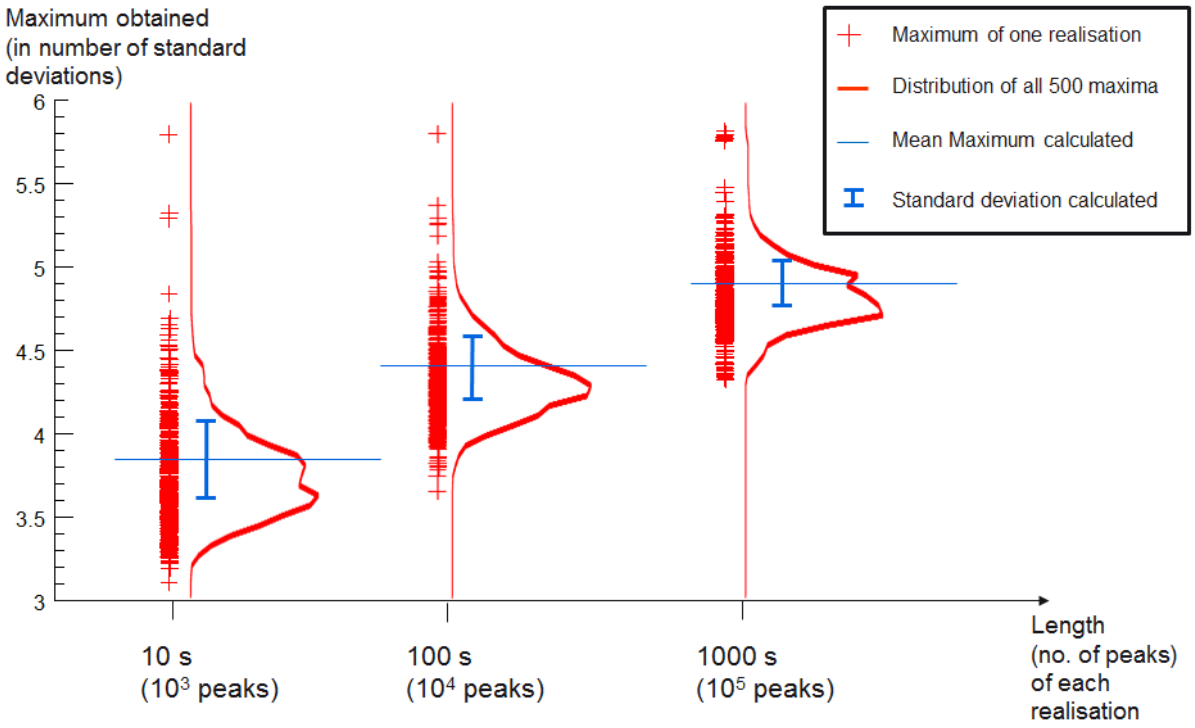


**Figure 21: Mean and standard deviation of extreme values observed for various signal lengths**

From Figure 21, it is clear that the greater the amount of data values are simulated for, i.e. a longer time history, the higher the probability of finding a high maximum. Also, the longer the signal, the less variation there is around a mean maximum. The mean and standard deviations were calculated using Equation 2.62 and Equation 2.64 respectively and seem to give sensible estimates.

It was seen in this section that each realisation of a time series of stress response produces another maximum value. Similarly each realisation will lead to another fatigue life estimation (see section 2.6). Since design engineers are looking for mean values and central tendencies, it is advisable to adopt a probabilistic approach.

## 2.3 Nonstationary random processes

So far, only stationary random processes have been introduced. Stationarity is a necessary condition to legitimately apply the signal processing techniques mentioned in the previous sections. However, stationarity is only a mathematical concept and is never fully met in practice. So stationarity is more a matter of convenience than of actuality [46]. Random data in nature is nonstationary when viewed as a whole [16]. In practice, only generated signals such as the excitation signals for shaker tests in the laboratory can be considered stationary.

A process which exhibits statistical properties that vary with translations in time is called a nonstationary process. Nonstationary data require more complex processing techniques compared to stationary data. Unfortunately, there is no general methodology for analysing the properties of any type of nonstationary data. The precise nature of the nonstationarity must be described to adopt an ad-hoc analysis technique. Several classes of nonstationary processes are considered in the literature [16, 47, 46]:

- Time-varying mean value
- Time-varying mean square value
- Time-varying frequency content

This thesis will focus on nonstationary data with time-varying mean square value because it represents well the type of nonstationary vibration encountered during the service life of many mechanical devices.

Nonstationary environmental loads with time-varying mean square value that are of concern in the field of civil engineering are due to wind [48, 49, 50], waves [50] and earthquakes [51]. Example nonstationary loads that are of concern for aerospace engineers are due to turbulent boundary flow [19, 52, 53]. Generally speaking, wheeled vehicle vibrations are likely to be nonstationary due to variations in road surface quality and vehicle speed [54, 55, 56, 57, 58]. Similarly, in the military [59] or in the rail industry [60] excitations show clear nonstationary segments of data.

A nonstationary process can often be represented as a signal with time-varying variance [16]. The nonstationary and non-Gaussian character of the atmospheric turbulence is now well recognized and gust loading is an important part of the fatigue induced on an aircraft structure [52]. Press and Steiner [61] established a formula giving the frequency of exceedance of gust velocities and induced loads and stresses on the aircraft structure. This formula also appears in the certification rules [62] to account for atmospheric variations such as horizontal gusts, penetration of jet streams and cold fronts. In this case, gusts with various amplitudes and directions must be considered. Similarly, road irregularities and vehicle speed variations are the primary cause of failure in automotive structures and components [59]. Both gust loading and road irregularities can be represented by signals with a smooth time-varying variance.

In this case, one can use a specific model consisting of deterministic factors applied to a stationary random process:

$$y(t) = a(t).x(t) \qquad \text{Equation 2.65}$$

where $x(t)$ is a sample record of a stationary random process with variance ${\sigma_x}^2$ and $a(t)$ is a deterministic function that is repeated exactly on each record. $x(t)$ and $a(t)$ are assumed to be independent. This model will largely be used in this study.

In some cases, the nonstationary data can be sliced into piecewise stationary segments and the analysis performed on the various segments separately [16].

Both piecewise stationary and "smooth" time-varying mean square value data will be studied hereafter.

### 2.3.1 Time-averaged probability structure

Analysing a single record of nonstationary data by time-averaging procedures is generally not appropriate since the statistical properties are not invariant with respect to translation in time. However, for long enough time series of time-varying mean square nonstationary random data, time averaging analysis procedures can produce meaningful results.

In practice, only one record or a limited number of records are available to study a nonstationary process. Bendat and Piersol [16] proved that considering a model of a time-varying mean square nonstationary random process, such as described in Equation 2.65, the time varying mean square value of the process $\{y(t)\}$ can be calculated from a single sample record as:

$$E[y^2(t)] = \mathrm{E}[a^2(t)x^2(t)] = E[a^2(t)]E[x^2(t)] = a^2(t){\sigma_x}^2 \qquad \text{Equation 2.66}$$

So that $a^2(t)$ can be interpreted as the instantaneous mean square value of the process $\{y(t)\}$.

Note that, similarly, the mean value of the process $\{y(t)\}$ can be calculated. If the sample record of a stationary random process $x(t)$ is zero centred, then the mean value of the process $\{y(t)\}$ is also zero.

A random signal is known as quasi-stationary if it can be divided into intervals of duration $T$ sufficiently long compared with the characteristic correlation time to allow treatment in each interval as if the signal were stationary [22]. In practice, if two sample records of stationary time history with PDFs $p_1$and $p_2$, lasting $t_1$ seconds and $t_2$ seconds respectively, then the concatenated signal would last $t_1 + t_2$ seconds and its PDF would be the weighted sum of the PDFs of both records, namely [16] :

$$\hat{p}(x) = \frac{t_1}{t_1 + t_2}p_1(x) + \frac{t_2}{t_1 + t_2}p_2(x) \qquad \text{Equation 2.67}$$

The weighting factors applied to $p_1$and $p_2$ ensure the resulting PDF has still a unit area. These factors are actually representing the fraction of the signal that stays at a particular variance. More generally, if $N$ signals were concatenated, each lasting $t_i$ seconds, then the overall PDF would be:

$$\hat{p}(x) = \frac{1}{T}\sum_{i=1}^{N} t_i . p_i(x) \qquad \text{Equation 2.68}$$

with $T = \sum_{i=1}^{N} t_i$.

If the PDF of the various sample records of stationary time histories are normally distributed and have zero mean, then it can be shown [16] that the resulting PDF will tend to increase the probability density of low and high values at the expense of intermediate values. This means that the PDF computed by time averaging of a single record of time-varying mean square random data will not be Gaussian and will show a high kurtosis value ($\kappa > 3$).

Road vibration tests on public roads or on proving ground show a divergence of the actual distribution from the normal distribution at the tails [59]. This indicates that the actual measured values at the extreme ends of the distribution are larger in magnitude than would be predicted by the assumption of a normal distribution. The kurtosis values generally exceeded a value of 3.0 (3.0 is the expected value for a Gaussian distribution).

Figure 22 (a) shows a time domain extraction of an example vertical excitation signal measured on a paved test track at the French car manufacturer Renault SA [63]. The measured signal, represented with a blue line, was normalised to a unit RMS. It has a kurtosis value of 7. Figure 22 (b) shows a random stationary Gaussian signal which has the same PSD and therefore the same overall vibration level.

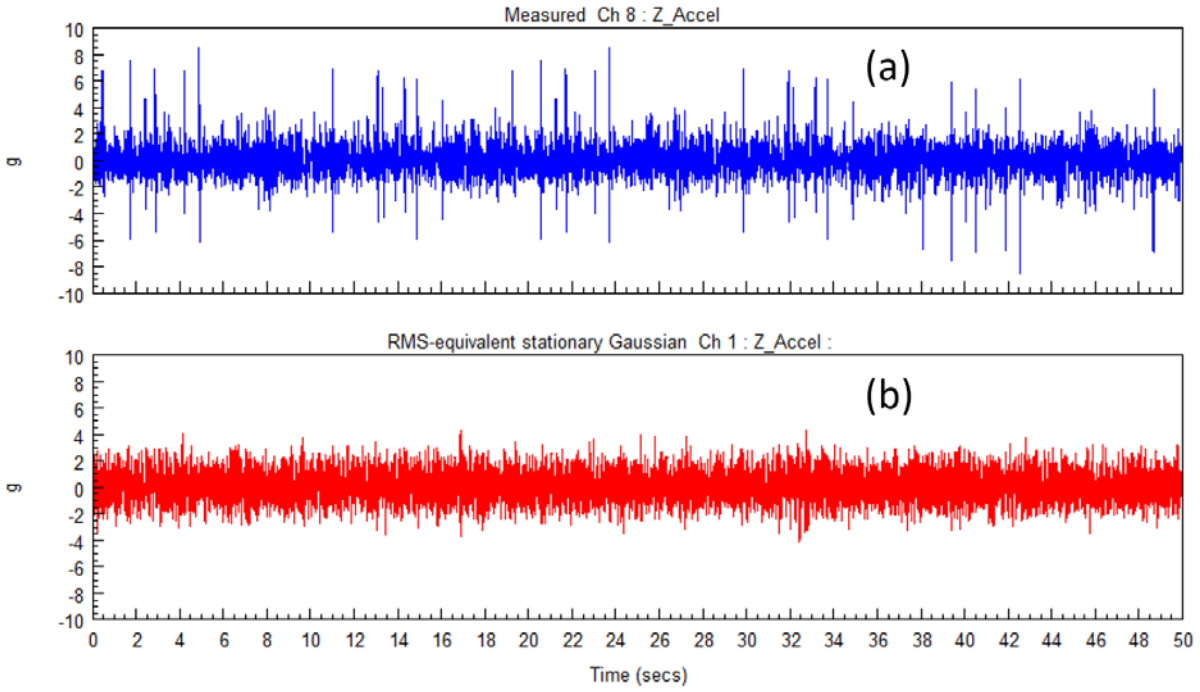


**Figure 22: comparison of a measured automotive road excitation signal (blue) with an RMS-equivalent Gaussian signal (red)**

It is clear that the measured data has much higher peaks than the RMS-equivalent stationary Gaussian signal. Even though most measured service excitation signal have such non-Gaussian

features, it is typical that they are considered under the form of PSDs. In practice, due to lack of time and experimental data, the necessary checks for stationarity and ergodicity are rarely properly carried out before any vibration analysis [22].

### 2.3.2 Cyclostationary processes

It is not appropriate to apply the same processing techniques established for ergodic data to a single record of time-varying mean square data since the statistical properties are not invariant with respect to translation in time [16]. However, there exist alternative techniques that are applicable to cyclostationary processes.

Cyclostationary is a class of random process, which can represent the random excitation for a wide class of structural systems, such as turbine blades, submarine propellers and internal combustion engines. A key characteristic of a cyclostationary excitation is that its statistics are not constant in time, as a stationary model would assume, but they vary periodically in time [47, 46].

Physical phenomena that involve periodicities give rise to random data for which appropriate probabilistic models exhibit periodically time-variant parameters. Most of the precursory works pertain to the field of communications, where it was recognised that the process of modulating a signal for Hertzian transmission naturally led to a cyclostationary behaviour [46]. However, the cyclostationary framework is appropriate for any physical phenomenon that gives rise to data with periodic statistical characteristics. For example, in mechanical-vibration monitoring and diagnosis for machinery, periodicity arises from rotation, revolution and reciprocation of gears, belts, chains, shafts, propellers, bearings, pistons, etc. For these and many other examples, the periodicity can be an important characteristic that should be reflected in an appropriate probabilistic model. Therefore, stationary processes, with their time-invariant probabilistic parameters, are in general inadequate for the study of such phenomena, and cyclostationary processes are indicated. For example, a stationary random signal modulated with a periodic amplitude modulation function is a second-order cyclostationary signal [46]. Some application [64] showed that the road excitation on a vehicle could be modelled as a cyclostationary process too.

A process $y(t)$ is said to be cyclostationary in the wide sense if its mean and autocorrelation are periodic with some period $T$:

$$\mu_y(t+T) = \mu_y(t) \qquad \text{Equation 2.69}$$

$$R_{yy}(t+T, u+T) = R_{yy}(t,u) \qquad \text{Equation 2.70}$$

for all $t$ and $u$.

The attention will be primarily focused on the autocorrelation function. Using Equation 2.70, the autocorrelation can be re-expressed as:

$$R_{yy}\left(t+T+\frac{\tau}{2},t+T-\frac{\tau}{2}\right)=R_{yy}\left(t+\frac{\tau}{2},t-\frac{\tau}{2}\right)$$

$R_{yy}\left(t+\frac{\tau}{2},t-\frac{\tau}{2}\right)$ is a function of two independent variables, $t$ and $\tau$, and is periodic with period $T$. It is assumed that the Fourier series representation for this periodic function converges, so that $R_{yy}$ can be expressed as:

$$R_{yy}\left(t+\frac{\tau}{2},t-\frac{\tau}{2}\right)=\sum_{\alpha}R_{yy}^{\alpha}(\tau)e^{j2\pi\alpha t}$$

For which $\left\{R_{yy}^{\alpha}\right\}$ are the Fourier coefficients and $\alpha$ ranges over all integer multiples of the fundamental frequency $1/T$.

$R_{yy}^{\alpha}(t)$ is referred to as the cyclic autocorrelation function and $\alpha$ is called the cyclic frequency parameter. $R_{yy}^{\alpha}(t)$ can be written [47]:

$$R_{yy}^{\alpha}(\tau)=\frac{1}{T_0}\int_{-T_0/2}^{T_0/2}R_{yy}\left(t+\frac{\tau}{2},t-\frac{\tau}{2}\right)e^{-j2\pi\alpha t}\,dt \qquad \text{Equation 2.71}$$

Modelling the signal as cyclostationary therefore results in a two-dimensional autocorrelation function, where the extra dimension is denoted $\alpha$, i.e., the cycle frequency at which the one-dimensional autocorrelation function has been computed. For each $\alpha$, a Fourier transform of the cyclic autocorrelation function produces a cyclic-spectrum-cut for that particular frequency separation $\alpha$. Repeating this process for other values of $\alpha$ gives rise to a three-dimensional cyclic spectrum with the three axes being: $f$, $\alpha$, and magnitude. The cyclic spectrum is given as:

$$S_{yy}^{\alpha}(f)=\int_{-\infty}^{\infty}R_{yy}^{\alpha}(\tau)\,e^{-j2\pi f\tau}d\tau \qquad \text{Equation 2.72}$$

Note that, for $\alpha=0$ the cyclic autocorrelation function $R_{yy}^{\alpha}$ and the cyclic spectrum $S_{yy}^{\alpha}$ reduce to the conventional autocorrelation and the conventional PSD [47]. Equation 2.72 is therefore comparable to Equation 2.38 giving the conventional two-sided PSD $S_{xx}$ from the autocorrelation function $R_{xx}$. Also, for a stationary process, $R_{yy}^{\alpha}\equiv 0$ and $S_{yy}^{\alpha}\equiv 0$ for all $\alpha\neq 0$ [65]. Therefore, for a stationary random signal, the cyclic spectrum is given by:

$$S_{yy}^{\alpha}(f)=\begin{cases}S_{yy}(f), & \alpha=0\\ 0, & otherwise\end{cases} \qquad \text{Equation 2.73}$$

Now, the random signal $y(t)=a(t)x(t)$ is considered, where $x(t)$ is a stationary random signal, $a(t)$ is a periodic modulation function, with period $T$, and $x(t)$ and $a(t)$ are statistically independent (in the sense that their joint probability distributions factor into the product of the two individual marginal distributions, cf. section 2.1.7). The cyclic autocorrelation function and the cyclic spectrum of $y(t)$ will be calculated next.

The periodic modulation function $a(t)$ can be decomposed into Fourier series:

$$a(t) = \sum_k a_k e^{j2\pi\frac{kt}{T}} \qquad \text{Equation 2.74}$$

The autocorrelation function of $y(t)$ is [47]:

$$R_{yy}(t,\tau) = a(t+\tau/2)a^*(t-\tau/2)R_{xx}(\tau)$$

where $R_{xx}(\tau)$ is the autocorrelation function of the stationary process $x(t)$.

Inserting Equation 2.74, the expression for the autocorrelation function becomes:

$$R_{yy}(t,\tau) = \sum_{k,l} a_k a_l^* e^{j2\pi\frac{(k-l)t}{T}} e^{j2\pi\frac{(k+l)\tau}{2T}} R_{xx}(\tau)$$

The cyclic autocorrelation function is therefore (see Equation 2.71)

$$R_{yy}^{\alpha}(\tau) = \langle R_{yy}(t,\tau)e^{-j2\pi\alpha t}\rangle$$

which is equivalent to [65]:

$$R_{yy}^{\alpha}(\tau) = \begin{cases} R_{xx}(\tau)\sum_k a_k a_{k-\alpha T}^* \, e^{j2\pi\left(\frac{k}{T}-\frac{\alpha}{2}\right)\tau}, \alpha \text{ multiple of } 1/T \\ 0, \text{ otherwise} \end{cases} \qquad \text{Equation 2.75}$$

The cyclic spectrum is obtained using Equation 2.72:

$$S_{yy}^{\alpha}(f) = \begin{cases} \sum_k a_k a_{k-\alpha T}^* \, S_{xx}\left(f - \frac{k}{T} + \frac{\alpha}{2}\right), \alpha \text{ multiple of } 1/T \\ 0, \text{ otherwise} \end{cases} \qquad \text{Equation 2.76}$$

with $S_{xx}(f)$ the two-sided PSD of $x(t)$.

Or, considering the harmonic cyclic frequency $\alpha = p/T$,

$$S_{yy}^{p/T}(f) = \sum_k a_k a_{k-p}^* \, S_{xx}\left(f - \frac{k}{T} + \frac{p}{2T}\right) \qquad \text{Equation 2.77}$$

where $\sum_k a_k a_{k-p}^*$ is the correlation function of the Fourier coefficients $a_k$ of the periodic modulation function.

N.B.: if the period $T$ is large compared to the autocorrelation of $x(t)$, then this expression can be approximated:

$$S_{yy}^{p/T}(f) \approx S_{xx}(f)\sum_k a_k a_{k-p}^* \qquad \text{Equation 2.78}$$

## 2.4 Dynamic characteristics of physical systems

A system is typically defined as a collection of mathematical models, hardware, components or subsystems that is typically mapping a set of inputs to a set of outputs. In this thesis, the principal system is a mechanical component, the input is the excitation e.g. the drive signal of acceleration in the case of a shaker and the output is a response signal representing acceleration, displacement or more specifically stress. The impulse response of the system is denoted $h(\tau)$. The system's behaviour can usually be modelled or represented mathematically.

### 2.4.1 Linear and time-invariant systems

Linear and time-invariant (LTI) systems with constant parameters will be mainly considered in this thesis.

A system $L_h$ is linear if the response characteristics are additive and homogeneous [16, 20]. This means that $L_h[N.a + M.b] = N.L_h[a] + M.L_h[b]$, where $a$, $b$ are inputs and $N$, $M$ are some arbitrary linear scaling.

A system has constant parameters if all fundamental properties of the system are invariant with respect to time. A system is time invariant if any shift $t_0$ of the input $x(t)$ to $x(t + t_0)$ causes a similar shift of the output $y(t)$ to $y(t + t_0)$:

$$L_h[x(t + t_0)] = y(t + t_0)$$

A system is considered to be stable if the output to a bounded input is bounded.

Note that for a system to be physically realisable, it is necessary that the system responds only to past inputs i.e. its impulse response function $h(\tau) = 0$ for $\tau < 0$. In this case, the system is called causal.

If the input $x(t)$ is from a stationary random process and if the system $L_h$ is linear and time invariant, then the output $y(t) = L_h[x(t)]$ will form a stationary random process. This result is proved in reference [16].

Also, if $x(t)$ follows a Gaussian distribution and if the system $L_h$ is linear, then $y(t) = L_h[x(t)]$ will also follow a Gaussian distribution. This result is proved in reference [36].

It is worth noting that the converse of the two previous properties of an LTI system is not true i.e. a nonstationary random input will not necessarily lead to a nonstationary output and a non-Gaussian input will not necessarily lead to a non-Gaussian output [66].

Figure 23 represents a linear system with one input $x$ and one output $z$.

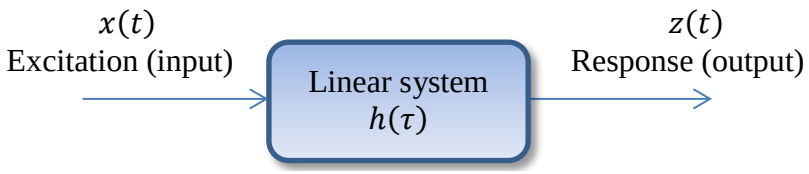


**Figure 23: Simple system with one input and one output**

If the input is a constant amplitude fixed harmonic sine wave of frequency $f$:

$$x(t) = x_0 sin(2\pi f t)$$

Then, by definition of a linear system, the steady state output must also be a constant amplitude sine wave of the same frequency but, in general, with a different amplitude and phase:

$$z(t) = z_0 sin(2\pi f t - \varphi)$$

The dynamic characteristics of an LTI system can be modelled mathematically. In the time domain, the impulse response function of the system - generally denoted $h(\tau)$ - is defined as the output of the system at any time to a unit impulse input applied a time $\tau$ before. The relationship between the input $x(t)$ and the output $z(t)$ is given by the convolution integral [20]:

$$z(t) = \int_{-\infty}^{t} h(t-\tau).x(\tau)d\tau \qquad \text{Equation 2.79}$$

In the frequency domain, the dynamic characteristics of an LTI system can be described by a frequency response function (FRF) $H(f)$, which is defined as the Fourier transform of $h(\tau)$.

Equation 2.80 gives the relationship between $h(\tau)$ and $H(f)$:

$$H(f) = \int_{0}^{\infty} h(\tau).e^{-j2\pi f\tau}d\tau \qquad \text{Equation 2.80}$$

The equivalent of Equation 2.79 can be obtained in the frequency domain. Indeed, the frequency response function $H(f)$ can be used to relate the Fourier transforms of the input and output [16, 20] as expressed in Equation 2.81 :

$$Z(f) = H(f).X(f) \qquad \text{Equation 2.81}$$

A similar expression exists to relate the PSDs of the input and output of a linear system. It is obtained by using Equation 2.79 to write the autocorrelation function of the output $z(t)$. Newland [20] then shows that taking the Fourier transforms of both parts of the equation gives the relationship linking the PSDs and the frequency response function $H(f)$:

$$G_{zz}(f) = H^*(f).H(f).G_{xx}(f) \qquad \text{Equation 2.82}$$

where $H^*$ is the complex conjugate of $H$. $G_{zz}$ and $G_{xx}$ are the PSDs of the input to and output of the system respectively.

The system considered in this thesis is typically a component fixed on a shaker table. Figure 24 shows an outlined view of the shaker system with its principal sub-systems.

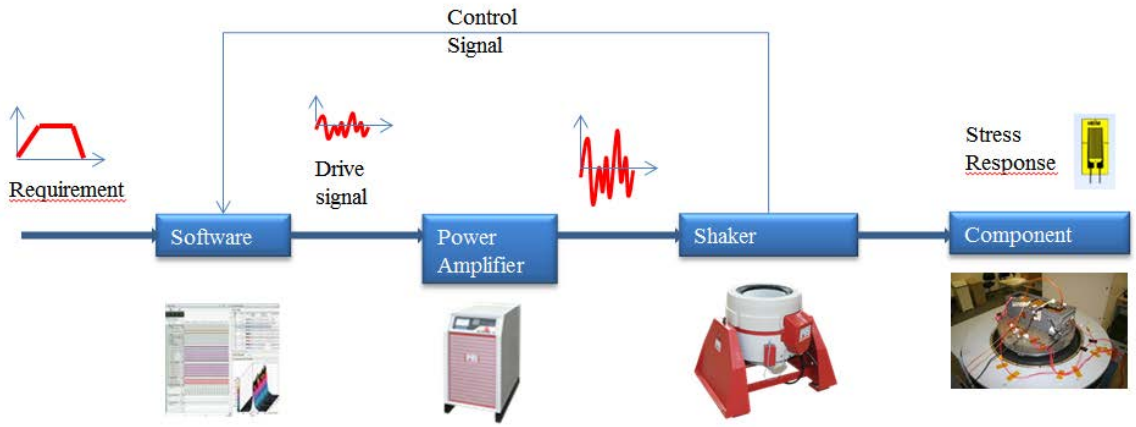


**Figure 24: global view of the vibration test system**

### 2.4.2 Non-linear systems

In this thesis the system is assumed to be linear, i.e. the relationship between the control signal and the stress response follows Equation 2.79 and Equation 2.81 presented in the previous section. However, in practice, nonlinearities always occur to some degree. A common case of non-linearity in the component is when it is made of materials with nonlinear properties. Elastomer materials (e.g. rubber) are common examples that exhibit nonlinear load deflection responses. Plastic and elastomeric materials often have a complex modulus that changes with temperature and loading frequency [12, 67, 14]. Another example is in the case of large deformation and material response, where the stress is above the yield strength and complicated cyclic hardening occurs [13].

There are a number of analysis methods for nonlinear response prediction. More complete reviews of the various methods are given by Worden [68, 69] or by Sweitzer [12].

The linearity assumption taken in this thesis is based on the fact that the (stress) response characteristics for many mechanical systems may be assumed to be linear, at least over some limited range of inputs, without involving unreasonable errors [16].

## 2.5 Static failure analysis

Although static failure is not the main concern of this thesis, some basic concepts are introduced in this section. It illustrates the probabilistic aspects of static failure under random loading. The objective is to design a structure such that the probability of failure during service life is acceptably small. Two approaches are presented; the three-sigma and the first passage failure. In both approaches, the mechanical stress is considered as a random variable.

### 2.5.1 The "three-sigma" design criterion

The "three-sigma" design criterion is typically used to design structures where brittle fracture or fatigue are not considered to be the principal failure modes [21, 70].

The mechanical stress $z(t)$ is assumed to be a random Gaussian variable with RMS $\sigma_z$ and zero mean value. The strength $R$ is deterministic. A basic requirement could be that, for a safe design, $R \geq 3\sigma_z$ [21].

Since the random stress $z(t)$ is assumed to be Gaussian, the probability that stress will exceed three times its RMS value is $P(z \geq 3\sigma_z) = 0.00135$ (see Table 2. in section 2.1.5, where the Gaussian PDF is introduced). Thus, the stress exceeds the strength only less than 0.15% of the time if $R = 3\sigma_z$.

In reality, the strength $R$ is a random variable, with known mean and standard deviation.

The stress-strength analysis used in reliability engineering can be seen as a generalized "three-sigma" criterion. Figure 25 shows an example of the stress and strength distributions. In this example, stress and strength are considered as independent random variables. The overlap of these distributions, referred to as stress-strength interference, represents the probability of failure [71, 72].

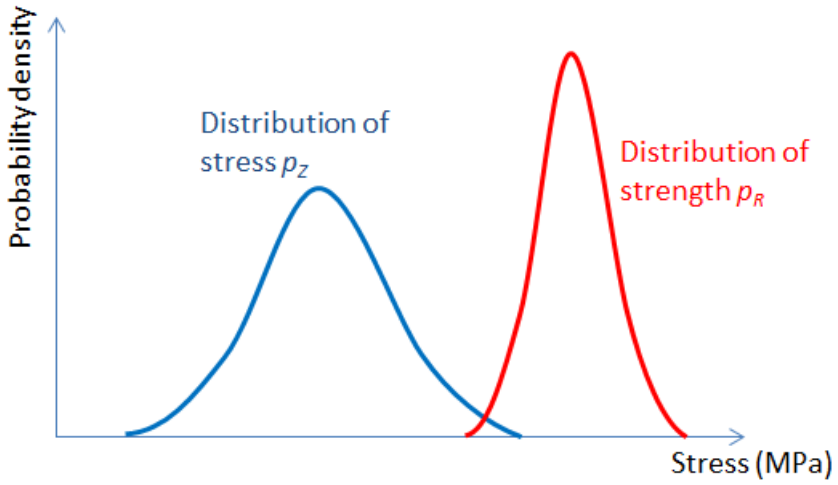


**Figure 25: Example stress-strength diagram**

### 2.5.2 The first passage failure

In the first passage failure criterion, failure is defined as the first time the stress $z(t)$ exceeds the strength $R$. The goal of design is to ensure that the probability of a first-passage failure in service life $T_s$ is acceptably small [21].

The term "first passage failure", however, does not necessarily indicate that a structure fails immediately at the first time the response exceeded a given threshold level. Instead, the first

passage probability is frequently used to measure the probability that the structural response exceeds certain design limit conditions, such as yield stress at least once within a specific time interval. So the first passage problem is meaningful as a measure of likelihood for the structure to be in a design limit state, which is an important indicator for structural safety [25].

Over the years, several investigators have addressed the first-passage problem. Some of the pioneers have been Lin [19], Yang and Shinozuka [24, 25], Winterstein [50] or Ortiz [21].

The probability of a first-passage failure $P_f$ can be formulated as:

$$P_f = P(T_f < T_s)$$

with $T_f$ time to failure and $T_s$ service life.

In the case where the strength $R$ is deterministic and constant, the probability of a first-passage failure can be written:

$$P_f = P(Z_m > R) = 1 - P_{Z_m}(R)$$

where $Z_m$ is the largest stress peak value during $T_s$ and $P_{Z_m}$ is the CDF of the random variable $Z_m$.

An important application is the special case of a fatigue problem, where crack growth is modelled by the fracture mechanics fatigue model [21]. As the crack grows, the ultimate strength becomes smaller (regardless of whether a ductile or brittle fracture model is used). Failure occurs the first time that the random stress $z(t)$ exceeds the ultimate strength.

Other important applications of the first passage problem are related to the reliability of structures when subjected to earthquake [25] or ocean wave [50] excitations modelled as random processes.

## 2.6 Fatigue failure analysis

### 2.6.1 Introduction to fatigue phenomenon and modelling

The majority of component design involve parts subjected to fluctuating or cyclic loads. Such loading induces fluctuating or cyclic stresses that often result in failure by fatigue [73].

According to the ASTM standard [74], material fatigue is “the process of progressive localized permanent structural change occurring in a material subject to conditions that produce fluctuating stresses and strains at some point or points and that may culminate in cracks or complete fracture after a sufficient number of fluctuations”. Another more conceptual definition of material fatigue is “failure under a repeated or otherwise varying load which never reaches a level sufficient to cause failure in a single application” [75].

Between 1852 and 1870 the German railway engineer August Wöhler set up and conducted the first systematic fatigue investigation [76]. Some of Wöhler's data are plotted in terms of nominal stress versus cycles to failure, on what has become well known as the S-N diagram, as shown in Figure 26. Each curve on such a diagram is still referred to as a Wöhler curve.

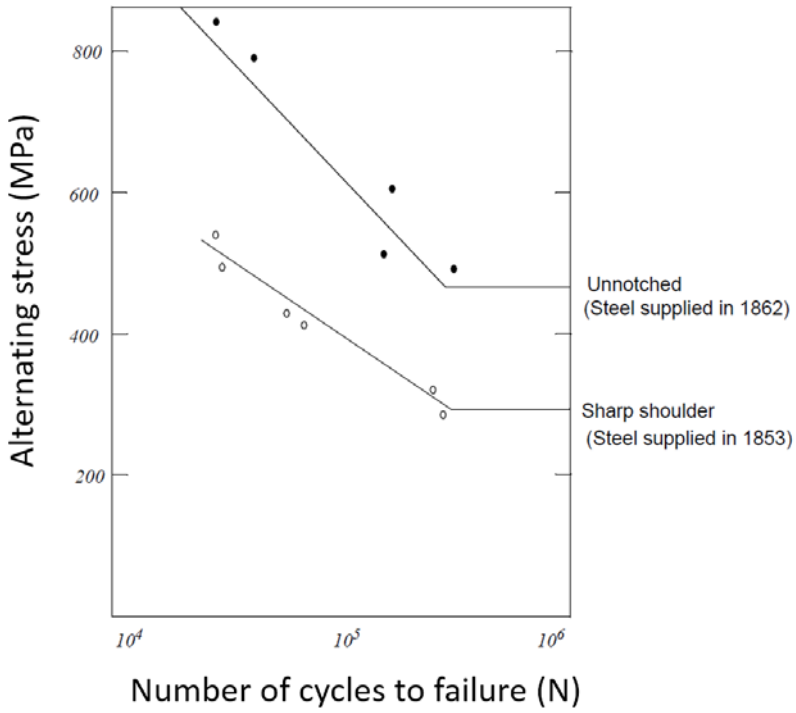


**Figure 26: Example Wöhler curves showing alternating stress versus number of cycles to failure**

From the Wöhler curve, it becomes obvious that the fatigue life of a structure is largely dependent upon the amplitudes of local stress - also called stress response in this thesis.

It is widely accepted that the fatigue process actually embraces two domains of cyclic stressing or straining that are distinctly different in character, and in each of which failure occurs by apparently different physical mechanisms. One domain of cyclic loading is that for which significant plastic strain occurs during at least some of the loading cycles. This domain involves some large stress response cycles, relatively short lives and is usually referred to as low cycle fatigue. The other domain of cyclic loading is that for which the stress or strain cycles are largely confined to the elastic range. This domain is associated with low loads and long lives and is commonly referred to as high-cycle fatigue. Low cycle fatigue is typically associated with fatigue lives between about 10 to 100,000 cycles and high cycle fatigue to lives greater than 100,000 cycles. The assumption of high-cycle fatigue will be adopted in this thesis.

The high-cycle fatigue approach is really only valid where the applied stress is nominally within the elastic range of the material and the number of cycles to failure is large. Typical types of cyclic stresses which contribute to the fatigue process are shown in Figure 27.

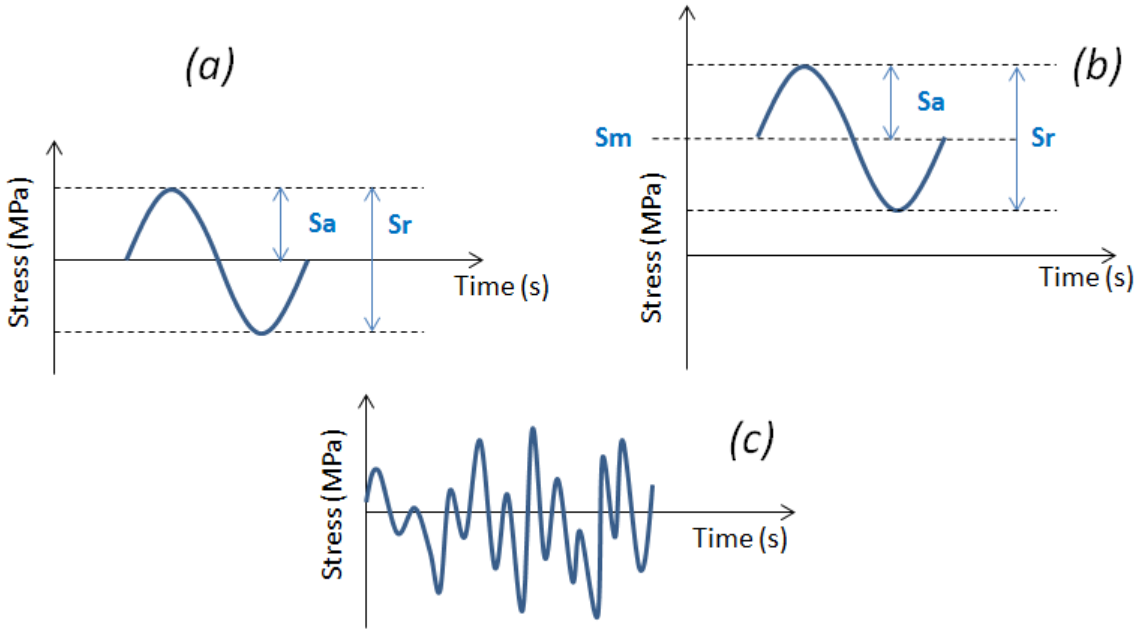


**Figure 27: Typical Fatigue stress cycles: (a) fully reversed, (b) mean and dynamic stress components and (c) random stress response**

Figure 27(a) illustrates a fully reversed stress cycle with a sinusoidal form. Figure 27 (b) illustrates the more general situation where the maximum and minimum stresses are not equal, in this case they are both tensile, and so define an offset for the cyclic loading. Figure 27 (c) illustrates a more complex, random loading pattern which is more representative of the cyclic stresses found in structures during real service life. From the above it is clear that a fluctuating stress cycle can be considered to be made up of two components, a static or steady state stress $S_m$, and an alternating or variable stress amplitude $S_a$. It is also often necessary to consider the stress range, $S_R$, which is the algebraic difference between the maximum and minimum stress in a cycle.

S-N data is nearly always presented in the form of a log-log plot of alternating stress, amplitude $S_a$ or range $S_R$, versus cycles to failure, with the actual Wöhler line representing the mean life. Certain materials, e.g. steels, display a fatigue limit, $S_e$, which represents an alternating stress level below which the material has an infinite life. When plotted on log-log scales, the relationship between alternating stress, $S_R$, and number of cycles to failure, $N_f$ can be described by the Basquin power-law relationship [73, 77] given in Equation 2.83.

$$C = N_f . {S_R}^b \qquad \text{Equation 2.83}$$

where $S_R$ is the stress range in MPa, $N_f$ is the number of rainflow cycles to failure, $C$ is the Basquin coefficient (intercept of the SN curve with the stress axis) and $b$ is the Basquin exponent (gradient of the SN curve in log-log space). Figure 28 shows an example S-N curve. This curve is curve fitted through the life data of the various coupons tested. The life data of each coupon is represented using either a cross (for the failed coupons) or an arrow for the ones that did not fail).

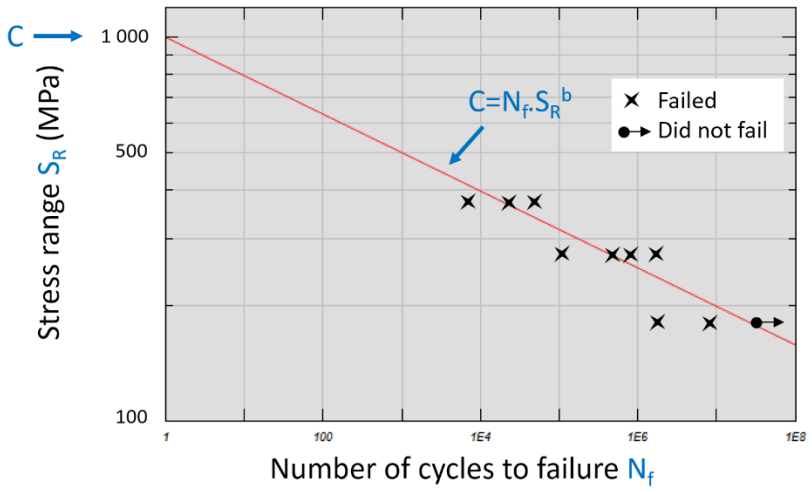


**Figure 28: Example stress-life fatigue curve showing the test data points and the curve fit using the Basquin equation**

Fatigue tests can be conducted using a given nonzero mean stress. Corrections for the effect of mean stress can be adopted. This would typically modify the stress range of a cycle with any mean stress value to obtain a fatigue-equivalent cycle, whose mean stress correspond to the one of the fatigue curve [73]. Note that the stress range $S_R$ is the most significant aspect to consider in a cycle and the mean stress $S_m$ has a secondary effect [73].

It is worth noting that, according to Equation 2.83, fatigue damage is related exponentially to stress. This means that a small under-estimation in stress leads to a large under-estimation of the fatigue damage.

### 2.6.2 Deterministic rainflow cycle count

Fatigue lives of specimens are determined from constant amplitude tests. Real structures however rarely experience constant amplitude loading. The rainflow cycle counting (RFC) method [78] is a cycle counting scheme employed to reduce a complex irregular loading history into a series of constant amplitude events, each defined by its range and its mean value. This method defines cycles as closed stress/strain hysteresis loops [79].

For decades now, RFC has been the most popular and effective way of extracting cycles for fatigue life assessment [80, 81, 29]. The rule for the four points algorithm [80] is described as follows:

Take four consecutive points, starting from the first data point. A cycle is found when the second and third points are within the range defined by the first and last points.

To illustrate this, an example is given based on the red signal displayed in Figure 29:

- Consider points 1, 2, 3, 4: there is no cycle since point 3 is lower than 1.
- Continue with points 2,3,4,5: no cycle since 4 is higher than 2
- Continue with points 3,4,5,6: no cycle since 4 is higher than 6
- Continue with points 4,5,6,7: Cycle C1 is counted. Its range is 4 and mean is 7.
- Now remove the cycle C1, join points 4 and 7 and continue from point 4:

- Continue with points 4,7,8,9: Cycle C2 is counted. Its range is 1 and mean is 3.5.
- Now remove C2, join points 4 and 9 and continue from point 4:
- Etc.

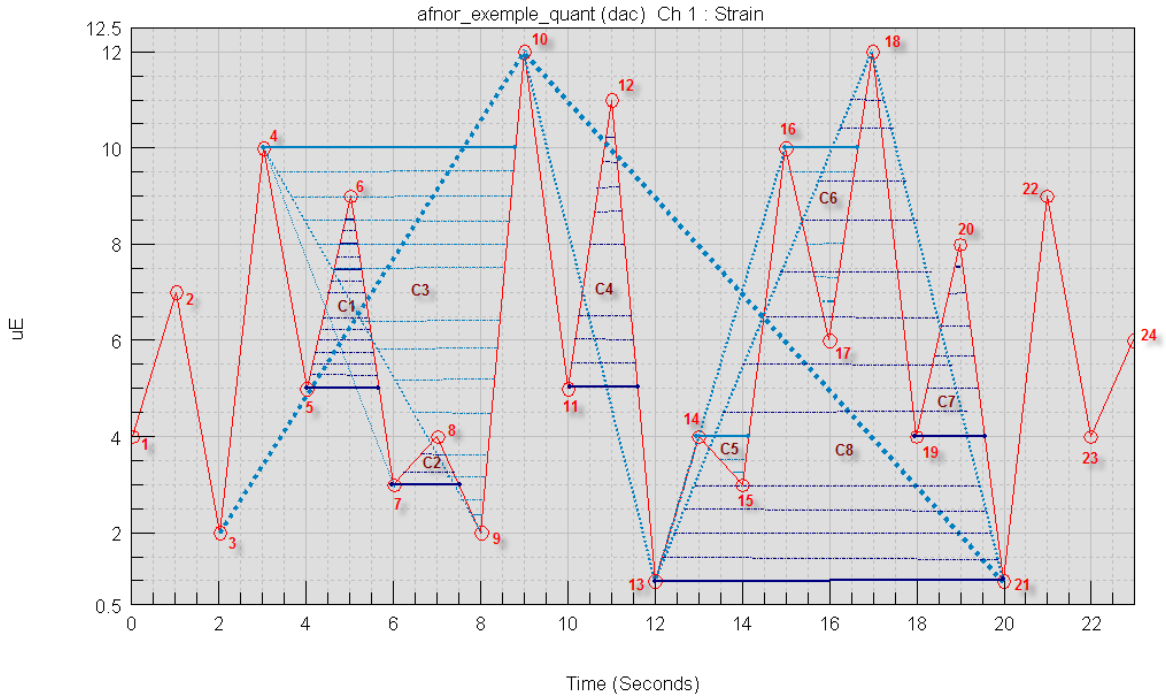


**Figure 29: Example rainflow cycle extraction. For example, a cycle comprising points 4, 5, 6, 7 is identified and extracted.**

The result of a rainflow cycle count can be represented as a matrix showing how many cycles were counted for various {Min; Max} values. In practice, a histogram representation is often preferred. An example MinMax histogram is illustrated in Figure 30. It shows the number of cycles along the vertical axis counted for various {Min; Max} bins.

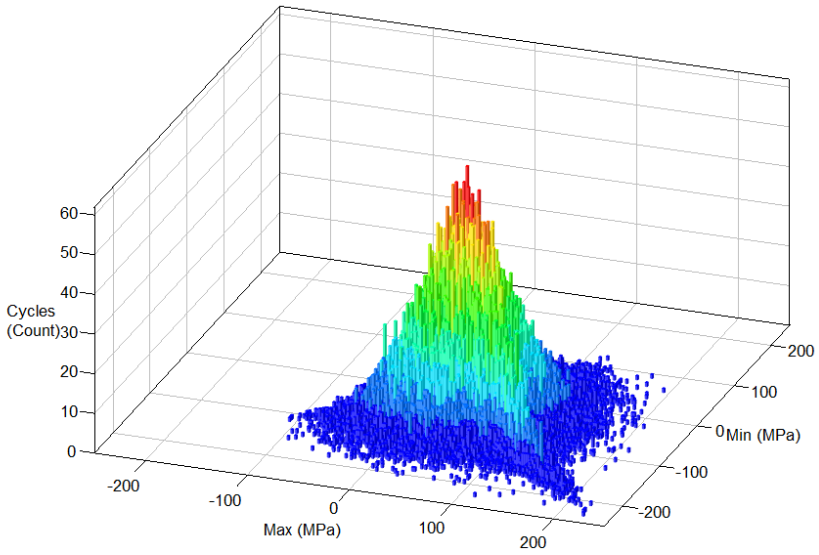


**Figure 30: Example MinMax rainflow histogram**

Alternative representations of the rainflow cycles include the so-called RangeMean histogram, as illustrated in Figure 31.

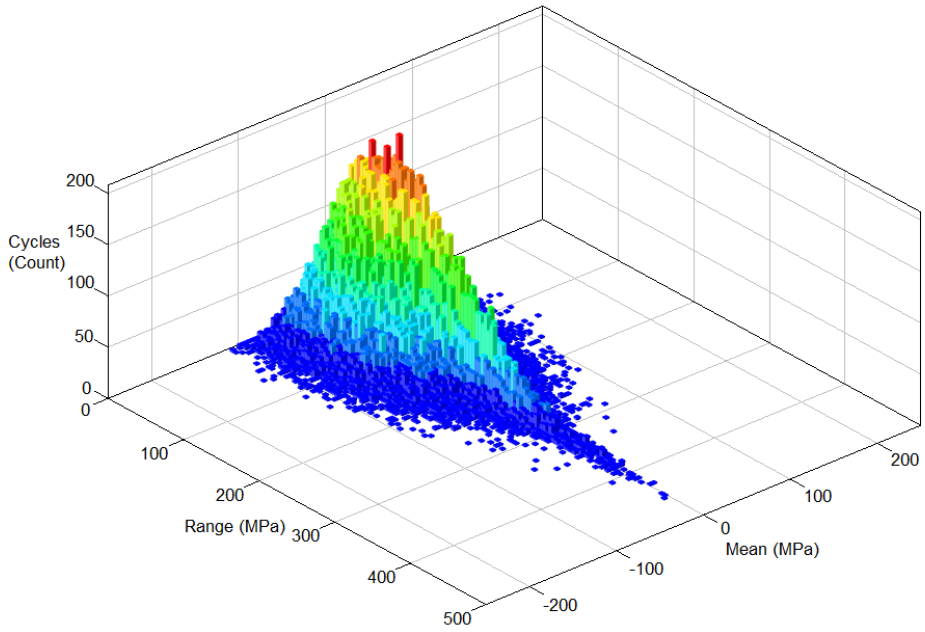


**Figure 31: Example RangeMean rainflow histogram**

Note that in some cases, where the influence of the mean values is considered negligible, the range-only 2D histogram, written $N(S_R)$ is often preferred. An example range-only rainflow histogram is illustrated in Figure 32.

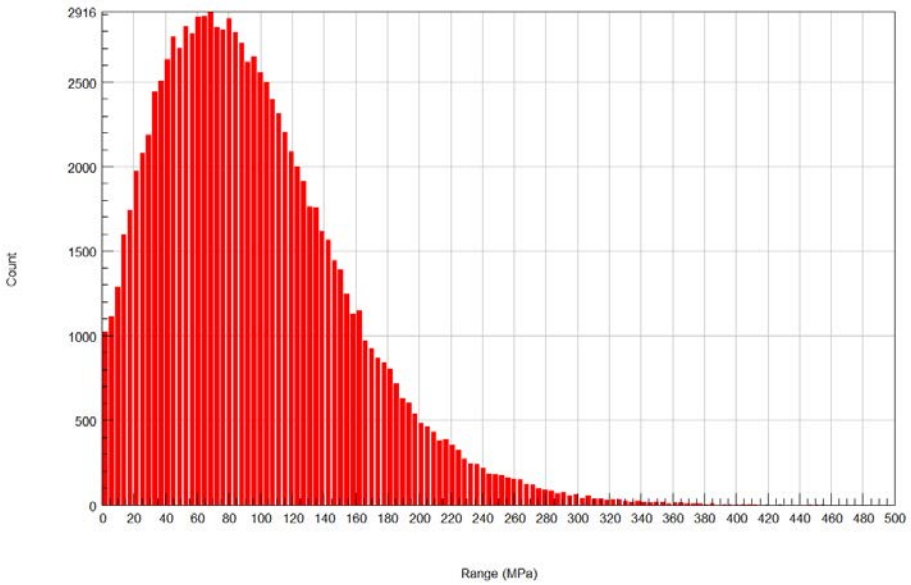


**Figure 32: Example range-only 2D histogram**

### 2.6.3 Probabilistic rainflow cycle count

When a time history of stress is random, deterministic cycle counting becomes prohibitive and shows risks of inaccuracy. Indeed, a time domain simulation raises the question of how long the signal should be to ensure convergence on fatigue life estimate. The time domain approach can therefore be time consuming and this is the main reason why a spectral approach is relevant. While an exact distribution for the peaks of a Gaussian random process is known (see section 2.2.8 Distribution of peaks), an exact distribution for the ranges of rainflow cycles is unknown.

The random variable considered is stress and is represented by the symbol $z$. The stress range is noted $z_R$.

The objective of this section is to deduce the PDF of the ranges of rainflow-like cycles from the PDF of the peaks and the PDF of the valleys. The range of a rainflow cycle is defined as {peak – valley} of that cycle. Section 2.6.2 shows that finding a rainflow cycle is by definition a deterministic process. Modelling such a complex process is not straightforward and the rainflow cycles cannot be obtained from the peak distribution alone. Some observations can however be made:

- The peak and valley of a cycle are not necessarily consecutive.
- The biggest cycle is always made of the highest peak and the lowest valley.

Those observations lead one to consider several ways of combining peaks and valleys to form rainflow cycles:

- 1. Peaks and valleys are randomly associated to form a range
- 2. Peaks and valleys are paired as they arrive in the time history. The range is the distance between successive peaks and troughs.
- 3. Each peak is paired with the valley of the same magnitude i.e. the highest peak goes with the lowest valley, the second highest peak goes with the second lowest valley, etc.

It is clear that, in the case of random stress responses, the last case (case 3) is the most conservative because it will lead to a calculation which considers cycles with the highest ranges and will therefore lead to the highest predicted damage.

#### *2.6.3.1 The consequences of the peaks and valleys paired randomly*

In this case, the PDF of the ranges is calculated considering the random variable "range" as the sum of the peaks and the valleys, which are considered as two independent random variables. The PDF of the sum of two independent variables with PDF $p_{z_p}$ and $p_{z_v}$ is expressed using the convolution product of both marginal PDF, as expressed in Equation 2.14:

$$p_{z_R}(z) = p_{z_p}(z) * p_{z_v}(z) \qquad \text{Equation 2.84}$$

where $*$ represents the convolution product.

The PDF obtained has negative ranges. These are due to negative peaks associated with some positive valleys. Instead of ignoring such cycles with negative ranges, it is suggested to fold them back and add them to the positive side of the ranges, as per Equation 2.85.

$$p_{Z_R}(z) = \begin{cases} 0, & z < 0 \\ p_{Z_R}(z) + p_{Z_R}(-z), & z \geq 0 \end{cases}$$ Equation 2.85

This gives the range PDF corresponding to the event where all peaks and valleys are randomly mixed. The PDF of the mean values could be extracted in a similar manner.

Figure 33 shows the resulting range distribution obtained in the random association case for the narrow and broadband cases compared with the rainflow range distributions obtained from Monte-Carlo simulations of the spectra presented in Figure 11. The theoretical PDFs are in blue whereas the PDFs of the time domain simulation are in red.

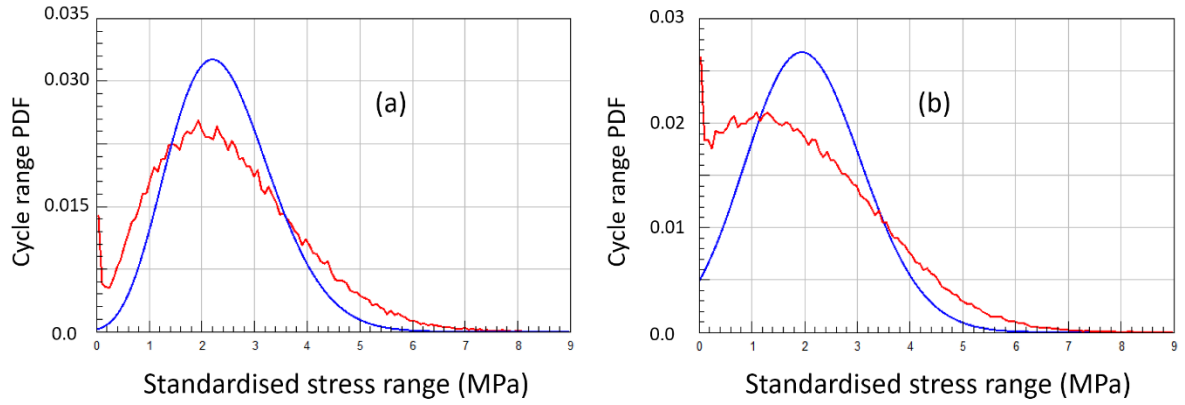


**Figure 33: Theoretical range distribution when peaks and valleys are randomly mixed (blue) versus rainflow range distribution (red) in the case of a narrowband process (a) broadband process (b)**

The random association of peaks and valleys to form cycles does not suit the way the cycles are combined in a rainflow procedure (see section 2.6.2). For instance, according to this random mixture, the probability of the maximum peak being paired with the minimum valley is $1/(N_p T)$, which is extremely low, whereas this event is the maximum range that the material will experience and it will always be counted by the rainflow counting algorithm (see previous section 2.6.2 Deterministic rainflow cycle count).

### *2.6.3.2 The consequences of the peaks and valleys paired in sequence*

A rise is defined as the difference between the value of $z(t)$ at a valley and the value of $z(t)$ at the next peak. A fall is the difference between the value of the signal at a peak and at the next valley. If the process is stationary, the distributions of rise and fall are symmetric [21, 82]. The rises and falls of a random process are of interest in oceanography, as they correspond to the heights of waves in the ocean [21]. The rises and falls were also considered of interest in engineering design for metal fatigue, as fatigue damage is better related to cyclic stress ranges than to stress peaks [21, 82].

J. R. Rice et al. [82] studied the 'rise and fall' densities for stationary Gaussian random processes. The PDFs are determined from the joint probability density functions of $z(t)$, $\dot{z}(t)$ and $\ddot{z}(t)$ with a 6-by-6 correlation matrix and their computation is complex. In this study, it was observed that the rise and fall densities showed an unexpected likelihood (referred to as a 'hump' in the paper) near the origin, and the authors were unable to say if it was due to

numerical inaccuracies or if it was inherent in the approximation developed. It appears that this PDF local maximum at low stress ranges is observed in the rise and fall PDF computed from time domain simulations (see Figure 34), especially for small irregularity factors. This is due to the higher number of small fluctuations introduced by a broadband signal compared to a narrowband signal. For example, in Figure 12 (b), showing a signal regenerated from a bimodal PSD, a number of high frequency cycles are distorted because they sit on the top of low frequency cycles, which leads to smaller rises and falls.

Ortiz et al. [21] developed an approximation for the rise and fall distributions, based on a Rayleigh distribution. Similarly, Dirlik [29] defined 'an ordinary range' as the distance between successive peaks and troughs and proposed a model for the ordinary range PDF based on a sum of a Rayleigh distribution and an exponential distribution. Note that the exponential distribution was used to model the PDF local maximum near the origin. Figure 34 compares a rise and fall distribution using a blue line with the rainflow-range density using a red line for both the narrowband and broadband cases presented in Figure 11. Both were computed from time domain simulations. The approximations introduced by Ortiz et al. [21] and Dirlik [29] are represented in dashed and dotted lines respectively.

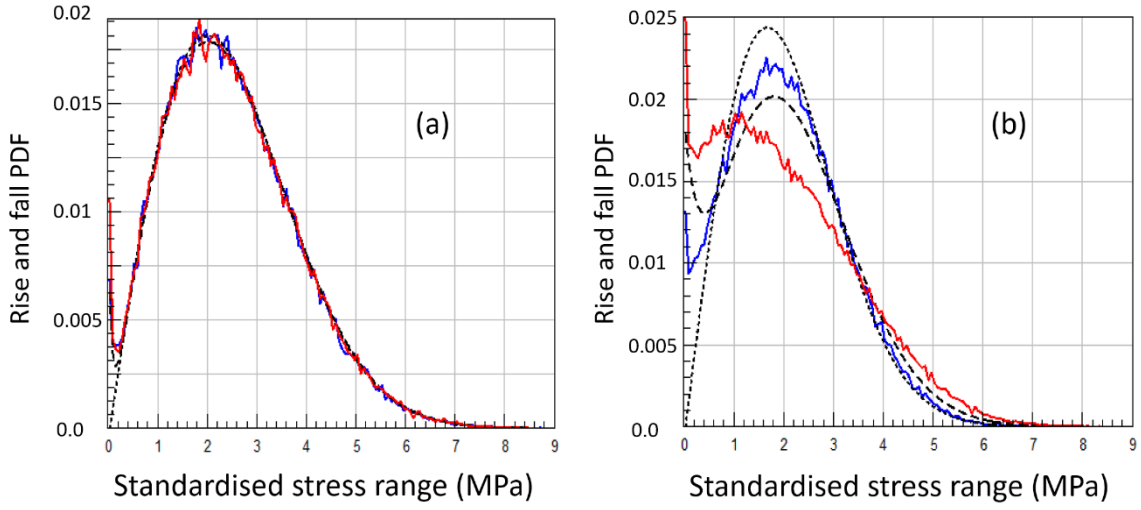


**Figure 34: Rise and fall PDF (blue) versus rainflow range PDF (red) of the numerical simulations of a narrowband process (a) broadband process (b), overlaid with the theoretical rise and fall PDFs from Ortiz et al. [21] (dashed black) and Dirlik [29] (dotted black)**

Both the Ortiz and Dirlik models approximate well the rise and fall PDFs. Dirlik's has the advantage of representing the PDF local maximum behaviour at low stress ranges. A comparison of rise and fall PDFs and rainflow-range PDFs shows distinctive differences between the two sets of densities corresponding to the same power spectrum, especially in the broadband case. The most important difference from fatigue damage point of view, is that the rainflow range density becomes considerably higher than the rise and fall density at higher ranges. For example, in Figure 34 (b), the rise and fall PDFs approach zero much sooner than the rainflow-range density, which exhibits higher probabilities for large ranges.

The rise and fall distribution (or ordinary-range distribution), where the peaks and valleys are paired in sequence, does not suit the rainflow distribution. The peaks and valleys are combined

in a more specific way to form rainflow cycles (see section 2.6.2) and the probability of finding cycles with high range is underestimated when using the models presented in this section for approximating the rise and fall distributions. Therefore the models presented in this section for approximating the rise and fall distributions are not retained as valid candidates for the estimation of fatigue damage.

#### *2.6.3.3 The consequences of the peaks and valleys paired by magnitude*

In this case, the PDF of the ranges is obtained by considering that each peak is paired with a valley of the same magnitude but with a negative value. Therefore, the random variable representing stress range is written

$$z_R = 2\,.\,z_p \qquad \text{Equation 2.86}$$

where $z_R$ represents the stress range and $z_p$ the value of a peak in stress.

So, using Equation 2.13 from section 2.1.8 referred to as the PDF transform, the range PDF is directly obtained from the PDF of the peaks, as expressed in Equation 2.87.

$$p_{z_R}(z) = \frac{1}{2} p_{z_p}\left(\frac{z}{2}\right) \qquad \text{Equation 2.87}$$

Note that in this way of pairing peaks and valleys, the cycles formed are considered to have zero mean values. The range PDF is eventually found by inserting Equation 2.54 into Equation 2.87:

$$p_{z_R}(z) = \frac{1}{2\sigma_z}\left\{\frac{\sqrt{1-\gamma^2}}{\sqrt{2\pi}} e^{\frac{-z^2}{8{\sigma_z}^2(1-\gamma^2)}} + \frac{z.\gamma}{4\sigma_z} e^{\frac{-z^2}{8{\sigma_z}^2}}\left[1 + erf\left(\frac{z.\gamma}{\sigma_z\sqrt{8(1-\gamma^2)}}\right)\right]\right\} \qquad \text{Equation 2.88}$$

where $\sigma_z$ is the RMS value of the stress signal $z(t)$.

Figure 35 shows the resulting range distribution obtained with this way of pairing peaks and valleys by magnitude for the narrow and broadband cases compared with the deterministic rainflow range distributions obtained from Monte-Carlo simulations of time series corresponding to the spectra presented in Figure 11. The theoretical PDF are in red whereas the PDF of the time domain simulation are in blue.

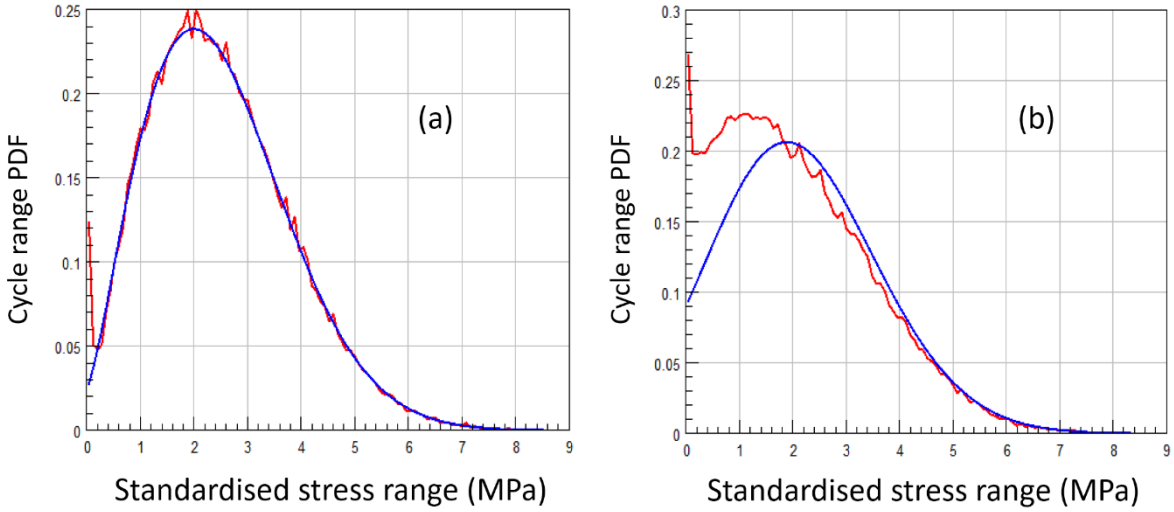


**Figure 35: Rainflow ranges distribution of the numerical simulations (red) overlaid with the range distribution when peaks and valleys are symmetrically paired (blue) in the narrow band (right) and broadband (left) cases**

This distribution matches extremely well the tail of the rainflow-range distribution, but gets less and less similar as the ranges decrease. This difference happens essentially in the broadband case, since in the narrowband case every peak is associated with its corresponding valley and the distribution of ranges follows a Rayleigh distribution (see section 2.2.8). In the broadband case the discrepancy is quite obvious up to the mid-range area.

Figure 36 illustrates why some cycles are transferred from the mid stress range area to the very low stress levels as in Figure 35 (b). It is due to the potential presence of low frequency cycles which distort some cycles of higher frequency and make the rainflow algorithm consider lower-range cycles.

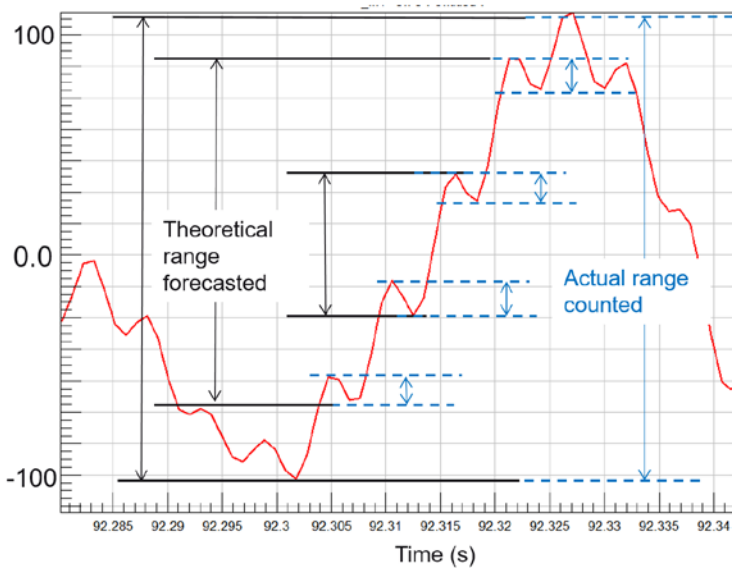


**Figure 36: Example of the range distribution derived from Rice's peak distribution not being the same as the rainflow distribution**

Note that, from a fatigue view point, it is clear that the high ranges have more importance as fatigue damage and stress range are linked in a power law. Therefore, the proposed theoretical

distribution of the ranges obtained in Equation 2.88 and displayed in Figure 35 can be considered satisfactory.

This way of pairing peaks and valleys will however introduce some conservatism in the case of broadband stress results as illustrated in Figure 36. This conservatism will be more pronounced for applications, where the slope *b* of the fatigue curve is not sufficiently steep as to be able to neglect the influence of the cycles of small and mid amplitudes on fatigue damage. See section 2.6.4 for more details on how the fatigue damage is computed from the rainflow cycle histogram.

In the rest of this thesis, the histogram of the rainflow ranges will be calculated from the PDF of the peaks using Equation 2.88. A zero mean value will be considered.

#### *2.6.3.4 Empirical approaches from the literature*

Empirical methods exist to derive the distribution of the rainflow stress ranges [26, 27, 28, 29, 30, 31, 32, 41, 42, 56] for stationary and Gaussian stress responses. Figure 37 shows Dirlik's empirical is compared with the rainflow-range distribution from time domain simulations and the pairing method where each peak is paired with the valley of the same magnitude (i.e. peaks and valleys are paired symmetrically).

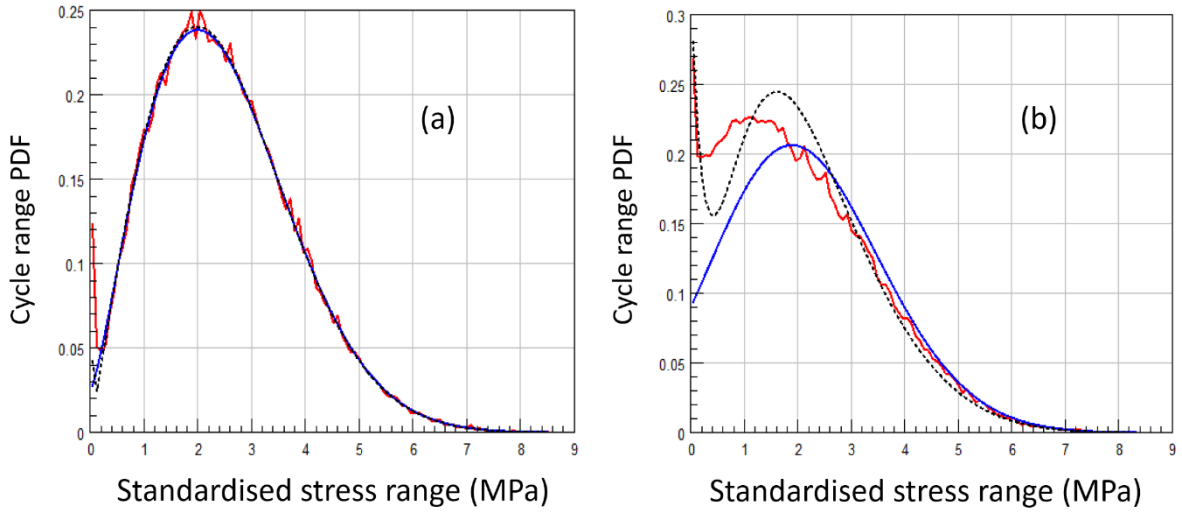


**Figure 37: Rainflow range PDF (red) of the numerical simulations overlaid with the theoretical range PDF when the peaks and valleys are paired symmetrically (blue) and with Dirlik's theoretical rainflow range PDF (dotted black) in the narrow band (right) and broadband (left) cases**

Although the Dirlik method has been used successfully for many years and offers good correlation with the time domain simulation [26]; it is empirical in its derivation which makes it difficult to develop mathematically. The method where peaks and valleys are paired symmetrically is based on Rice's peak distribution. It gives comparable results to Dirlik's approach [28] and it is derived analytically. Therefore the method where peaks and valleys are paired according to their magnitude will be used for the development of this thesis with regards to non-Gaussian stress responses.

### 2.6.4 Fatigue damage and fatigue life

The rainflow cycle count histogram can be obtained from the PDF of ranges by multiplying it with the total number of expected cycles during the exposure duration, that is $\mathrm{E}[P].T_t$, with $\mathrm{E}[P]$ the expected number of peaks per unit time (as per Equation 2.48) and $T_t$ the exposure duration.

One obtains the general equation giving the number of cycles at stress range $z_R$:

$$N(z_R) = E[P].T_t.p_{z_R}(z_R) \qquad \text{Equation 2.89}$$

where $p_{z_R}(z_R)$ is the PDF of stress ranges as per Equation 2.88.

This histogram will be called the range-only rainflow histogram. The damage from each individual cycle extracted by the RFC method is determined from the fatigue life curve (see example SN curve in Figure 26). Equation 2.83 can be used to find the number of cycles to failure $N_f$ for every individual cycle. The damage is computed as the number of cycles of a given stress range counted divided by the number of cycles to failure for that specific stress range. The damage is then summed linearly using the Miner damage accumulation law [83], as described by Equation 2.90:

$$D = \sum \frac{N(z_R)}{N_f(z_R)} \qquad \text{Equation 2.90}$$

where $N(z_R)$ is the number of cycles counted having a stress range $z_R$ and $N_f(z_R)$ is the total number of cycles stress range $z_R$ that the material is capable to withstand.

Considering a Range-only histogram $N(z_R)$, as described in chapter 2.6.1, fatigue damage is determined by inserting Equation 2.83 into Equation 2.90:

$$D = \frac{1}{C}\sum N(z_R).{z_R}^b \qquad \text{Equation 2.91}$$

$D$ is the fatigue damage ratio. If $D \geq 1$, then the component is likely to fail within the test duration $T_t$. If $D < 1$, then the fatigue life can be determined as $T_t/D$ in seconds.

For random vibration data, the cycle mean stress effect is usually ignored because the effect is much less significant than stress range and the cycles are approximately symmetric; therefore, the more damaging effect of a tensile mean is largely negated by the less damaging effect of a compressive mean [28].

In this study, it will be considered that the fatigue damage is dependent on the number of cycles of stress response and their amplitudes and not the frequency at which the cycles occur.

## 2.7 Accelerated vibration endurance tests

Test engineers want to accelerate a test whilst keeping the same failure mechanisms. Accelerating a test certainly helps reduce the time-to-market, but it is also extremely useful from an engineering point of view. If the test fails, the engineers will know it soon enough and they will have the means to remedy it. If a test is successful, the engineers may want to push it further to assess the safety margins.

### 2.7.1 Vibration testing systems

Accelerated endurance vibration tests are typically performed by fixing the test article on a hydraulic or electrodynamic vibration testing system, generally referred to as a shaker.

The controller is a software, which performs closed-loop control during a shaker test. The controller generates an electronic signal which, once amplified, becomes the drive signal to the vibration testing system. It is a closed-loop control because the component under test is instrumented and its response, typically acceleration, is fed back to the controller. This ensures that the test article effectively sees vibrations as defined in the vibration specification. A vibration specification can be random, harmonic, shock, sine-on-random or the replication of a time domain signal.

For random vibration testing, the Fast Fourier Transform (FFT) is typically used to correct the input signal using the feedback signal [84]. The input signal's FFT is performed and compared to the FFT of the control signal. If there is a difference between both spectra, then the correction to apply is added to the next drive spectrum and a new drive signal is generated from it. See chapter 3 for more details on signal generation.

### 2.7.2 Deterministic vibration endurance tests

Deterministic loads should always be represented by time histories. Example deterministic test specifications include sine dwells, sine sweeps and Time Waveform Replication (TWR) [1, 2]. The TWR technique is sometimes used for simulating loads that are random in nature. In the TWR technique, the actual signal measured in operational conditions is reproduced on a shaker. Although this method seems useful, it doesn't capture the variability which can actually occur in the field since the waveform produced in the test is just one field measurement. For example, in the automotive sector, two drivers will behave differently, will take different routes, etc., so simply reproducing and repeating a single trip removes this variability. Note also that it is seldom practical nor possible to conduct durability tests using real measured data because of the volume of data necessary, the duration over which components must survive and inherent problems in achieving correlation between the actual test rig output and that desired [84].

Although the TWR technique is well suited for the reproduction of deterministic excitation loads, it is not adapted nor practical for random loads with inherent variability. This thesis is about random vibrations and will therefore concentrate on spectral approaches.

### 2.7.3 The load amplification method

For endurance tests, a classic way to accelerate a test is the "load amplification method" [2, 6]. The load amplification method simply scales the input signal by an appropriate amount in order to reduce the test duration. Scaling the load will reduce the test duration exponentially. The scale factor is calculated using Equation 2.92.

$$Scale = \left(\frac{T_s}{T_t}\right)^{1/b} \qquad \text{Equation 2.92}$$

Where $T_s$ is the target life, typically the service life, $T_t$ is the reduced test duration and $b$ is the slope of the Wöhler line as per Equation 2.83.

Considerable care is required when using this method to ensure that loads are not scaled excessively thereby inducing local yield, which alters the load path away from the observed failure point. The engineer must always ensure a sufficient margin in the scale factor to avoid local yielding.

The method is ideal for components that are designed to resist a high load event like a collision, for example, but require fatigue testing for many repeats of a lower amplitude load. In this case the lower amplitude loads can be scaled quite significantly without exceeding the design envelope. Typically, in the automotive or aerospace industry, test reduction factors vary from 5 to 500 or more [85, 86].

### 2.7.4 The kurtosis control method

Kurtosis control is primarily presented as a way to better simulate service loads. In some cases, product failures are caused by high excursions in the excitation [11] and running a Gaussian test will not reproduce these peaks, or at least not with the sufficient rate. Increasing the global RMS value is no longer representative of the real environment and the failure mode reproduced on the shaker may be different to the one in service. Kurtosis control focusses on the ability to produce high excursions in the excitation signal. The excitation signal has the prescribed frequency content and global RMS (i.e. its PSD is matching the target the PSD profile), but its wave form contains high peaks that are meant to be more realistic compared to what is encountered in real life. The generation of such excitation signals with high kurtosis will be presented in chapter 3.

Another application of kurtosis control is to accelerate a test. The higher excursions of the excitation signal are likely to cause higher stress responses, which in turn will increase the damage rate. Since the damage rate is higher, the test duration could be reduced while reproducing the same overall damage. The main objective of this thesis is to provide engineers with a way to estimate the fatigue life of a structure under non-Gaussian random loads, and especially loads with high kurtosis. Once this objective is achieved, the engineer will be able to use a similar rule to the one presented in Equation 2.92, whereby the test duration can be reduced by applying both a scale factor and a specific kurtosis value to the excitation. However, obtaining this relationship is not straightforward as the damage depends on how the leptokurtic

excitation signal was generated, how the leptokurtic properties are transferred to the stress response and how the characteristics of the response influence the fatigue life. The generation of leptokurtic random excitation signals, the transfer of the excitation's non-Gaussian features to the stress response and the effects on fatigue life will be presented in chapters 3, 4 and 5 respectively.

### 2.7.5 Conclusions

Although the load amplification method is referenced in standards and used in practice, it suffers from limitations such as the potential for it not to reproduce the same failure mode. Kurtosis control is a fairly recent technique. It has the advantage of causing the test article to experience more time duration at high accelerations without necessarily changing the global RMS.

One outstanding question to answer in this thesis is how the kurtosis of the excitation can be related to the test reduction.

Note that to further reduce the duration of a test, one could potentially combine both approaches.

## 2.8 Final conclusions

This chapter provided a review of some of the fundamental aspects of random processes, the linear dynamics of physical systems excited by random processes and mechanical failure prediction.

When the vibration environment is random, then the response stress is a random variable too. Providing the statistical properties of the random stress are known, one can adopt a probabilistic fatigue analysis to determine the mean fatigue damage. If conditions of stationarity and ergodicity are met and if the stress response is Gaussian, then the fatigue analysis including a probabilistic rainflow cycle count as described in section 2.6.3 can be carried out. It is convenient to consider a random load as ergodic and Gaussian, since statistics such as the peak distribution are readily available for this specific class of Gaussian random time histories. In this case, statistics can be extracted from one relatively short realisation or measurement of a phenomenon. A fatigue analysis should theoretically be carried out from the stress response, over a given timeframe.

However, if an excitation signal cannot be considered as Gaussian, then further characterisation of the excitation and stress response is required and a dedicated probabilistic analysis must take place. The objective of this work is to find a statistical (as opposed to deterministic) approach to some specific non-Gaussian loadings that does not require realisations of long time domain signals.

Chapter 3 introduces how to generate stationary Gaussian random signals and some specific non-Gaussian random signals. These signals will then be used for investigations of the statistics of the response of linear systems and comparison with theoretical and experimental data.

From this point forward in this thesis, all metrics are considered along the vibration random process as opposed to ensemble averages (through the process) e.g. statistical moments are based on temporal averages and PDFs are the probability distributions of instantaneous values.

# 3 Non-Gaussian signal generation

## 3.1 Introduction and assumptions

In this chapter some methods for simulating non-Gaussian signals are presented. Some existing methods presented and a new method is introduced and developed.

The generated signals represent non-Gaussian loadings, which are typically applied in environmental tests. The signals produced will be used only for simulations and validations of the distributions and statistics that will be derived later in chapters 4 and 5. The excitation signals considered are real valued with zero mean and zero skewness values.

The types of non-Gaussian random excitation signals produced include:

i. Clipped random signals: to simulate how the drive signal is limited during a shaker test.
ii. Random signals with high kurtosis: to simulate non-Gaussian loads found in service such as inputs due to potholes in roads for the automotive industry.

A new method for generating random signals with high kurtosis is presented and is shown to give the required statistics.

In this thesis only the four first statistical moments (see section 2.1.10) will be considered and more specifically two of them namely the standard deviation and the kurtosis.

The kurtosis value considered in this thesis is not a function of frequency, such that when used as an excitation signal all resonances must be impacted by the increased kurtosis and not just some of them. The global time averaged kurtosis is considered in this thesis. Also, the phase of the excitation signals is always considered to be distributed uniformly, so that the kurtosis or skewness are not due to any phase relationship between different frequency components.

Note that shaker controllers typically prevent signal clipping to be used with kurtosis control since the produced leptokurtic signal is more likely to reach higher levels than the equivalent Gaussian one and the test is likely to be rapidly aborted. To avoid a test with high kurtosis to be systematically aborted, the sigma clipping parameter is often required to be set to a very high value. This enables the study of leptokurtic and clipped excitations to be done separately without the need to consider any interaction between the two.

## 3.2 Stationary random Gaussian noise generation

A very common approach to characterize random vibrations is to compute the temporal average Power Spectral Density (PSD) of the vibrations [22]. PSDs are useful for identifying prevalent frequencies and the overall RMS vibration level. When the process is both Gaussian and stationary, the nature of the signal is well defined by the normal distribution and its associated statistical moments (see section 2.2).

The generation of Gaussian and stationary signals is presented in this section. The method presented is based on an Inverse Fourier Transform, as it is the method typically used by vibration controllers [84].

### 3.2.1 The inverse Fourier transform technique

The signal generation technique is based on the inverse discrete Fourier transform (IDFT) of a frequency domain spectrum constructed with amplitudes directly related to the target PSD and a random phase. The approach to obtain a random time domain signal $x(t)$ is described in Equation 3.1. [9, 15, 87]:

$$x(t) = \sum_{k=1}^{M} A_k \cos(2\pi k \Delta f t - \varphi_k) \qquad \text{Equation 3.1}$$

with $A_k$ the amplitudes of the harmonics determined from the shape of the PSD, $G_{XX}$, that is discretized over $M$ frequency lines, with the frequency increment, $\Delta f$, as given in Equation 3.2:

$$A_k = \sqrt{2\Delta f G_{xx}(k\Delta f)} \qquad \text{Equation 3.2}$$

The phase angles, $\varphi_k$, are defined as samples of a random variable uniformly distributed in the range from 0 to $2\pi$ radians, mutually independent of each other and of the amplitudes $A_k$. The signal produced can be considered as a random phase multisine signal.

The length and sample rate of the signal generated depend on the frequency resolution and the maximum frequency of the PSD respectively.

### 3.2.2 Applications

When a random excitation is known to be stationary and Gaussian, then all the statistics of it can be derived from its PSD [16, 20, 22, 15]. When applied as an input to a known or specified linear system, the response is also perfectly known in terms of spectral content and statistics.

Time domain simulations of a stationary and Gaussian process can be used:

- to validate some theoretically derived statistics
- to simulate the excitation of a non-linear system
- as an intermediate step in the creation of a non-Gaussian signal (see sections 3.3 to sections 3.5)

Table 3.1 shows an example PSD from the international standard MIL STD 810-G [2] corresponding to the general exposure to vibrations due to a jet aircraft cargo. The overall RMS vibration level is 4.02 g.

| Frequency (Hz) | Acceleration Spectral Density ($g^2$/Hz) |
|---|---|
| 15 | 0.01 |
| 106 | 0.01 |
| 150 | 0.02 |
| 500 | 0.02 |
| 2000 | 0.0013 |
| *Global RMS = 4.02 g* | |

**Table 3.1: Example PSD profile from MIL STD 810G [2]**

The spectrum profile described in Table 3.1 is displayed in Figure 38:

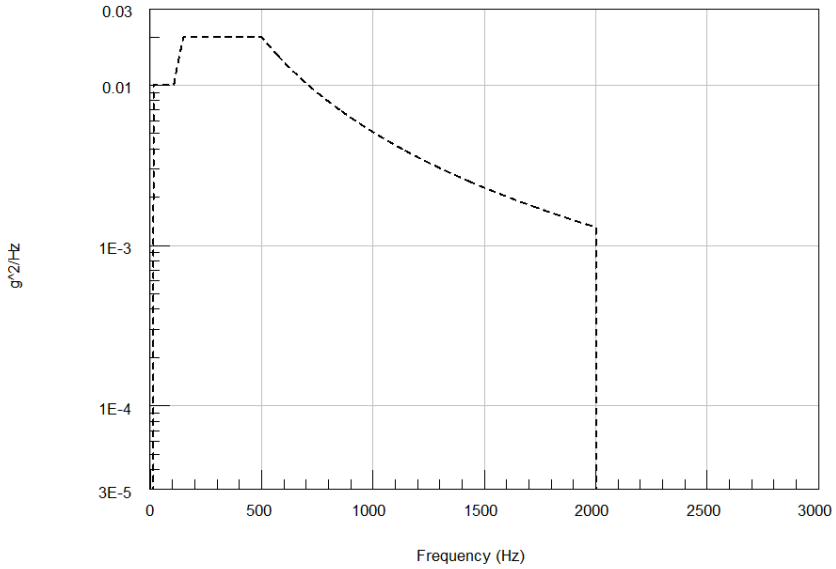


**Figure 38: Example PSD**

The vibration environment for materiel installed in jet aircraft stems from four principal mechanisms. These are:

1. engine noise impinging on aircraft structures,
2. turbulent aerodynamic flow over external aircraft structures,
3. turbulent aerodynamic flow and acoustic resonance phenomena within cavities open to the external airflow, and
4. airframe structural motions due to manoeuvres, aerodynamic buffet, landing, taxi, etc.

A signal of 100s sampled at 8192 points per seconds was generated using the methodology based on the inverse Fourier transform. Figure 39 shows an extract of the obtained signal.

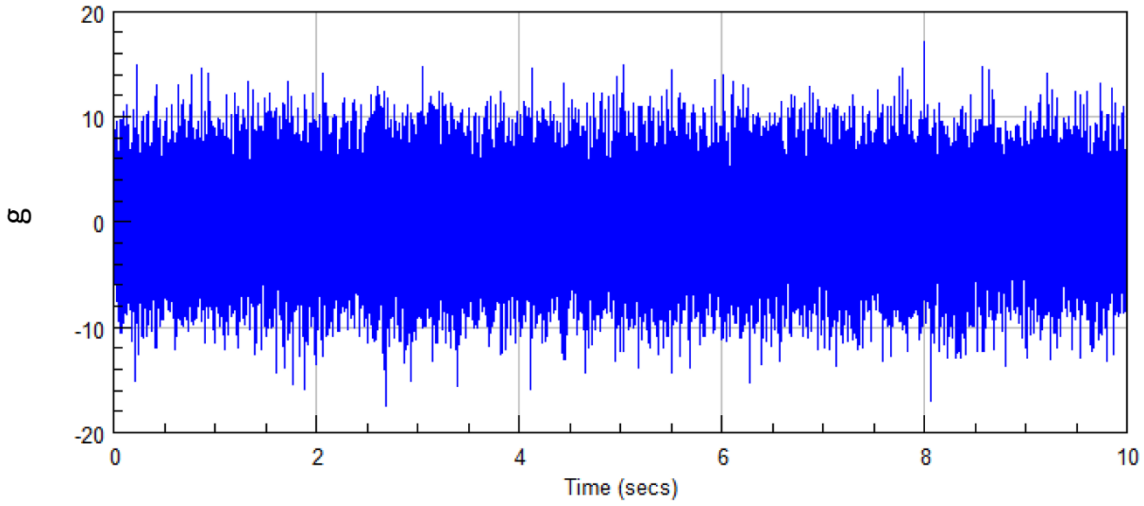


**Figure 39: Example stationary and Gaussian Signal realisation corresponding to target PSD**

The PSD and the PDF of the obtained signal are displayed in Figure 40. The PSD and PDF are overlaid with the target PSD profile and the ideal Gaussian distribution respectively in dashed black lines.

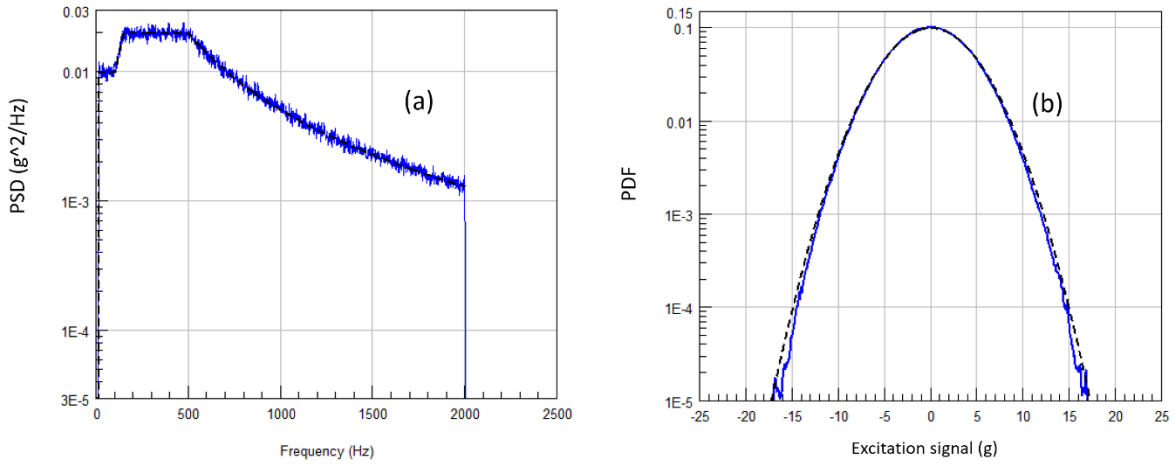


**Figure 40 : (a) PSD of the obtained signal (blue) overlaid with target PSD (dashed black), (b) PDF the obtained signal (blue) overlaid with ideal Gaussian PDF (dashed black)**

Note that in Figure 40 the ideal PDF and the calculated PDF don't perfectly match, especially for extreme values. This is typically due to an insufficient number of samples, i.e. the longer the signal, the more chances to find extreme values. The error between the ideal PDF and the calculated PDF reduces when several realisations of time signals are concatenated.

### 3.2.3 Limitations

The signal obtained with the IDFT method is generally considered as having a lower level of randomness than a natural random noise [88]. For instance, a natural random noise is expected to be unbounded, whereas the maximum of a signal obtained with the IDFT method is limited to:

$$\max_t\big(x(t)\big) \leq \sum_{k=1}^{M} A_k$$

This limitation can be problematic when $M$, the number of spectral lines is small.

In the rest of this thesis, stationary random Gaussian noise generation will be done using the so-called 'inverse Welch' method, as it was modelled after the Welch method for estimating the spectral density [89, 88]. Sections of random data obtained from the IFT method are multiplied by a window function, overlapped and added to form a nearly stationary output. The weighting windows allow continuous frequency content and help limit leakage. A typical window is the Hanning window. The level of overlap dictates whether the resulting signal will be stationary or not. For instance, a typical window such as the Hanning window will provide a uniform statistical weighting when overlapped by 67%, which in turn will generate a stationary signal.

## 3.3 Clipped signal generation

Shaker controllers often limit the drive signal to prevent high amplitude peaks. Limiting therefore allows the shaker system to deliver more power, because it can represent random signals of greater RMS power by eliminating the rare high amplitude peaks. Because the high amplitudes are removed above a given level, the resulting limited signal is no longer Gaussian. In the PDF of a clipped signal, the tails will appear modified compared to the Gaussian PDF. Methods for limiting a drive signal will be presented in this section.

### 3.3.1 Limiting the excitation signal

The high amplitude peaks may either be truncated at a given level (a so-called brick wall limiting or abrupt clipping), or compressed (soft limiting), resulting in drive signals which are no longer Gaussian [90]. Both techniques are presented in the next two sections.

#### *3.3.1.1 Abrupt clipping*

Brick wall limiting or abrupt clipping is a technique that simply cuts off the peaks at a given level. The resulting signal is therefore non-Gaussian. Abrupt clipping directly influences the resulting signal's crest factor, $CF$, which is defined as the maximum value divided by the RMS of the signal. The maximum value reached by a clipped signal is denoted as $x_{th}$.

The probability density function (PDF) of an abruptly clipped signal shows peaks at the clipping level [16]. Figure 41 shows the PDF of a signal with abrupt clipping occurring at $x_{th} = \pm 6g$ compared with the PDF of the original unclipped Gaussian signal.

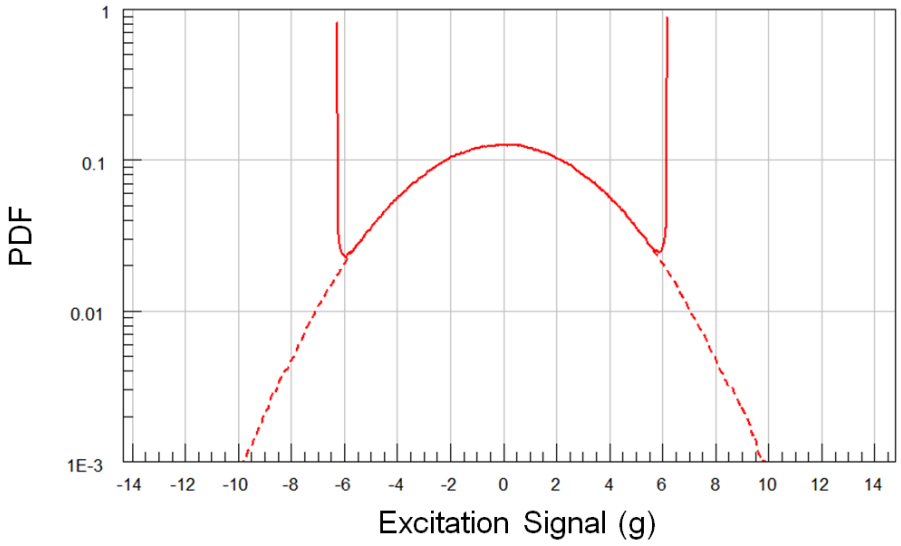


**Figure 41: PDF of a brick wall limited signal (solid) versus a Gaussian signal (dashed). The abrupt clipping occurs at +/- 6 g**

The PDF of an abrupt clipped signal can be expressed as:

$$p_y(y) = \begin{cases} p_x(y) & if|y| < x_{th} \\ \frac{1}{2}\left(1 - erf\left(\frac{|x_{th}|}{\sqrt{2}\sigma_x}\right)\right) & if|y| = x_{th} \\ 0 & if|y| > x_{th} \end{cases} \quad \text{Equation 3.3}$$

where $p_x(x)$ is the PDF of a centered Gaussian distribution with standard deviation $\sigma_x$. It can be verified that the area under the abrupt clipped PDF equals 1.0. The PDF obtained is an even function and therefore the 1st and 3rd central moments are zero, giving zero mean $\mu_y$ and skewness $\lambda_y$. The root-mean-square (RMS) is then equal to the standard deviation.

The 2nd and 4th central moments, $M_2$ and $M_4$, of the abrupt clipped signal can be calculated from the definition of the moments of a probability distribution (see Equation 2.17). The probability distribution of the abrupt clipped signal is given in Equation 3.3. The expressions obtained for $M_2$ and $M_4$ are then:

$$M_2 = {\sigma_x}^2\left(CF^2 + (1 - CF^2)\,\mathrm{erf}\left(\frac{CF}{\sqrt{2}}\right) - \frac{2CF}{\sqrt{2\pi}}e^{-\frac{1}{2}CF^2}\right) \quad \text{Equation 3.4}$$

$$M_4 = {\sigma_x}^4\left(CF^4 + (3 - CF^4)\,\mathrm{erf}\left(\frac{CF}{\sqrt{2}}\right) - \frac{2CF}{\sqrt{2\pi}}e^{-\frac{1}{2}CF^2}(CF^2 + 3)\right) \quad \text{Equation 3.5}$$

The kurtosis $\kappa_y$ is related to the 2nd and 4th moments as per Equation 2.19.

Equation 3.4 and Equation 3.5 clearly express that both the RMS and the kurtosis of the signal are reduced when a random Gaussian signal is clipped. Figure 42 shows how the RMS and kurtosis evolve against the crest factor $CF$. The theoretical RMS and the theoretical kurtosis are represented using dashed black lines and the RMS and the kurtosis values obtained from time series simulations are represented using red lines. The kurtosis value is particularly sensitive to the level of clipping.

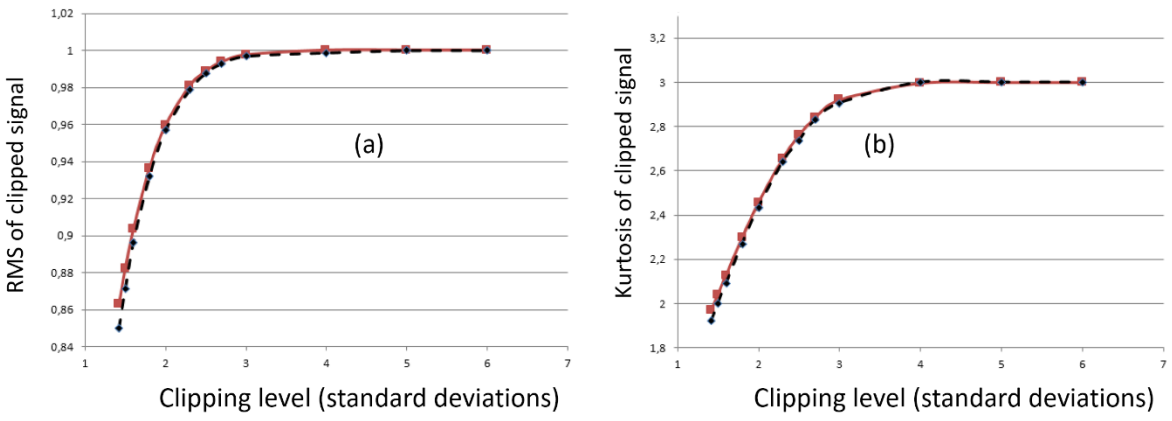


**Figure 42: (a) Theoretical RMS value (dashed black) versus RMS value (red) of the numerical simulations and (b) theoretical kurtosis value (dashed black) versus kurtosis value (red) of the numerical simulations**

### *3.3.1.2 Soft Clipping*

Soft clipping, or compression, is an alternative way of limiting a signal. The main advantage of soft clipping is to reduce the high frequency distortion. Different compression techniques exist. One simple way is to use a logistic sigmoid function such as the hyperbolic tangent, the arctangent or the error function to limit the amplitudes of a Gaussian signal. In this work, the hyperbolic tangent was used as the nonlinear zero-memory transformation of a Gaussian random signal $x(t)$ with standard deviation $\sigma_x$ into a non-Gaussian signal $y(t)$, according to:

$$y(t) = CF\sigma_x tanh\left(\frac{x(t)}{CF\sigma_x}\right) \qquad \text{Equation 3.6}$$

Applying the PDF transform (see Equation 2.12 in section 2.1.8) leads to the following expressions for the PDF of a compressed signal [91]:

$$p_y(y) = \begin{cases} \dfrac{1}{\sqrt{2\pi}\sigma_x}\dfrac{1}{1-(y/x_{th})^2}e^{-\frac{1}{2}CF^2 atanh^2(y/x_{th})} & if\,|y| \le x_{th} \\ 0 & if\,|y| > x_{th} \end{cases} \qquad \text{Equation 3.7}$$

It can be verified that the area under the PDF of a compressed signal equals 1.0. As for the abrupt clipped signal, the PDF obtained is even and therefore, the 1st and 3rd central moments are zero. The 2nd and 4th central moments, $M_2$ and $M_4$, can be calculated via numerical integration of Equation 3.7. An example PDF for a compressed signal showing reduced tails is illustrated in Figure 43.

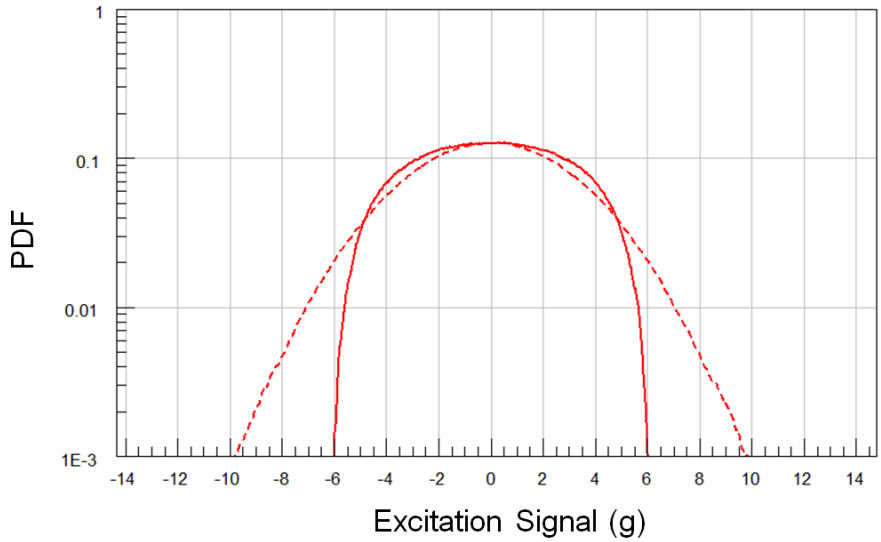


**Figure 43: PDF of compressed signal (solid) versus Gaussian signal (dashed).**

Finally, Figure 44 shows a time domain comparison of a Gaussian drive signal (red) with its clipped versions. One is obtained from abrupt clipping (blue) and the other from soft clipping (green). The abrupt clipping version is seen to generate a flat top response at the clipped peak.

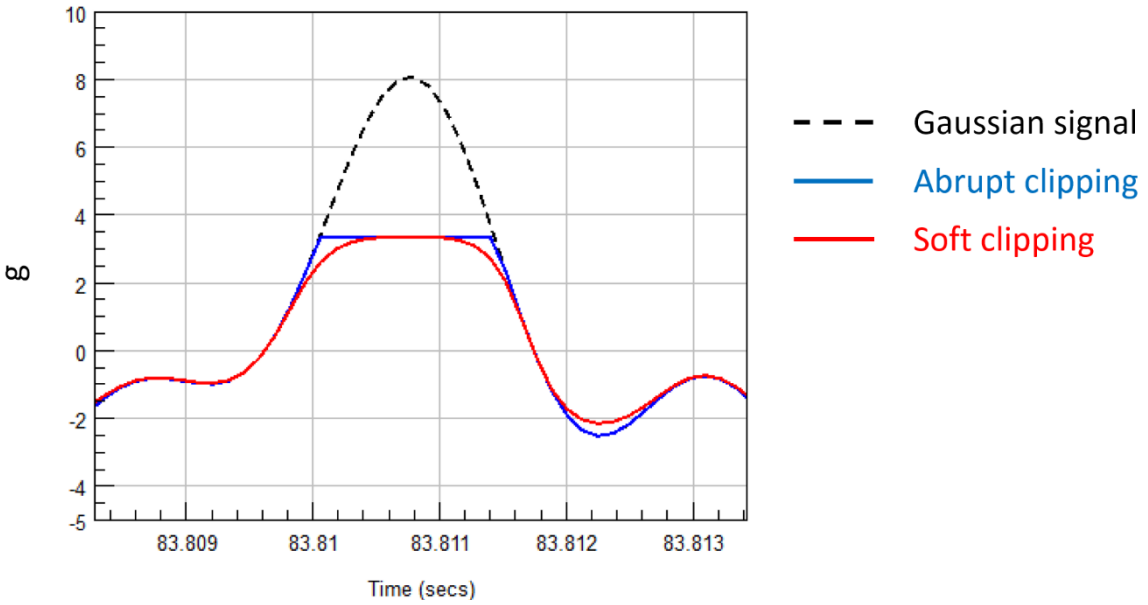


**Figure 44: Effect of abrupt clipping versus compression shown in the time domain.**

### 3.3.2 Applications

The same example presented in Table 3.1 and in Figure 38 is used here. A signal of 100s sampled at 8192 points per seconds was generated using first the abrupt clipping technique and then the soft clipping technique. In both cases, a prescribed crest factor of 2 was used. Figure 45 shows an extract of the signal obtained after abrupt clipping.

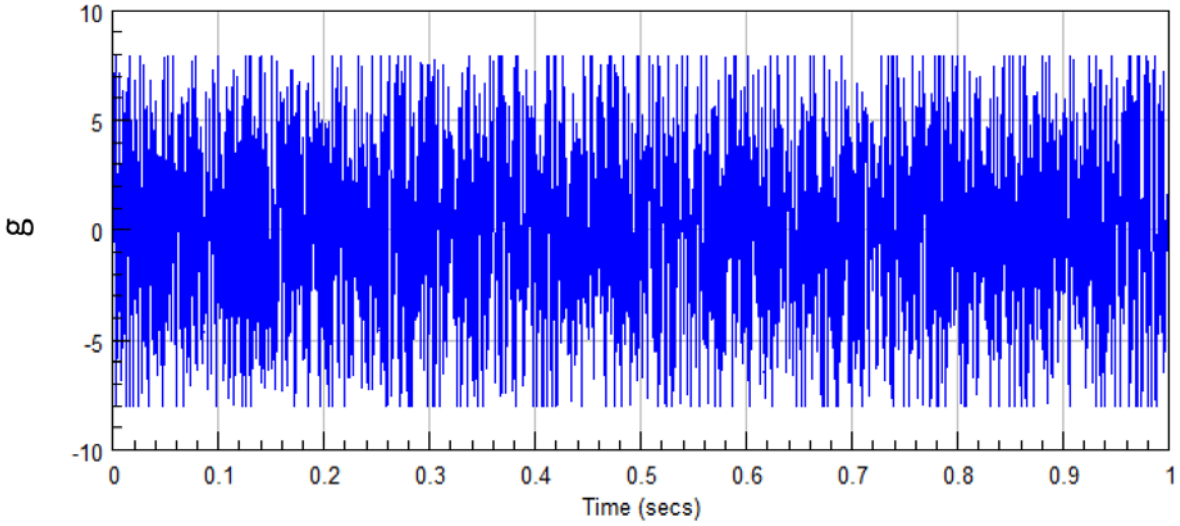


**Figure 45 : Example of a signal obtained after "abrupt" clipping of a stationary and Gaussian signal**

Figure 46 shows an extract of the signal obtained after soft clipping.

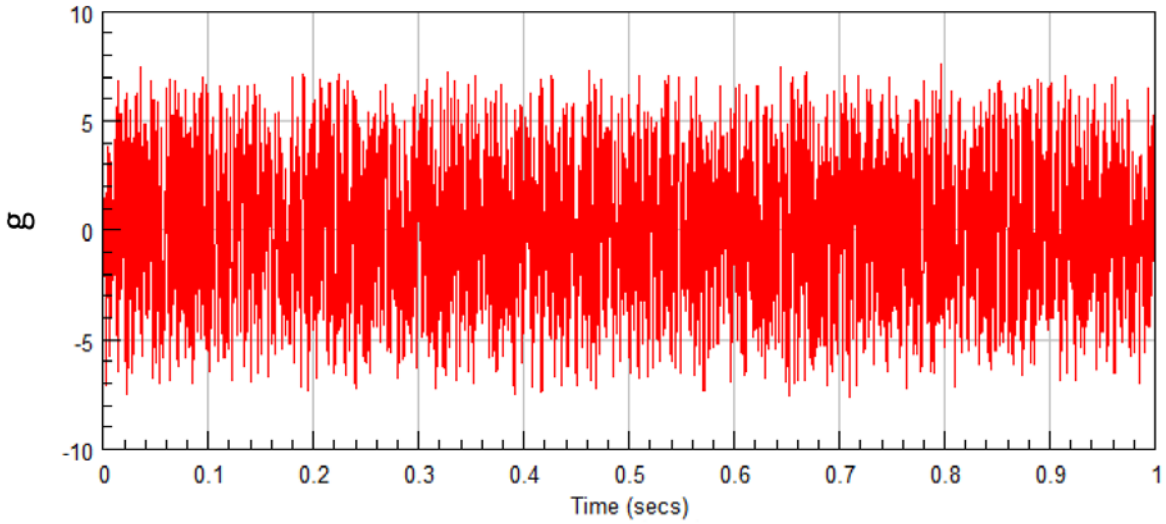


**Figure 46: Example of a signal obtained after "soft" clipping of a stationary and Gaussian signal**

None of the clipped signals obtained exceed indeed a level corresponding to twice the RMS value (i.e. 8.04 g). It is however difficult to detect soft clipping through a simple visual inspection of the time history record. A stronger detection is achieved by computing the PDF of the clipped data.

The PSD and the PDF of the obtained signals are displayed in Figure 47. The PSD and PDF corresponding to the abrupt clipped signal are represented in blue line, the PSD and PDF corresponding to the soft clipped signal are represented in red line and the target PSD profile and the ideal Gaussian distribution are in dashed black lines.

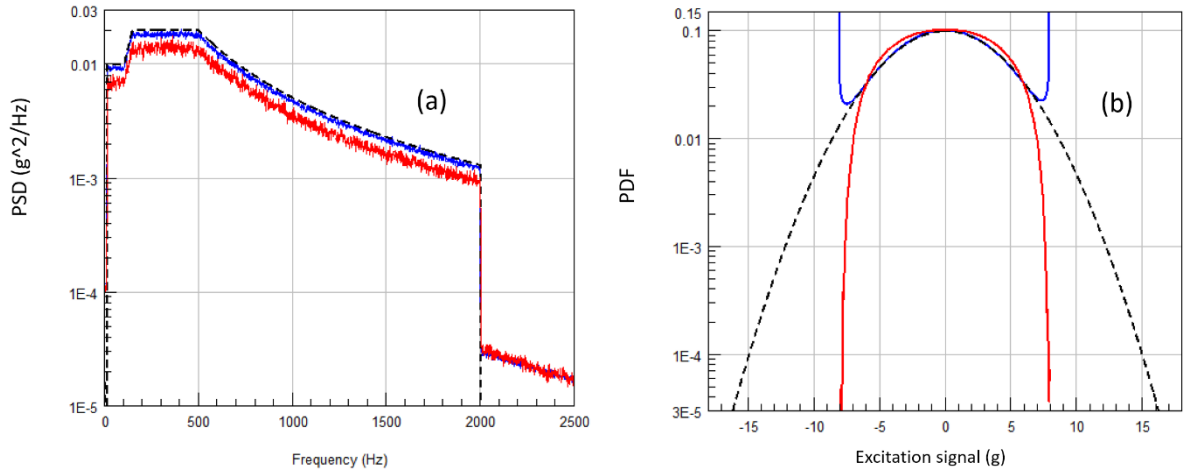


**Figure 47 : (a) PSD of the "abruptly" clipped signal in blue overlaid with the PSD of the "soft" clipped signal in red and with the target PSD in dashed black lines. (b) PDF the "abruptly" clipped signal overlaid with the PDF of the "soft" clipped signal and with the ideal Gaussian PDF**

Note that in Figure 47 (a), the ideal and the calculated PSD don't match perfectly. This is due to clipping, which reduces the variance of the signal. For the case of abrupt clipping, using Equation 3.4, one obtains $M_2$= 14.87 which corresponds to an RMS value of 3.86, instead of the original value of 4.02, representing a loss in the RMS value of about 4%. For the case of soft clipping, $M_2$ can be calculated from Equation 3.7, and is found to be $M_2$= 11.3 in this case

which corresponds to an RMS value of 3.36, representing a loss in the RMS value of about 17%. Clearly, this loss reduces as the crest factor increases.

Note also the high frequency distortion introduced in the PSD of both clipped signals in Figure 47 (a).

### 3.3.3 Limitations

Although very easy to implement, using either analogue or digital means, abrupt clipping introduces strong high frequency distortion in the resulting spectrum [50, 92]. Conceptually, this can be understood by thinking of clipping a sine wave, where the spectrum of a sine wave is a single line at the fundamental frequency. The more the sine wave is clipped, the closer it gets to resemble a square wave. The Fourier series of a square wave is made up of one component at the fundamental frequency and an infinite number of odd harmonics, whose amplitudes decrease as $1/f$. Soft clipping produces less high frequency distortion compared to abrupt clipping but introduces a greater reduction in variance.

Random vibration tests with various values for sigma clipping have been made and reported on a test article instrumented with strain gauges [90]. It was concluded that for endurance tests the user should avoid sigma clipping below 3.0 for several reasons. Firstly, clipping the signal introduces high frequency distortion. The extra energy above the required cut-off frequency can cause damage to components that are sensitive to the additional higher frequency excitation and this may not be representative of the real-world excitation. Secondly, it also leads to a reduction of energy in the bandwidth of the originally specified test. Finally, and most importantly, it noticeably reduces the fatigue damage potential on the test article, due to the reduced number of stress cycles of high amplitudes.

## 3.4 Steady leptokurtic signal generation

Modern shaker controllers generate drive signals with specific RMS and kurtosis value by means of kurtosis control [8]. As previously discussed in section 2.6, damage depends strongly on the amplitudes of a process and a high kurtosis means a more impulsive signal with therefore higher amplitude peaks in the excitation.

There are a number of benefits in generating synthetic leptokurtic time series:

- Simulating a more realistic vibration environment than standard Gaussian distributed signals
- Creating a more severe test to precipitate the failure and reveal probable failure modes
- Creating a more severe test specification in order to reduce the duration of an endurance test while cumulating the same amount of fatigue damage. (i.e. Accelerated testing)

The kurtosis value represents only one statistical moment and a complex non-Gaussian PDF could require a very high number of statistical moments for a perfect match; since the probability density function of a random variable is uniquely defined only if all its moments are known [36]. There are therefore a multitude of possible PDFs verifying the four lowest order

moments, which means that different signals may have the same four lowest order moments but different PDFs. Note also that the PDF alone cannot intrinsically differentiate between a stationary non-Gaussian signal and a nonstationary signal [16, 58]. So, depending on how kurtosis is implemented, a leptokurtic signal will match only some specific non-Gaussian PDFs obtained from measured data. There are a number of existing methods in the literature for generating random time histories with specified spectral density and kurtosis [88, 50, 84, 87, 40, 42, 93].

Two different algorithms for the generation of excitation signals with a high kurtosis are presented in this thesis. The first algorithm, described in this section, generates a stationary signal with instantaneous, high-excursion peaks. This first technique can be used to generate response signals due to nonlinearities in a structure, typically used to obtain a non-Gaussian stationary signal that deviates from the normal distribution, showing a steady rate of instantaneous peaks [93]. This algorithm has been described in a number of reference papers [42, 50] and it is used in this study primarily for comparison purposes with the second algorithm.

The second algorithm, developed in this study as a novel approach and presented in section 3.5, creates non-stationary signals with bursts of high amplitude excursions, typically representing varying-variance signals.

### 3.4.1 The polynomial transform technique

When there is a one-to-one monotonic relationship between two different random signals $x(t)$ and $y(t)$, that is, $y(t) = g(x(t))$, the PDF of $y(t)$ can be deduced from the PDF of $x(t)$ using the PDF transform, as expressed in Equation 2.12. Several formulae for the transformation $g(.)$ have been proposed in the literature [50, 94, 95, 96, 97] to adjust the kurtosis of a Gaussian random variable. The idea is based on the fact that squaring part of a Gaussian signal will have the effect of skewing it, whereas cubing a Gaussian signal will make it leptokurtic. Several authors [50, 95, 96] proposed a polynomial transform of the general form:

$$y(t) = c_0 + c_1 x(t) + c_2 x(t)^2 + c_3 x(t)^3 \qquad \text{Equation 3.8}$$

where $c_0$, $c_1$, $c_2$ and $c_3$ are real coefficients driving the type and amount of non-Gaussianity that is required. The coefficients can take any value positive, zero or negative, as long as the transformation $g(.)$ remains monotonic. Typically, the constant $c_0$ in Equation 3.8 specifies the mean value, while $c_1$ controls the standard deviation of $y(t)$. The $c_2$ and $c_3$ coefficients influence the skewness and kurtosis respectively. The goal is therefore to find a relationship between the coefficients in Equation 3.8 and the required statistics for $y(t)$.

Note that choosing the transformation $g(.)$ as a monotonically increasing function allows the process $x(t)$ and its corresponding transformed $y(t)$ to have zero crossings, peaks or valleys at the same instants in time and in the same sequence [42]. Consequently, both $x(t)$ and its transformed version $y(t)$ will share the same irregularity factor. Moreover, since the rainflow counting extracts cycles by pairing peaks and valleys based on their relative positions and time

sequence (ref section 2.6.2), the same number of rainflow cycles will be counted in the $x(t)$ and transformed $y(t)$ random signals.

Winterstein [50] considered using Hermite polynomials to expand a Gaussian PDF to match the first statistical moments required of the transformed signal $y(t)$. For a leptokurtic process, Winterstein's second order model [50, 56] defines the direct transformation $g$ that allows one to obtain $y(t)$ from a standardised Gaussian normal signal $x(t)$ as:

$$y(t) = \mu_Y + \sigma_Y . K . \left[x(t) + \tilde{h}_3(x(t)^2 - 1) + \tilde{h}_4(x(t)^3 - 3x(t))\right] \qquad \text{Equation 3.9}$$

with:

$$K = \frac{1}{\sqrt{1 + 2\tilde{h}_3{}^2 + 6\tilde{h}_4{}^2}}$$

$$\tilde{h}_3 = \frac{\lambda_y}{6\left(1 + 6\tilde{h}_4\right)}$$

$$\tilde{h}_4 = \frac{\sqrt{1 + 1.5\left(\kappa_y - 3\right)} - 1}{18}$$

where $\lambda_y$ and $\kappa_y$ are the expected skewness and kurtosis respectively.

So, typically, values for $\lambda_y$ and $\kappa_y$ are specified and the corresponding coefficients $K$, $\tilde{h}_3$ and $\tilde{h}_4$ are calculated and used in Equation 3.9 to create a leptokurtic signal with the required statistical properties from $x(t)$, the realisation of a stationary Gaussian signal.

The Winterstein second order model was adopted in this thesis for the generation of steady non-Gaussian signals, because it appears to be widely accepted and it is known to provide an accurate representation of a wide range of nonlinear behaviour [56]. Although it is limited by the fact that the transformation $g(.)$ must be monotonic i.e. the first derivative of Equation 3.9 must always be positive. This last condition implies that not all values of skewness and kurtosis can be treated by the Hermite model, but for zero skewness, all kurtosis values can be modelled [42, 50].

Note that Equation 3.9 is an approximate solution using only the first four Hermite coefficients $\tilde{h}_n$ and neglecting the cross terms $\tilde{h}_n\tilde{h}_m$. This approximation is considered sufficient to capture the non-Gaussian characteristics of the signal generated [50, 42].

Note also that only "softening" responses are considered here (with wider than Gaussian distribution tails; e.g. $\kappa_y > 3$). Another model [50, 56] covers the "hardening" responses (with narrower than Gaussian distribution; e.g. $\kappa_y < 3$).

Winterstein [50] used the orthogonal properties of the Hermite polynomials to calculate the autocovariance function $C_{yy}(\tau)$ and the spectral density $S_{yy}(f)$ of a nonlinear transformed

signal $y(t)$ in terms of functions related to the original Gaussian process $x(t)$. In the case of a four Hermite coefficients approximation, the autocovariance function $C_{yy}(\tau)$ and the spectral density $S_{yy}(f)$ are approximated as follows:

$$C_{yy}(\tau) = \left(\sigma_y . K\right)^2 . \left[C_{xx}(\tau) + 2\tilde{h}_3{}^2 C_{xx}(\tau) * C_{xx}(\tau) + 6\tilde{h}_4{}^2 C_{xx}(\tau) * C_{xx}(\tau) * C_{xx}(\tau)\right] \quad \text{Equation 3.10}$$

and therefore:

$$S_{yy}(f) = \left(\sigma_y . K\right)^2 . \left[S_{xx}(f) + 2\tilde{h}_3{}^2 S_{xx}(f) * S_{xx}(f) + 6\tilde{h}_4{}^2 S_{xx}(f) * S_{xx}(f) * S_{xx}(f)\right] \quad \text{Equation 3.11}$$

where $K$, $\tilde{h}_3$ and $\tilde{h}_4$ are defined in Equation 3.9 as a function of the expected skewness and kurtosis and $*$ represents the convolution product.

Looking at the expression giving the spectral density $S_{yy}(f)$, the 2 and 3-fold convolution products will induce sub and superharmonics to the original spectral density $S_{xx}(f)$. These extra harmonics will be subsequently more pronounced as the prescribed kurtosis is high. This shows that the zero-memory polynomial transform technique generates some signal power redistribution across the frequencies.

### 3.4.2 Applications

The polynomial transform method is straightforward to implement, in both an open or closed-loop algorithm. This technique generates stationary signals that represent responses to zero-memory nonlinear systems [12, 50]. The signal generated can match the PDF of the structural response of a softening or hardening nonlinear system (i.e. with nonlinear stiffness), by applying an appropriate monotone function, $g$, to a Gaussian process.

The non-Gaussian characteristics of the structural response may be due to actual softening/ hardening properties of the nonlinear system or to non-Gaussian excitation. For instance, systems with nonlinear stiffness subjected to Gaussian stationary excitation will show non-Gaussian responses. Alternatively, linear responses to typical wind and wave (non-Gaussian) loads show leptokurtic characteristics [50]. Note that this method has the advantage of potentially modelling the skewness typically due to wind and wave loads.

It is useful to note that the signal generated $y(t)$ shows peaks that are exaggerated (in the case $\kappa_y > 3$) or attenuated (in the case $\kappa_y < 3$) compared to the peaks in the Gaussian signal $x(t)$. This makes this approach also useful to simulate soft clipping [9, 10].

The same example presented in Table 3.1 and in Figure 38 is used here. A signal of 100s sampled at 8192 points per seconds was generated using the methodology based on the polynomial transform technique. A prescribed kurtosis of 12 was used. Figure 48 shows an extract of the leptokurtic signal obtained.

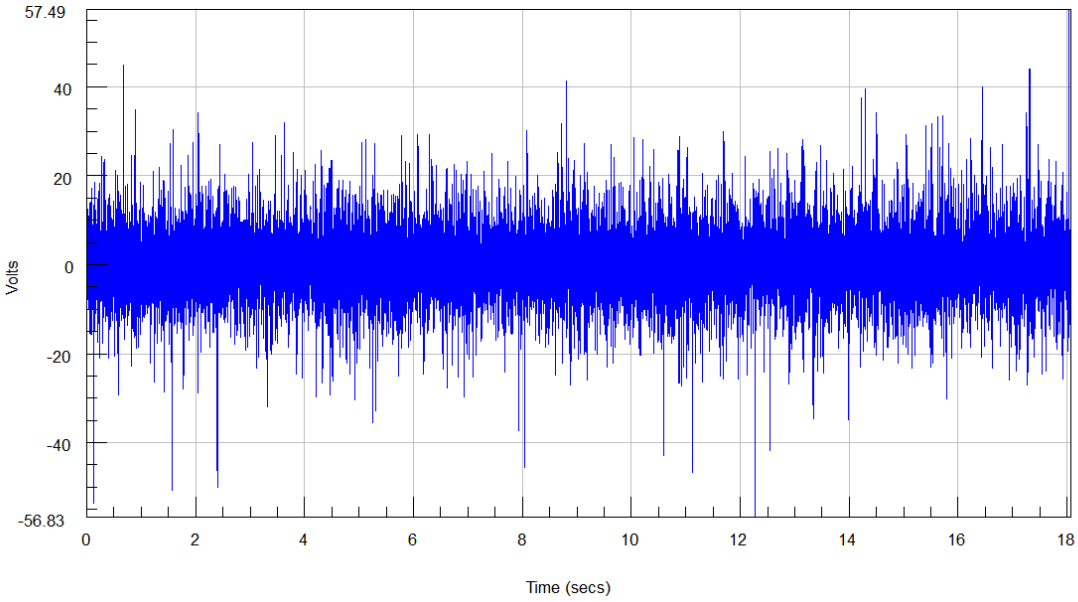


**Figure 48: Example stationary non-Gaussian Signal realisation corresponding to the target PSD and with kurtosis of 12**

The PSD and the PDF of the obtained signal are displayed in Figure 49. The PSD and PDF are overlaid with the target PSD profile and the ideal Gaussian distribution respectively in dashed black lines.

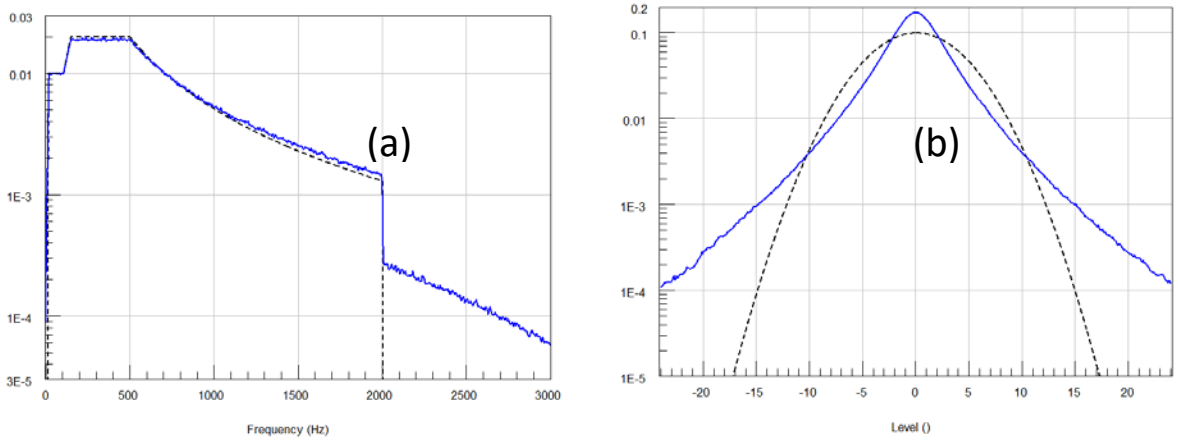


**Figure 49 : (a) PSD of the obtained signal with kurtosis of 12 overlaid with the target PSD and (b) PDF of the obtained signal overlaid with the ideal Gaussian PDF**

The difference with the Gaussian signal is very clear in the PDF, where the leptokurtic signal shows a much higher probability of finding high values compared to the Gaussian signal. The PSD of the transformed signal is clearly evidencing the harmonic distortions due to the non-linear transform of the original Gaussian signal. This phenomenon is explained at the end of the previous section 3.4.1.

### 3.4.3 Limitations of the polynomial transform technique

The first limitation of the polynomial transform technique is that, as discussed in section 3.4.1, the zero-memory nonlinear $g$ transformation function has to be monotonic, which introduces a limitation on the values of skewness and kurtosis that can be treated by the Hermite model. In

other words, not all combinations of skewness and kurtosis are allowed. However, for the present case of a generally zero skewness process, then all kurtosis values are possible [50, 42].

Now, as shown in section 3.4.1 and reported in [9, 88], a high prescribed kurtosis introduces harmonic distortions which reduce the dynamic range for the spectral density of the generated data. This phenomenon can be seen in Figure 49 (a). In the context of shaker tests, it is difficult for the controller to compensate for such distortions when driving a vibration test, especially when there is a resonance of the test article within the excited frequency band [98]. If the control loop is not successful in limiting the induced harmonic distortions, then frequencies that are expected to lie outside of the frequency band of interest may well end up being excited.

However, the main limitation of this technique is that it fails to correctly model the nature of some excitations. For instance, the primary cause of the leptokurtic nature of road vehicles vibrations is the result of the nonstationarity of the process rather than an inherent non-Gaussian character. Often, field data show a continuously varying class of non-stationary signals and this approach does not succeed in reproducing the variations in the processes' amplitude that are considered essential if realistic simulations are to be achieved [54, 57].

## 3.5 Nonstationary leptokurtic signal generation

Two different algorithms for the generation of excitation signals with a high kurtosis are proposed in this thesis. The first algorithm was presented in section 3.4. The second algorithm, developed in this study and proposed here, creates non-stationary signals with bursts of high amplitude excursions, typically representing varying-variance signals. This second algorithm is a novel approach.

Such a non-stationary signal can be obtained through a modulation process. A stationary Gaussian signal is first generated. This signal is then amplitude modulated by a low frequency wave, independent of the Gaussian signal. Although any periodic amplitude modulation function could be used to turn a stationary Gaussian process into a nonstationary non-Gaussian one, the amplitude modulation comprising spaced and non-centred sine waves will be adopted in the rest of this thesis.

### 3.5.1 The amplitude modulation technique

Let us assume the nonstationary random process $y(t)$ can be represented as:

$$y(t) = a(t).x(t) \qquad \text{Equation 3.12}$$

where $x(t)$ is a stationary Gaussian random process with zero mean and variance ${\sigma_x}^2$ and where $a(t)$ is a periodic function, each period being made of the concatenation of a constant amplitude flat portion and a half sine pulse representing a burst.

It is suggested that the burst is made of a sine wave window in order to produce a continuous junction between the burst and the flat portion, resulting in a nonstationary random signal with a continuously varying variance. Bursts have a length of $T_0$ and appear once every $T$ seconds (i.e. at a rate $1/T$) with $T_0 \leq T$, such that they cover $100 * T_0/T$ % of the total time.

An example modulation function $a(t)$ is illustrated in Figure 50.

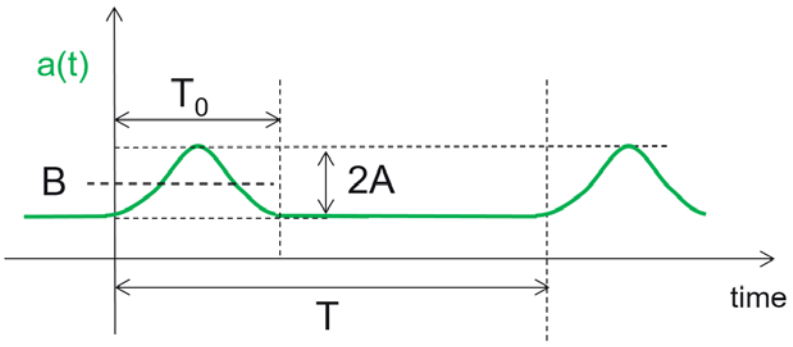


**Figure 50: an example modulation function containing spaces**

Over one period lasting $T$ seconds and starting at zero second, the deterministic modulation function $a(t)$ is defined as:

$$a(t) = \begin{cases} A.\sin(2\pi t/T_0) + B & if\ 0 \leq t < T_0 \\ B - A & if\ T_0 \leq t \leq T \end{cases}$$

where $A$ is the amplitude of the sine wave making a burst in a period of the modulation function, $T_0$ its period and $B$ its offset.

In the rest of this thesis, $B$ and $A$ are chosen such that $B > A$, so the modulating function is always strictly positive. It is assumed in the rest of this section that $a(t)$ and $x(t)$ are independent. Note also that the period $T$ of the modulation function is assumed to be chosen such that $1/T$ is below the range of frequencies contained in the original stationary signal $x(t)$. The resulting modulated signal $y(t)$ is a nonstationary random process with a constant (zero) mean and a time-dependent variance. The variance increases in the vicinity of a burst and decreases to a lower, steady value between the bursts of energy. By analogy with amplitude modulation in radio communications, the modulation index can be defined as $A/B$.

Note that in real life, the bursts are not identical. For instance, Rouillard [99] studied the distribution of the length of the various bursts of energy found in vehicles during road measurements. Also, the amplitudes $A$ of the bursts should not be constant but should fluctuate according to some distribution. Some assumptions were made in the rest of this thesis to keep the theory simple and tractable:

(i) The length of the bursts pulse will be considered constant.
(ii) The amplitudes of the bursts will remain constant.
(iii)The bursts may appear at random instants within a period but they will not overlap.

It is believed that the pure random nature of the underlying stationary signal tends to mask the deterministic aspects of the amplitude modulation function. Note that the position in time of the bursts within a period, the global statistics of the nonstationary process remain the same, as long as the bursts do not overlap.

The proportion of the burst deviation in a period is noted $r_b$ and is calculated as:

$$r_b = T_0/T \qquad \text{Equation 3.13}$$

with $T_0 \leq T$ such that $0 \leq r_b \leq 1$.

The PDF of the amplitude modulated process can be calculated as the weighted sum of the PDF of the Gaussian part and the PDF of the burst, as described in section 2.3.1, Equation 2.67. Considering one period of $T$ seconds, the Gaussian part lasts $T - T_0 = T(1 - r_b)$ seconds, whereas the burst lasts $T_0 = Tr_b$ seconds. Therefore, the statistical moments associated with the amplitude modulated process are the weighted sum of the statistical moments of the Gaussian part and the statistical moments of the bursts (see the definition of statistical moments in section 2.1.10).

Three cases of amplitude modulation will be considered and compared next. These are namely no burst, only bursts with no stationary portion inbetween and the general case where bursts are interlaced with stationary non-modified portions. In each case, the PDF of the random signal obtained will be calculated and its statistical moments will be deduced.

#### *3.5.1.1 Amplitude modulation using a constant modulation*

If $r_b = 0$, in other words, if the bursts of energy have a zero length $T_0 = 0$, then the signal obtained is stationary random with variance ${\sigma_x}^2(B-A)^2$, where $(B-A)$ is the value of the "flat" or constant part of the modulation function.

In this case, the PDF of $y(t)$ is Gaussian and can be calculated using Equation 2.13 in section 2.1.8 as:

$$p_y(y) = \frac{1}{\sqrt{2\pi}.(B-A).\sigma_x} e^{-\frac{y^2}{2.(B-A)^2{\sigma_x}^2}} \qquad \text{Equation 3.14}$$

The statistical moments are those of a Gaussian-distributed random time history (see section 2.1.10). The first statistical moment $E[y]$ is zero, the second moment is $E[y^2] = {\sigma_x}^2(B-A)^2$, third moment $E[y^3]$ is zero and the fourth moment is $E[y^4] = 3{\sigma_x}^4(B-A)^4$. Note that the Kurtosis is 3.

#### *3.5.1.2 Amplitude modulation using successive bursts*

If $r_b = 1$, then the variance of the process is constantly oscillating. The modulation function is made purely of a non-centred sine wave of amplitude $A$ and mean value $B$. The periodic modulation function $a(t)$ is defined as:

$$a(t) = A.\cos(2\pi f_0 t + \varphi) + B$$

where $A$ is the amplitude of the modulation function, $f_0$ its frequency, $\varphi$ its phase and $B$ its offset such that $B > A$

If the initial phase of this sine wave is considered a random variable, the PDF giving the probability of finding a value between $(B-A)$ and $(B+A)$ is given as [20, 15]:

$$p_a(s) = \begin{cases} \dfrac{1}{\pi\sqrt{A^2-(s-B)^2}} & if\ |s-B| < A \\ 0 & if\ |s-B| \geq A \end{cases} \qquad \text{Equation 3.15}$$

The PDF of the underlying random noise $x(t)$ follows a Gaussian law.

The formula for determining the distribution of the product of two independent random variables (see section 2.1.9.2, Equation 2.15) can be used to find the distribution of $y(t)$, which can be written:

$$p_Y(y) = \frac{1}{\sqrt{2\pi}.\pi.\sigma_x} \int_{y/(A+B)}^{y/(B-A)} e^{-\frac{a^2}{2.{\sigma_x}^2}} \frac{1}{\sqrt{a^2A^2-(y-aB)^2}} da \qquad \text{Equation 3.16}$$

No closed form solution to this integral has been found after an extensive search was conducted.

The statistical moments of $y(t)$ though can be derived. The underlying Gaussian signal $x(t)$ has a variance $E[x^2] = {\sigma_x}^2$. Since the modulating function $a(t)$ is the sum of a harmonic signal of amplitude A and a constant B, its variance can be easily calculated as $E[a^2] = \left(B^2 + \frac{1}{2}A^2\right)$. Therefore, the global variance of the signal obtained is $E[y^2] = E[a^2]E[x^2] = \left(B^2 + \frac{1}{2}A^2\right){\sigma_x}^2$. Note that since $a(t)$ and $y(t)$ are nonstationary, the expectation operator $E[.]$ is defined here as an average over an infinite time so that the results obtained are independent of the time $t$.

Similarly, the fourth statistical moment is calculated using $E[y^4] = E[a^4]E[x^4]$. The fourth statistical moment of the underlying Gaussian signal $x(t)$ is $E[x^4] = 3{\sigma_x}^4$. Based on the additive property of cumulants, the fourth statistical moment of the modulating function $a(t)$ is calculated in Appendix B as: $E[a^4] = \frac{3}{8}A^4 + B^4 + 3A^2B^2$. Finally, the fourth statistical moment of $y(t)$ is obtained as:

$$E[y^4] = E[a^4]E[x^4] = \left(\frac{3}{8}A^4 + B^4 + 3A^2B^2\right)3{\sigma_x}^4$$

Note that the kurtosis of $y(t)$ is:

$$\kappa_y = 3\frac{\left(\frac{3}{8}A^4 + B^4 + 3A^2B^2\right)}{\left(B^2 + \frac{1}{2}A^2\right)^2}$$

which can be rearranged as:

$$\kappa_y = \frac{3}{2}A^2.\frac{(A^2 + 16B^2)}{(A^2 + 2B^2)^2} + 3 \qquad \text{Equation 3.17}$$

Note that for a given value of the offset $B$, when $0 \leq A \leq B$, $\kappa_y$ is an increasing function of $A$ because its derivative with respect to $A$ is always positive.

The value of $\kappa_y$ takes its maximum when $A = B$. This means the maximum kurtosis obtained using this approach is 35/6. Also, it is clear from Equation 3.17 that $\kappa_y$ is always greater than 3.0.

The case of successive bursts is analogous to an amplitude modulation process with a non-centered sine wave. Such a signal is always leptokurtic, with a kurtosis value in the range $3 \leq \kappa_y \leq 35/6$. Figure 51 illustrates the value of the kurtosis obtained for various values of $B$ ($0 < B \leq 1$) and for various values of $A$ ($A \leq B$).

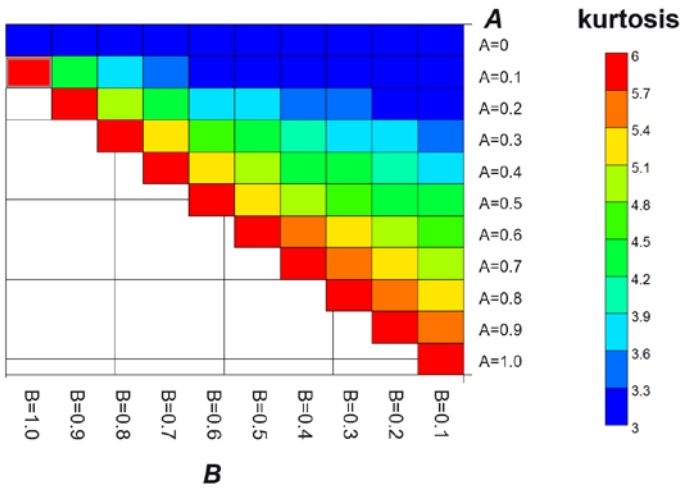


**Figure 51 : The kurtosis for a random signal amplitude modulated with successive sinusoidal bursts having various amplitude *A* and offset *B* values**

For a given offset $B$, the maximum kurtosis is obtained when the amplitude of the modulating function $A$ gets close to $B$. This corresponds to the case where bursts of energy are dominant and the stationary amplitude modulation part inbetween bursts is comparatively very low.

### *3.5.1.3 Amplitude modulation using spaced bursts*

In the general case, when $0 \leq r_b \leq 1$, the global PDF of $y(t)$ is a weighted sum of the PDFs of :

- the stationary part (see Equation 3.14) that is present during $(1 - r_b)$ of a period,
- the purely oscillating part (see Equation 3.16) that is present the remaining fraction $r_b$ of a period.

The PDF of the concatenated time history can be calculated using Equation 2.67 in chapter 2.3.1. The global PDF $p_Y$ of $y(t)$ can be expressed as:

$$p_Y(y) = \frac{(1 - r_b)}{\sqrt{2\pi}.(B - A).\sigma_x} e^{-\frac{y^2}{2.(B-A)^2{\sigma_x}^2}} + \frac{r_b}{\sqrt{2\pi}.\pi.\sigma_x} \int_{\frac{y}{A+B}}^{\frac{y}{B-A}} e^{-\frac{a^2}{2.{\sigma_x}^2}} \frac{1}{\sqrt{a^2A^2 - (y - aB)^2}} da \qquad \text{Equation 3.18}$$

The PDF obtained in Equation 3.18 is the sum of two parts. The first part is due to the stationary sections in the excitation signal; it is a Gaussian PDF with standard deviation $(B - A)\sigma_x$. No closed form solution to the integral present in Equation 3.18 has been found. It is therefore recommended to use a numerical integration to solve it.

Note that the PDFs of the particular cases with no bursts or successive bursts presented in the two previous sections can be found by setting $r_b = 0$ and $r_b = 1$ respectively.

The second and fourth statistical moments of the concatenated process can deduced from their definition, based on PDFs (see Equation 2.16 in chapter 2.1.10). They are therefore calculated as a weighted sum of the second and fourth statistical moments of the stationary and the amplitude modulated processes.

$$\begin{cases} E[y^2] = r_b.{\sigma_x}^2.\left(\frac{A^2}{2} + B^2\right) + (1 - r_b).{\sigma_x}^2.(B - A)^2 \\ E[y^4] = r_b.\left(\frac{3}{8}.A^4 + B^4 + 3A^2B^2\right).3{\sigma_x}^4 + (1 - r_b).3{\sigma_x}^4.(B - A)^4 \end{cases}$$

Equation 3.19

The expression for the kurtosis is then deduced:

$$\kappa_y = 3 \cdot \frac{r_b\left(\frac{3}{8}.A^4 + B^4 + 3A^2B^2\right) + (1 - r_b).(B - A)^4}{\left(r_b.\left(\frac{A^2}{2} + B^2\right) + (1 - r_b)(B - A)^2\right)^2}$$

Equation 3.20

Note that the variance and kurtosis of the particular cases with no bursts or successive bursts presented in the two previous sections can be found by setting $r_b = 0$ and $r_b = 1$ respectively.

The system of equations given in Equation 3.19 can be simplified. The generated nonstationary excitation $y(t)$ is meant to have the same variance as the original stationary Gaussian signal it is obtained from, so $E[y^2] = {\sigma_x}^2$. Also, using the definition of the kurtosis value, the fourth moment of the generated excitation signal $E[y^4]$ can be substituted with $\kappa_y E[y^2]^2$, which is known since $\kappa_y$ is the value of the prescribed kurtosis.

In this more general case, $r_b$ can be very small, leading to a very peaky amplitude modulation signal, which in turn leads to an amplitude modulated signal with a very high kurtosis value.

Let $B$ be a fixed value and let $\kappa_y$ be a function of two variables $A$ and $r_b$. For a given value of B, virtually any kurtosis bigger than 3.0 can be obtained by varying $A$ and $r_b$. Figure 52 shows a surface plot showing kurtosis for a fixed value of $B = 1$ and for $0 \leq A \leq 1$ and various values of $r_b$.

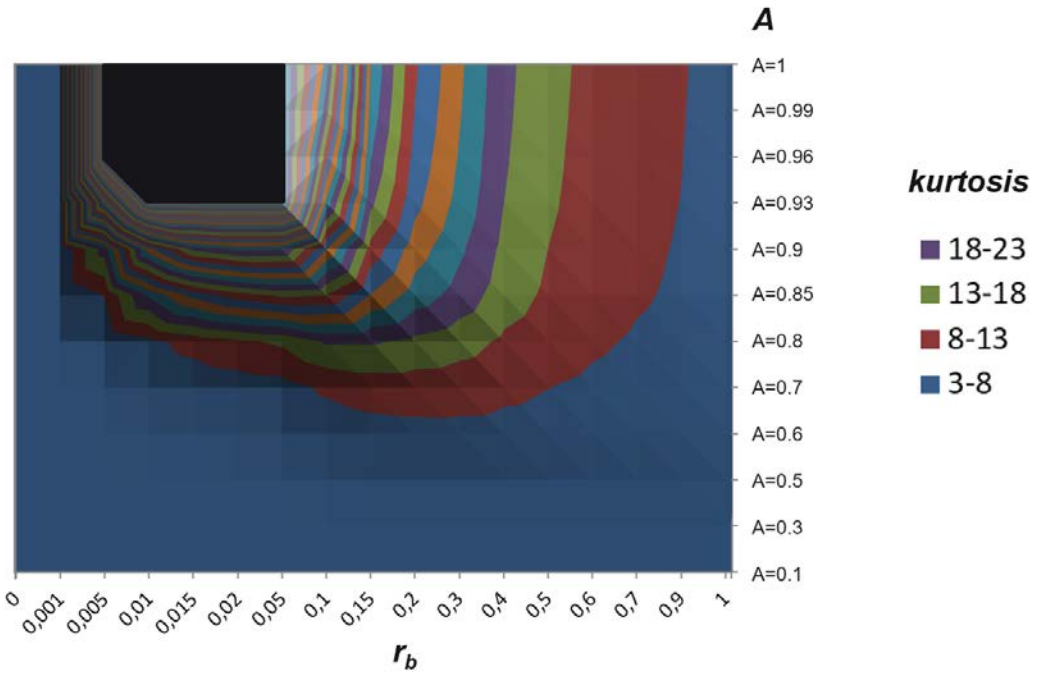


**Figure 52: The kurtosis value for a random signal amplitude modulated with spaced sinusoidal bursts having a fixed offset *B* and varying amplitude *A* and proportion of bursts $r_b$**

Only the first four colours corresponding to the lowest ranges of kurtosis (3-23) are displayed in the legend for the sake of clarity. The other colours correspond to kurtosis values above 23 and the black area contains kurtosis values higher than 150. The horizontal and vertical scales are not linear, but concentrate around low values of $r_b$ and high values of $A$, where high values of kurtosis are typically obtained. This area corresponds to scenarios where bursts of energy are dominant and the stationary part inbetween is comparatively very low.

By examination of the contour curves, it appears that there are several different cases leading to a similar value of kurtosis. For instance, a signal with very rare bursts of low amplitudes (low $r_b$ and low $A$) may have the same kurtosis as a signal mostly made of high fluctuations (high $r_b$ and high $A$). Both signals will have very different PDF distributions though and will therefore represent different physical phenomena. Also, as will be shown in section 4.4, when both signals are used as excitations to a component with a given frequency response, they will lead to responses with very different kurtosis values. This is why the rate of bursts shall be typically left as a user input parameter when it comes to simulating some leptokurtic nonstationary excitations.

To produce a signal that follows both the prescribed PSD and kurtosis using amplitude modulation, it is proposed to first derive a stationary signal $x(t)$ from the PSD, as described in section 3.2 and then multiply it by a modulation function $a(t)$. The characteristics of $a(t)$ are calculated based on the value of the target kurtosis and the rate of bursts $r_b$, chosen based on the type of phenomenon – more or less impulsive – that one wants to simulate.

The objective is therefore to solve the system of equations given in Equation 3.19 to find the unknown coefficients $A$ and $B$ for a prescribed kurtosis value and a given proportion of bursts $r_b$. Newton's method [100] can be used to solve the system of nonlinear equations in Equation

3.19. This type of iterative algorithm requires initial estimates for $A$ and $B$ to converge more rapidly. Also, in case where there are multiple solutions, the algorithm will converge to the solution closest to the initial guess.

The calculation of the initial estimates is given in Appendix B. An initial estimate for $A$ and $B$ can be: $A_{estimate} = 0.5\sqrt{\frac{1}{\left|{r_b}^2 - \frac{3}{2}r_b\right|}}$ and

$B_{estimate} = A_{estimate}(1 - r_b) + \sqrt{{A_{estimate}}^2({r_b}^2 - 3/2r_b) + 1}.$

Routines based on Newton's method such as zeros_sys_eqn in IMSL [101] can be used to solve the system of nonlinear equations using the provided initial estimates $A_{estimate}$ and $B_{estimate}$.

In actual fact, different physical phenomena may lead to bursts of energy having different durations. In some cases, bursts can be quite instantaneous, whereas in other case, they are made of a rather continuous and slow variation of the variance of the signal. Also, bursts can occur more or less often, depending on how many bursts occur per unit time. So there is a need to give the user the ability to define the proportion of bursts with two properties: the burst duration in seconds and the burst rate in the number of bursts per second. The proportion of bursts $r_b$ is therefore obtained as the product of the burst's duration with the burst rate.

Note that only the proportion of bursts $r_b$ has a role at this stage. The burst's duration will play a role, however, on the kurtosis value of the response of a linear system which responds to this excitation (see section 4.4).

To define the spectral structure of time series, it is not appropriate to apply the same processing techniques established for stationary data to time-varying mean square data (see section 2.2). Alternative techniques do exist that are dedicated to nonstationary data such as poly-spectra [38] and time-frequency instantaneous spectra [16]. These techniques are used generically for many different types of nonstationary signals. However, the signal of interest is very specific i.e. a stationary random signal modulated with a periodic function. It can be considered as cyclostationary and specific techniques apply to such a class of random signal [46, 47].

Assuming the underlying zero mean stationary Gaussian random process $x(t)$ and the modulation function $a(t)$ are independent, the mean of the amplitude modulated signal $y(t)$ is then calculated as $E[y] = E[a]E[x] = 0$.

Using the Parseval identity, the sum of the moduli squared of the complex Fourier coefficients $a_k$ of the periodic function $a(t)$ is equal to the average value of $|a(t)|^2$ over one period. One can thus write: $E[a^2] = \sum|a_k|^2$ and the variance of $y(t)$ is:

$$E[y^2] = E[a^2]E[x^2] = \sigma_x^2 \sum_k |a_k|^2$$

where $\sigma_x^2$ is the variance of the stationary ergodic signal $x(t)$ and $a_k$ are the Fourier coefficients of the periodic function $a(t)$. Note that since $a(t)$ and $y(t)$ are nonstationary, the expectation

operator $E[.]$ is defined here as an average over an infinite time so that the results obtained are independent of the time $t$.

The derivations to obtain the kurtosis $\kappa_y$ presented next are based on the theory of cyclostationary processes (see section 2.3.2) and constitute a novel approach developped in this thesis.

The fourth statistical moment of $y(t)$ is :

$$E[y^4] = E[a^4]E[x^4] = \sum_p |R_a(p)|^2 \,.\, \kappa_x . \sigma_x^4$$

where $R_a(p) = \sum_k a_k a_{k-p}^*$ is the correlation function of the Fourier coefficients $a_k$ of the periodic modulation function and $\kappa_x$ the kurtosis of the stationary Gaussian signal $x(t)$. Noting that $\sum_k |a_k|^2 = R_a(0)$, the kurtosis $\kappa_y$ of the signal $y(t)$ can be expressed as :

$$\kappa_y = \frac{\sum_p |R_a(p)|^2}{|R_a(0)|^2} \kappa_x$$

This expression can be modified to include the cyclic autocorrelation function [102]. This is done by noting that using Equation 2.75, $R_{yy}^{p/T}(0) = R_{xx}(0) \sum_k a_k a_{k-p}^* = R_{xx}(0)\, R_a(p)$, hence $R_a(p) = R_{yy}^{p/T}(0)/R_{xx}(0)$ and :

$$\kappa_y = \frac{\sum_p \left| R_{yy}^{p/T}(0) \right|^2}{\left| R_{yy}^{0}(0) \right|^2} \kappa_x$$

The kurtosis $\kappa_y$ of the signal $y(t)$ can be obtained in terms of the cyclic spectrum:

$$\kappa_y = \frac{\sum_p \left| \int S_{yy}^{p/T}(f) df \right|^2}{\left| \int S_{yy}^{0}(f) df \right|^2} \kappa_x \qquad \text{Equation 3.21}$$

Equation 3.21 shows that the kurtosis $\kappa_y$ of the signal $y(t)$ depends on the sum of the cyclic spectral variances and on the kurtosis of the input $\kappa_x$. Note that $\kappa_x = 3$ in the present case, but the underlying stationary random signal does not need to be Gaussian. The number of cyclic spectra considered ($p$ here) depend on the number of Fourier coefficients required to represent the modulation function $a(t)$.

Replacing $S_{yy}^{p/T}(f)$ with its expression given in Equation 2.77 and noting that $\int_{-\infty}^{\infty} S_{xx}\left(f - \frac{k}{T} + \frac{p}{2T}\right) df$ is independent on $k$ or $p$, one obtains the relationship relating the kurtosis of the amplitude modulated signal with the characteristics of the amplitude modulation function as:

$$\kappa_y = \frac{\sum_p \left|\sum_k a_k a_{k-p}^*\right|^2}{\left|\sum_k a_k a_k^*\right|^2} \kappa_x \qquad \text{Equation 3.22}$$

The amplitude modulated signal $y(t)$ is cyclostationary of order 2 [46]. Its cyclic spectrum is derived in section 2.3 and is found to be:

$$S_{yy}^{p/T}(f) = \sum_k a_k a_{k-p}^* S_{xx}\left(f - \frac{k}{T} + \frac{p}{2T}\right) \qquad \text{Equation 2.77}$$

with $S_{xx}(f)$ the PSD of the underlying stationary signal $x(t)$ and $a_k$ the Fourier coefficients of the modulating function. In the case where the modulation function comprises a half sine wave interlaced with stationary portions, the Fourier coefficients $a_k$ are calculated in Appendix B and are:

$$a_k = A.r_b.\left(1 + \frac{k^2}{(1/r_b)^2 - k^2}\right)\left(\frac{sin(\pi k r_b)}{\pi k r_b}\right) \qquad \text{Equation 3.23}$$

for all $k \neq 0$, and for $k = 0$, $a_0 = (B - A) + r_b A$.

Note that $a_k$ are not defined in Equation 3.23 for $r_b = 1$ i.e. when the modulation function is a non-centred sine wave expressed as $a(t) = Acos(2\pi f_0 t) + B$. In this trivial case, the Fourier coefficients $a_k$ are all zero except $a_0 = B$ and $a_{\pm 1} = A/2$.

Note that for $p = 0$, the cyclic spectrum reduces to the conventional PSD [47]. Using Equation 2.77, $S_{yy}^0(f)$ is expressed as $\sum_k |a_k|^2 S_{xx}\left(f - \frac{k}{T}\right)$, which reveals the presence of sidebands due to the spectrum being shifted by $\frac{k}{T}$. The level of the sidebands is reduced when the rate $a_k/a_0$ is reduced. In order to reduce the out of band effects in the PSD of the nonstationary signal generated, it is suggested to have a very high value for $T$ i.e. a very low burst rate (typically below the range of frequencies contained in $S_{xx}$), with a low proportion of bursts $r_b$ and with a small modulation index $A/B$. It is worth noting that limiting the modulation index can limit the value of the kurtosis obtained (see Figure 52). So in practice, if a very high kurtosis is required then there will be sideband effects.

Figure 53 shows the values of the 20 first Fourier coefficients calculated using Equation 3.23 for two proportion of bursts $r_b = 0.1$ (represented using triangles) and $r_b = 0.01$ (represented using circles) in the case of a modulating function with $A = 1$ and $B = 2$. Note that the values were normalised with respect to $a_0$. It clearly illustrates the values that the rate $a_k/a_0$ can take for different proportions of bursts $r_b$.

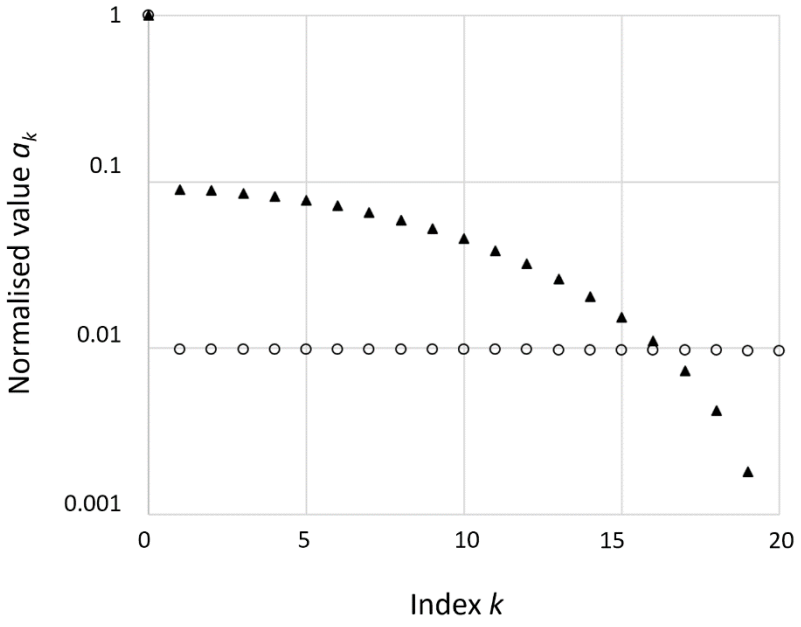


**Figure 53: Fourier coefficients for a modulating function with $r_b$ = 0.1 (triangles) and $r_b$ =0.01 (circles)**

The kurtosis of the excitation $y(t)$ can be obtained by applying Equation 3.22 linking the Fourier coefficients $a_k$ and the kurtosis of a cyclostationary process.

Equation 3.22 is a generic expression for the kurtosis of an amplitude modulated signal $\kappa_y$ using the Fourier coefficients $a_k$ of the periodic modulation function. A closed form solution can be found in the case of successive half-sine bursts, i.e. when the modulation function is a non-centred sine wave. In this specific case, the Fourier coefficients $a_k$ and $b_k$ are zero for all $k$ but for $k = 0$ and for $k = \pm 1$, where $a_k = B$ and $a_k = A/2$ respectively.

Using Equation 3.22, the kurtosis $\kappa_y$ becomes:

$$\kappa_y = \frac{\frac{3}{8}A^4 + B^4 + 3A^2B^2}{\left(B^2 + \frac{1}{2}A^2\right)^2}\kappa_x$$

This is the same expression as given in Equation 3.17, found by calculating the statistical moments of the amplitude modulated random signal.

The cyclostationary theory will be used in section 4.4 to calculate the cyclic spectrum of the response signal obtained when the excitation signal is filtered with the frequency response function of the component of interest. Then the kurtosis of the response will be calculated using Equation 3.21.

Note that since the bursts are randomly distributed in time, the process is not strictly cyclostationary. The theory of cyclostationarity is however used here, because it is convenient to understand the relationship between the input and output statistics. Looking at the global time-averaged statistical moments only, providing the bursts do not overlap, their position in

time relative to each other does not play any role. In section 4.4 it will be assumed that the statistics of the response can be derived using the theory of cyclostationarity.

Note also that the calculation of the kurtosis of the signal only requires the proportion of time duration containing bursts $r_b$. There is no parameter for the burst width $T_0$ nor for the length of the modulator $T$. So, for the global statistics, having 10 bursts per second of 0.01 s each is equivalent to having 1 burst per second of 0.1s each. In section 4.4, however, the prediction of the kurtosis of the response to a linear and time-invariant (LTI) system will require one to know how large each burst is and how spaced they are apart.

### 3.5.2 Applications

Some specific vibratory environments such as road vehicle vibrations can be significantly non-stationary mainly due to variations in road roughness and vehicle speed [54, 55]. Some authors [54, 55] argue that non-stationary random vehicle vibrations consist of segments of Gaussian stationary data. So, a road excitation signal can be seen as an amplitude modulated process. Road sections with a high degree of roughness are of special interest, since these have a significant impact on the fatigue life of a vehicle. It has been shown [57, 103] that most of the fatigue damage accumulated in a vehicle are consequence of short-duration oscillations caused by local irregularities on the road surface. The road excitation can be modelled as Gaussian loads with superimposed bursts of energy due to a sudden short change of surface variability. Similarly, in the military [59] or in the rail industry [60], excitations show clear nonstationary segments of data.

Gaussian loads with time-varying mean square values are present in many other fields. For example, responses of a sailing vessel can be modelled as a Gaussian process with bursts due to ‘slams’ which occur when a ship proceeds at certain speeds in rough seas and the front part of the underside of the hull sustains large forces as the result of impact with the sea surface [57]. In the field of civil engineering, bursts of energy are due to wind [48, 49, 50], waves [50] and earthquakes [51], whereas in the aerospace industry they are typically due to turbulent boundary flow [19, 52, 53]. Other typical examples are found in mechanical systems consisting of rotating parts, where bursts of energy are released a number of times per revolution [46]: combustion of gas in internal combustion engines, admission and exhaust of fluids in pumps, turbulence around fan blades, etc.

The same example presented in Table 3.1 and in Figure 38 is used here.

A signal of 100s sampled at 8192 points per seconds was generated using the methodology based on the amplitude modulation technique described in this section. A prescribed kurtosis of 12 was used. Figure 54 shows an extract of the leptokurtic signal obtained.

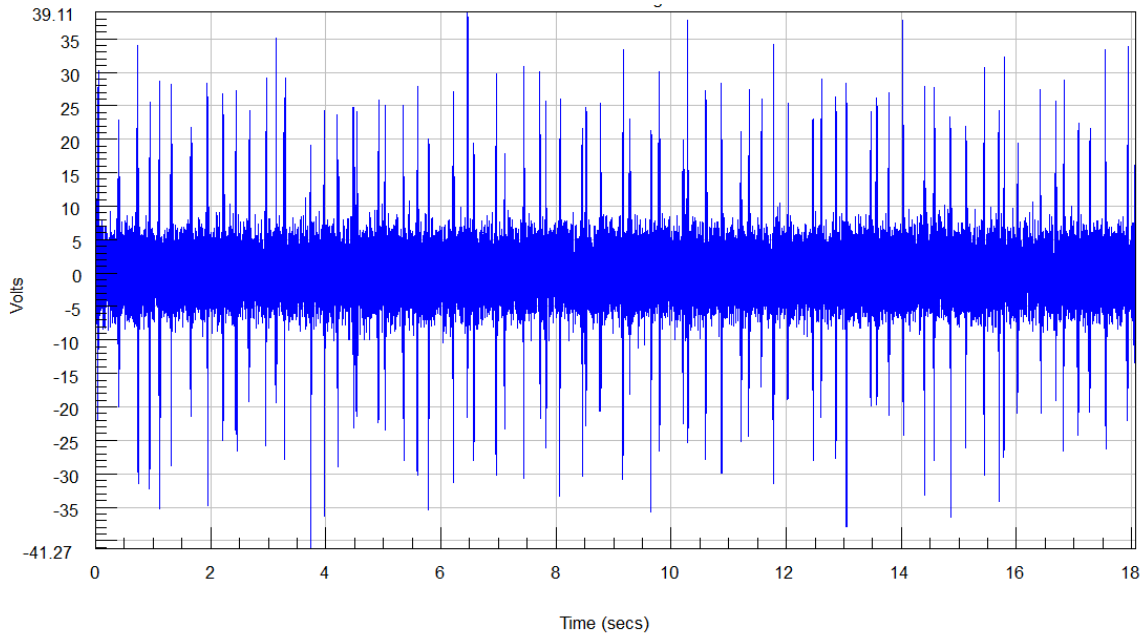


**Figure 54: An example nonstationary non-Gaussian Signal realization corresponding to target PSD and kurtosis of 12**

The PSD and the PDF of the signal obtained are displayed in Figure 55. The PSD and PDF are overlaid with the target PSD profile and the ideal Gaussian distribution respectively in dashed black lines.

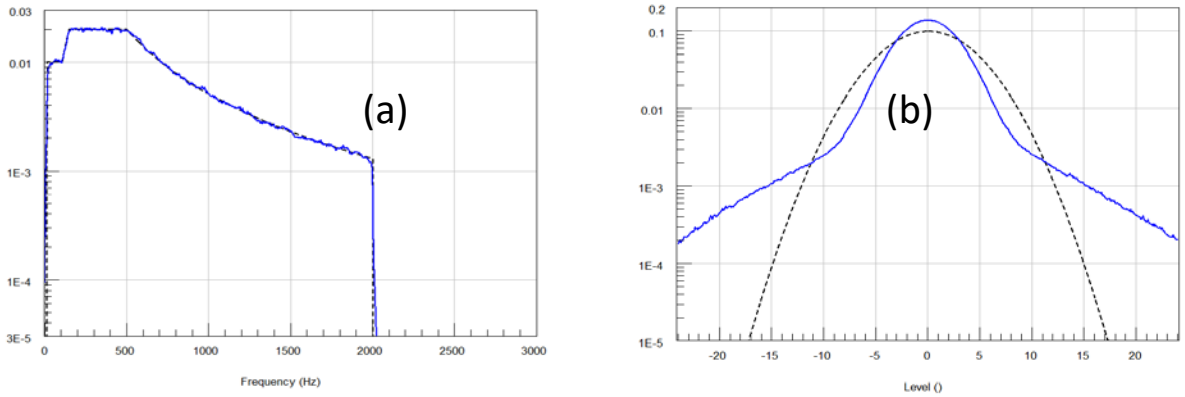


**Figure 55 : (a) PSD of the obtained signal with kurtosis of 12 overlaid with the target PSD and (b) PDF of the obtained signal overlaid with the ideal Gaussian PDF**

The difference with the Gaussian signal is very clear in the PDF, where the leptokurtic signal shows a much higher probability of finding high values compared to the Gaussian signal. As expected from Equation 3.18, the PDF is indeed made of two constituents. This is revealed by the change in slope in the shape of the non-Gaussian PDF obtained.

Both techniques for generating leptokurtic signals can be compared. The PSD and the PDF of the signals obtained are compared in Figure 56. The PSD and PDF corresponding to the steady leptokurtic signal are represented in blue line, the PSD and PDF corresponding to the nonstationary leptokurtic signal are represented in red line and the target PSD profile and the ideal Gaussian distribution are in dashed black lines.

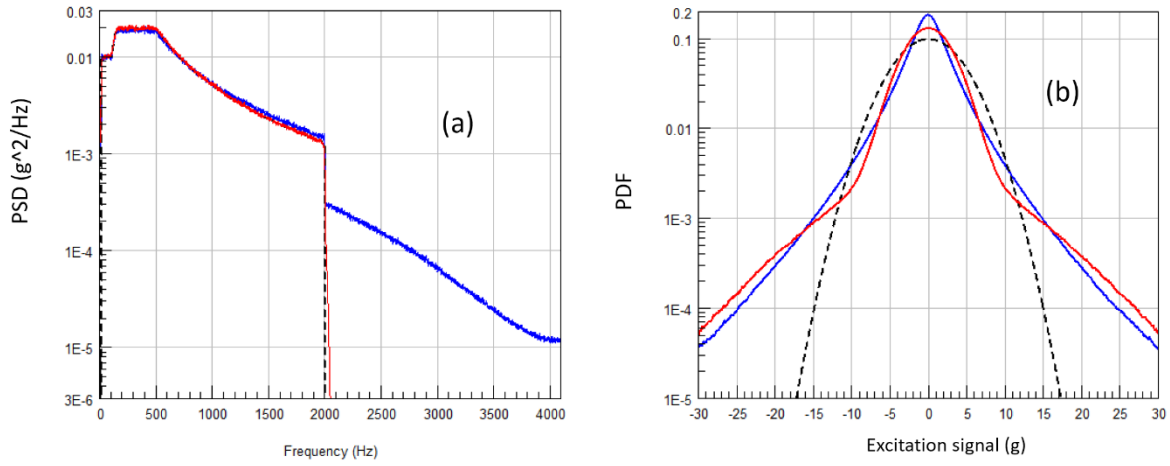


**Figure 56: (a) PSD of the steady leptokurtic signal generated in blue overlaid with the PSD of the nonstationary leptokurtic signal in red and with the target PSD in dashed black lines. (b) PDF the steady leptokurtic signal overlaid with the PDF of the nonstationary leptokurtic signal and with the ideal Gaussian PDF. Both leptokurtic signals have the same kurtosis value of 12.**

Both leptokurtic signals share the same target kurtosis value of 12. Figure 56 (a) reveals how much harmonic distortion can be introduced by the polynomial transform technique, when used to generate a steady leptokurtic random signal. Comparatively, the amplitude modulation technique shows a much better dynamic range. Indeed, the sidebands generated by the amplitude modulation can be drastically reduced by adopting a low proportion of bursts $r_b$ with a small modulation index $A/B$.

### 3.5.3 Limitations

This method requires not only the kurtosis but also additional parameters, which define the proportion of the time duration of the bursts of energy. Depending on the proportion of bursts $r_b$, not all values for the kurtosis can be achieved. For instance, using a proportion of bursts of 1.0 will lead to a sinusoidal modulation function, which only allows a maximum kurtosis of 5.83 (see section 3.5.1.2). Basically, according to Figure 52, $r_b$ must be strictly positive and smaller than 1 for the amplitude modulated signal obtained to be able to reach high kurtosis values.

This method, being based on amplitude modulation, will introduce sidebands which in turn reduce the dynamic range for the spectral density of the generated data. However, for a given kurtosis value, the out of band energy introduced by the amplitude modulation technique is typically much smaller than the one introduced by the polynomial transform technique (see Figure 56 (a)). This is a benefit of this novel approach proposed in this section for generating nonstationary leptokurtic excitation signals.

So far, the method proposed produces signals with zero skewness and does not allow modelling or introduction of any non-zero skewness value.

## 3.6 Conclusions

Chapter 3 introduced methods that can be used to generate stationary Gaussian random signals and some specific non-Gaussian random signals including:

i. Clipped random signals: to simulate how the excitation signal is typically limited during a shaker test.
ii. Random signals with high kurtosis: to simulate non-Gaussian loads found in service such as potholes in the automotive industry.

Two different algorithms for the generation of excitation signals with a high kurtosis were presented. The first algorithm generates a stationary signal with instantaneous, high-excursion peaks, whereas the second algorithm creates non-stationary signals with bursts of high amplitude excursions, typically representing varying-variance signals. For this second methodology, the relationship between the characteristics of the modulation function and the kurtosis desired was developed in this study as an original contribution.

Each method was detailed and applications were discussed. Each signal generation procedure was illustrated with numerical examples. Finally, the known limitations of each technique were described and explained.

Chapter 3 will now serve for simulation and validation purposes in the rest of this thesis. Indeed, the next chapters will concentrate on statistical methods for deriving output distributions and fatigue damage; the various theories presented will be validated and supported by generating signals and running time domain numerical simulations.

Chapter 4 will discuss the statistics of the response of a linear system to Gaussian and various non-Gaussian excitations. The linear system is considered to be a mechanical component and the response is expressed in terms of the stress response. The reader will realise that, for some specific non-Gaussian loadings, it is possible to determine the statistics of the response knowing only the statistics of the excitation and the dynamic characteristics of the linear system, without having to perform simulations requiring the production of long excitation time histories.

# 4 Relationship between the input and output statistics

## 4.1 Introduction and assumptions

Various means to generate a signal with a specified power spectral density (PSD) and kurtosis have been identified and studied in chapter 3. A signal generated using the techniques presented in chapter 3 is meant to represent the excitation applied to a mechanical device, not the stress response at a critical location.

In this chapter, the mechanical device or object is considered to be a linear and time invariant system (see section 0) and is represented by a linear filter. The linearity assumption taken in this thesis is based on the fact that the (stress) response characteristics for many mechanical systems may be assumed to be linear, at least over some limited range of inputs, without involving unreasonable errors [16]. The linear system is represented by a frequency response function (FRF), which can represent a multimodal system. The output stress obtained has specific characteristics and statistics such as root mean square (RMS) and kurtosis values.

The response of linear systems to non-Gaussian inputs have been previously documented [51, 104, 105], but they are often based on simulations and none of them provide a clear relationship between the input and output kurtosis for instance. The so-called Papoulis rule [66] states that the response of a narrowband filter will tend towards a Gaussian process, as the bandwidth of the filter tends to zero. This is irrespective of the distribution associated with the input signal.

The main objective of this chapter is to find out the non-Gaussian characteristics of the output stress signal, knowing the non-Gaussian characteristics of the input excitation signal; without the need for numerical simulations. Formulations are proposed that give the statistics of the response due to specific non-Gaussian random excitations, including steady non-Gaussian loadings, non-stationary signals with high amplitude excursions.

The synoptic presented in Figure 57 illustrates the inputs and results obtained in this chapter, more specifically related to the kurtosis. Note that in the case of clipped excitations, the crest factor used is associated with the excitation PSD instead of the kurtosis value.

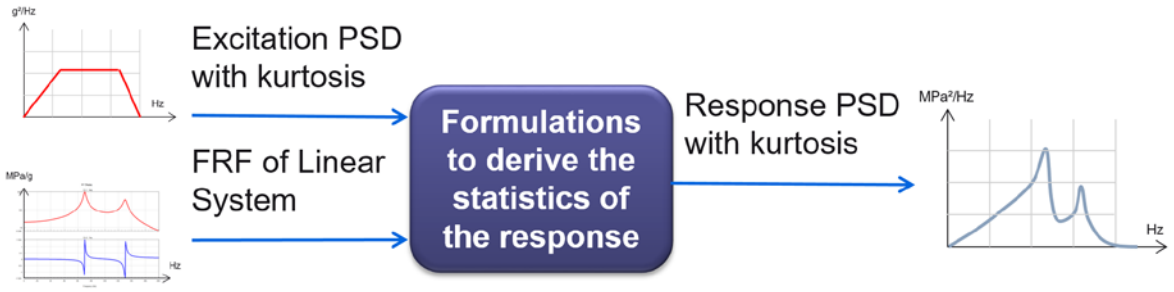


**Figure 57 : Inputs required and results obtained in this chapter in the case of kurtosis controlled excitations**

Three types of random excitations will be considered next: stationary random Gaussian noise, stationary non-Gaussian excitations, including clipped and leptokurtic signals and finally

nonstationary excitations. For the non-Gaussian cases, theoretical expressions will be developed and proposed to predict the non-Gaussian characteristics of the output stress signal.

## 4.2 Output statistics from a stationary random Gaussian noise excitation

Section 2.4 presents the input-output relationships for a stationary Gaussian excitation of a linear system. Ways to calculate the output signal waveform are also described in section 2.4, with Equation 2.79:

$$z(t) = \int_{-\infty}^{t} h(t-\tau).x(\tau)d\tau \qquad \text{Equation 2.79}$$

where $h(\tau)$ is the impulse response function of the system, $x(t)$ the input signal and $z(t)$ the output signal.

And the calculation of the output PSD is done using Equation 2.82 :

$$G_{zz}(f) = H^*(f).H(f).G_{xx}(f) \qquad \text{Equation 2.82}$$

where $H^*$ is the complex conjugate of $H$. $G_{zz}$ and $G_{xx}$ are the PSDs of the input to and output of the system respectively.

The RMS of the response $\sigma_z$ can be calculated by incorporating Equation 2.82 into Equation 2.42 as:

$${\sigma_z}^2 = \int_{0}^{\infty} H^*(f).H(f).G_{xx}(f)df \qquad \text{Equation 4.1}$$

Note that these expressions (Equation 2.79, Equation 2.82 and Equation 4.1) are valid for all types of excitations, stationary Gaussian or not, as long as the system is linear and time-invariant (LTI) [20].

Section 2.4 especially states that when the input $x(t)$ is from a stationary random process and if the system $f$ is linear and time invariant, then the output $z(t) = f[x(t)]$ will form a stationary random process [16]. Also, if $x(t)$ follows a Gaussian distribution, then $z(t) = f[x(t)]$ will also follow a Gaussian distribution [36].

## 4.3 Output statistics from a stationary, non-Gaussian random excitation

In recent work by Rizzi et al. [106], it was found that a leptokurtic loading having a steady rate of instantaneous, high-excursion peaks produced essentially the same response as if the load was Gaussian. It was found that the linear response to a non-Gaussian loading was Gaussian when the length of the system impulse response is much greater than the rate of the peaks in the loading. Practically, lower damping would typically reduce the excess kurtosis in the response, since a lower damping means a longer impulse response function which averages out

the peak values during the convolution process. This section introduces a formulation to calculate the kurtosis of the response due to specific non-Gaussian stationary signals.

A non-Gaussian stationary signal $y(t)$ can be obtained from a Gaussian stationary signal $x(t)$ using the polynomial transform as described in section 3.4. This non-Gaussian stationary signal $y(t)$ will be then used as the input of a linear system where the statistics of the response $z(t)$ will be of interest. Figure 58 illustrates this process and the associated notations.

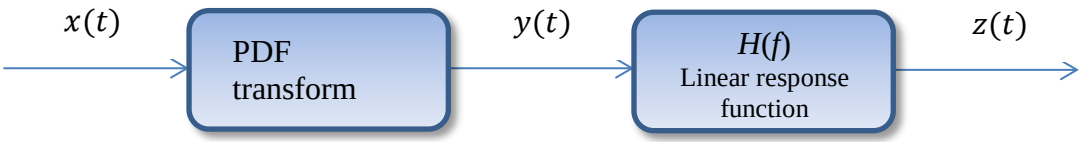


**Figure 58: Synoptic showing how to obtain a filtered non-Gaussian stationary signal**

### 4.3.1 Output statistics from a white noise non-Gaussian excitation

Consider a random stationary non-Gaussian and white noise process $y(t)$ that is filtered through a LTI system of impulse response function defined by its coefficients $h_i$. Using the fact that the cumulants are additive under convolution, Lacoume [18] proves that the cumulants $c_{z,k}$ of the output signal $z(t)$ can be calculated from the cumulants $c_{y,k}$ of the input signal $y(t)$ and the coefficients $h_i$ of the impulse response function as:

$$c_{z,k} = c_{y,k} \sum_i (h_i)^k \qquad \text{Equation 4.2}$$

Details of the derivation to obtain Equation 4.2 are given in Appendix D.

In practice, setting $k = 2$ and $k = 4$, the 2nd and 4th cumulants of the response signal $c_{z,2}$ and $c_{z,4}$ can be derived from the 2nd and 4th cumulants of the input signal $c_{y,2}$ and $c_{y,4}$ respectively and from the coefficients $h_i$ of the impulse response function as:

$$c_{z,2} = c_{y,2} \sum_i (h_i)^2$$

$$c_{z,4} = c_{y,4} \sum_i (h_i)^4$$

From Equation 4.2 and using Equation 2.25 that defines standardised cumulants $C_{z,k}$, the input-output relationship for the standardised cumulants becomes:

$$C_{z,k} = C_{y,k} \frac{\sum_i (h_i)^k}{\left(\sum_i {h_i}^2\right)^{k/2}} \qquad \text{Equation 4.3}$$

Donoho [107] demonstrates that the output cumulants are always smaller (i.e. closer to zero) than the input cumulants of a white noise signal - unless the IRF is a zero signal with only its

first value at 1.0 (i.e. corresponding to an all-pass system). This means that a linear filter applied to a non-Gaussian white noise signal will always tend to make the response more Gaussian than the input.

The kurtosis $\kappa_z$ is defined as the 4th standardized statistical moment. In the case of a zero-mean stationary process, the kurtosis $\kappa_z$ is related to the 4th standardized cumulant $C_{z,4}$ by [18]:

$$\kappa_z = C_{z,4} + 3 \qquad \text{Equation 4.4}$$

Inserting Equation 4.3 with $k = 4$ into Equation 4.4, one obtains the expression giving the output kurtosis $\kappa_z$ from the system's impulse response function $h_i$ and the input kurtosis $\kappa_y$:

$$\kappa_z = \frac{\sum h_i^4}{(\sum h_i^2)^2}\left(\kappa_y - 3.0\right) + 3.0 \qquad \text{Equation 4.5}$$

The expression in Equation 4.5 only depends on the coefficients $h_i$ of the discrete Impulse Response Function (IRF) of the dynamic system and the input kurtosis $\kappa_y$.

The IRF corresponding to a system with very low damping will oscillate longer than the IRF corresponding to a highly damped system. In relation to Equation 4.5, when both the numerator and the denominator are divided by $h_0$, it becomes evident that an IRF with long decaying oscillations will maximize the squared terms in the denominator compared to the terms raised to the 4th power in the numerator. This will lead to a lower output kurtosis for a lightly damped system than for a more heavily damped one. A mathematical demonstration of this phenomenon is given in Appendix D. This behaviour is consistent with the observation that the output signal tends to be Gaussian as the bandwidth of the filter, i.e, the amount of damping, decreases [66, 106]. Appendix D also shows that this tendency towards Gaussianity is even more pronounced for the higher order statistical moments.

Equation 4.5 also shows that the output kurtosis $\kappa_z$ cannot exceed the input kurtosis $\kappa_y$ since $\frac{\sum h_i^4}{(\sum h_i^2)^2} < 1$.

Equation 4.5 gives the kurtosis of the response knowing the kurtosis of the excitation and the dynamic characteristics of the linear system and it is only applicable to steady, non-Gaussian and white noise processes. Such processes are typically generated using a polynomial transform method. The next section shows how the kurtosis input-output relationship can be generalized to coloured noise.

### 4.3.2 Generalisation to coloured noise

The formulation found in the previous section (Equation 4.5) is applicable to white noise input signals only. A coloured noise can be obtained from a white noise by using a linear numerical filter. The colouring process is illustrated in Figure 59:

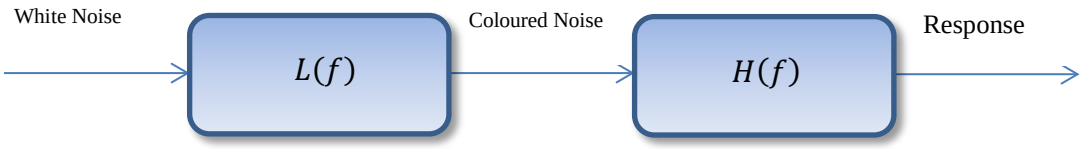


**Figure 59: White noise to coloured noise process for simulation**

In Figure 59, $L(f)$ is a 'colouring filter' that turns an original white noise to the coloured noise of interest. This coloured noise is then filtered using $H(f)$, the frequency response function of the system. This process is equivalent to using one combined system frequency response function, illustrated in Figure 60:

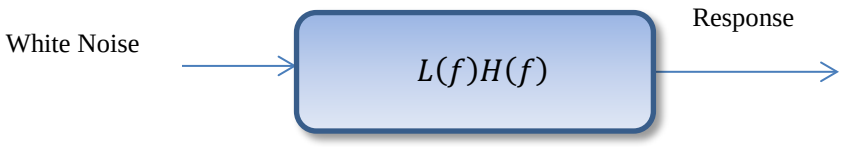


**Figure 60: Combining two consecutive transfer functions into one**

The computation of the output kurtosis is using the same formulae as in the previous section; the impulse response function $f_i$ to consider is obtained by convolving the impulse response function $l_i$ associated with the colouring filter $L(f)$ with the impulse response function of the system $h_i$:

$$f_i = l_i * h_i \qquad \text{Equation 4.6}$$

where the sign * represents the convolution product.

Note that the coefficients $l_i$ are the coefficients of the autocorrelation function of the excitation (coloured) signal.

Applying Equation 4.5 using $f_i$ as the coefficients of the impulse response function, one obtains:

$$\kappa_z = \frac{\sum f_i^4}{(\sum f_i^2)^2}(\kappa_w - 3.0) + 3.0 \qquad \text{Equation 4.7}$$

with $\kappa_w$ the kurtosis associated with the white noise.

The limitation in using Equation 4.7 is that the kurtosis associated with the white noise $\kappa_w$ is not known. The prescribed kurtosis $\kappa_y$ is indeed associated with the coloured noise. So, in order

to use Equation 4.7, we need to calculate what the kurtosis of the white noise process should be, knowing the colouring filter frequency response $L(f)$ and $\kappa_y$, the kurtosis associated with the coloured input noise. Inverting Equation 4.5 and noting $l_i$ the coefficients of the IRF associated with the colouring filter $L(f)$, one finds:

$$\kappa_w = \frac{(\sum l_i^2)^2}{\sum l_i^4}\left(\kappa_y - 3.0\right) + 3.0 \qquad \text{Equation 4.8}$$

Therefore, inserting Equation 4.8 into Equation 4.7, the output kurtosis is obtained from the system's impulse response function, the autocorrelation function of the excitation and the input kurtosis as:

$$\kappa_z = \frac{\sum f_i^4}{(\sum f_i^2)^2}\frac{(\sum l_i^2)^2}{\sum l_i^4}\left(\kappa_y - 3.0\right) + 3.0 \qquad \text{Equation 4.9}$$

Note that for a white noise excitation, then $l_i = \delta[i]$, and $f_i = l_i * h_i = h_i$ and Equation 4.9 becomes identical to Equation 4.5.

Note also that, if the input noise is Gaussian, then $\kappa_y = 3$ and $\kappa_z = 3$. Similarly, the output higher order cumulants $c_{z,k}$ (for $k > 2$) calculated in Appendix D are zero when the input higher order cumulants $c_{y,k}$ are zero – which is property of a Gaussian signal [18]. This supports the statement that a Gaussian signal remains Gaussian after linear filtering [20].

Following the same logic discussed after establishing Equation 4.5, Equation 4.9 shows that to maximise the output kurtosis, the system must be rather heavily damped. Similarly, it appears in Equation 4.9 that a narrowband leptokurtic input signal will allow more kurtosis in the response signal.

In the particular case where the system is responding almost instantaneously to the input i.e. the first natural frequency is above the frequencies of the applied load, the output kurtosis is maximised. This can be shown mathematically by using Equation 4.5 or understood conceptually by considering that the system's behaviour is close to an all-pass filter.

Figure 61 illustrates by numerical examples the relationship between the input and the output kurtosis for input signals of various bandwidth and single degree of freedom systems with a natural frequency at 150 Hz and various damping ratios. The input signal is leptokurtic with kurtosis 5. It was obtained using the polynomial transform of a 100 second random noise sampled at 4096 Hz, centred around 100 Hz, with various bandwidths. The vertical axis of Figure 61 (a) shows the output kurtosis observed from numerical simulations and the vertical axis of Figure 61 (b) shows the output kurtosis calculated using Equation 4.9:

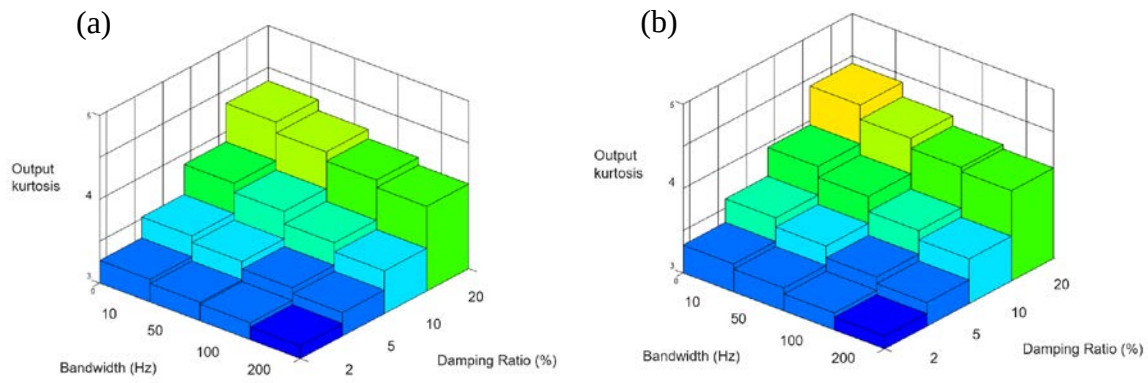


**Figure 61: (a) output kurtosis observed from numerical simulations of a narrowband input signal with kurtosis of 5 with various bandwidths filtered using a linear unimodal FRF with various damping ratios and (b) theoretical output kurtosis calculated**

Figure 61 illustrates indeed that the output kurtosis is maximised, when the system is highly damped and/or the input signal is narrowband. The output kurtosis calculated using Equation 4.9 is in good agreement with the output kurtosis observed after digital filtering with less than 2% error in this case.

Equation 4.9 gives the kurtosis of the response knowing the kurtosis of the excitation and the dynamic characteristics of a single or multi-degree of freedom linear system. Equation 4.9 is valid for stationary coloured excitation signals, which can be leptokurtic or platykurtic. This means that Equation 4.9 is also applicable in the case of a clipped input signal to understand the statistics of the response after linear filtering. This section provides mathematical expressions showing why and how an LTI filter tends to turn a stationary non-Gaussian signal into a Gaussian signal. The next section shows how the kurtosis input-output relationship can be calculated in the case of non-stationary excitation signals with high amplitude excursions.

## 4.4 Output statistics from an amplitude modulated random excitation

In recent work by Rizzi et al. [106], it was found that the response to a non-Gaussian leptokurtic loading with bursts of high input values was non-Gaussian and also leptokurtic, even when filtered through a lightly damped linear system. This was in contrast with using steady leptokurtic excitations, where the output signal produced was essentially the same as if the input was Gaussian. This section introduces a formulation to calculate the kurtosis of the response due to specific non-stationary signals with high amplitude excursions obtained using an amplitude modulation function comprising spaced and non-centred sine waves.

A nonstationary random signal $y(t)$ obtained by an amplitude modulation technique can be represented as:

$$y(t) = a(t).x(t)$$

with $a(t)$ is a deterministic periodic modulation function, each period comprising a constant amplitude flat portion and a half sine pulse representing a burst. See section 3.5.1 for details.

The modulation function $a(t)$ can be calculated in order to produce a nonstationary random signal $y(t)$ with a prescribed kurtosis value as described in section 3.5. The nonstationary random signal $y(t)$ obtained will then be used as the input to a linear system and the statistics of the response $z(t)$ will be investigated. Figure 62 illustrates this process and the associated notations.

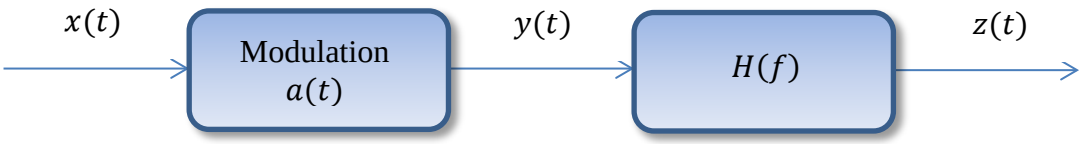


**Figure 62: Synoptic showing how to obtain a filtered non-stationary signal**

The excitation signal $y(t)$ considered is therefore a stationary random signal modulated with a periodic function. Its statistics vary periodically in time and it can therefore be considered as cyclostationary [47, 46]. The reader is referred to section 2.3.2 for more background on cyclostationary processes and on the specific techniques that apply to such a class of random signals. The cyclostationary theory will be used in this section to calculate the cyclic spectrum of the response signal and the kurtosis of the response using Equation 3.21.

Note that the same assumptions as used in section 3.5, where the generation of the excitation signal $y(t)$ is described, are used in this section:

i. The length of the bursts pulse will be considered constant.
ii. The amplitudes of the bursts will remain constant.
iii. The bursts may appear at random instants within a period but they will not overlap.

The third assumption (iii) is particularly important here, as the theory of cyclostationarity requires the amplitude modulation function to be periodic. By looking at the global time-

averaged statistical moments only, providing the bursts do not overlap, their position in time relative to each other does not play any role. It is therefore assumed that the theory of cyclostationarity can be used to understand the relationship between the input and output statistics. The cyclostationarity assumptions used for this signal are discussed in chapter 3.5.

In chapter 2.4, Equation 2.82 gives the input-output relationship for conventional power spectra. The extension to the input-output cyclic spectrum relation for LTI systems is given by Gardner [47]:

$$S_{zz}^{\alpha}(f) = H\left(f + \frac{\alpha}{2}\right).S_{yy}^{\alpha}(f).H^{*}\left(f - \frac{\alpha}{2}\right) \qquad \text{Equation 4.10}$$

where $H(f)$ is the frequency response function of the linear system and $S_{zz}^{\alpha}(f)$ and $S_{yy}^{\alpha}(f)$ are the cyclic spectra for $z(t)$ and $y(t)$ respectively. $\alpha$ is the cyclic frequency, ranging over all integer multiples of the fundamental frequency $1/T$ of the modulation function. The spectral frequency $f$ and the cyclic frequency $\alpha$ are illustrated using an example signal in Figure 63.

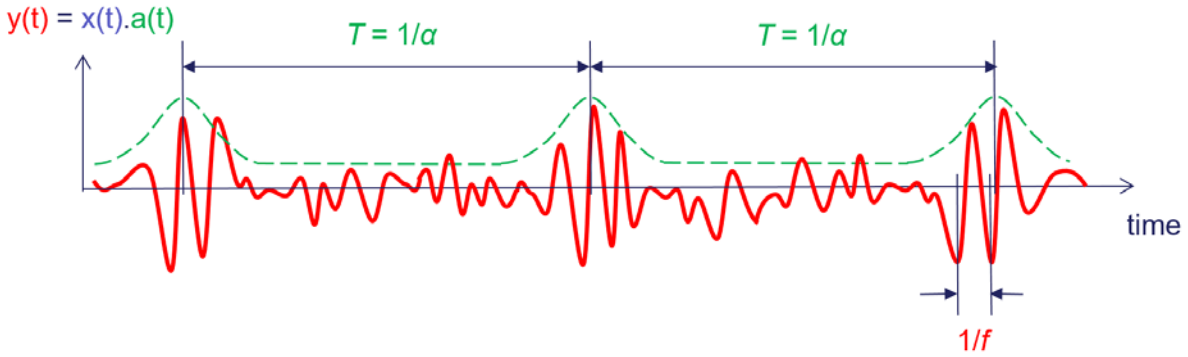


**Figure 63: Example amplitude modulated signal illustrating the spectral frequency *f* and the cyclic frequency *α* of a cyclostationary waveform.**

Note that when the process is stationary, then $\alpha = 0$, $S_{zz}^{\alpha}(f) = S_{zz}(f)$ (see Equation 2.73), and Equation 4.10 becomes $S_{zz}(f) = H^{*}(f).S_{xx}(f).H(f)$, which is identical to Equation 2.82.

The kurtosis of the response $z(t)$ can be obtained from Equation 3.21 linking the kurtosis of an amplitude modulated cyclostationary process $\kappa_y$ and its cyclic spectrum $S_{yy}^{\alpha}$. The amplitude modulated cyclostationary excitation $y(t)$ is filtered through an LTI filter to obtain the response signal $z(t)$, which is assumed to be also an amplitude modulated cyclostationary signal. Then, Equation 3.21 can be used again to obtain the kurtosis of the response $\kappa_z$ from the cyclic spectrum of the response $S_{zz}^{\alpha}$ :

$$\kappa_z = \frac{\sum_p |\int S_{zz}^{\alpha}(f)df|^2}{|\int S_{zz}^{0}(f)df|^2}\kappa_x \qquad \text{Equation 4.11}$$

where $p$ is an integer. The harmonic cyclic frequency $\alpha$ being considered to be a multiple of the fundamental frequency $1/T$ of the modulation function, $p = \alpha T$.

Using the input-output cyclic spectrum relation for LTI systems given in Equation 4.10,

$$\kappa_z = \frac{\sum_p \left| \int H\left(f + \frac{\alpha}{2}\right) . S_{yy}^{\alpha}(f) . H^*\left(f - \frac{\alpha}{2}\right) df \right|^2}{\left| \int H(f) . S_{yy}^{0}(f) . H^*(f) df \right|^2} \kappa_x \qquad \text{Equation 4.12}$$

Replacing $S_{yy}^{\alpha}$ with its expression given in Equation 2.77:

$$\kappa_z = \frac{\sum_p \left| \int H\left(f + \frac{\alpha}{2}\right) . \left\{ \sum_k a_k a_{k-\alpha T}^* S_{xx}\left(f - \frac{k}{T} + \frac{\alpha}{2}\right) \right\} . H^*\left(f - \frac{\alpha}{2}\right) df \right|^2}{\left| \int H(f) . \left\{ \sum_k a_k a_k^* S_{xx}\left(f - \frac{k}{T}\right) \right\} . H^*(f) df \right|^2} \kappa_x$$

where $a_k$ are the Fourier coefficients of the modulation function, $H(f)$ is the frequency response function of the linear system and $S_{xx}(f)$ is the PSD of $x(t)$, the original stationary Gaussian random signal.

Knowing that the harmonic cyclic frequency $\alpha$ is a multiple of $1/T$, it can be replaced with $\alpha = p/T$, with $p \in \mathbb{Z}$ (all integers, including zero) and the equation giving $\kappa_z$ can be re-expressed as:

$$\kappa_z = \frac{\sum_p \left| \int H\left(f + \frac{p}{2T}\right) . \left\{ \sum_k a_k a_{k-p}^* S_{xx}\left(f + \frac{p-2k}{2T}\right) \right\} . H^*\left(f - \frac{p}{2T}\right) df \right|^2}{\left| \int H(f) . \left\{ \sum_k a_k a_k^* S_{xx}\left(f - \frac{k}{T}\right) \right\} . H^*(f) df \right|^2} \kappa_x \qquad \text{Equation 4.13}$$

Note that the kurtosis $\kappa_z$ of the response signal is predicted by considering both the period $T$ of the modulating function $a(t)$ and the proportion of bursts $r_b$ ($r_b$ is used in the computation of the Fourier coefficients $a_k$ – see Equation 3.23).

Note also that $\kappa_z \geq \kappa_x$ because the response kurtosis is obtained from a sum over a number of positive terms for various $p$ values and in the case $p = 0$, then the numerator equals the denominator.

For a narrowband system whose bandwidth is much smaller than the frequency of the modulator $\frac{1}{T}$, then the modulus of $H\left(f + \frac{p}{2T}\right)$ and $H^*\left(f - \frac{p}{2T}\right)$ almost do not overlap for $p \neq 0$ and the numerator in Equation 4.13 tends to be equal to the denominator, which in turn means that the output kurtosis tends towards $\kappa_x$. This is in agreement with the so-called Papoulis rule [66], which states that the response to a narrowband filter will tend towards a Gaussian process, as the bandwidth of the filter tends to zero. Indeed, in the case of a very narrowband filter, close bursts may be smoothed out in the response leading to a more stationary response signal with a smaller kurtosis.

On the other hand, if the frequency of the modulator $\frac{1}{T}$ is less than half the bandwidth of the narrowband filter, then the numerator is maximised and the output kurtosis can be much higher than $\kappa_x$. Comparing Equation 4.13 and Equation 3.22 giving $\kappa_z$ and $\kappa_y$ respectively, it is clear that $\kappa_z \leq \kappa_y$. In other words, the output kurtosis $\kappa_z$ is always smaller than the input kurtosis $\kappa_y$, unless the frequency response function corresponds to an all pass system i.e. $H(f) \equiv 1$.

The proportion of bursts $r_b$ also plays an important role in maximising the output kurtosis. The smaller the proportion of bursts $r_b$, the more the Fourier coefficients $a_k$ are comparable to an impulse function, with a relatively high first value $a_0$ followed by comparatively small values with a small decay rate (see Figure 53 comparing the Fourier coefficients for two different values of $r_b$, obtained using Equation 3.23 linking the Fourier coefficients $a_k$ and $r_b$). On the other hand, a high value for the proportion of bursts $r_b$ will lead to a high values for the Fourier coefficients immediately following $a_0$ but with a lower decay rate. Therefore a large proportion of bursts will tend to increase the product $a_k a_{k-p}^*$ and thus increase the value for the output kurtosis $\kappa_z$. This means that the response signal obtained from an excitation with wider bursts will tend to be more leptokurtic. Inversely, a leptokurtic excitation signal containing very short bursts will be less successful in transmitting a high kurtosis value to the response.

Three cases of amplitude modulated excitations will be analysed next: excitation with no burst ($r_b = 0$), excitation with only bursts with no stationary portion inbetween ($r_b = 1$) and the general case where the excitation comprises bursts interlaced with stationary portions ($0 \leq r_b \leq 1$). In each case, the output kurtosis $\kappa_z$ will be calculated from Equation 4.13.

### 4.4.1 Response to an excitation with constant amplitude modulation

If $r_b = 0$, in other words, if the bursts of energy have a zero length $T_0 = 0$, then the excitation signal $y(t)$ is stationary random with variance ${\sigma_x}^2(B-A)^2$, where $(B-A)$ is the value of the "flat" or constant part of the modulation function.

The Fourier coefficients $a_k$ of the modulation function are zero except for $k = 0$, where $a_0 = B - A$. The numerator in Equation 4.13 is non-zero only when $p = 0$ and in this case it is equal to the denominator: therefore $\kappa_z = \kappa_x = 3.0$, as expected in the case of a stationary random Gaussian excitation.

### 4.4.2 Response to an excitation with successive bursts

If $r_b = 1$, then the excitation signal $y(t)$ is constantly oscillating, with a sine wave modulation function. The Fourier coefficients $a_k$ of the modulation function are all zero except $a_0 = B$ and $a_{-1} = a_1 = A/2$. Using these values for the coefficients $a_k$, Equation 4.13 is developed in Appendix B and the expression for the output kurtosis is:

$$\kappa_z = \left( 1 + \frac{A^2B^2}{2} \frac{\left| \int H\left(f+\frac{1}{2T}\right).\left\{S_x\left(f-\frac{1}{2T}\right)+S_x\left(f+\frac{1}{T}\right)\right\}.H^*\left(f-\frac{1}{2T}\right)df \right|^2}{\left| \int H(f).\left\{B^2S_x(f)+\frac{A^2}{4}S_x\left(f-\frac{1}{T}\right)+\frac{A^2}{4}S_x\left(f+\frac{1}{T}\right)\right\}.H^*(f)df \right|^2} + \frac{A^4}{8} \frac{\left| \int H\left(f+\frac{1}{T}\right).S_x(f).H^*\left(f-\frac{1}{T}\right)df \right|^2}{\left| \int H(f).\left\{B^2S_x(f)+\frac{A^2}{4}S_x\left(f-\frac{1}{T}\right)+\frac{A^2}{4}S_x\left(f+\frac{1}{T}\right)\right\}.H^*(f)df \right|^2} \right) \kappa_x \quad \text{Equation 4.14}$$

Note that for a narrowband system whose bandwidth is smaller than half the frequency of the modulator, then the modulus of $H\left(f+\frac{1}{T}\right)$ and $H^*\left(f-\frac{1}{T}\right)$ do not overlap and the numerators in Equation 4.14 tend to zero, which means that the output kurtosis $\kappa_z$ tends towards $\kappa_x$.

### 4.4.3 Response to an excitation with spaced bursts

In the general case, when $0 \leq r_b \leq 1$, the excitation comprises bursts interlaced with stationary portions. The Fourier coefficients $a_k$ of the modulation function are introduced and discussed in section 3.5 and given in Equation 3.23 as:

$$a_k = A.r_b.\left(1 + \frac{k^2}{(1/r_b)^2 - k^2}\right)\left(\frac{sin(\pi k r_b)}{\pi k r_b}\right) \qquad \text{Equation 3.23}$$

for all $k \neq 0$, and for $k = 0$, $a_0 = (B - A) + r_b A$.

Inserting Equation 3.23 in Equation 4.13, the output kurtosis can be calculated numerically. Note that the output kurtosis of the specific cases with no bursts or successive bursts are found by setting $r_b = 0$ and $r_b = 1$ respectively.

Figure 64 illustrates the relationship between the input and the output kurtosis when a leptokurtic input signal is filtered through a single degree of freedom system with various damping ratios. The degree of freedom system has a natural frequency at 150 Hz with damping ratios ranging from 1% to 10% of critical damping. The input signal is leptokurtic with a kurtosis value of 5. It was obtained by amplitude modulating a 100 second random noise sampled at 4096 Hz and centred around 100 Hz, with a 10 Hz bandwidth. The amplitude modulating function has the following characteristics: a period $T$ of 0.5 second with bursts lasting 0.02 second ($T_0$), which corresponds to a proportion of bursts $r_b = 4\%$. The vertical axis of Figure 64 compares the output kurtosis observed after a numerical simulation of a leptokurtic signal is filtered through a single degree of freedom system with various damping ratios represented with blue circles and the output kurtosis calculated using Equation 4.13 represented using red circles:

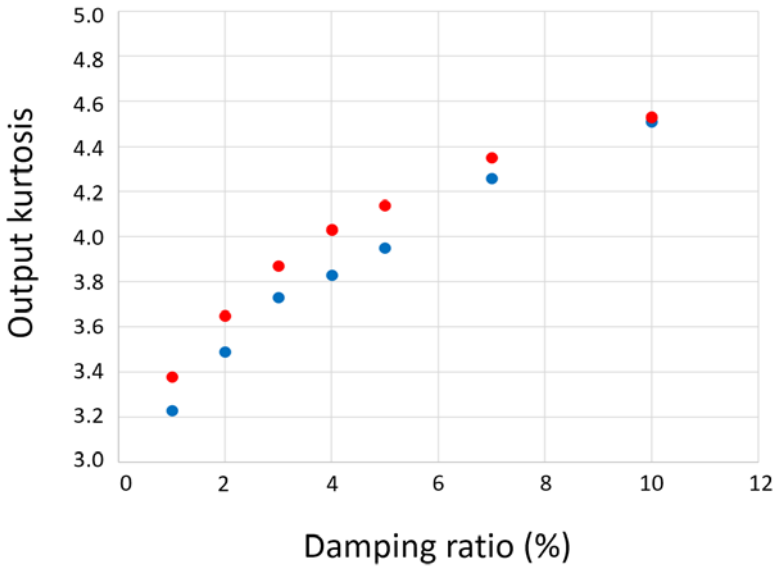


**Figure 64: Comparison of the output kurtosis obtained from numerical simulations (blue circles) and the theoretical expression (red circles) when filtered through a one degree of freedom system with various damping ratios.**

Figure 64 shows indeed that the output kurtosis is maximised when the system is highly damped. The output kurtosis calculated using Equation 4.13 is in good agreement with the output kurtosis observed after digital filtering with less than 5% error in this case. This over-prediction of the estimate of the kurtosis is explained later in this section.

Figure 65 illustrates the influence of the duration of the bursts to the output kurtosis when the leptokurtic signal is filtered through a single degree of freedom system. The degree of freedom system has a natural frequency at 150 Hz with a fixed damping ratio of 2 % of critical damping. The input signal is leptokurtic with a kurtosis value of 5. It was obtained by amplitude modulating a 100 second random noise sampled at 4096 Hz and centred around 100 Hz, with a 10 Hz bandwidth. The amplitude modulating function has the following characteristics: a period $T$ of 0.5 second with bursts duration $T_0$ ranging from 0.01 second to 0.08 second, which correspond to proportions of bursts $r_b$ ranging from 2% to 16%. The vertical axis of Figure 65 compares the output kurtosis observed after a numerical simulation of a leptokurtic signal with various bursts durations filtered through a single degree of freedom system represented with blue circles and the output kurtosis calculated using Equation 4.13 represented using red circles:

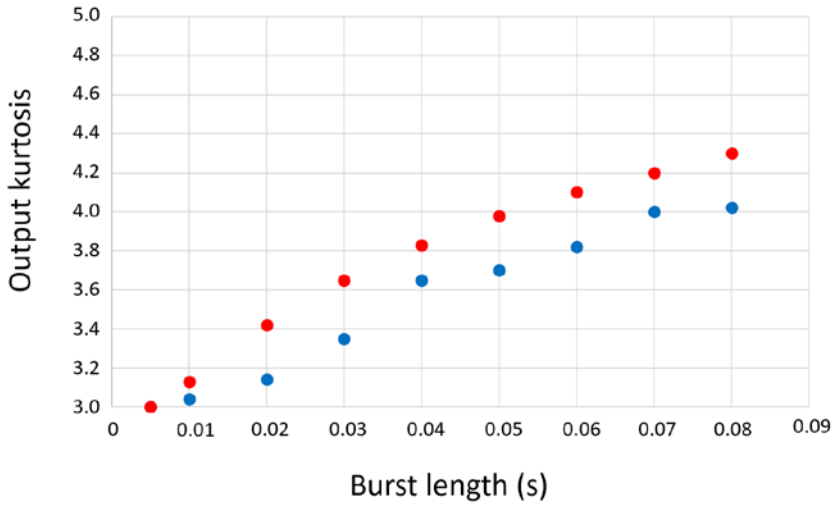


**Figure 65: Comparison of the output kurtosis obtained from numerical simulations (blue circles) and the theoretical expression (red circles) for various lengths of bursts when filtered through a one degree of freedom system**

Figure 65 shows indeed that the output kurtosis increases with the length of the bursts in the leptokurtic excitation signal. In practice, consider two leptokurtic excitation signals with same RMS and same kurtosis, one with very short, high amplitude bursts (e.g. almost instantaneous peaks) and the other with longer bursts with relatively smaller amplitudes. Once filtered through the same linear multimodal system with low damping, the kurtosis of the output signal due to the excitation with short bursts will be lower than the kurtosis of the output signal due to the excitation with longer bursts.

Note that the spacing of the bursts also has an important role. A larger period $T$ for the modulation function of the excitation signal will provide more kurtosis in output (for a fixed proportion of bursts $r_b$). Conceptually, once an excitation signal containing bursts close to each other is filtered through a system with low damping, the response due to one burst might not

have died out before the following burst appears, leading to a more stationary response with less pronounced excursions and therefore a smaller kurtosis.

The output kurtosis calculated using Equation 4.13 is in good agreement with the output kurtosis observed after digital filtering. It provides a conservative estimate of the kurtosis of a response signal with typically less than 10% error. This conservatism is due to a number of reasons, the main one being that the bursts in the time domain numerical simulations are randomly positioned in time, sometimes getting close to each other (without overlapping though, see section 3.5), whereas the algorithm considers that the modulation function is periodic and hence the bursts are equidistant in time. The error between the output kurtosis calculated and observed would reduce considerably if the bursts were occurring at a fixed period and the error would tend to zero as the duration of the input signal increases.

Equation 4.13 gives the kurtosis of the response knowing the characteristics of the modulation function used to create a nonstationary excitation signal and the dynamic characteristics of a single or multi-degree of freedom linear system. Equation 4.13 is valid for non-stationary excitation signals with high amplitude excursions obtained by amplitude modulation with a periodic modulation function. This section gave mathematical expressions showing why and how a narrowband LTI filter tends to turn a nonstationary excitation signal with high amplitude excursions into a stationary and Gaussian signal.

## 4.5 Comparison of the output kurtosis from the two leptokurtic signal generation techniques

The resulting kurtosis values after the filtering of leptokurtic signals generated using both the polynomial transform approach and the amplitude modulation technique are compared using example signals filtered through various linear systems.

As an illustration, the same example of a leptokurtic excitation signal considered in section 3.4.2 is used here. Both leptokurtic signal generation techniques were used to produce excitation signals with a kurtosis value of 12 and an RMS value of 4.02g. The excitation signals were then filtered through bi-modal linear systems with natural frequencies 200 and 350 Hz and modal damping ratios ranging from 1% to 10%. Figure 66 illustrates the various gains of the FRF of the linear systems used, in units of MPa/g.

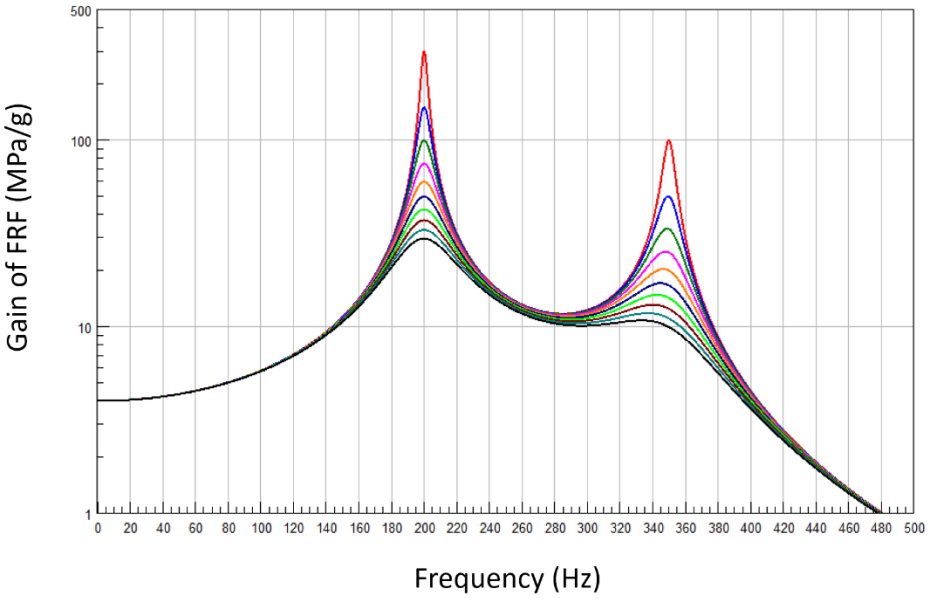


**Figure 66: The modulus of the bimodal FRF representing a linear system with modes nominally at 200 and 350 Hz, and with modal damping ratios ranging from 1% (red) to 10% (black)**

The values for the output kurtosis of the bimodal system using the expressions given in this chapter are compared in Figure 67. Note that the characteristic of the modulation function considered were a period of 0.25 second and a burst length of 0.03 second (so a proportion of bursts of 12%).The calculated kurtosis corresponding to the steady leptokurtic signal are represented using circles, the calculated kurtosis corresponding to the nonstationary leptokurtic signal are represented using triangles.

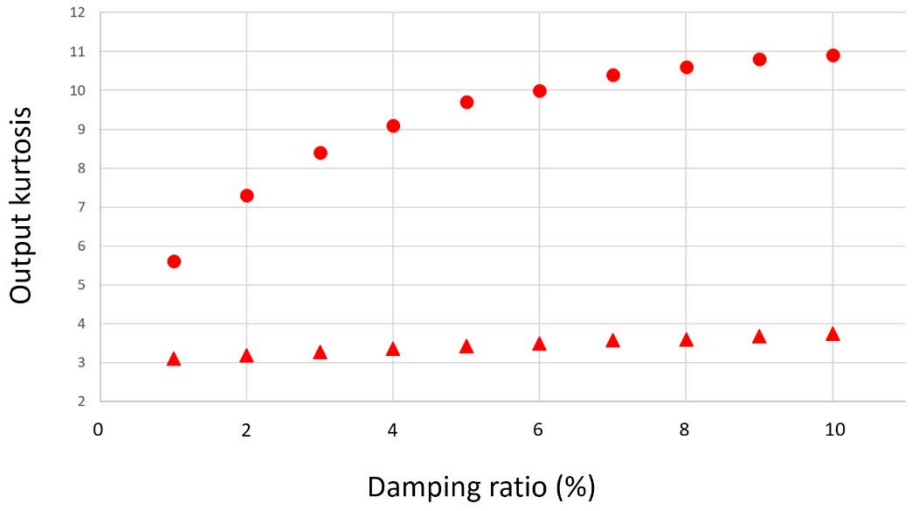


**Figure 67: Comparison of the theoretical output kurtosis from a stationary leptokurtic excitation (triangles) and from a nonstationary leptokurtic excitation (circles)**

Figure 67 reveals that using an amplitude modulation technique (with sufficiently long and spaced bursts) can be far more effective in terms of output kurtosis than using a polynomial transform technique, which essentially creates instantaneous peaks in the excitation signal.

## 4.6 Conclusions

Chapter 4 provided the theoretical expressions that can be used to predict the non-Gaussian characteristics of the output response or stress signal, knowing the non-Gaussian characteristics of the input excitation signal; without the need for numerical simulations. Characterising the input excitation with its PDF or its kurtosis alone is not sufficient. For instance, a nonstationary signal comprising long bursts and a non-Gaussian steady state signal may have similar kurtosis and even similar PDFs but they will produce very different responses with different PDFs once filtered. Original formulations were proposed that give the statistics of the response due to specific non-Gaussian random signals, including steady non-Gaussian loadings and non-stationary signals with high amplitude excursions.

In the case of leptokurtic excitation signals, the kurtosis of the response is generally lower than the kurtosis of the excitation signal i.e. the LTI system tends to make the output signal Gaussian. This phenomenon is more pronounced as the bandwidth of the LTI system reduces, in agreement with the so-called Papoulis rule [66]. This phenomenon was explained mathematically for both cases of leptokurtic excitations studied in this thesis; stationary leptokurtic signals obtained by applying a polynomial transform and nonstationary leptokurtic signals obtained by amplitude modulation. The kurtosis of a response signal due to a non-Gaussian stationary excitation to an LTI system will be maximised when the system is heavily damped and if the excitation signal is narrowband. In the case of a signal due to an amplitude modulated nonstationary exciting an LTI system, the kurtosis of the response will be maximised when the system is heavily damped and if the frequency of the modulator is small compared to the bandwidth of the LTI system. In both cases, the minimum kurtosis obtained for the response signal is 3.0 and the maximum kurtosis cannot exceed the kurtosis of the excitation.

The amplitude modulation technique for generating leptokurtic excitation signals can produce filtered responses with much higher kurtosis values compared to the kurtosis obtained from polynomial transformed excitations. In the case of an amplitude modulated excitation, the level of the response kurtosis depends on the distance between the bursts and the length of the bursts, which can be set by the user.

Chapter 5 will propose formulations to predict the various statistical distributions for a non-Gaussian stress response, knowing the non-Gaussian characteristics of the stress response without the need for numerical simulations. This will allow one to compute fatigue damage and fatigue life knowing the excitation PSD with its associated non-Gaussian characteristics (clipping level or kurtosis value) and the dynamic characteristics of the linear system representing the mechanical component subjected to the random non-Gaussian excitation.

# 5 Distributions of the peaks and rainflow ranges for filtered non-Gaussian processes

## 5.1 Introduction and assumptions

Various non-Gaussian excitation signals were studied in chapter 3, with chapter 4 introducing the means to predict their time averaged kurtosis after linear filtering. This chapter focusses on the stress response and more specifically on the distributions of its instantaneous values, the distributions of its peaks and the distributions of its rainflow cycles. Statistical approaches will be presented to predict these distributions.

The distribution of the instantaneous values, the distribution of the peaks and the distribution of the rainflow cycles for a stationary Gaussian random stress response have been documented in many places [15, 16, 19, 20, 21, 26, 27, 28, 29, 31], but the expressions are not applicable to non-Gaussian random stress responses. Several spectral approaches exist in the literature to address the non-Gaussian random stress responses [50, 94, 95, 96, 97, 56]. These latter approaches provide analytical formulae to derive the level cross counting histogram, the peak distributions or the distribution of the rainflow cycles from the stress response spectrum and a prescribed kurtosis value. Typically, they do not study the transfer of the non-Gaussian features from the excitation to the response due to the dynamic characteristics of the mechanical component. Moreover, they are often based on a polynomial transform approach and are therefore more adapted to the specific type of steady leptokurtic stress responses.

The previous chapter showed that the non-Gaussian features of an input signal are still present, to a certain extent, in the output response of a linear filter. When the response is non-Gaussian, the use of spectral methods developed under the Gaussian assumption can lead to underestimates of the number of high level cycles and their related fatigue damage contribution [50, 42].

The main aim of this chapter is to predict the various statistical distributions for a non-Gaussian stress response, knowing the non-Gaussian characteristics of the stress response without the need for numerical simulations. Formulations are proposed that give the various distributions of the response due to specific filtered non-Gaussian random signals, including steady non-Gaussian loadings and non-stationary excitations with high amplitude excursions.

The diagram presented in Figure 68 illustrates the inputs and results obtained in this chapter, more specifically related to the kurtosis.

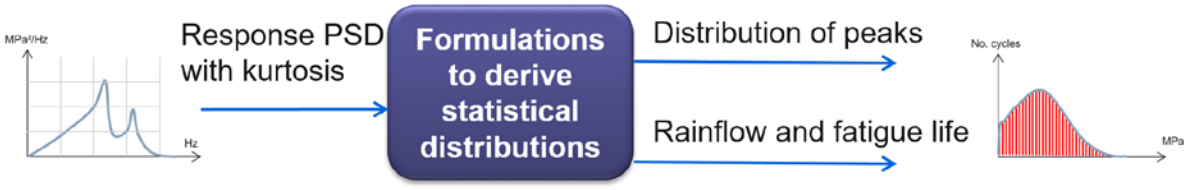


**Figure 68 : Inputs required and results obtained in this chapter in the case of kurtosis controlled excitations**

In the case where a structure is designed against static failure (see section 2.5), it is useful to predict what maximum stress value could be present in the leptokurtic random response. This chapter also provides formulations to predict the maximum value of the response due to specific non-Gaussian random signals, that might occur during the exposure duration.

The characteristics of the responses to several specific excitations will be considered next: stationary random inputs, stationary polynomial transformed leptokurtic excitations and non-stationary amplitude modulated loadings excitations.

For each of the specific non-Gaussian excitations considered, the response is assumed to be of the same nature as the excitation. For instance, the response due to a stationary leptokurtic random excitation can be approximated as a polynomial transform of the stationary Gaussian response of the identical linear system when subjected to a Gaussian excitation having the same RMS as the non-Gaussian excitation. Similarly, an amplitude modulated signal remains amplitude modulated after linear filtering.

## 5.2 PDF of instantaneous values in the response resulting from non-Gaussian excitations

For all the cases presented below, the stress response is represented by a PSD, calculated using Equation 2.82 with an associated kurtosis value calculated using either Equation 4.9 (for steady non-Gaussian excitations) or Equation 4.13 (for nonstationary excitations). In this section, it is proposed to predict the distributions of the instantaneous response values, the peaks and the ranges from the response PSD and response kurtosis only.

### 5.2.1 PDF of instantaneous values in the response resulting from a stationary, leptokurtic random excitation

Two types of clipped excitations are described in chapter 3: a Gaussian random signal can be indeed truncated at a given level (a so-called brick wall limiting or abrupt clipping), or compressed (soft limiting). Both techniques generate a stationary non-Gaussian signal.

It is assumed that the response due to a stationary leptokurtic random excitation can be approximated as a polynomial transform of the stationary Gaussian response of the identical linear system when subjected to a Gaussian excitation having the same RMS as the non-Gaussian excitation.

Winterstein [50] proposed a monotonic function $g$ acting as a zero-memory nonlinear system to model leptokurtic responses. For more details on the polynomial transform technique, please refer to section 3.4. In the case of a zero mean, symmetric, standardised Gaussian signal $x(t)$, the transformation $g$ that allows one to obtain $z(t)$ is given by Equation 3.9. Winterstein [50] also gave the inverse transform. When used with $\tilde{h}_3 = 0$ (i.e. zero skewness – see section 3.4), the inverse transform $g^{-1}\big(z(t)\big)$ giving a centred Gaussian random signal with unit variance $x(t)$ is:

$$x = \left( \sqrt{\left( \frac{z}{2K\tilde{h}_4\sigma_z} \right)^2 + \left( \frac{1-3\tilde{h}_4}{3\tilde{h}_4} \right)^3} + \frac{z}{2K\tilde{h}_4\sigma_z} \right)^{\frac{1}{3}} - \left( \sqrt{\left( \frac{z}{2K\tilde{h}_4\sigma_z} \right)^2 + \left( \frac{1-3\tilde{h}_4}{3\tilde{h}_4} \right)^3} - \frac{z}{2K\tilde{h}_4\sigma_z} \right)^{\frac{1}{3}}$$

Equation 5.1

where $\sigma_z$ is the RMS value of the response signal calculated using Equation 4.1 and where $K$ and $\tilde{h}_4$ are the same coefficients as in Equation 3.9, which are defined as:

$$K = \frac{1}{\sqrt{1 + 6\tilde{h}_4{}^2}}$$

$$\tilde{h}_4 = \frac{\sqrt{1 + 1.5(\kappa_z - 3)} - 1}{18}$$

where $\kappa_z$ is the output kurtosis value calculated in Equation 4.9.

The derivative of the transformation $g$ is given by:

$$\frac{dz}{dx} = g'(x) = \frac{K}{\sigma_x}\left(1 - 3\tilde{h}_4 + 3\tilde{h}_4\frac{x^2}{\sigma_x{}^2}\right)$$

Equation 5.2

Since the transformation $g$ is a piecewise one-to-one monotonic function, the PDF transform (see section 2.1.8) can be applied to obtain the PDF of instantaneous values for the response. The PDF for the response $z(t)$ is hence obtained as:

$$p_z(z) = \frac{p_x\left(g^{-1}(z)\right)}{\left|g'\left(g^{-1}(z)\right)\right|}$$

Equation 5.3

where $p_x$ is a Gaussian PDF with unit variance.

As an illustration, the same example of a leptokurtic signal considered in section 3.4.2 is used here. A prescribed kurtosis value of 12 was used and the signal has an RMS value of 4.02. Figure 48 shows an extract of the leptokurtic signal obtained. This excitation signal was then filtered through a bi-modal linear system with natural frequencies 200 and 350 Hz and a modal damping ratio of 5%. Figure 69 illustrates the gain of the FRF of the linear system used, in units of MPa/g.

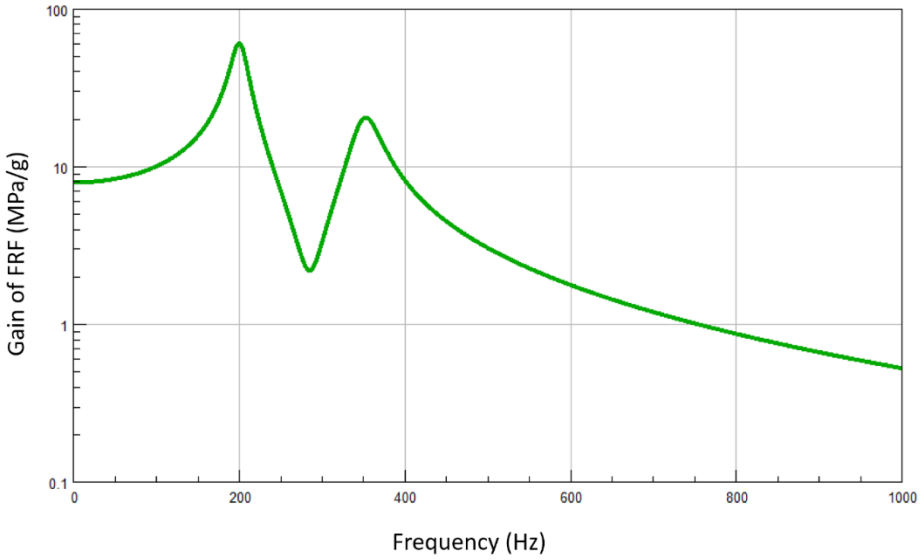


**Figure 69: The modulus of the bimodal FRF representing a linear system with modes nominally at 200 and 350 Hz, and with 5% modal damping**

Both the theoretical approach and numerical simulations were carried out. The theoretical method is using a purely spectral approach, whereas numerical simulations use realisations of time histories. The response signal obtained from numerical simulations has an RMS value of 52 MPa and a kurtosis of 4. When using the theoretical expressions given in chapter 4, the RMS value for the stress response calculated from Equation 4.1 is 52 MPa and the output kurtosis value calculated using Equation 4.9 is 4, which is in very good agreement with the values observed from numerical simulations. The irregularity factor is 0.78, which means the response has to be considered broadband (see section 2.2.8 for more details on the irregularity factor).

Figure 70 shows the normalised PDF of the stress response obtained from time domain numerical simulations (in blue), overlaid with the theoretical PDF obtained using Equation 5.3 using a red line and with the theoretical distribution corresponding to a Gaussian random response signal with same RMS using a dashed black line. The horizontal axis represents normalised stress, i.e. the stress divided by the RMS value.

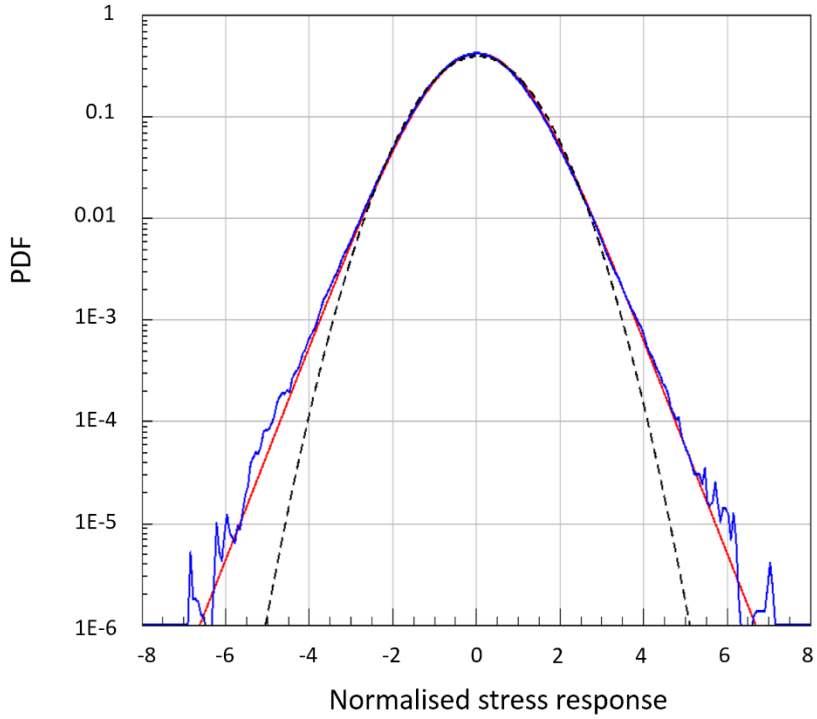


**Figure 70: The PDF of the response to the bimodal linear system from numerical simulations (blue), from the theoretical prediction (red) and using the Gaussian assumption (dashed black)**

The theoretical PDF obtained using Equation 5.3 (red) is a good fit of the PDF of the stress response obtained from time domain numerical simulations. Even though the response kurtosis is only 4, assuming a Gaussian response (dashed black) dramatically underestimates the response PDF, especially for high response levels where fatigue damage might occur.

### 5.2.2 PDF of instantaneous values in the response resulting from a clipped excitation

Winterstein [15] proposed a monotonic function $g$ acting as a zero-memory nonlinear system to model hardening responses, that is, platykurtic responses with kurtosis < 3. It uses Hermite polynomials to approach a non-Gaussian distribution and is perfectly suited for mild deviations from a normal law. In the case of a symmetric, standardised Gaussian signal $x(t)$, the inverse transform $g^{-1}(z(t))$ giving a centred Gaussian random signal with unit variance $x(t)$ is:

$$x = \left(1 + 3\tilde{h}_4\right)\frac{z}{K\sigma_z} - \tilde{h}_4\left(\frac{z}{K\sigma_z}\right)^3 \qquad \text{Equation 5.4}$$

where $\sigma_z$ is the RMS value of the response signal calculated using Equation 4.1 and where $K$ and $\tilde{h}_4$ are defined for hardening responses as [42]:

$$K = \frac{1}{\sqrt{1 + 6\tilde{h}_4{}^2}}$$

$$\tilde{h}_4 = \frac{\kappa_z - 3}{24}$$

where $\kappa_z$ is the output kurtosis value calculated in Equation 4.9.

The monotonic function $g$ acting as a zero-memory nonlinear system to model hardening responses, that is, platykurtic responses with kurtosis < 3 can be calculated as the inverse of the expression given in Equation 5.4 and expressed as:

$$\frac{z}{K\sigma_z} = \left(\sqrt{\left(\frac{x}{2\tilde{h}_4}\right)^2 - \left(\frac{1+3\tilde{h}_4}{3\tilde{h}_4}\right)^3} - \frac{x}{2\tilde{h}_4}\right)^{\frac{1}{3}} - \left(\sqrt{\left(\frac{x}{2\tilde{h}_4}\right)^2 - \left(\frac{1+3\tilde{h}_4}{3\tilde{h}_4}\right)^3} + \frac{x}{2\tilde{h}_4}\right)^{\frac{1}{3}} \quad \text{Equation 5.5}$$

The derivative of the transformation $g$ is calculated as:

$$\frac{dz}{dx} = g'(x) = \frac{K\sigma_z}{3}\left(\frac{\frac{x}{4\tilde{h}_4^2}}{\sqrt{\left(\frac{x}{2\tilde{h}_4}\right)^2 - \left(\frac{1+3\tilde{h}_4}{3\tilde{h}_4}\right)^3}} - \frac{1}{2\tilde{h}_4}\right)\left(\sqrt{\left(\frac{x}{2\tilde{h}_4}\right)^2 - \left(\frac{1+3\tilde{h}_4}{3\tilde{h}_4}\right)^3} - \frac{x}{2\tilde{h}_4}\right)^{-\frac{2}{3}} - \frac{K\sigma_z}{3}\left(\frac{\frac{x}{4\tilde{h}_4^2}}{\sqrt{\left(\frac{x}{2\tilde{h}_4}\right)^2 - \left(\frac{1+3\tilde{h}_4}{3\tilde{h}_4}\right)^3}} + \frac{1}{2\tilde{h}_4}\right)\left(\sqrt{\left(\frac{x}{2\tilde{h}_4}\right)^2 - \left(\frac{1+3\tilde{h}_4}{3\tilde{h}_4}\right)^3} + \frac{x}{2\tilde{h}_4}\right)^{-\frac{2}{3}} \quad \text{Equ. 5.6}$$

As discussed in chapter 3, the zero-memory nonlinear function $g$ is an approximate solution using only the first four Hermite coefficients $\tilde{h}_n$ (only $\tilde{h}_4$ in this case) and neglecting the high order coefficients and the cross terms $\tilde{h}_n\tilde{h}_m$. This approximation is considered sufficient to capture the mild non-Gaussian characteristics of the signal generated [50, 42]

Since the transformation $g$ is a piecewise one-to-one monotonic function, the PDF transform (see section 2.1.8) can be applied to obtain the PDF of instantaneous values for the response. The PDF for the response $z(t)$ is expressed using Equation 5.3 from the previous section:

$$p_z(z) = \frac{p_x\left(g^{-1}(z)\right)}{\left|g'\left(g^{-1}(z)\right)\right|} \quad \text{Equation 5.3}$$

where $p_x$ is a Gaussian PDF with unit variance.

As an illustration, the same example of a leptokurtic signal considered in section 3.3.2 is used here. An abrupt clipping technique was used with a prescribed crest factor of 2. The clipped signal obtained has an RMS value of 3.85, i.e. smaller than the 4.02 obtained with the original Gaussian signal generated before clipping. Figure 45 shows an extract of the clipped signal obtained. This excitation signal was then filtered through a bi-modal linear system with natural

frequencies 200 and 350 Hz and damping ratio of 5%. Figure 69 illustrates the gain of the FRF of the linear system used, in units of MPa/g.

Both the theoretical approach and numerical simulations were carried out. The theoretical method is using a purely spectral approach, whereas numerical simulations use realisation of time histories. The response signal obtained from numerical simulations has an RMS value of 49 MPa and a kurtosis of 2.95. When using the theoretical expressions given in chapter 4, the RMS value for the stress response calculated from Equation 4.1 is 49 MPa and the output kurtosis value calculated using Equation 4.9 is 2.95, which is in excellent agreement with the values observed from time domain numerical simulations.

Figure 72 shows the normalised PDF of the stress response obtained from time domain numerical simulations (in blue), overlaid with the theoretical PDF obtained using Equation 5.3 using a red line and with the theoretical distribution corresponding to a Gaussian random response signal with same RMS using a dashed black line. The horizontal axis represents normalised stress, i.e. the stress divided by the RMS value.

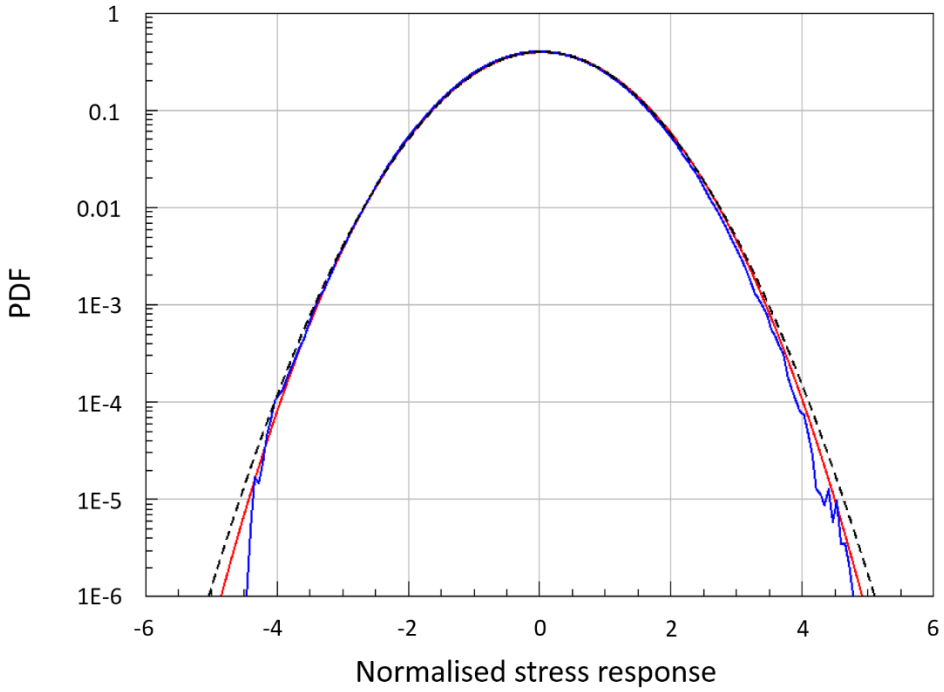


**Figure 71: The PDF of the platykurtic response to the bimodal linear system from numerical simulations (blue), from the theoretical prediction (red) and using the Gaussian assumption (dashed black)**

The theoretical non-Gaussian PDF obtained using Equation 5.3 (red) shows indeed a lower probability of obtaining instantaneous values of the response occurring at a high levels. The theoretical non-Gaussian PDF obtained is a good fit of the PDF observed from the time domain simulations (blue), although it slightly overestimates the probability of values occurring at a high level. This last observation can be explained by the finite length of the time series simulations. The proposed theoretical PDF is conservative and closer to the results than when assuming a Gaussian response (dashed black), especially for high response levels, where fatigue damage might occur.

### 5.2.3 PDF of instantaneous values in the response resulting from an amplitude modulated excitation

The stress response is assumed to be of the same nature as the input signal, i.e. amplitude modulated. The response signal is therefore made of a stationary Gaussian signal multiplied by a periodic, modulating signal. The output modulating function is assumed to have excursions made of the same waveform as in the input modulating function (i.e. sine bursts), occurring at the same rate but having a different amplitude due to the filtering process. The reader is referred to section 3.5 for more details on the modulation function. Although, it is expected that the modulating function be distorted by the convolution with the system impulse response, this assumption is adopted for practical reasons.

The stress response $z(t)$ is nonstationary random with a constant (zero) mean and a time-dependent variance. The variance increases in the vicinity of a burst and decreases to a lower, steady value between the bursts of energy. The response is therefore considered as being the concatenation of:

- a stationary part lasting $(1 - r_b)T$ seconds over a period of $T$ seconds,
- an oscillating part lasting $r_b T$ seconds over a period of $T$ seconds.

The output kurtosis for a cyclostationary excitation is given in Equation 4.13. The first objective is therefore to find the characteristics of the amplitude modulating signal, i.e. the amplitude of the bursts which is used to produce the calculated output kurtosis.

Using the same logic as in section 3.5, the second and fourth statistical moments of the amplitude modulated response are calculated as a weighted sum of the second and fourth statistical moments of the stationary and the amplitude modulated signals respectively:

$$E[z^2] = {\sigma_{sr}}^2 r_b \left( \frac{{A_r}^2}{2} + {B_r}^2 \right) + {\sigma_{sr}}^2 (1 - r_b)(B_r - A_r)^2 \qquad \text{Equation 5.7 (a)}$$

$$E[z^4] = 3{\sigma_{sr}}^4 r_b \left( \frac{3}{8} {A_r}^4 + {B_r}^4 + 3{A_r}^2 {B_r}^2 \right) + 3{\sigma_{sr}}^4 (1 - r_b)(B_r - A_r)^4 \qquad \text{(b)}$$

where ${\sigma_{sr}}^2$ is the variance of the stationary response (which is amplitude modulated), $A_r$ and $B_r$ are the amplitude and offset of the modulation function applied to the stationary response respectively and $r_b$ is the proportion of the burst deviation in a period.

The output kurtosis is expressed as:

$$\kappa_z = 3 \cdot \frac{r_b \left( \frac{3}{8} {A_r}^4 + {B_r}^4 + 3{A_r}^2 {B_r}^2 \right) + (1 - r_b).(B_r - A_r)^4}{\left( r_b . \left( \frac{{A_r}^2}{2} + {B_r}^2 \right) + (1 - r_b)(B_r - A_r)^2 \right)^2} \qquad \text{Equation 5.8}$$

The system of equations given in Equation 5.7 can be simplified. The variance of the nonstationary response $E[z^2]$ and the variance of the underlying stationary response ${\sigma_{sr}}^2$ are both calculated from Equation 4.1 and are equal, i.e. $E[z^2] = {\sigma_{sr}}^2$. Also, by definition of the kurtosis, the fourth moment of the response signal $E[z^4]$ can be substituted with $\kappa_z E[z^2]^2$.

The objective is therefore to solve the system of equations given in Equation 5.7 to find the unknown coefficients $A_r$ and $B_r$ for a prescribed output kurtosis value $\kappa_z$ and a given proportion of bursts $r_b$. Newton's method [100] can be used to solve the system of nonlinear equations in Equation 5.7. This type of iterative algorithm requires initial estimates for $A_r$ and $B_r$ to converge more rapidly. The original values $A$ and $B$, representing the amplitude and the offset of the modulation function of the excitation, can be taken as initial estimates. Routines based on Newton's method such as zeros_sys_eqn in IMSL [101] can be used to solve the system of nonlinear equations using the initial estimates provided.

In the general case, when $0 \leq r_b \leq 1$, the global PDF of $z(t)$ is a weighted sum of the PDFs of :

- the stationary part (see Equation 3.14) that is present during $(1 - r_b)$ of a period,
- the purely oscillating part (see Equation 3.16) that is present $r_b$ of a period,

The PDF of the concatenated time history can be calculated using Equation 2.67 in chapter 2.3.1 as a weighted sum of PDFs. The global PDF of $z(t)$ can be expressed as:

$$p_z(z) = \frac{(1-r_b)}{\sqrt{2\pi}.(B_r - A_r).\sigma_z} e^{-\frac{z^2}{2.(B_r-A_r)^2{\sigma_z}^2}} + \frac{r_b}{\sqrt{2\pi}.\pi.\sigma_z} \int_{\frac{z}{A_r+B_r}}^{\frac{z}{B_r-A_r}} e^{-\frac{a^2}{2.{\sigma_z}^2}} \frac{1}{\sqrt{a^2{A_r}^2 - (z - aB_r)^2}} da \qquad \text{Equation 5.9}$$

This equation is similar to Equation 3.18, that gives the PDF of the input excitation. No closed form solution to the integral in Equation 5.9 has been found. It is therefore recommended to use a numerical integration to solve it.

As an illustration, the same example of a leptokurtic signal considered in section 3.5.2 is used here. A prescribed kurtosis value of 12 was used and the signal has an RMS value of 4.02. Figure 54 shows an extract of the leptokurtic signal obtained. This excitation signal was then filtered through a bi-modal linear system with natural frequencies 200 and 350 Hz and damping ratio of 5%. Figure 69 illustrates the gain of the FRF of the linear system used, in units of MPa/g.

Both the theoretical approach and numerical simulations were carried out. The theoretical method is using a purely spectral approach, whereas numerical simulations use realisation of time histories. The response signal obtained from numerical simulations has an RMS value of 52 MPa and a kurtosis of 8.4. When using the theoretical expressions given in chapter 4, the RMS value for the stress response calculated from Equation 4.1 is 52 MPa and the output kurtosis value calculated using Equation 4.9 is 9, which is in agreement with the values observed from numerical simulations.

Figure 72 shows the PDF of the stress response obtained from time domain numerical simulations (in blue), overlaid with the theoretical PDF obtained using Equation 5.9 using a red

line and with the theoretical distribution corresponding to a Gaussian random response signal with same RMS using a dashed black line.

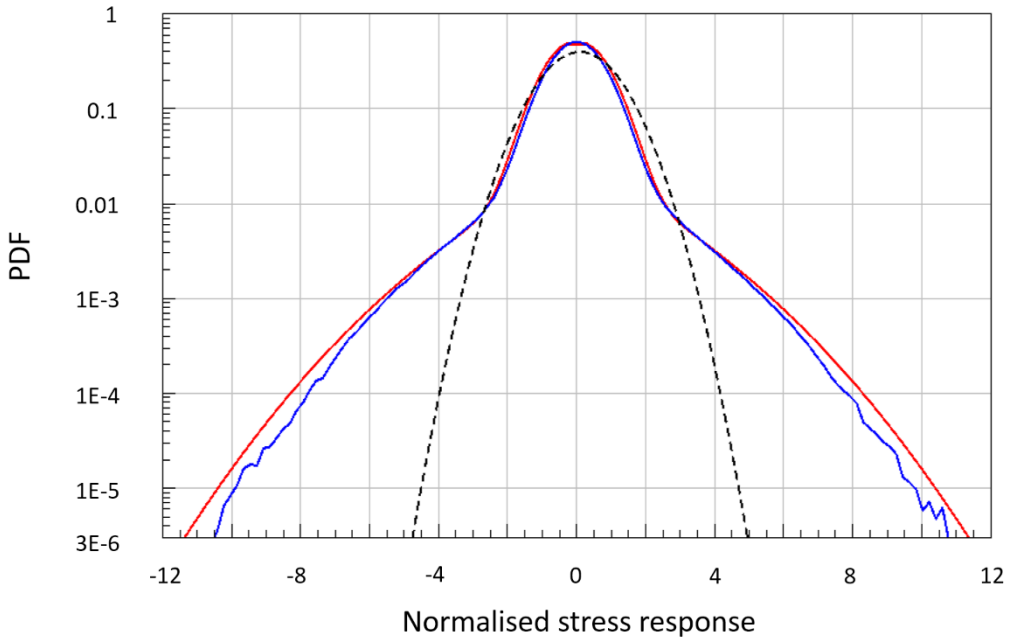


**Figure 72: The PDF of the response to the bimodal linear system from numerical simulations (blue), from the theoretical prediction (red) and using the Gaussian assumption (dashed black)**

The theoretical non-Gaussian PDF obtained using Equation 5.9 (red) is indeed made of two constituents. This is revealed by the change in slope in its shape. The theoretical non-Gaussian PDF obtained is matching the curvature of the PDF observed from the time domain simulations (blue), although it slightly overestimates the probability of values occurring at the higher levels. This last observation can be explained by the finite length of the time series simulations. The proposed theoretical PDF is conservative and much closer than the expected results than when assuming a Gaussian response (dashed black), especially for high response levels where fatigue damage might result.

Figure 70 and Figure 72 can be compared, because both result from an excitation with the same kurtosis value exciting the same bimodal system. Figure 70 is due to a steady leptokurtic excitation, whereas Figure 72 is due to a nonstationary leptokurtic excitation. After the filtering process, the response signal obtained from the latter has a much higher kurtosis value and shows a much higher probability of values occurring at a higher levels.

## 5.3 Peak response distribution in the response resulting from non-Gaussian excitations

The derivation of theoretical expressions to predict the distribution of the peaks for the various non-Gaussian cases studied is proposed in this section as an original contribution.

### 5.3.1 Peak response distribution in the response resulting from a stationary, leptokurtic random excitation

In the case of a stationary leptokurtic excitation, the distribution of the peaks $p_{z_p}$ for the response $z(t)$ is based on the PDF transform of the PDF for the peaks corresponding to a Gaussian case. The peak PDF $p_{z_p}$ for the response $z(t)$ is hence obtained as:

$$p_{z_p}(z) = \frac{p_{x_p}\left(g^{-1}(z)\right)}{\left|g'\left(g^{-1}(z)\right)\right|} \qquad \text{Equation 5.10}$$

where $p_{x_p}$ is the peak distribution for a Gaussian process with unit variance, as defined in Equation 2.54, $g'$ is the derivative of the monotonic function $g$ used to model the leptokurtic response, as defined in Equation 3.9 and $g^{-1}$ its inverse.

The following example uses the same response signal as in section 5.2.1. This response signal was obtained from a leptokurtic signal with kurtosis 12 described in section 3.4.2, filtered using a bi-modal linear system whose gain is represented in Figure 69. Figure 73 illustrates the normalised PDF of the stress peaks obtained from time domain numerical simulations (in blue), overlaid with the theoretical PDF of the stress peaks obtained using Equation 5.10 using a red line and with the theoretical distribution corresponding to a Gaussian random response signal with the same (unitary) RMS shown by the dashed black line.

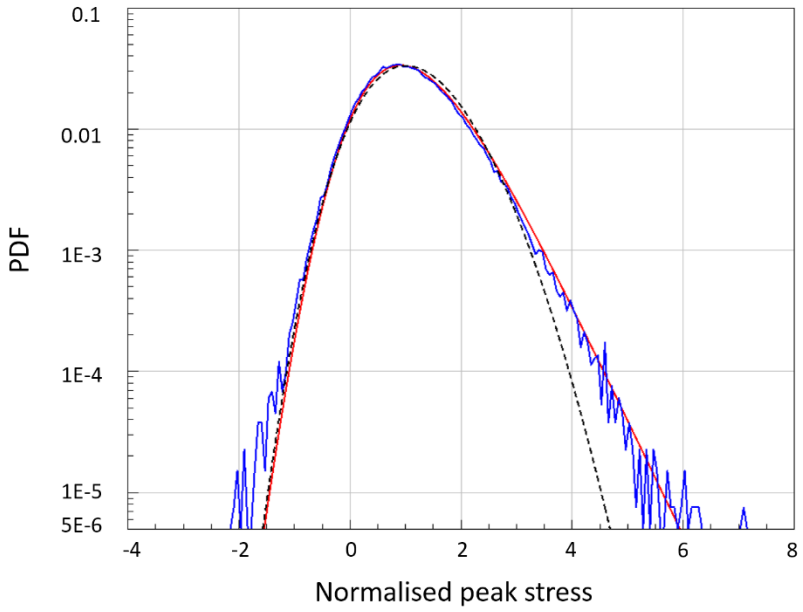


**Figure 73: The peak distributions for the leptokurtic response of the bimodal linear system from numerical simulations (blue), from the theoretical expression (red) and using the Gaussian assumption (dashed black)**

Once again, the theoretical distribution provides a very good fit for the probability of finding peaks. Due to the finite length of the simulated signal, the peak PDF obtained from time domain numerical simulations is not well defined at high positive response levels but the theoretical distribution seems to provide a good estimate of the mean probability of finding peaks, especially for positive values of the peaks. Apart from the extreme values, there is a slight overestimation of the probability of finding positive stress peaks due to the fact that the instantaneous peaks in the response are actually smoothed by the filtering process, making them less sharp and smaller in amplitude than expected by the polynomial transform modelling.

Note that the distribution of the valleys is equally as well predicted, especially for the negative valleys. The negative peaks (and positive valleys) are underestimated by this approach, but this is less problematic since the rainflow cycles are built by pairing the peaks and valleys of equal magnitude (see section 5.5) and the large cycles are of particular interest compared to the small cycles for the assessment of fatigue and strength of a material. When assuming a Gaussian response (dashed black in Figure 73) the theoretical peak distribution underestimates dramatically the response PDF, especially for high response levels, where fatigue damage might occur.

Other example results are shown in Appendix E. One is showing the theoretical output kurtosis and peak distribution obtained from the same input signal and the same FRF but with a lighter damping ratio of 2% (see Figure 89) and the other one is using a unimodal FRF with only the resonance at 200 Hz and still with a lighter damping ratio of 2% (see Figure 90). The theoretical approach gives equally as good results in both cases. Note that the case presented in this chapter is considered as a quite extreme one, because the kurtosis value chosen for the excitation signal is quite high in practice and the response signal is rather broadband (with an irregularity factor of 0.78) and tends to show a higher kurtosis value of 4.0 compared to the cases shown in appendix E.

### 5.3.2 Peak response distribution in the response resulting from a clipped excitation

In the case of a platykurtic excitation, the distribution of the peaks $p_{z_p}$ in the response $z(t)$ is based on the PDF transform of the PDF for the peaks corresponding to a response under a Gaussian excitation. The peak PDF $p_{z_p}$ for the response $z(t)$ is expressed using Equation 5.10 from the previous section:

$$p_{z_p}(z) = \frac{p_{x_p}\left(g^{-1}(z)\right)}{\left|g'\left(g^{-1}(z)\right)\right|} \qquad \text{Equation 5.10}$$

where $p_{x_p}$ is the peak distribution for a Gaussian process with unit variance, as defined in Equation 2.54, $g'$ is the derivative of the monotonic function $g$ used to model the platykurtic response, as defined in Equation 5.5 and $g^{-1}$ its inverse.

The following example uses the same response signal as in section 5.2.2. Figure 74 illustrates the normalised PDF of the stress peaks obtained from time domain numerical simulations (in

blue), overlaid with the theoretical PDF of the stress peaks obtained using Equation 5.10 using a red line and with the theoretical distribution corresponding to a Gaussian random response signal with the same (unitary) RMS shown by the dashed black line.

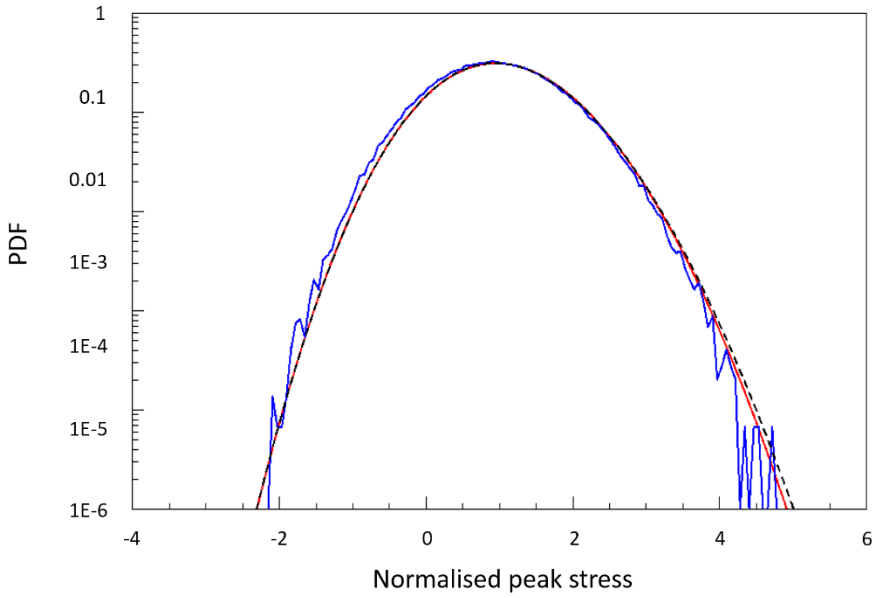


**Figure 74: The peak distributions for the platykurtic response of the bimodal linear system from numerical simulations (blue), from the theoretical expression (red) and using the Gaussian assumption (dashed black)**

As previously, the theoretical distribution provides a good fit for the probability of finding peaks. The theoretical peak PDF is closer to the results from the time domain simulations than when assuming a Gaussian response (dashed black). The theoretical peak PDF is slightly conservative as it slightly overestimates the probability of finding peaks at high response levels where fatigue damage might occur.

### 5.3.3 Peak response distribution in the response resulting from an amplitude modulated excitation

In the case of an amplitude modulated excitation, the peaks of the output signal are obtained by multiplying the peaks of the underlying stationary Gaussian signal by the modulating function. Therefore the peak distribution of the response can be calculated using the rule to find the PDF of the product of two independent random variables, namely the peaks of the underlying stationary Gaussian signal and the instantaneous values of the modulating function. The expression for the peak distribution of the response $p_{z_p}(z)$ can be calculated based on Equation 2.15 (see Section 2.1.9):

$$p_{z_p}(z) = \int_{-\infty}^{\infty} p_{x_p}(a) \frac{1}{|a|} p_a\left(\frac{z}{a}\right) da \qquad \text{Equation 5.11}$$

with $p_{x_p}$ the peak PDF of the underlying stationary Gaussian signal and $p_a$ the PDF of the modulating function. This expression requires the PDF of the modulating function $p_a$ to be determined.

Considering a periodic modulation function made of half sine pulses, covering $r_b$ of a period, as described in chapter 3.5.1, then the PDF of the modulating function $p_a$ is a weighted sum of the PDFs of:

- the constant amplitude flat portion that is present during $(1 - r_b)$ of a period, which PDF is expressed using the Dirac delta function
- the purely oscillating part that is present $r_b$ of a period, which PDF is given in Equation 3.15

The PDF of the concatenated time history can be calculated using Equation 2.67 in chapter 2.3.1. The PDF of the modulating function $p_a$ can be expressed as:

$$p_a(s) = \begin{cases} r_b \dfrac{1}{\pi\sqrt{{A_r}^2 - (s - B_r)^2}} + (1 - r_b)\delta(s + A_r - B_r) & if\ |s - B_r| < A_r \\ 0 & if\ |s - B_r| \geq A_r \end{cases} \quad \text{Equation 5.12}$$

where $A_r$ and $B_r$ are the amplitude and offset of the modulation function applied to the stationary response, $r_b$ is the proportion of the burst deviation in a period and $\delta$ is the Dirac delta function, which satisfies the identity $\int_{-\infty}^{\infty} \delta(x)dx = 1$.

The peak PDF for a stationary Gaussian process of arbitrary bandwidth is given in Equation 2.54 in section 2.2.8 as:

$$p_{x_p}(s) = \frac{1}{\sigma_X}\left\{\frac{\sqrt{1-\gamma^2}}{\sqrt{2\pi}}.e^{-\frac{s^2}{2.{\sigma_X}^2(1-\gamma^2)}} + \frac{s.\gamma}{2\sigma_X}.e^{-\frac{s^2}{2.{\sigma_X}^2}}.\left(1 + \text{erf}\left(\frac{s.\gamma}{\sigma_X\sqrt{2(1-\gamma^2)}}\right)\right)\right\} \quad \text{Equation 2.61}$$

Inserting this expression for $p_{x_p}$ and Equation 5.12 for $p_a$ into Equation 5.11, one obtains an expression for the peak PDF for the amplitude modulated stress response as:

$$\begin{aligned} p_{z_p}(z) = {} & r_b \frac{\sqrt{1-\gamma^2}}{\sqrt{2\pi}\sigma_X} \int_{z/(A_r+B_r)}^{z/(B_r-A_r)} \frac{1}{|a|} \frac{1}{\pi\sqrt{{A_r}^2 - (\frac{z}{a} - B_r)^2}} e^{-\frac{a^2}{2.{\sigma_X}^2(1-\gamma^2)}} da \\ & + r_b \frac{z.\gamma}{2{\sigma_X}^2} \int_{z/(A_r+B_r)}^{z/(B_r-A_r)} \frac{1}{|a|} \frac{1}{\pi\sqrt{{A_r}^2 - (\frac{z}{a} - B_r)^2}} e^{-\frac{z^2}{2.{\sigma_X}^2}}.\Bigg(1 \\ & + \text{erf}\left(\frac{z.\gamma}{\sigma_X\sqrt{2(1-\gamma^2)}}\right)\Bigg) da + (1 - r_b).\frac{1}{B_r - A_r} f_X\left(\frac{z}{B_r - A_r}\right) \end{aligned} \quad \text{Equation 5.13}$$

This expression has to be evaluated numerically as no closed form solution has been found.

Note that the integration goes from $z/(A_r + B_r)$ to $z/(B_r - A_r)$. This avoids the integrand containing the square root of a negative value.

Note that in the case of a Gaussian narrowband random process, the peak PDF tends towards a Rayleigh distribution and is given in Equation 2.51 in section 2.2.8 as:

$$p_{x_p}(s) = \frac{s}{{\sigma_X}^2}.\mathrm{e}^{-\frac{1}{2}\left(\frac{s}{\sigma_X}\right)^2} \qquad \text{Equation 2.54}$$

When inserting this expression for $p_{x_p}$ into Equation 5.11, the expression for the peak PDF obtained for the amplitude modulated response signal is expressed in a simpler form as:

$$p_{z_p}(z) = r_b \int_{z/(A_r+B_r)}^{z/(B_r-A_r)} \frac{1}{|a|} \frac{1}{\pi\sqrt{{A_r}^2 - (\frac{z}{a} - B_r)^2}} \frac{a}{{\sigma_X}^2} e^{-\frac{a^2}{2.{\sigma_X}^2}} da + \frac{(1-r_b)}{B_r - A_r} f_X\left(\frac{z}{B_r - A_r}\right)$$

The following example uses the same response data as in section 5.2.3. Figure 75 illustrates the normalised PDF of the stress peaks obtained from time domain numerical simulations (in blue), overlaid with the theoretical PDF of the stress peaks obtained using Equation 5.13 using a red line and with the theoretical distribution corresponding to a Gaussian random response signal with the same (unitary) RMS shown by the dashed black line.

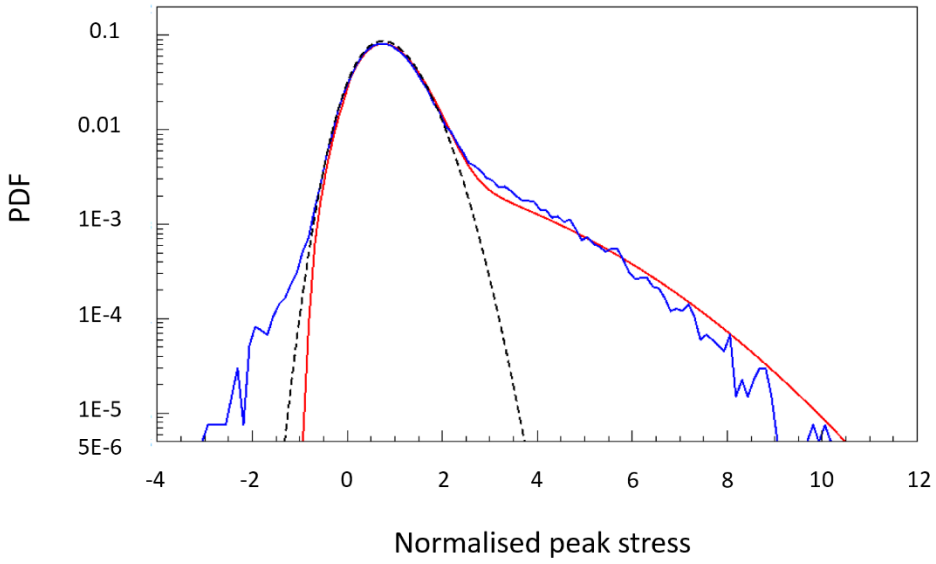


**Figure 75: The peak distributions for the leptokurtic response of the bimodal linear system from numerical simulations (blue), from the theoretical expression (red) and using the Gaussian assumption (dashed black)**

The theoretical non-Gaussian peak PDF obtained using Equation 5.13 (red) is indeed made of two constituents. This is revealed by the change in slope in its shape. The theoretical non-Gaussian PDF obtained is matching the curvature of the PDF observed from the time domain simulations (blue). The proposed theoretical PDF is slightly conservative due to the conservatism associated with the theoretical kurtosis of the response (see section 4.4). It is nevertheless much closer than the expected results than when assuming a Gaussian response (dashed black), especially for high response levels where fatigue damage might occur.

Figure 73 and Figure 75 can be compared, because both result from an excitation with the same kurtosis value exciting the same bimodal system. Figure 73 shows the peak PDF due to a steady leptokurtic excitation, whereas Figure 75 shows the peak PDF due to a nonstationary leptokurtic excitation. After the filtering process, the response signal obtained from the latter has a much higher kurtosis value and shows a much higher probability of peaks at higher levels.

Other example results are shown in Appendix E. One is showing the theoretical output kurtosis and peak distribution obtained from the same input signal and the same FRF but with a lighter damping ratio of 2% (see Figure 91) and the other one is using a unimodal FRF with only the resonance at 200 Hz and still with a lighter damping ratio of 2% (see Figure 92). The theoretical approach gives equally as good results in both cases. Note that the case presented in this chapter is considered as a quite extreme one because the kurtosis value chosen for the excitation signal is quite high in practice and the response signal is rather broadband (with an irregularity factor of 0.78) and tends to show a higher kurtosis value of 4.0 compared to the cases shown in appendix E.

## 5.4 Maximum peak in the response resulting from non-Gaussian excitations

Another typical requirement for design purpose is to calculate the largest peak in the non-Gaussian response from the response PSD and its associated kurtosis value. The average value of the largest peak together with the distribution of the extreme values can be used to define a limit for the theoretical peak and range distributions.

### 5.4.1 Maximum peak in the response resulting from a stationary, leptokurtic random excitation

In the Gaussian case, the average value of the largest peak out of $N_p T$ peaks is given in Equation 2.62 and can be adapted to calculate the largest peak in the response signal resulting from a stationary and Gaussian excitation $\overline{Z_m^g}$ as:

$$\overline{Z_m^g} \approx \sigma_z \left( \sqrt{2\ln(\gamma N_p T)} + \frac{\varepsilon}{\sqrt{2\ln(\gamma N_p T)}} \right) \qquad \text{Equation 5.14}$$

where $\sigma_z$ is the RMS value of the response signal calculated using Equation 4.1, $\gamma$ is the irregularity factor, $N_p$ is the number of expected peaks per unit time, $T$ is the exposure duration and $\varepsilon$ is the Euler constant.

The expression proposed for the average value of the largest peak out of $N_p T$ peaks in the leptokurtic response is based on a modification of the expression given for a Gaussian response. The nonlinear memoryless transformation $g$ used in Winterstein's second order model [50] (see Equation 3.9 in section 3.4) is assumed to hold at all instants in time. It can therefore be used to relate the maximum peak in the leptokurtic case $\overline{Z_m}$ with the maximum peak in the Gaussian

case $\overline{Z_m^g}$. So, inserting Equation 5.14 into Equation 3.9, one obtains an estimate of the largest peak out of $N_p T$ peaks for a steady leptokurtic response signal as:

$$\overline{Z_m} = \sigma_z K \left[ \frac{\overline{Z_m^g}}{\sigma_z} + \tilde{h}_4 \left( \left( \frac{\overline{Z_m^g}}{\sigma_z} \right)^3 - 3 \frac{\overline{Z_m^g}}{\sigma_z} \right) \right] \qquad \text{Equation 5.15}$$

where $\sigma_z$ is the RMS value of the response signal calculated using Equation 4.1, $K$ and $\tilde{h}_4$ are the same coefficients as in Equation 5.1 and $\overline{Z_m^g}$ is the largest peak in the response signal resulting from a stationary and Gaussian excitation.

Winterstein [50] also proposed an expression for the distribution of the extreme values.

### 5.4.2 Maximum peak in the response resulting from a clipped excitation

The probability distribution and the average value of the largest peak in the response signal can be calculated from the response PSD and its associated kurtosis value. The expression proposed here for the average value of the largest peak out of $N_pT$ peaks in the platykurtic response is the same as the expression given for a Gaussian response. This will provide a slight overestimation of the real average value, which is acceptable in the case of mild platykurtic responses.

### 5.4.3 Maximum peak in the response resulting from an amplitude modulated excitation

The probability distribution of the largest peak in the response signal is obtained from Equation A.10 (see appendix A):

$$p_{Z_m}(z) = N_pTp_p(z)\left(P_p(z)\right)^{N_pT-1}$$

where $p_p$ is the PDF of the peaks given in Equation 5.13 and $P_p$ is the cumulative distribution function of the peaks.

The expected value for the largest peak $\overline{Z_m}$ i.e. the average value of the largest peak out of $N_pT$ peaks is obtained using Equation 2.4 as:

$$\overline{Z_m} = \int_{-\infty}^{\infty} sp_{Z_m}(s)ds$$

This expression has to be evaluated numerically as no closed form solution has been found.

## 5.5 Rainflow cycle count histogram

The PDF of the rainflow ranges is calculated from the PDF of the peaks based on the fact that the peaks and valleys are paired symmetrically (as discussed in chapter 2.6.3), i.e. a peak is paired with a valley of same magnitude. Note that this way of pairing peaks and valleys will however introduce some conservatism in the case of broadband stress results, as illustrated in Figure 36 in section 2.6.3. So the PDF of the ranges is obtained from the distribution of peaks using Equation 2.87, which is

$$p_{z_R}(z_R) = \frac{1}{2}p_{z_p}\left(\frac{z_R}{2}\right) \qquad \text{Equation 2.87}$$

where $z_R$ is the stress range, $p_{z_p}$ is the PDF of the peaks and $p_{z_R}$ is the PDF of the ranges.

The rainflow cycle count histogram can be obtained from the PDF of the ranges by multiplying it with the total number of expected cycles during the exposure duration, that is $N_pT_t$, with $N_p$ the expected number of peaks per unit time and $T_t$ the exposure duration. The assumption is made that the polynomial transform does not change the number of peaks per unit time $N_p$, nor

the number of zero crossings per unit time $N_0{}^+$. So both values are calculated from the response PSD using Equation 2.48 and Equation 2.46 respectively, applicable to any stationary random data with any PDF [16].

One obtains the general equation giving the number of cycles at a particular stress range $N(z_R)$ using Equation 2.89:

$$N(z_R) = N_p . p_{z_R}(z_R) \qquad \text{Equation 2.89}$$

where $N(z_R)$ forms the rainflow cycle count histogram.

### 5.5.1 Rainflow cycle count histogram resulting from a stationary, leptokurtic random excitation

The following example uses the same response signal as in section 5.2.1. This response signal was obtained from a leptokurtic signal with kurtosis 12 described in section 3.4.2, filtered using a bi-modal linear system whose gain is represented in Figure 69. Figure 76 illustrates the rainflow cycle count histogram obtained from time domain numerical simulations (in blue), overlaid with the theoretical rainflow cycle count histogram obtained using Equation 2.89 shown by the red line and with the theoretical rainflow cycle count histogram corresponding to a Gaussian random response signal with same RMS given using the dashed black line.

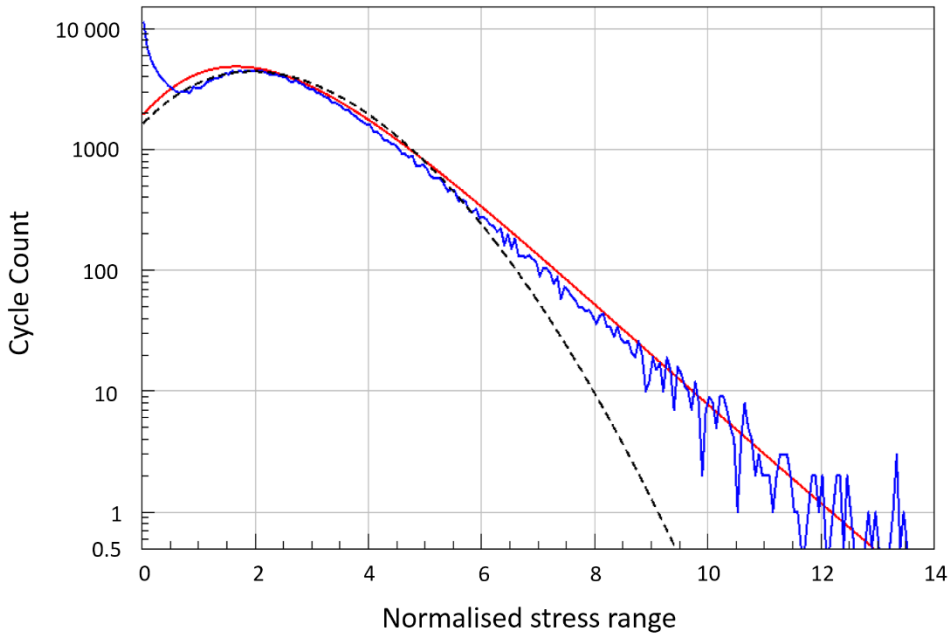


**Figure 76: The rainflow range distributions for the leptokurtic response of the bimodal linear system from numerical simulations (blue), from the theoretical expression (red) and using the Gaussian assumption (dashed black)**

The theoretical rainflow cycle count histogram provides a very good fit for the probability of finding cycles at the high ranges. The theoretical rainflow cycle count histogram is slightly conservative when assessing the number of stress cycles of mid-range values. The discrepancy at the low ranges is due to the complex way peaks and valleys are paired. This is discussed in

section 2.6.3. From a fatigue view point, it is however clear that the high ranges have more importance as fatigue damage and stress range are linked in a power law.

Due to the finite length of the simulated signal, the rainflow histogram obtained from time domain numerical simulations shows a high variability at high range levels, but the theoretical histogram seems to provide a good estimate of the mean number of cycles. When assuming a Gaussian response (dashed black), the theoretical rainflow cycle count histogram dramatically underestimates the observed rainflow cycle count histogram, especially for high ranges where most fatigue damage might occur.

Note that the PDF transform can be applied to Dirlik's empirical approach [29] too. In this case the quality of the fit is enhanced in the low range region but provides no particular benefit for the mid or high ranges.

### 5.5.2 Rainflow cycle count histogram resulting from a clipped excitation

The following example uses the same response data as in section 5.2.2. Figure 77 illustrates the rainflow cycle count histogram obtained from time domain numerical simulations (in blue), overlaid with the theoretical rainflow cycle count histogram obtained using Equation 2.89 shown by the red line and with the theoretical rainflow cycle count histogram corresponding to a Gaussian random response signal with same RMS given using the dashed black line.

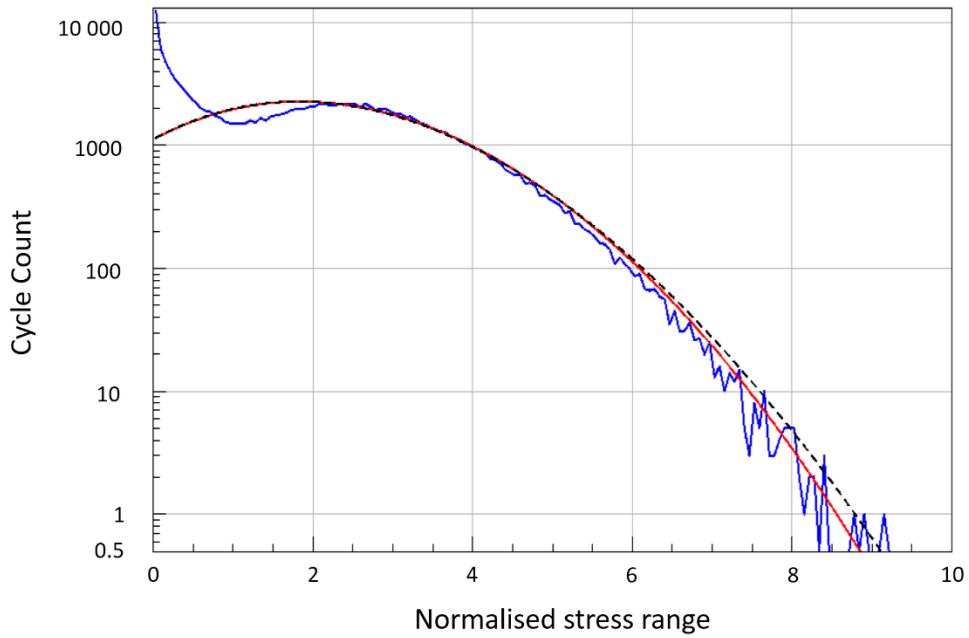


**Figure 77: The rainflow range distributions for the platykurtic response of the bimodal linear system from numerical simulations (blue), from the theoretical expression (red) and using the Gaussian assumption (dashed black)**

As previously, the theoretical rainflow cycle count histogram obtained using Equation 2.89 (red) and taking into account the platykurtic nature of the response provides a good fit to the rainflow cycle histogram obtained from the time domain simulation (blue). Due to the finite length of the simulated signal, the rainflow histogram obtained from time domain numerical simulation shows a high variability at high range levels but the theoretical histogram seems to

provide a good estimate of the mean number of rainflow cycles. When assuming a Gaussian response (dashed black) the theoretical rainflow cycle count histogram overestimates slightly the observed rainflow cycle count histogram, especially for high ranges where most fatigue damage might occur.

### 5.5.3 Rainflow cycle count histogram resulting from an amplitude modulated excitation

The following example uses the same response data as in section 5.2.3. Figure 78 illustrates the rainflow cycle count histogram obtained from time domain numerical simulations (in blue), overlaid with the theoretical rainflow cycle count histogram obtained using Equation 2.89 shown by the red line and with the theoretical rainflow cycle count histogram corresponding to a Gaussian random response signal with same RMS given using the dashed black line.

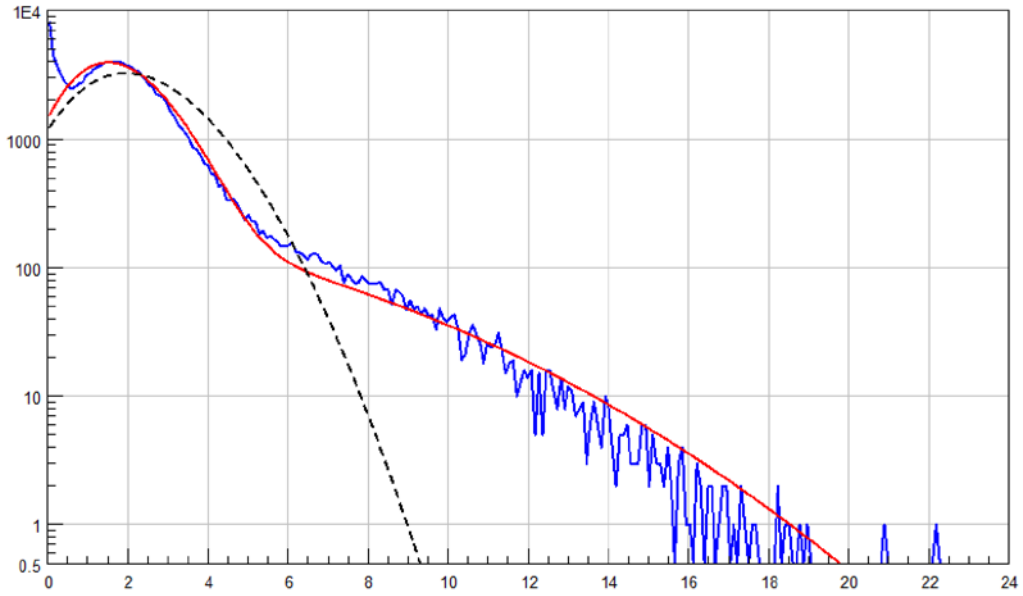


**Figure 78: The rainflow range distributions for the leptokurtic response of the bimodal linear system from numerical simulations (blue), from the theoretical expression (red) and using the Gaussian assumption (dashed black)**

Once again, the theoretical rainflow cycle count histogram obtained using Equation 2.89 (red) and taking into account the amplitude modulated nature of the response provides a good fit to the rainflow cycle histogram obtained from the time domain simulation (blue). The theoretical rainflow cycle count histogram is quite conservative, particularly for high cycle ranges where fatigue damage might occur. When assuming a Gaussian response (dashed black) the theoretical rainflow cycle count histogram underestimates dramatically the observed rainflow cycle histogram, especially for high ranges.

## 5.6 Fatigue life predictions

The estimate of fatigue damage here is determined based on the rainflow cycle count histogram, as described in chapter 2.6.4 using Equation 2.91 with various values for the Basquin exponent $b$ accounting for the fatigue material curves:

- $b = 4$ typically used with electronic components [70],
- $b = 8$ adequate for metallic materials such as steels and aluminium alloys [1, 5],
- $b = 12$ to represent certain steels alloys [27]

To illustrate the importance of the $b$ coefficient, Figure 79 shows an example rainflow histogram overlaid with several fatigue curves. Note that the axes of the rainflow histogram are transposed.

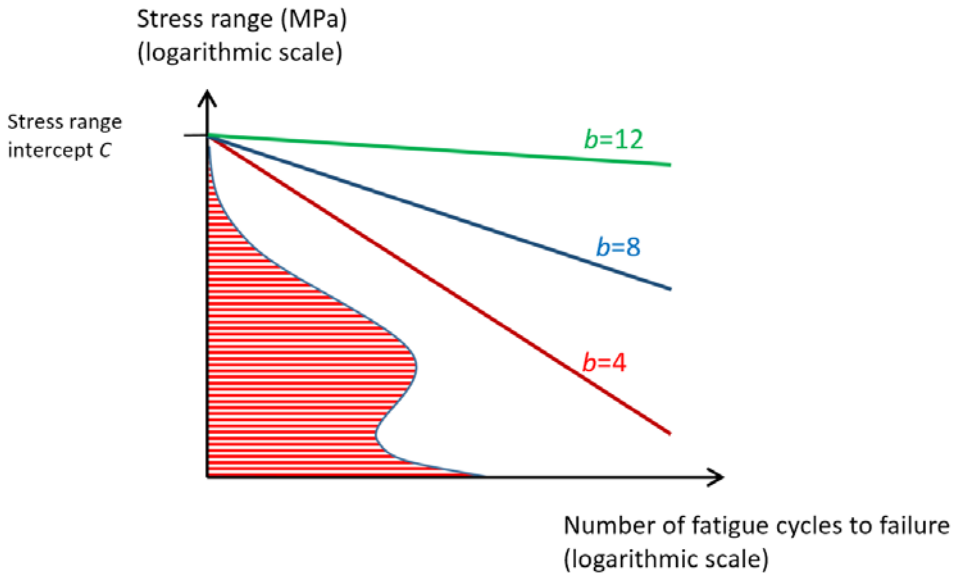


**Figure 79: Illustration of an example rainflow cycle histogram overlaid with three fatigue curves, with different slopes. As the slope value increases, the cycles with high stress range have more importance.**

In most practical situations, fatigue curves with higher values for the exponent $b$ only exist beyond the endurance limit, where the amount of cumulated damage is less significant. In most practical situations, the effective fatigue damage at the critical failure location is governed by notches, surface finish effects, or welds; and the Basquin exponent $b$ usually lies in the range 3 – 7 [28]. The stress range intercept $C = 2000$ MPa was used and no fatigue limit was considered.

### 5.6.1 Fatigue life predictions resulting from a stationary, leptokurtic random excitation

Based on the same example response as in the previous sections, Table 5.1 compares the fatigue damage values obtained from time domain numerical simulations with the damage values obtained based on the theoretical statistical rainflow cycle count histogram, considering the leptokurtic nature of the stress response and with the theoretical statistical rainflow cycle count histogram considering a Gaussian random response.

Ten realisations of 500 sec time domain signals were produced and the maximum, minimum and mean damage observed are reported in Table 5.1, together with the damage values calculated from the theoretical rainflow histograms considering both a leptokurtic and a Gaussian stress response.

**Table 5.1: Comparison of relative fatigue damage values calculated for various materials**

| Basquin exponent | Interval of damage from time domain simulations | Mean damage from time domain simulations | Damage from theoretical rainflow - leptokurtic | Damage from theoretical rainflow – Gaussian |
|---|---|---|---|---|
| $b$=4 | [6.2 – 6.4] | 6.3 | 7 | 5.4 |
| $b$=8 | [3.9 $10^{-3}$ – 6.0 $10^{-3}$] | 4.5 $10^{-3}$ | 4.3 $10^{-3}$ | 1.5 $10^{-3}$ |
| $b$=12 | [1.0 $10^{-5}$ – 4.1 $10^{-5}$] | 1.7 $10^{-5}$ | 1.2 $10^{-5}$ | 0.1 $10^{-5}$ |

In Table 5.2, the damage values are scaled with respect to the mean damage out of the ten time domain simulations and displayed in percent.

**Table 5.2: Percent damage values with respect to the mean damage from the time domain simulations**

| Basquin exponent | Interval of damage from time domain simulations | Mean damage from time domain simulations | Damage from theoretical rainflow - leptokurtic | Damage from theoretical rainflow – Gaussian |
|---|---|---|---|---|
| $b$=4 | [98% – 102%] | 100% | 112% | 86% |
| $b$=8 | [86% – 125%] | 100% | 95% | 33% |
| $b$=12 | [55% – 245%] | 100% | 73% | 6% |

The theoretical damage obtained from the classical (Gaussian) spectral approach is always below the lower limit of the interval of observed damages from time domain simulations. Also, this underestimation of the damage is even more significant as the Basquin exponent $b$ increases.

The theoretical damage predicted with the proposed leptokurtic spectral approach is much higher than the Gaussian spectral approach and is closer to the mean damage observed from time domain simulations. For a more shallow fatigue curve (Basquin exponent $b$=12), the fatigue damage is governed essentially by the larger cycles in the tail of the distribution. This is where the observed rainflow histogram shows a significant variability mostly due to the limited duration of the reconstructed signals, inadequate to statistically capture the extreme amplitude cycles (see section 2.2.9 on extreme values, showing how the standard deviation of the distribution of extreme values decreases as the signal duration increases). Therefore, in the case of a high Basquin exponent, the few cycles of extreme stress range that appear beyond the theoretical distribution (as illustrated in Figure 76) have an important contribution to the overall damage, hence the larger spread in the observed damage values as $b$ increases. This is also why the damage from the leptokurtic spectral approach slightly underestimates the mean damage observed from time domain simulations. For a steeper fatigue curve (Basquin exponent $b$=4),

extreme cycles are less influential and stress cycles in the mid-range can govern the fatigue damage more easily, providing they are sufficiently numerous. The proposed formulation for the leptokurtic spectral approach shows a slight overestimation of the number of stress cycles (as illustrated in Figure 76), which is the reason why the damage from the leptokurtic spectral approach slightly overestimates the mean damage observed from time domain simulations, when using a low value for the Basquin exponent.

### 5.6.2 Fatigue life predictions resulting from a clipped excitation

Based on the same example as in the previous sections, Table 5.3 compares the fatigue damage values obtained from time domain numerical simulations with the damage values obtained based on the theoretical statistical rainflow cycle count histogram, considering the leptokurtic nature of the stress response and with the theoretical statistical rainflow cycle count histogram considering a Gaussian random response. Ten realisations of 500 sec time domain signals were produced and the maximum and minimum damages found are reported in Table 5.3.

**Table 5.3: Comparison of relative fatigue damage values calculated for various materials**

| Basquin exponent | Interval of damage from time domain simulations | Mean damage from time domain simulations | Damage from theoretical rainflow - platykurtic | Damage from theoretical rainflow – Gaussian |
|---|---|---|---|---|
| $b$=4 | [4.75 – 4.85] | 4.8 | 5 | 5.5 |
| $b$=8 | [1.0 $10^{-3}$ – 1.1 $10^{-3}$] | 1.1 $10^{-3}$ | 1.2 $10^{-3}$ | 1.5 $10^{-3}$ |
| $b$=12 | [5.1 $10^{-7}$ – 5.7 $10^{-7}$] | 5.3 $10^{-7}$ | 7.0 $10^{-7}$ | 10 $10^{-7}$ |

In Table 5.4, the damage values are scaled with respect to the mean damage found out of the ten time domain simulations and displayed in percent.

**Table 5.4: Percent damage values with respect to the mean damage from the time domain simulations**

| Basquin exponent | Interval of damage from time domain simulations | Mean damage from time domain simulations | Damage from theoretical rainflow - platykurtic | Damage from theoretical rainflow – Gaussian |
|---|---|---|---|---|
| $b$=4 | [99% – 101%] | 100% | 104% | 114% |
| $b$=8 | [97% – 101%] | 100% | 109% | 136% |
| $b$=12 | [96% – 106%] | 100% | 131% | 188% |

The theoretical damage obtained from the classical (Gaussian) spectral approach is always above the higher limit of the range of observed damages from time domain simulations and this overerestimation of the damage is more significant as the Basquin exponent $b$ increases. The theoretical damage obtained from the proposed platykurtic spectral approach seems to take into account the beneficial effect on damage that the clipping of the excitation has produced. Although slightly conservative, the theoretical damage obtained from the proposed platykurtic spectral approach is very close to the mean damage obtained from the time domain simulations.

In addition to the numerical approach exposed here, random vibration tests with various values for sigma clipping were made on a test article instrumented with strain gauges [90]. It was concluded that for endurance tests, the user should avoid sigma clipping below 3 because it noticeably reduces the fatigue damage potential on the test article, due to the reduced number of stress cycles at high amplitudes. It was also shown how the "classical" spectral fatigue approach using a Gaussian assumption could overestimate the fatigue damage on the test article.

### 5.6.3 Fatigue life predictions resulting from an amplitude modulated excitation

Based on the same example as in the previous sections, Table 5.5 compares the fatigue damage values obtained from time domain numerical simulations with the damage values obtained based on the theoretical statistical rainflow cycle count histogram, considering the leptokurtic nature of the stress response and with the theoretical statistical rainflow cycle count histogram considering a Gaussian random response. Ten realisations of 500 second time domain signals were produced and the maximum and minimum damages found are reported in Table 5.5.

**Table 5.5: Comparison of relative fatigue damage values calculated for various materials**

| Basquin exponent | Interval of damage from time domain simulations | Mean damage from time domain simulations | Damage from theoretical rainflow - leptokurtic | Damage from theoretical rainflow – Gaussian |
|---|---|---|---|---|
| $b$=4 | [15.9 – 17.6] | 16.7 | 19.6 | 5.4 |
| $b$=8 | [13 $10^{-2}$ – 19 $10^{-2}$] | 15 $10^{-2}$ | 29 $10^{-2}$ | 0.15 $10^{-2}$ |
| $b$=12 | [28 $10^{-4}$ – 66 $10^{-4}$] | 38 $10^{-4}$ | 136 $10^{-4}$ | 0.01 $10^{-4}$ |

In Table 5.6, the damage values are scaled with respect to the mean damage found out of the ten time domain simulations and displayed in percentages.

**Table 5.6: Percent damage values with respect to the mean damage from the time domain simulations**

| Basquin exponent | Interval of damage from time domain simulations | Mean damage from time domain simulations | Damage from theoretical rainflow - leptokurtic | Damage from theoretical rainflow – Gaussian |
|---|---|---|---|---|
| $b$=4 | [95% – 105%] | 100% | 117% | 32% |
| $b$=8 | [87% – 122%] | 100% | 188% | 1% |
| $b$=12 | [75% – 175%] | 100% | 357% | 0.03% |

The theoretical damage obtained from the classical (Gaussian) spectral approach is always far below the lower limit of the interval of observed damages from time domain simulations. Also, this underestimation of the damage is even more significant as the Basquin exponent $b$ increases. The theoretical damage predicted with the proposed leptokurtic spectral approach is closer to the mean damage observed from time domain simulations with an increasing degree of conservatism as the the fatigue exponent $b$ increases.

When looking at the comparison between the theoretical rainflow cycle count histogram and the one obtained from time domain simulations (see previous section), the overestimation of the probability of obtaining cycles in the high response ranges leads one to expect a conservative predicted damage compared to the time domain simulations. This is indeed the case here. It is even more pronounced in the case of high values for the fatigue exponent $b$, where damage is almost purely driven by the stress response cycles with high amplitudes (section 5.6 discusses the importance of the $b$ coefficient in more details).

The damage predicted from the theoretical expression taking into account the leptokurtic nature of the loading is clearly conservative. In contrast, the standard approach (for Gaussian responses) underestimates severely the damage and may therefore lead to an under-design of a structure. Hence it is critical that predictions do not use the Gaussian assumption where it is suspected that the stress response might be leptokurtic. A test for Gaussianity in the response is thus a priority.

## 5.7 Conclusions

Chapter 5 introduced novel formulations to predict the PDF of instantaneous values, the maximum stress value, the peak PDF and the rainflow cycle count histogram for a non-Gaussian stress response, knowing its PSD and kurtosis without the need for numerical simulations.

The distributions and histograms obtained were compared with those obtained from time domain signal realisations and fatigue estimates were calculated from the rainflow cycle count histograms.

In the leptokurtic case (kurtosis higher than 3), two sorts of leptokurtic responses were studied separately; the stationary one, typically modelled using a zero-memory polynomial transform of a stationary Gaussian signal and the nonstationary one, generated by amplitude modulating a stationary Gaussian signal. It was shown that making the Gaussian assumption in presence of a leptokurtic response can significantly underestimate the damage, even for steep fatigue material curves. Both stationary and nonstationary leptokurtic responses show a much higher probability of obtaining cycles with large ranges than when the Gaussian assumption is made. This is also reflected when comparing the fatigue damage estimates, i.e. the damage due to a leptokurtic response can be orders of magnitudes higher than when compared to the damage due to a Gaussian response with same RMS. This fact gets more pronounced as the kurtosis increases.

In the platykurtic case (kurtosis smaller than 3), the theoretical damage obtained making the Gaussian assumption is overerestimated. The theoretical damage obtained from the proposed platykurtic spectral approach takes into account the beneficial effect of a lower kurtosis and provides fatigue damage estimates that are in better correlation with numerical simulations and experimental tests.

This chapter illustrated how the standard approach (for Gaussian responses) severely underestimates the damage and may therefore lead to an under-design of a structure. Hence it is critical that predictions do not use the Gaussian assumption where it is suspected that the stress response might be leptokurtic. A test for Gaussianity properties for the response, such as the one proposed by Bendat and Piersol [16], is thus a priority.

# 6 Overall conclusions

## 6.1 Conclusions of the research

Engineers want to estimate the fatigue life of a structure subjected to random vibrations. When the mechanical environment is random, it is typically characterised by Power Spectral Density (PSD) and a common way to proceed is to adopt a spectral fatigue analysis, which is based on a statistical approach to assess the number of stress peaks at various levels or the stress cycles of various ranges.

In modern CAE-based fatigue analysis tools, the user specifies the excitation PSD, and a FE results file representing the frequency response function linking the excitation and the stress response. The stress response PSD is obtained and the statistical rainflow histogram is extracted. Fatigue life estimates can be derived by associating the statistical rainflow histogram with the material fatigue curve. Such a spectral fatigue approach can offer an efficient and accurate fatigue life estimation compared to using time domain realisations.

However, statistical approaches are currently limited to random stationary and Gaussian excitations only.

The global objective of this PhD thesis was to extend the existing statistical approach for fatigue analysis under non-Gaussian random loads. Non-Gaussian random excitations found in industrial applications and studied in this thesis include clipped random excitations and excitations with high kurtosis. These objectives were gradually achieved in the various chapters in this thesis. After an introduction and an overview of the background literature, the means to generate non-Gaussian signals were exposed in chapter 3, expressions for the statistics of the response to a linear filter were presented in chapters 4 and the rainflow cycle distribution and fatigue damage estimates were obtained in chapter 5. This means that it is sufficient to know the characteristics of the excitation and the linear filter for the proposed formulations to provide the theoretical distributions for the response stress cycle ranges - the fatigue damage being then derived from it. Time domain signals were simulated only to compare the statistics and histograms obtained from the theoretical formulations with those resulting from the counting algorithms applied to the signals. They have shown the robustness and accuracy of the theoretical expressions.

This thesis has therefore brought new techniques to extend the usage of the spectral fatigue analysis to non-Gaussian cases, including clipped and leptokurtic processes. The novel formulations can be used to improve the time-to-failure estimates for more realistic loadings. The proposed expressions are robust, with no empiricism and are compatible with any fatigue curve. It was clearly shown that the standard approach for Gaussian responses can dramatically underestimate the damage due to leptokurtic excitations and may therefore lead to an under-design of a structure. Hence it is highly recommended to do a Gaussianity test when it is suspected that the stress response might be leptokurtic.

A noticeable benefit of being able to assess the fatigue life in the case of a structure subjected to a leptokurtic random excitation is to create an accelerated test specification. The idea is to associate a specific kurtosis value to a given PSD in order to reduce the exposure duration, while encompassing the same fatigue damage potential as the original stationary and Gaussian random test. The use of kurtosis control in addition to the usual load amplification method leads to an accelerated test that has a smaller RMS value than the equivalent random stationary and Gaussian test which is accelerated using the load amplification method only. So an advantage of the leptokurtic test is that it can reach very short durations without using exaggerated RMS levels.

## 6.2 Perspective for future research

Whilst performing this work, some additional avenues of research have been identified that may be of interest. The main ones being:

- Derivation of the range-mean rainflow matrix of the response stress due to random Gaussian and non–Gaussian excitations. The mean stress can have a significant impact on the fatigue life [108] and it would be interesting to be able to take it into account.
- Accounting for material nonlinearity when the structure subjected to Gaussian and non–Gaussian random excitations. Material non-linearity occurs typically when the excitation is severe enough to produce large deformations and large material response. In this case, the linear relationship relating the excitation and the stress response is no longer valid. In some other cases, a high temperature can affect the material properties and activate nonlinear phenomena such as viscosity.
- Consideration of other high order statistics such as the skewness. For instance, the skewness helps to account for asymmetric probability distributions, which occurs in road vehicles under certain circumstances [96].
- Further research on the damage induced by sine-on-random excitations, especially when the frequencies of the sine tones are multiple of each other, which typically occurs with helicopters [86], thermal engines [85] or more generally with machinery with rotating parts [46].

## References


[1] NATO Standardisation Agency, STANAG 4370. AECTP 200 (Edition 3) Mechanical Conditions, NATO, 2006.

[2] USA Department of Defense, Test Method Styandard MIL-STD-810G Environmental Engineeering Considerations and Laboratory Tests, 2008.

[3] UK Ministry of Defence, Defence Standard 00-35 Issue 4 (2006). Environmental Handbook for Defence Materiel: Part 3: Environmental Test Methods.

[4] “RCA/DO-160 Revision G: Environmental Conditions and Test Procedures for Airborne Equipment”, RTCA, 2010.

[5] "GAM EG-13 – Annexe Générale Mécanique", France, Ministère de la Défense, Délégation Générale pour l’Armement, 2002.

[6] A. Halfpenny and F. Kihm, "Mission Profiling and Test Synthesis Based on Fatigue Damage Spectrum. Ref. FT342.," in *9th Intl. Fatigue Congress*, Atlanta, USA, 2006.

[7] International Test Operation Procedure (ITOP) 1-1-050, Development of Laboratory Vibration Schedules., 6 June 1997.

[8] J. Zhuge, D. Formenti and M. Richardson, "A Brief History of Modern Digital Shaker Controllers," *Sound and Vibration*, vol. 44, no. 9, pp. 12-16, 2010.

[9] A. Steinwolf, "Shaker random testing with low kurtosis: Review of the methods and application for sigma limiting," *Shock and Vibration*, vol. 17, no. 3, pp. 219-231, 2010.

[10] A. Steinwolf, "Two methods for random shaker testing with low kurtosis," *Sound and Vibration*, vol. 42, no. 10, p. 18–22, 2008.

[11] F. Kihm, A. Halfpenny and K. Munson, "Synthesis of Accelerated and More Realistic Vibration Endurance Tests Using Kurtosis," in *SAE Technical Paper 016-01-0275*, 2016.

[12] K. Sweitzer, "Random vibration response statistics for fatigue analysis of nonlinear structures," PhD Thesis, Institute of Sound and Vibration Research, Southampton, UK, 2006.

[13] H. Rognon, "Comportement en fatigue sous environnement vibratoire: Prise en compte de la plasticité au sein des méthodes spectrales," PhD Thesis, SUPMECA, 2013.

[14] K. Worden, D. Hickey and M. Haroon, "Nonlinear system identification of automotive dampers: a time and frequency-domain analysis.," *Mechanical Systems and Signal Processing*, vol. vol. 23, no. no. 1, pp. p. 104-126, 2009.

[15] S. Rice, "Mathematical analysis of random noise," in *Selected papers on noise and stochastic processes*, New York, 1954.

[16] J. Bendat and A. G. Piersol, Random Data: Probability, random variables, New York: 3rd ed. John Wiley & Sons, 2000.

[17] J. Bendat, "Probability functions for random responses," NASA report on contract NAS-5-4590, 1964.

[18] J.-L. Lacoume, P.-O. Amblard and P. Comon, Statistiques d’ordre supérieur pour le traitement du signal, Masson, 1997.

[19] Y. Lin, Probabilistic theory of structural dynamics, McGraw-Hill, 1967.

[20] D. Newland, Random Vibrations, Spectral & Wavelet analysis (3rd edition), New York: Dover Publications, 1993.

[21] P. H. Wirsching, T. L. Paez and K. Ortiz, Random vibrations: theory and practice, Courier Corporation, 2006.

[22] C. Lalanne, Mechanical Vibration and Shock Analysis, Random Vibration (Vol. 3), John Wiley & Sons, 2013.

[23] D. E. Cartwright and M. S. Longuet-Higgins, "The Statistical distribution of the maxima of a random function," *Proceedings of the Royal Society*, vol. 237, no. 1209, p. 212–232, 1956.

[24] J.-N. Yang and M. Shinozuka, "On the first excursion probability in stationary narrow-band random vibration," *Journal of Applied Mechanics*, vol. 38, no. 4, pp. 1017-1022, 1971.

[25] M. Shinozuka and W. F. Wu, "On the first passage problem and its application to earthquake engineering," in *Proceedings of the Ninth World Conference on Earthquake Engineering*, Tokyo and Kyoto, Japan, 1988.

[26] N. W. M. Bishop and F. Sherratt, "Fatigue life prediction from power spectral density data. II: Recent developments," *Environmental engineering*, vol. 2, no. 2, pp. 11-15, 1988.

[27] C. Lalanne, Mechanical vibration and shock Analysis, Fatigue Damage (Vol 4), John Wiley & Sons, 2010.

[28] A. Halfpenny, "Rainflow Cycle Counting and Fatigue Analysis from PSD," in *Proceedings of the ASTELAB conference*, Paris, 2007.

[29] T. Dirlik, "Application of computers to fatigue analysis," PhD Thesis, Warwick University, 1985.

[30] A. Halfpenny and F. Kihm, "Rainflow Cycle Counting and Acoustic Fatigue Analysis Techniques for Random Loading," in *10th International Conference RASD*, Southampton, UK, 2010.

[31] I. Rychlik, "On the "narrow-band" approximation for expected fatigue damage," *Probabilistic Engineering Mechanics*, vol. 8, pp. 1-4, 1993.

[32] I. Rychlik, "Rain-Flow-Cycle distribution for ergodic load processes," *SIAM Journal on Applied Mathematics*, vol. 48, no. 3, pp. 662-679, 1988.

[33] S. Rice, "Probability distributions for noise plus several sine waves–The problem of computation," *IEEE Trans. Commun.*, no. 22, pp. 851-853, 1974.

[34] S. Rice, "Statistical Properties of a Sine Wave Plus Random Noise," *Bell System Technical Journal*, vol. 27, no. 1, p. 109–157, 1948.

[35] I. M. Ryzhik and I. Gradshteyn, Table of integrals, series, and products, 1965.

[36] A. Papoulis , Probability, Random Variables, and Stochastic Processes, McGraw-Hill, Inc., 1991.

[37] H. Cramér, Mathematical methods of statistics, Princeton University Press, 1999.

[38] W. B. Collis, P. R. White and J. K. Hammond, "Higher-order spectra: the bispectrum and trispectrum," *Mechanical Systems and Signal Processing*, vol. 12, no. 3, pp. 375-394, 1998.

[39] K. Shin and J. Hammond, Fundamentals of signal processing for sound and vibration engineers, John Wiley & Sons, 2008.

[40] B. Puig, "Modélisation et simulation de processus stochastiques non gaussiens," Doctoral dissertation, Université Pierre et Marie Curie-Paris VI, Paris, 2003.

[41] X. Pitoiset, "Méthodes spectrales pour l'analyse en fatigue des structures métalliques sous chargements aléatoires multiaxiaux.," PhD thesis, Université libre de Bruxelles, Bruxelles, 2001.

[42] D. Benasciutti, "Fatigue analysis of random loadings," PhD thesis, University of Ferrara, Ferrara, 2004.

[43] R. A. Fisher and L. H. C. Tippett, "Limiting forms of the frequency distribution of the largest or smallest member of a sample," *Mathematical Proceedings of the Cambridge Philosophical Society,* vol. 24, pp. 180-190, 1928.

[44] M. S. Longuet-Higgins, "On the statistical distribution of heights of sea waves," *Journal of Marine Research,* vol. 11, no. 3, pp. 245-266, 1952.

[45] E. J. Gumbel, Statistics of extremes., Courier Corporation, 2012.

[46] J. Antoni, "Cyclostationarity by examples," *Mechanical Systems and Signal Processing,* vol. 23, no. 4, pp. 987-1036, 2009.

[47] W. A. Gardner, "The spectral correlation theory of cyclostationary time-series," *Signal processing,* vol. 11, no. 1, pp. 13-36, 1986.

[48] A. Halfpenny, "Dynamic analysis of both on and offshore wind turbines in the frequency domain," PhD Thesis, University of London, 1998.

[49] L. M. Fitzwater and S. R. Winterstein, "Predicting design wind turbine loads from limited data: Comparing random process and random peak models," *Journal of solar energy engineering,* vol. 123, no. 4, pp. 364-371, 2001.

[50] S. Winterstein, "Nonlinear vibration models for extremes and fatigue," *ASCE Journal of Engineering Mechanics,* vol. 114, no. 10, pp. 1772-1790, 1988.

[51] B.-F. Peng and J. P. Conte, "Closed-form solutions for the response of linear systems to fully nonstationary earthquake excitation," *Journal of engineering mechanics,* vol. 124, no. 6, pp. 684-694, 1998.

[52] T. Reytier, "Modelling fatigue spectra of aircraft structure under gust loads. Thèse de doctorat.," Université Toulouse III-Paul Sabatier, 2012.

[53] A. Steinwolf and S. A. Rizzi, "Non-Gaussian PDF Modeling of Turbulent Boundary Layer Fluctuating Pressure Excitation," in *Eighth International Conference on Recent Advances in Structural Dynamics,* Southampton, UK, 2003.

[54] V. Rouillard, "On the Non-Gaussian Nature of Random Vehicle Vibrations," *World Congress on Engineering,* pp. 1219-1224, July, 2007.

[55] D. Charles, "Derivation of Environment Descriptions and Test Severities from Measured Road Transportation Data," *Journal of the Institute of Environmental Sciences,* pp. 37-42, Feb. 1993.

[56] D. Benasciutti and R. Tovo, "Cycle distribution and fatigue damage assessment in broad-band non-Gaussian random processes," *Probabilistic Engineering Mechanics,* vol. 20, pp. 115-127, 2005.

[57] K. Bogsjö, "Road profile statistics relevant for vehicle fatigue, Ph.D. thesis," Lund University, 2007.

[58] D. Richards, "A Review of Analysis and Assessment Methodologies for Road Transportation Vibration and Shock Data," *Environmental Engineering,* pp. 23-26, Dec. 1990.

[59] W. Connon, "Comments on Kurtosis of Military Vehicle Vibration Data," *Journal of the Institute of Environmental Sciences,* no. September/October, pp. 38-41, 1991.

[60] P. Wolfsteiner and W. Breuer, "Fatigue assessment of vibrating rail vehicle bogie components under non-Gaussian random excitations using power spectral densities," *Journal of Sound and Vibration,* vol. 332, no. 22, pp. 5867-5882, 2013.

[61] H. Press and R. Steiner, "An Approach to the Problem of Estimating Severe and Repeated Gust Loads for Missile Operations," NACA TN 4332, 1958.

[62] "CS-25 Certifications specifications for large aeroplanes," European Aviation Safety Agency, 2003.

[63] L. Girardeau, *Personal communication. Renault SA, France.*

[64] A. Jha, E. Nikolaidis and S. Gangadharan, "Vibration of dynamic systems under cyclostationary excitations," *AIAA journal,* vol. 38, no. 12, pp. 2284-2291, 2000.

[65] W. A. Gardner, Statistical spectral analysis: a nonprobabilistic theory, Prentice-Hall, Inc., 1986.

[66] A. Papoulis, "Narrow-Band Systems and Gaussianity," *IEEE Transactions on Information Theory,* vol. 18, no. 1, pp. 20-27, 1972.

[67] B. Thomas, "Dynamique d'une structure complexe à non linéarités localisées sous environnement vibratoire évolutif : Application à l'isolation vibratoire d'un équipement automobile," PhD Thesis, INSA de Lyon, 2012.

[68] K. Worden, C. R. Farrar and J. Haywood, "A review of nonlinear dynamics applications to structural health monitoring," *Structural Control and Health Monitoring,* vol. 15, no. 4, pp. 540-567, 2008.

[69] G. Kerschen, K. Worden and A. Vakakis, "Past, present and future of nonlinear system identification in structural dynamics," *Mechanical systems and signal processing,* vol. 20, no. 3, pp. 505-592, 2006.

[70] D. Steinberg, Vibration analysis for electronic equipment, New York: Wiley-Interscience, 1988.

[71] L. K. I. Utkin, "Stress-Strength Reliability Models Under Incomplete Information".

[72] R. Melchers , Structural Reliability Analysis and Prediction (2nd Edition), Chichester, UK: John Wiley & Sons, 1999.

[73] J. A. Bannantine, J. J. Comer and J. L. Handrock, Fundamentals of Metal Fatigue Analysis, Prentice Hall, 1990.

[74] ASTM, ASTM E1823-13, Standard Terminology Relating to Fatigue and Fracture Testing, West Conshohocken, PA: ASTM International, 2013.

[75] A. Halfpenny, "A practical introduction to fatigue," in *New technology 2001*, Warwickshire, UK, 2001.

[76] A. Wöhler, "Tests to determine the forces acting on railway wagon axles, and the capacity of resistance of the axles.," *Z. Bauw.,* vol. 10, pp. pp. 583-616, 1860.

[77] O. Basquin, "The Exponential Law of Endurance Tests," *American Society for Testing and Materials Proceedings,* vol. 10, pp. 625-630, 1910.

[78] M. Matsuishi and T. Endo, "Fatigue of Metals Subjected to Varying Stress," in *Japan Society of Mechanical Engineers,* Jukvoka, Japan, 1968.

[79] S. Downing and D. Socie, "Simple rainflow counting algorithms," *Int. J Fatigue,* pp. 31-40, 1982.

[80] Y. Lee, M. Barkey and H. Kang, Metal Fatigue Analysis Handbook: Practical Problem-solving Techniques for Computer-aided Engineering, Butterworth-Heinemann, 2011.

[81] P. Watson and B. J. Dabell, "Cycle Counting and Fatigue," in *Proc. of SEE Symposium held at Warwick Uni.*, 1975.

[82] J. R. Rice and F. P. Beer, "On the Distribution of Rises and Falls in a Continuous Random Process," *Journal of Basic Engineering*, vol. 87, pp. 398-404, 1965.

[83] M. Miner, "Cumulative damage in fatigue," *J. Applied Mechanics*, vol. 67, 1945.

[84] A. Steinwolf, “Closed-loop shaker simulation of non-Gaussian random vibrations,” *Test Engineering and Management*, vol. 63, no. 3, p. 10, 2006.

[85] F. Kihm, A. Halfpenny and Beaum, B., "Obtaining a Swept Sine on Random Vibration Profile for Powertrain Mounted Component Qualification," in *SAE Technical Paper 2015-01-0430*, 2015.

[86] A. Halfpenny and T. C. Walton , "New techniques for vibration qualification of vibrating equipment on aircraft," in *Proceedings Aircraft Airworthiness & Sustainment*, 2010.

[87] S. R. Winterstein, T. C. Ude and G. Kleiven, "Springing and slow-drift responses: predicted extremes and fatigue vs. simulation," in *Proc., BOSS-94*, 1994.

[88] D. Smallwood, "Vibration with non-Gaussian noise," *Journal of the IEST*, 2009.

[89] F. Kihm, S. Rizzi and N. Ferguson, "Understanding how kurtosis is transferred from input acceleration to stress response and it's influence on fatigue life," in *11th International Conference RASD*, Pisa, 2013.

[90] F. Kihm and D. Delaux, "Vibration fatigue and simulation of damage on shaker table tests: the influence of clipping the random drive signal," *Procedia Engineering*, vol. 66, pp. 549-564, 2013.

[91] F. Kihm and S. A. Rizzi, "The Effect of Drive Signal Limiting on High Cycle Fatigue Life Analysis," in *International Conference on Vibration and Vibro-acoustics*, Harbin, China, 2014.

[92] J. Van Vleck and D. Middeton, "The spectrum of clipped noise," *Proc. IEEE*, vol. 54, pp. 2 -19, 1966.

[93] D. Smallwood, "Generation of time histories with a specified auto spectral density,skewness and kurtosis," in *Proceedings of the Institute of Environmental Sciences*, 1996.

[94] I. Rychlik, P. Johannesson and M. Leadbetter, "Modelling and statistical analysis of ocean-wave data using transformed Gaussian processes," *Marine Structures*, vol. 10, pp. 13-44, 1997.

[95] M. Ochi and K. Ahn, "Probability distribution applicable to non-Gaussian random processes," *Probabilistic Engineering Mechanics*, vol. 9, pp. 255-264, 1994.

[96] A. Steinwolf and N. Ng, "Random vibration testing with PSD simulation supplemented by kurtosis and skewness control," in *Proceedings of the 7th EUROMECH Solid Mechanics Conference*, Lisbon, 2009.

[97] S. Sarkani, D. P. Kihl and J. E. Beach, "Fatigue of welded joints under narrowband non-Gaussian loadings," *Probabilistic Engineering Mechanics*, vol. 9, no. 3, pp. 179-190, 1994.

[98] A. Steinwolf, "Random vibration testing beyond PSD limitations," *Sound and Vibration*, vol. 40, no. 9, pp. 12-21, 2006.

[99] V. Rouillard, "On the Statistical Distribution of Stationary Segment Lengths of Road Vehicles Vibrations," in *World Congress on Engineering*, 2007.

[100] M. Abramowitz and I. Stegun, Handbook of mathematical functions: with formulas, graphs, and mathematical tables, Courier Corporation, 1964.

[101] V. Numerics, IMSL MATH/LIBRARY.: Fortran subroutines for mathematical applications (Vol. 2)., Visual Numerics, Incorporated, 1994.

[102] J. Antoni, *Personal communication. INSA Lyon, France.*

[103] F. Oijer and S. Edlund, "Identification of transient road obstacle distributions and their impact on vehicle durability and driver comfort," *Vehicle system dynamics,* vol. 41, pp. 744-753, 2004.

[104] A. Steinwolf and R. Ibrahim, "Numerical and experimental studies of linear systems subjected to non-Gaussian random excitations," *Probabilistic engineering mechanics,* vol. 14, no. 4, pp. 289-299, 1999.

[105] C. Wu and G. Q. Cai, "Effects of excitation probability distribution on system responses," *International Journal of Non-Linear Mechanics,* vol. 39, pp. 1463-1472, 2004.

[106] . S. Rizzi, A. Przekop and T. Turner, "On the response of a nonlinear structure to high kurtosis non-Gaussian random loadings," in *EURODYN 2011, 8th International Conference on Structural Dynamics, Paper 41*, Leuven, Belgium, 2011.

[107] D. Donoho, "On minimum entropy deconvolution," *Applied time-series analysis II,* p. 565–609, 1981.

[108] K. Sweitzer and N. S. Ferguson, "Mean stress effects on random fatigue of nonlinear structures," in *Twelfth International Congress on Sound and Vibration*, Lisbon, 2005.

[109] I. S. Gradsteyn and I. M. Ryzhik, Tables of integrals, series and products, New York: Academic Press, 1961.

[110] F. Kihm, A. Halfpenny and N. S. Ferguson, "Fatigue Life from Sine-on-random Excitations," *Procedia Engineering,* vol. 101, pp. 235-242, 2015.

[111] R. Lambert , "Fatigue damage accumulation prediction for combined sine and random stresses," *The Journal of Environmental Sciences,* vol. 31, no. 3, pp. 53-63, 1988.

[112] A. Halfpenny, *Personal communication. HBM Prenscia, UK.*.

[113] C. Lalanne, Mechanical Vibration and Shock Analysis, Specification Development (Vol. 5), John Wiley & Sons, 2013.

[114] R. Pinnington, "Tyre–road contact using a particle–envelope surface model," *Journal of Sound and Vibration,* vol. 332, no. 26, p. 7055–7075, 2013.

[115] I. Rychlik, "A new definition of teh rainflow cycle counting method," *International journal of fatigue,* vol. 9, no. 2, pp. 119-121, 1987.

[116] E. Van der Ouderaa, J. Schoukens and J. Renneboog, "Peak factor minimization using a time-trequency domain swapping algorithm," *IEEE Transactions on Instrumentation and Measurement,* vol. 37, no. 1, pp. 145-147, 1988.

[117] J.-L. Sauvaget, *Personal communication. PSA Peugeot Citröen, France.*.

[118] A. Jha, E. Nikolaidis and S. Gangadharan, "Vibration of dynamic systems under cyclostationary excitations," *AIAA journal,* vol. 38, no. 12, pp. 2284-2291, 2000.

# APPENDICES

## APPENDIX A: Statistics and Derivations

### The characteristic function of a normal process

The probability density function $p_r$ of a normally distributed stationary time history with zero mean and variance ${\sigma_x}^2$ is:

$$p_x(x) = \frac{1}{\sqrt{2\pi}\sigma_x} e^{-x^2/2{\sigma_x}^2}$$

The characteristic function $\varphi_x$ of a PDF $p_x$ is written:

$$\varphi_x(k) = \int_{-\infty}^{+\infty} p_x(u) e^{jku} du$$

where $k$ is a real value representing the transform variable and $j$ the imaginary number.
So, for a normal and cantered distribution:

$$\varphi_x(k) = \int_{-\infty}^{+\infty} \frac{1}{\sqrt{2\pi}\sigma_x} e^{-\frac{1}{2}\left(\frac{u}{\sigma_x}\right)^2} e^{jku} du$$

Which can be also written:

$$\varphi_x(k) = \frac{1}{\sqrt{2\pi}\sigma_x} \int_{-\infty}^{+\infty} e^{jku - \frac{1}{2}\left(\frac{u}{\sigma_x}\right)^2} du$$

Rearranging:

$$\varphi_x(k) = \frac{1}{\sqrt{2\pi}\sigma_x} \int_{-\infty}^{+\infty} e^{\frac{-1}{2{\sigma_x}^2}\left[\left(u - jk{\sigma_x}^2\right)^2 + k^2{\sigma_x}^4\right]} du$$

Using the variable substitution $\lambda = \frac{u - jk{\sigma_x}^2}{\sqrt{2}\sigma_x}$, characteristic function $\varphi_x$ becomes

$$\varphi_x(k) = \frac{1}{\sqrt{2\pi}\sigma_x} e^{-\frac{k^2{\sigma_x}^2}{2}} \sqrt{2}\sigma_x \int_{-\infty}^{+\infty} e^{\lambda^2} d\lambda$$

The Gaussian integral is identified:

$$\int_{-\infty}^{+\infty} e^{\lambda^2} d\lambda = \sqrt{\pi}$$

Then,

$$\varphi_x(k) = e^{-\frac{1}{2}{\sigma_x}^2 k^2}$$

This is Equation 2.23.
Note that if $\mu_x \neq 0$, then

$$\varphi_x(k) = e^{\mu_x k - \frac{1}{2}{\sigma_x}^2 k^2}$$

### Level crossings for a stationary and Gaussian process

The expected number of crossings of the level $\alpha$ per unit time with a positive slope is written ${N_\alpha}^+$ and is given by [16, 20, 15]:

$${N_\alpha}^+ = \int_0^\infty y.p_{x,y}(\alpha, y)dy \qquad \text{Equation A.1}$$

Where $p_{x,y}(x, y)$ is the joint probability density function of the random data $x(t)$ and its derivative $y(t) = \dot{x}(t)$. To calculate the joint probability density function $p_{x,y}(x, y)$, both variables are assumed to be Gaussian. The variances of the process and its derivative are respectively ${\sigma_x}^2$ and ${\sigma_{\dot{x}}}^2$, where ${\sigma_{\dot{x}}}^2$ is calculated from the area under the PSD of the derivative, also called the second spectral moment of the PSD $G_{xx}$:

$${\sigma_{\dot{x}}}^2 = \int_0^\infty f^2.G_{xx}(f)df \qquad \text{Equation A.2}$$

The covariance is $\sigma_{xy} = E[x(t).y(t)] = 0$ as proven by Bendat & Piersol [16] in the section called Derivative Random Processes or Newland [20] in chapter 8 "Statistics of narrow-band processes". Therefore, the random variables $x$ and $y$ are uncorrelated and the joint probability density function $p_{x,y}(x, y)$ is calculated as the product of $p_x(x)$ and $p_y(y)$ and expressed as:

$$p_{x,y}(x, y) = \frac{1}{\sigma_x\sqrt{2\pi}} exp\left(-\frac{x^2}{2{\sigma_x}^2}\right)\frac{1}{\sigma_{\dot{x}}\sqrt{2\pi}} exp\left(-\frac{y^2}{2{\sigma_{\dot{x}}}^2}\right) \qquad \text{Equation A.3}$$

Inserting Equation A.3 into Equation A.1, the expression for ${N_\alpha}^+$ becomes for Gaussian processes:

$${N_\alpha}^+ = \frac{1}{2\pi\sigma_x\sigma_{\dot{x}}} exp\left(-\frac{\alpha^2}{2{\sigma_x}^2}\right)\int_0^\infty y.exp\left(-\frac{y^2}{2{\sigma_x}^2}\right)dy$$

Using entries in section 3.321 of [109], the integral is solved and its value is ${\sigma_x}^2$. For a stationary Gaussian random process, the expected number of crossings of the level $\alpha$ per unit time with a positive slope ${N_\alpha}^+$ is now expressed:

$${N_\alpha}^+ = \frac{1}{2\pi}\frac{\sigma_{\dot{x}}}{\sigma_x} exp\left(-\frac{\alpha^2}{2{\sigma_x}^2}\right) \qquad \text{Equation A.4}$$

This is Equation 2.44

### The peak PDF of a narrowband process

The expression in Equation 2.51 can be derived using the Rice representation of narrowband noise. Rice [15] suggests a representation of the random noise $x(t)$ based on the Fourier series:

$$x(t) = \sum_{k=1}^{M} (\alpha_k . \cos(2\pi f_k t) + \beta_k . \sin(2\pi f_k t)) \qquad \text{Equation A.5}$$

where $M$ is a large number ($M \to \infty$) and $\alpha_k$, $\beta_k$ are independent coefficients distributed normally. Or more conveniently:

$$x(t) = \sum_{k=1}^{M} c_k . \cos(2\pi f_k t - \varphi_k) \qquad \text{Equation A.6}$$

where $M$ is a large number ($M \to \infty$), $\varphi_k$ are independent random phase angles with a uniform distribution on the interval [0,2π[ and the coefficients $c_k$ are distributed normally [23].

Let $f_m$ be a representative mid-band frequency for the narrowband noise. The noise signal may be written as:

$$x(t) = \sum_{k=1}^{M} c_k . \cos(2\pi f_k t - 2\pi f_m t - \varphi_k + 2\pi f_m t)$$

Using simple trigonometric relationships:

$$x(t) = \cos(2\pi f_m t) . x_c(t) - \sin(2\pi f_m t) . x_s(t)$$

where $x_c$ and $x_s$ are the components of the random noise that are respectively "in phase" and "in quadrature" with the mid-band frequency $f_m$. Those components can be expressed as:

$$x_c(t) = \sum_{k=1}^{M} c_k . \cos(2\pi f_k t - 2\pi f_m t - \varphi_k)$$

$$x_s(t) = \sum_{k=1}^{M} c_k . \sin(2\pi f_k t - 2\pi f_m t - \varphi_k)$$

Rice [15] showed that $x_c$ and $x_s$ are independent random variables, distributed normally around zero and with the same variance ${\sigma_x}^2$ as $x(t)$.

A typical narrowband signal is depicted in Figure 80.

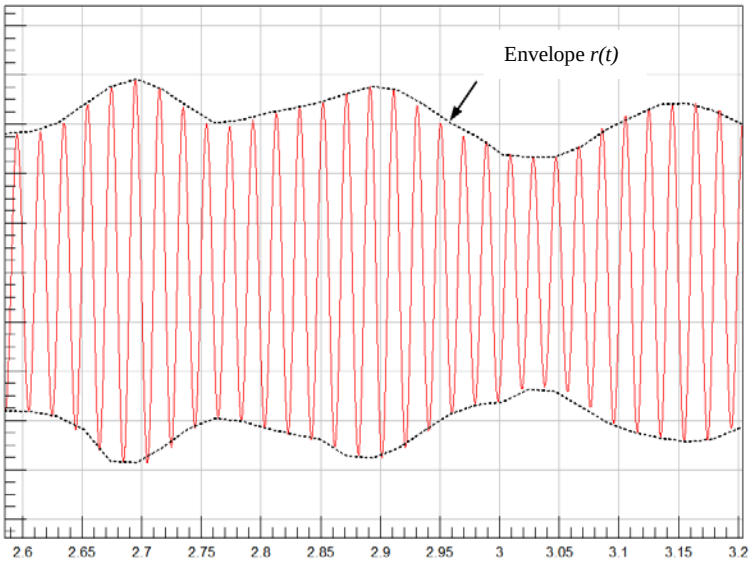


**Figure 80: Example narrowband signal and its envelope**

Such a signal can be expressed:

$$x(t) = r(t)\,.\cos\left(2\pi f_m t + \theta(t)\right) \qquad \text{Equation A.7}$$

where $r(t)$ is the signal's envelope and $\theta(t)$ the phase angle.

$r(t)$ and $\theta(t)$ are slowly varying functions of time relative to the mid-band frequency $f_m$.

The envelope can be expressed as $r(t) = \sqrt{x_c(t)^2 + x_s(t)^2}$.

Papoulis [36] gives the distribution of the root mean square (RMS) value of two independent normal distributions, (see example 6.15 in [36]) and the resulting probability density function is found to be:

$$f_R(r) = \frac{\mathrm{r}}{{\sigma_X}^2}.\mathrm{e}^{-\left(\frac{r^2}{2{\sigma_X}^2}\right)}$$

This is the same Rayleigh distribution with scale parameter $\sigma_X$ as found in Equation 2.51.

### PDF of peaks and valleys for a broadband random process

Rice [15] stated that a local maximum is obtained when the first derivative of the signal is equal to zero and when the second derivative is negative. The marginal distribution of peaks, called the peak probability density function is given by (see [15]):

$$p_{x_p}(s)=\frac{1}{N_p}\int_{-\infty}^{0} -z.\,\mathrm{p}_{X,Y,Z}(s,0,z)dz \qquad \text{Equation A.8}$$

where $\mathrm{p}_{X,Y,Z}(x,y,z)$ is the joint probability density function of the random data $x(t)$, its derivative $y(t)=\dot{x}(t)$ and its second derivative $z(t)=\ddot{x}(t)$. The joint probability density function $\mathrm{p}_{\mathrm{X,Y,Z}}(\mathrm{x,y,z})$ can be calculated if all variables are assumed to be Gaussian. Using the generic results from the section on N-dimensional normal distributions in [16], the joint probability density function $\mathrm{p}_{X,Y,Z}(x,y,z)$ can be calculated from the marginal distributions $p_x(x)$, $p_y(y)$ and $p_z(z)$ and the covariance matrix.

The variances of the process and its derivatives are respectively ${\sigma_x}^2$, ${\sigma_{\dot{x}}}^2$ and ${\sigma_{\ddot{x}}}^2$.

The covariances $\sigma_{XY}$ and $\sigma_{YZ}$ are zero as proven by Bendat & Piersol [16] in the section called Derivative Random Processes or Newland [20] in chapter 8 “Statistics of narrow-band processes”. The covariance $\sigma_{XZ}$ is ${\sigma_{\dot{X}}}^2$ as proven by Rice [15] in section 3.6.

Finally, an expression for $\mathrm{p}_{X,Y,Z}(s,0,z)$ is found and Equation A.8 can be solved. Rice [15] showed that in the case of a broadband process, the peak distribution is expressed by Equation 2.54.

### Distribution of the weighted sum of Rayleigh and Normal distributed random variables

The value of a peak $S$ is a random variable. It is assumed that the value of the random variable $S$ is a weighted sum of two independent random variables $S_r$ and $S_g$ which are respectively distributed according to Rayleigh and Normal laws.

$$S = \alpha.S_g + \beta.S_r$$

with $\alpha$ and $\beta$ two real valued weighting coefficients.

The first and second order statistical moments of $S$ are:

$$E[S] = E\left[\alpha.S_g + \beta.S_r\right] = \alpha.E[S_g] + \beta.E[S_r]$$

$$E[S^2] = E\left[\left(\alpha.S_g + \beta.S_r\right)^2\right] = \alpha^2.E[{S_g}^2] + \beta^2.E[{S_r}^2]$$

There are several possible solutions for $\alpha$ and $\beta$. Those solutions contain the irregularity factor γ since, as stated in previous section when γ tends to 1.0, S tends to $S_r$, and when γ tends to 0.0, S tends to $S_g$.

Taking the weighting coefficients to be $\alpha^2 = 1 - \gamma^2$ and $\beta^2 = \gamma^2$, S can be written:

$$S = \sqrt{1 - \gamma^2}.S_g + \gamma.S_r$$

The random variable $S_g$is normal with zero mean and variance ${\sigma_x}^2$, therefore $\sqrt{1 - \gamma^2}.S_g$ is normal with zero mean and variance ${\sigma_1}^2 = {\sigma_x}^2.(1 - \gamma^2)$ and its PDF is given as :

$$f_G(x) = \frac{1}{\sqrt{2\pi}\sigma_1} e^{\frac{-x^2}{2{\sigma_1}^2}}$$

The random variable $S_r$is distributed according to a Rayleigh distribution with scale parameter $\sigma_x$, therefore $\gamma.S_r$ is distributed as Rayleigh with scale parameter $\sigma_2 = \sigma_x.\gamma$ and its PDF is given as :

$$f_R(x) = \frac{x}{{\sigma_2}^2} e^{\frac{-x^2}{2.{\sigma_2}^2}}$$

Papoulis [5] demonstrates that the PDF of the sum of 2 independent variables with PDF $p_R$ and $p_G$ is expressed:

$$p_p(s) = \int_0^{+\infty} p_R(x).p_G(s - x)dx$$

Which can be then developed:

$$p_p(s) = \int_0^{+\infty} \frac{x}{{\sigma_2}^2} e^{\frac{-x^2}{2.{\sigma_2}^2}} . \frac{1}{\sqrt{2\pi}\sigma_1} e^{\frac{-(s-x)^2}{2.{\sigma_1}^2}} dx$$

$$p_p(s) = \frac{1}{\sqrt{2\pi}.\sigma_1.{\sigma_2}^2} \int_0^{+\infty} x.e^{\frac{-x^2({\sigma_1}^2+{\sigma_2}^2)}{2.{\sigma_2}^2.{\sigma_1}^2}} . e^{\frac{x.s}{{\sigma_1}^2}} . e^{\frac{-s^2}{2.{\sigma_1}^2}} dx$$

$$p_p(s) = \frac{1}{\sqrt{2\pi}.\sigma_1.{\sigma_2}^2} \int_0^{+\infty} x.e^{\frac{-x^2({\sigma_1}^2+{\sigma_2}^2)+x.2.s.{\sigma_2}^2-s^2.{\sigma_2}^2}{2.{\sigma_2}^2.{\sigma_1}^2}} dx$$

Using $a = \frac{{\sigma_1}^2+{\sigma_2}^2}{2.{\sigma_2}^2.{\sigma_1}^2}$, $b = \frac{s}{{\sigma_1}^2}$, $c = -\frac{s^2}{2.{\sigma_1}^2}$ , this simplifies to :

$$p_p(s) = \frac{1}{\sqrt{2\pi}.\sigma_1.{\sigma_2}^2} \int_0^{+\infty} x.e^{-x^2a+x.b+c} dx$$

Now rewriting the exponent:

$$-x^2a + x.b + c = -a\left(x - \frac{b}{2a}\right)^2 + c + \frac{b^2}{4a}$$

Therefore

$$e^{-x^2a+x.b+c} = e^{-a\left(x-\frac{b}{2a}\right)^2} . e^{c+\frac{b^2}{4a}}$$

$p_p(s)$ can be rewritten:

$$p_p(s) = \frac{e^{c+\frac{b^2}{4a}}}{\sqrt{2\pi}.\sigma_1.{\sigma_2}^2} \int_0^{+\infty} x.e^{-a\left(x-\frac{b}{2a}\right)^2} dx$$

writting $x = x - \frac{b}{2a} + \frac{b}{2a}$:

$$p_p(s) = \frac{e^{c+\frac{b^2}{4a}}}{\sqrt{2\pi}.\sigma_1.{\sigma_2}^2} \left( \int_0^{+\infty} \left(x - \frac{b}{2a}\right) . e^{-a\left(x-\frac{b}{2a}\right)^2} dx + \int_0^{+\infty} \frac{b}{2a} . e^{-a\left(x-\frac{b}{2a}\right)^2} dx \right)$$

And using the substitution $= x - \frac{b}{2a}$ , the first integral is evaluated and the second integral can be expressed in terms of the error function defined as :

$$erf(x) = \frac{2}{\sqrt{\pi}} \int_0^x e^{-t^2} dt = 1 - \frac{2}{\sqrt{\pi}} \int_x^{\infty} e^{-t^2} dt$$

Therefore:

$$p_p(s) = \frac{e^{c+\frac{b^2}{4a}}}{\sqrt{2\pi}.\sigma_1.{\sigma_2}^2}\left\{\frac{0.5}{a}.e^{-\frac{b^2}{4.a}} + \frac{b\sqrt{\pi}}{4a\sqrt{a}}.\left(1+\text{erf}\left(\sqrt{a}\left(\frac{b}{2a}\right)\right)\right)\right\}$$

Substituting $a$, $b$ and $c$ with $\sigma_1$ and $\sigma_2$ and then with $\gamma$ and ${\sigma_x}^2$ gives:

$$p_p(s) = \frac{1}{\sqrt{2\pi{\sigma_x}^2(1-\gamma^2)}.{\sigma_x}^2\gamma^2}.\left\{{\sigma_X}^2\gamma^2(1-\gamma^2).e^{-\frac{s^2}{2.{\sigma_x}^2(1-\gamma^2)}} + \frac{s.\gamma^3.\sqrt{2\pi{\sigma_x}^2(1-\gamma^2)}}{2}.e^{-\frac{s^2}{2.{\sigma_X}^2}}.\left(1+\text{erf}\left(\frac{s.\gamma}{\sqrt{2{\sigma_x}^2(1-\gamma^2)}}\right)\right)\right\}$$

Which simplifies as:

$$p_p(s) = \frac{\sqrt{1-\gamma^2}}{\sqrt{2\pi}\sigma_x}.e^{-\frac{s^2}{2.{\sigma_x}^2(1-\gamma^2)}} + \frac{s.\gamma}{2{\sigma_x}^2}.e^{-\frac{s^2}{2.{\sigma_x}^2}}.\left(1+\text{erf}\left(\frac{s.\gamma}{\sqrt{2{\sigma_x}^2(1-\gamma^2)}}\right)\right)$$

Factoring by $1/\sigma_x$:

$$p_p(s) = \frac{1}{\sigma_x}\left\{\frac{\sqrt{1-\gamma^2}}{\sqrt{2\pi}}.e^{-\frac{s^2}{2.{\sigma_x}^2(1-\gamma^2)}} + \frac{s.\gamma}{2\sigma_x}.e^{-\frac{s^2}{2.{\sigma_x}^2}}.\left(1+\text{erf}\left(\frac{s.\gamma}{\sigma_x\sqrt{2(1-\gamma^2)}}\right)\right)\right\}$$

Which is identical to the expression in Equation 2.54.

### PDF of the maximum peak

There are a number of research papers involved with finding the distribution for the maximum peak $X_m$ out of $N_pT$ peaks [43, 44, 23, 45]. If $P$ is the probability of an observation being less than $s$, the probability that the greatest of a sample of $N$ peaks is less than $s$ is $P^N$ [43]. Consequently, if $P_p$ is the Cumulative Distribution Function (CDF) of the peaks in a sample signal, then out of $N_pT$ peaks, the CDF of the maximum peak is:

$$P_{X_m}(s) = \big(P_p(s)\big)^{N_pT} \qquad \text{Equation A.9}$$

Note that the PDF of the largest peak value out of $N_pT$ peaks of a random process can be obtained by differentiation of Equation A.9 and is expressed as:

$$p_{X_m}(s) = N_pT p_p(s)\big(P_p(s)\big)^{N_pT-1} \qquad \text{Equation A.10}$$

The expected value for the largest peak i.e. the average value of the largest peak out of $N_pT$ peaks $\overline{X_m}$ is computed using Equation 2.4 as $\overline{X_m} = \int_{-\infty}^{\infty} s p_{X_m}(s) ds$.

In the case of a narrowband signal ($\gamma \to 1$), for a large value of peaks $N_pT$, an asymptotic expression for $\overline{X_m}$ was calculated to be [44]:

$$\overline{X_m} \approx \sigma_X \left( \sqrt{2\ln\big(N_pT\big)} + \frac{\varepsilon}{\sqrt{2\ln\big(N_pT\big)}} \right) \qquad \text{Equation A.11}$$

Here $\varepsilon$ denotes the Euler constant: $\varepsilon = 0.577215$ ...

In the case of a broadband signal ($0 < \gamma \leq 1$), for a large value of peaks $N_pT$, the asymptotic expression above was adapted to take into account the irregularity factor [23]:

$$\overline{X_m} \approx \sigma_X \left( \sqrt{2\ln\big(\gamma N_pT\big)} + \frac{\varepsilon}{\sqrt{2\ln\big(\gamma N_pT\big)}} \right) \qquad \text{Equation A.12}$$

When $\gamma$ approaches zero, the above expression is no longer valid. Fisher & Tippett [43] have shown that the average value of the largest peak out of $N_pT$ peaks in this case is given by:

$$\overline{X_m} \approx \sigma_X \left( \mathrm{m} + \frac{\varepsilon m}{m^2 + 1} \right) \qquad \text{Equation A.13}$$

where $m$ is the mode of the distribution of maximum peaks $m \approx \sqrt{ln\left(\frac{\left(N_pT\right)^2}{2\pi}\right) - ln\left[ln\left(\frac{\left(N_pT\right)^2}{2\pi}\right)\right]}$.

## APPENDIX B: Amplitude modulated random signals

### Kurtosis of an amplitude modulated signal with successive bursts

The fourth statistical moment of the amplitude modulated signal $y(t)$ is calculated using $E[y^4] = E[a^4]E[x^4]$.

The fourth statistical moment of the underlying Gaussian signal $x(t)$ is $E[x^4] = 3{\sigma_x}^4$.

The additive property of cumulants shall be used to calculate the fourth statistical moment of the modulating function $a(t)$. The fourth cumulant $C_{a,4}$ of the modulating function $a(t)$ is the sum of the fourth cumulants of the harmonic signal $C_{A,4}$ and the constant signal $C_{B,4}$ (see Equation 2.20 in section 2.1.11):

$$C_{a,4} = C_{A,4} + C_{B,4}$$

Then, using the cumulants-moments relationships (see Equation 2.24 in section 2.1.11)

$$C_{a,4} = M_{A,4} + M_{B,4} - 3\left(M_{A,2}\right)^2 - 3\left(M_{B,2}\right)^2$$

and since $C_{a,4} = M_{a,4} - 3\left(M_{a,2}\right)^2$

then, $M_{a,4} = M_{A,4} + M_{B,4} - 3\left(M_{A,2}\right)^2 - 3\left(M_{B,2}\right)^2 + 3\left(M_{a,2}\right)^2$.

Now, replacing $M_{A,2}$ with $\frac{1}{2}A^2$ , $M_{A,4}$ with $\frac{3}{2}\left(\frac{A^2}{2}\right)^2$ (since the kurtosis of a sine wave is $\frac{3}{2}$), $M_{B,2}$ with $B^2$ and $M_{B,4}$ with $B^4$ and $M_{a,2}$ with $\left(B^2 + \frac{1}{2}A^2\right)$, the expression for $M_{a,4}$ becomes:

$M_{a,4} = E[a^4] = \frac{3}{8}A^4 + B^4 + 3A^2B^2$

Finally, the fourth statistical moment of $y(t)$ is obtained as:

$E[y^4] = E[a^4]E[x^4] = \left(\frac{3}{8}A^4 + B^4 + 3A^2B^2\right)3{\sigma_x}^4$

Note that the kurtosis of $y(t)$ is:

$$\kappa_y = 3\frac{\left(\frac{3}{8}A^4 + B^4 + 3A^2B^2\right)}{\left(B^2 + \frac{1}{2}A^2\right)^2}$$

which can be rearranged as:

$$\kappa_y = \frac{3}{2}A^2.\frac{(A^2 + 16B^2)}{(A^2 + 2B^2)^2} + 3$$

This is Equation 3.17.

### Initial estimates of A and B for a prescribed Kurtosis value

To produce a signal that follows both the prescribed PSD and kurtosis using amplitude modulation, it is proposed to first derive a stationary signal $x(t)$ from the PSD, as described in section 3.2 and then multiply it by a modulation function $a(t)$. The characteristics of $a(t)$ are calculated based on the value of the target kurtosis and the rate of bursts $r_b$, chosen based on the type of phenomenon, more or less impulsive, that one wants to simulate.

The objective is therefore to solve the system of equations given in Equation 3.19 to find the unknown coefficients $A$ and $B$ for a prescribed kurtosis value and a given proportion of bursts $r_b$. Newton's method can be used to solve the system of nonlinear equations in Equation 3.19. Initial estimates for $A$ and $B$ are required for the iterative algorithm to converge more rapidly. The calculation of the initial estimates is given here.

First, note that the amplitude modulation is expected to keep the global energy of the signal, in other words, the variance of the amplitude modulated signal $y(t)$ should be the same as the variance of the underlying random signal $x(t)$. This means that $E[y^2] = {\sigma_x}^2$. Therefore, the first equation of the system of equations given in Equation 3.19 can be developed and re-written as:

$$B^2 + 2AB(r_b - 1) + \left(1 - \frac{1}{2}r_b\right)A^2 - 1 = 0$$

If one considers $B$ as the unknown, the discriminant of the quadratic equation $\Delta$ is found to be:

$$\Delta = 4A^2\left({r_b}^2 - \frac{3}{2}r_b\right) + 4$$

In order to obtain real roots, A must be chosen such that $A^2\left({r_b}^2 - \frac{3}{2}r_b\right) + 1 \geq 0$. In this case, the real roots obtained are:

$$B = A(1 - r_b) \pm \frac{\sqrt{\Delta}}{2}$$

Note that in the case of a zero discriminant, then $B = A(1 - r_b)$, which is not acceptable since in this case $B \leq A$ and the modulating function is therefore not always positive. So the discriminant must be strictly positive, which corresponds to a positive bound for:

$$A^2 < \frac{1}{\left|{r_b}^2 - \frac{3}{2}r_b\right|}$$

Note that ${r_b}^2 - 3/2r_b < 0$ for $0 < r_b \leq 1$, and the case $r_b = 0$ is excluded here since it would lead to a zero denominator.

So an initial estimate for $A$ can be: $A_{estimate} = 0.5\sqrt{\frac{1}{\left|{r_b}^2 - \frac{3}{2}r_b\right|}}$

Then, the initial estimate for $B$ can be deduced from the equation $B = A(1 - r_b) \pm \frac{\sqrt{\Delta}}{2}$. Since $B$ must be positive, the initial estimate for $B$ can be:

$$B_{estimate} = A_{estimate}(1 - r_b) + \sqrt{{A_{estimate}}^2({r_b}^2 - 3/2r_b) + 1}$$

Routines based on Newton's method such as zeros_sys_eqn in IMSL [101] can be used to solve the system of nonlinear equations using the provided initial estimates $A_{estimate}$ and $B_{estimate}$.

**Fourier coefficients of the modulating function**

Considering the random process $y(t) = a(t)x(t)$ where $x(t)$ stationary and $a(t)$ a periodic modulation function, with period $T$,

$$a(t) = \begin{cases} (B - A) & -T/2 \le t \le -T_0/2 \\ (Acos(2\pi f_0 t) + B) & -T_0/2 \le t \le T_0/2 \\ (B - A) & T_0/2 \le t \le T/2 \end{cases}$$

The modulation function is graphically represented below:

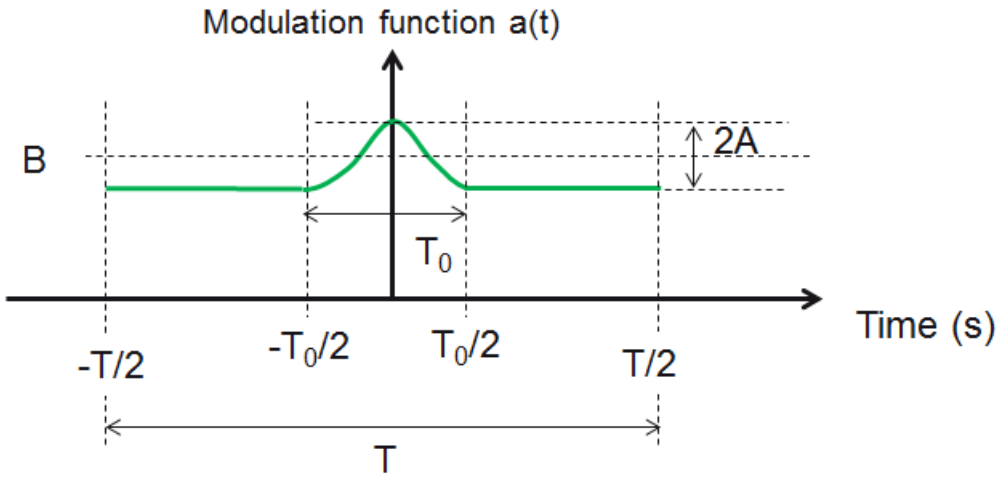


The modulation function has the following decomposition into Fourier series:

$$a(t) = a_0 + \sum_{k \neq 0} a_k \cos\left(2\pi \frac{kt}{T}\right) + \sum_{k \neq 0} b_k \sin\left(2\pi \frac{kt}{T}\right)$$

where

$$a_0 = \frac{1}{T} \int_{-T/2}^{T/2} a(t)dt$$

$$a_k = \frac{1}{T}\int_{-\frac{T}{2}}^{\frac{T}{2}} a(t)\cos\left(-2\pi\frac{kt}{T}\right)dt$$

$$b_k = \frac{1}{T}\int_{-T/2}^{T/2} a(t)\sin\left(-2\pi\frac{kt}{T}\right)dt$$

Since $a(t)$ is an even function of $t$, the $b_k$ coefficients are all zero. The $a_0$ coefficient is calculated as:

$$a_0 = \frac{1}{T}\left(2(B-A)\frac{T-T_0}{2} + T_0B + A\int_{-\mathrm{T}/2}^{\mathrm{T}/2} cos(2\pi f_0 t)dt\right)$$

$$a_0 = (B-A) + \frac{T_0}{T}A + \frac{A}{T}\left[\frac{sin(2\pi f_0 t)}{2\pi f_0}\right]_{-\mathrm{T}/2}^{\mathrm{T}/2}$$

$$a_0 = (B-A) + \frac{T_0}{T}A$$

And now the $a_k$ coefficients:

$$a_k = \frac{(B-A)}{T}\int_{-T/2}^{-T_0/2}\cos\left(2\pi\frac{kt}{T}\right)dt + \frac{A}{T}\int_{-T_0/2}^{T_0/2} cos(2\pi f_0 t)\cos\left(2\pi\frac{kt}{T}\right)dt + \frac{B}{T}\int_{-T_0/2}^{T_0/2}\cos\left(2\pi\frac{kt}{T}\right)dt + \frac{(B-A)}{T}\int_{T_0/2}^{T/2}\cos\left(2\pi\frac{kt}{T}\right)dt$$

Using $cos(2\pi f_0 t)\cos\left(2\pi\frac{kt}{T}\right) = \frac{1}{2}\left(cos\left(2\pi\left(f_0+\frac{k}{T}\right)t\right) + \cos\left(2\pi\left(f_0-\frac{k}{T}\right)t\right)\right)$, the coefficients become :

$$a_k = \frac{(B-A)}{T}\int_{-T/2}^{-T_0/2}\cos\left(2\pi\frac{kt}{T}\right)dt + \frac{A}{2T}\int_{-T_0/2}^{T_0/2} cos\left(2\pi\left(f_0+\frac{k}{T}\right)t\right)dt + \frac{A}{2T}\int_{-T_0/2}^{T_0/2} cos\left(2\pi\left(f_0-\frac{k}{T}\right)t\right)dt + \frac{B}{T}\int_{-T_0/2}^{T_0/2}\cos\left(2\pi\frac{kt}{T}\right)dt + \frac{(B-A)}{T}\int_{T_0/2}^{T/2}\cos\left(2\pi\frac{kt}{T}\right)dt$$

Writing the primitives:

$$a_k = \frac{(B-A)}{T}\left[\frac{sin\left(2\pi\frac{kt}{T}\right)}{2\pi\frac{k}{T}}\right]_{-T/2}^{-T_0/2} + \frac{A}{2T}\left[\frac{sin\left(2\pi\left(f_0+\frac{k}{T}\right)t\right)}{2\pi\left(f_0+\frac{k}{T}\right)}\right]_{-T_0/2}^{T_0/2}$$
$$+ \frac{A}{2T}\left[\frac{sin\left(2\pi\left(f_0-\frac{k}{T}\right)t\right)}{2\pi\left(f_0-\frac{k}{T}\right)}\right]_{-T_0/2}^{T_0/2} + \frac{B}{T}\left[\frac{sin\left(2\pi\frac{kt}{T}\right)}{2\pi\frac{k}{T}}\right]_{-T_0/2}^{T_0/2}$$
$$+ \frac{(B-A)}{T}\left[\frac{sin\left(2\pi\frac{kt}{T}\right)}{2\pi\frac{k}{T}}\right]_{T_0/2}^{T/2}$$

Developing:

$$a_k = \frac{(B-A)}{2\pi k}\left(sin\left(-\pi\frac{kT_0}{T}\right)\right) - \frac{A}{2T}\left(\frac{sin\left(\pi\frac{k}{T}T_0\right)}{\pi\left(f_0+\frac{k}{T}\right)}\right) + \frac{A}{2T}\left(\frac{sin\left(\pi\frac{k}{T}T_0\right)}{\pi\left(f_0-\frac{k}{T}\right)}\right)$$
$$+ \frac{B}{2\pi k}\left(2.sin\left(\pi\frac{kT_0}{T}\right)\right) + \frac{(B-A)}{2\pi k}\left(-sin\left(\pi\frac{kT_0}{T}\right)\right)$$

Which can be rearranged:

$$a_k = \frac{A}{\pi k}\left(sin\left(\pi\frac{kT_0}{T}\right)\right) - \frac{A}{2T}\left(\frac{sin\left(\pi\frac{k}{T}T_0\right)}{\pi\left(f_0+\frac{k}{T}\right)}\right) + \frac{A}{2T}\left(\frac{sin\left(\pi\frac{k}{T}T_0\right)}{\pi\left(f_0-\frac{k}{T}\right)}\right)$$

Factoring:

$$a_k = \frac{T_0}{T}\frac{A}{\pi\frac{kT_0}{T}}\left(sin\left(\pi\frac{kT_0}{T}\right)\right) + k\frac{T_0}{T}\frac{A}{2\pi\frac{k}{T}T_0}sin\left(\pi\frac{k}{T}T_0\right)\left(\frac{1}{(Tf_0-k)} - \frac{1}{(Tf_0+k)}\right)$$

Rearranging:

$$a_k = A\frac{T_0}{T}\left(\frac{sin\left(\pi\frac{kT_0}{T}\right)}{\pi\frac{kT_0}{T}}\right)\left(1 + \frac{k}{2(Tf_0-k)} - \frac{k}{2(Tf_0+k)}\right)$$

In more compact notations:

$$a_k = A\frac{T_0}{T}\left(1 + \frac{k^2}{(T/T_0)^2-k^2}\right)\left(\frac{sin\left(\pi\frac{kT_0}{T}\right)}{\pi\frac{kT_0}{T}}\right)$$

The real coefficients of the Fourier transform are even i.e. $a_{-k} = a_k$.

This is Equation 3.23

### Expression for the output kurtosis for an excitation made of successive bursts

When the modulation function is a non-centred sine wave : $a(t) = Acos(2\pi f_0 t) + B$, i.e. when $r_b = \frac{T_0}{T} = 1$, then the Fourier coefficients $a_k$ of the modulation function are all zero except $a_0 = B$ and $a_{-1} = a_1 = A/2$.

Using Equation 2.72, the cyclic spectrum of $y(t)$ is zero but for $\alpha = 0$, $\alpha = 1/T$ and $\alpha = 2/T$. The cyclic spectrum of the amplitude modulated excitation $S_{yy}^{\alpha}(f)$ is therefore given as:

$$S_{yy}^{\alpha}(f) = \begin{cases} B^2 S_{xx}(f) + \frac{A^2}{4} S_{xx}\left(f - \frac{1}{T}\right) + \frac{A^2}{4} S_{xx}\left(f + \frac{1}{T}\right), \alpha = 0 \\ \frac{AB}{2} S_{xx}\left(f + \frac{1}{2T}\right) + \frac{AB}{2} S_{xx}\left(f - \frac{1}{2T}\right), \alpha = 1/T \\ \frac{A^2}{4} S_{xx}(f), \alpha = 2/T \\ 0, \text{ otherwise} \end{cases}$$

Consider a non-centred sine wave where the Fourier coefficients $a_k$ are all zero except $a_0 = B$ and $a_{\pm 1} = A/2$.

Using Equation 4.13, the output kurtosis $\kappa_z$can be calculated for the cases $p = 0$, $p = \pm 1$ and $p = \pm 2$ with $k = 0$ or $k = \pm 1$:

$$\kappa_z = \left( \begin{array}{c} 1 + \frac{\left| \int H\left(f + \frac{1}{2T}\right) . \left\{ \frac{AB}{2} S_x\left(f - \frac{1}{2T}\right) + \frac{AB}{2} S_x\left(f + \frac{1}{2T}\right) \right\} . H^*\left(f - \frac{1}{2T}\right) df \right|^2}{\left| \int H(f) . \left\{ B^2 S_x(f) + \frac{A^2}{4} S_x\left(f - \frac{1}{T}\right) + \frac{A^2}{4} S_x\left(f + \frac{1}{T}\right) \right\} . H^*(f) df \right|^2} + \\ \frac{\left| \int H\left(f + \frac{1}{2T}\right) . \left\{ \frac{AB}{2} S_x\left(f - \frac{1}{2T}\right) + \frac{AB}{2} S_x\left(f + \frac{1}{2T}\right) \right\} . H^*\left(f - \frac{1}{2T}\right) df \right|^2}{\left| \int H(f) . \left\{ B^2 S_x(f) + \frac{A^2}{4} S_x\left(f - \frac{1}{T}\right) + \frac{A^2}{4} S_x\left(f + \frac{1}{T}\right) \right\} . H^*(f) df \right|^2} + \\ 2 \frac{\left| \int H\left(f + \frac{1}{T}\right) . \left\{ \frac{A^2}{4} S_x(f) \right\} . H^*\left(f - \frac{1}{T}\right) df \right|^2}{\left| \int H(f) . \left\{ B^2 S_x(f) + \frac{A^2}{4} S_x\left(f - \frac{1}{T}\right) + \frac{A^2}{4} S_x\left(f + \frac{1}{T}\right) \right\} . H^*(f) df \right|^2} \end{array} \right) \kappa_x$$

Noting that the 2 first lines are identical:

$$\kappa_z = \left( \begin{array}{c} 1 + 2\dfrac{\left|\int H\left(f+\frac{1}{2T}\right).\left\{\frac{AB}{2}S_x\left(f-\frac{1}{2T}\right)+\frac{AB}{2}S_x\left(f+\frac{1}{T}\right)\right\}.H^*\left(f-\frac{1}{2T}\right)df\right|^2}{\left|\int H(f).\left\{B^2S_x(f)+\frac{A^2}{4}S_x\left(f-\frac{1}{T}\right)+\frac{A^2}{4}S_x\left(f+\frac{1}{T}\right)\right\}.H^*(f)df\right|^2} + \\ 2\dfrac{\left|\int H\left(f+\frac{1}{T}\right).\left\{\frac{A^2}{4}S_x(f)\right\}.H^*\left(f-\frac{1}{T}\right)df\right|^2}{\left|\int H(f).\left\{B^2S_x(f)+\frac{A^2}{4}S_x\left(f-\frac{1}{T}\right)+\frac{A^2}{4}S_x\left(f+\frac{1}{T}\right)\right\}.H^*(f)df\right|^2} \end{array} \right) \kappa_x$$

Getting $\frac{AB}{2}$ and $\frac{A^2}{4}$ out of the integral :

$$\kappa_z = \left( \begin{array}{c} 1 + \dfrac{A^2B^2}{2}\dfrac{\left|\int H\left(f+\frac{1}{2T}\right).\left\{S_x\left(f-\frac{1}{2T}\right)+S_x\left(f+\frac{1}{T}\right)\right\}.H^*\left(f-\frac{1}{2T}\right)df\right|^2}{\left|\int H(f).\left\{B^2S_x(f)+\frac{A^2}{4}S_x\left(f-\frac{1}{T}\right)+\frac{A^2}{4}S_x\left(f+\frac{1}{T}\right)\right\}.H^*(f)df\right|^2} + \\ \dfrac{A^4}{8}\dfrac{\left|\int H\left(f+\frac{1}{T}\right).S_x(f).H^*\left(f-\frac{1}{T}\right)df\right|^2}{\left|\int H(f).\left\{B^2S_x(f)+\frac{A^2}{4}S_x\left(f-\frac{1}{T}\right)+\frac{A^2}{4}S_x\left(f+\frac{1}{T}\right)\right\}.H^*(f)df\right|^2} \end{array} \right) \kappa_x$$

Which is Equation 4.14.

## APPENDIX C: Sine-On-Random

The vibration environment generated by rotating machines such as internal combustion engines, turbines, pumps, electric motors for generators, etc. typically comprises harmonic tones superimposed on background noise [110].

Time domain simulations of a sine-on-random process can be used:

- to validate some theoretically derived statistics
- to simulate the excitation of a non-linear system

Sine-on-random excitations are specified in international standards such as in MIL STD 810G [2] or in DO 160G [4].

The description and various distributions associated with sine-on-random signals are presented in this section. The sine-on-random process is a composite process, comprising a deterministic sine wave and a random process. The random noise is considered to be stationary, ergodic and Gaussian. Mean values of the noise and harmonics are considered to be zero in the rest of this analysis. The random noise and the sine tones are considered to be independent processes.

### Sine-on-random representation and statistical properties

A sine-on-random process is typically represented by a Power Spectral Density (PSD) showing power spectral density versus frequency on the top of which there are vertical peaks representing the superimposed sine tones.

Note that if a sine-on-random process was represented with a PSD only, the presence of a pure tone of amplitude $A$ at frequency $f$ will produce a peak at that frequency with an infinite magnitude $\lim_{\Delta f \to 0} \frac{A^2}{4\Delta f}$ indicating that an unbounded quantity of energy is necessary to produce it [46]. Hence, checking for the presence of peaks in the PSD is the common practice to investigate whether the signal of interest contains periodic waveforms or whether it is purely random [46].

Figure 81 shows an example spectral representation of a sine-on-random process, as can be found in various military and civil standards [1, 4, 2].

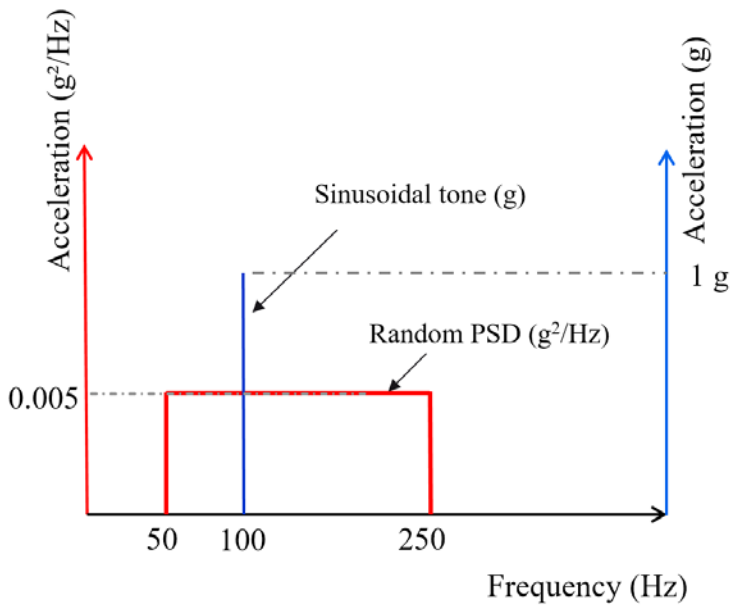


**Figure 81 : Spectral representation of a sine-on-random process**

A sine-on-random signal can be represented as:

$$y(t) = x(t) + \sum_{i=1}^{N} b_i . \cos(2\pi f_i t + \varphi_i) \qquad \text{Equation C.1}$$

with $x(t)$ some random noise and $b_i$, $f_i$ and $\varphi_i$ the amplitude, frequency and phase of the $N$ sine tones.

The probability density function $p_s$ of a sine wave of amplitude $A$ and random initial phase angle $\varphi_A$ is [20, 15]:

$$p_s(s) = \begin{cases} \dfrac{1}{\pi\sqrt{A^2 - s^2}} & if\ |s| < A \\ 0 & if\ |s| \geq A \end{cases} \qquad \text{Equation C.2}$$

The probability density function $p_x$ of a normally distributed stationary time history with zero mean and variance ${\sigma_x}^2$ is:

$$p_x(x) = \frac{1}{\sqrt{2\pi}\sigma_x} e^{-x^2/2{\sigma_x}^2} \qquad \text{Equation C.3}$$

Papoulis [36] demonstrates that the PDF of the sum of two independent variables with PDFs $p_x$ and $p_s$ is expressed as a convolution product of the individual PDFs (see Equation 2.14 in section 2.1.9.1). The PDF of a sine-on-random process $p_y$ is therefore expressed as:

$$p_y(y) = \int_{-\infty}^{\infty} p_x(y - \tau) . p_s(\tau)\, d\tau$$

Inserting the expressions for $p_x$ and $p_s$ one has:

$$p_y(y) = \frac{1}{\pi\sqrt{2\pi}\sigma_x}\int_{-A}^{A}\frac{e^{-(y-\tau)^2/2{\sigma_x}^2}}{\sqrt{A^2-\tau^2}}.d\tau$$

Using the change of variable $\tau = Acos\phi$ and $d\tau = -Asin\phi d\phi = -\sqrt{A^2-\tau^2}d\phi$, the expression for $p_y$ becomes:

$$p_y(y) = \frac{1}{\pi\sigma_x}\int_0^{\pi}\psi\left(\frac{y-Acos\phi}{\sigma}\right)d\phi \qquad \text{Equation C.4}$$

where $\psi(x) = \frac{1}{\sqrt{2\pi}}e^{-\frac{1}{2}x^2}$ is the standardized normal probability density function.

Note that this general expression for $p_y$ is identical to the one found by Bendat and Piersol [16].

Another expression can be obtained by considering the characteristic functions $\varphi_s$ and $\varphi_x$ of $p_s$ and $p_x$.

From the definition of the characteristic function:

$$\varphi_s(k) = \frac{1}{\pi}\int_{-A}^{+A}\frac{e^{-j2\pi kx}}{\sqrt{A^2-x^2}}dx$$

Adopting the change of variable $x = A.sin(y)$ leads to $dx = A.cos(y)dy$ and $A^2 - x^2 = A^2\,cos^2(y)$, therefore $\sqrt{A^2-x^2} = A\,cos(y)$ since $A^2 - x^2 \geq 0$.

The integral becomes:

$$\varphi_s(k) = \frac{1}{\pi}\int_{-\infty}^{\infty}e^{-j2\pi kA.sin(y)}\,dy$$

The integral can be limited to $\mp\pi/2$. Noting that $\sin(2\pi kA.sin(y))$ is an odd function and $\cos(2\pi kA.sin(y))$ is an even function, the integral becomes:

$$\varphi_s(k) = \frac{2}{\pi}\int_0^{\pi/2}\cos(2\pi kA.sin(y))dy$$

Using entry WA 30(7) in [109], $\varphi_s$ can be expressed using the Bessel function of the first kind $J_0$ as:

$$\varphi_s(k) = J_0(kA)$$

The characteristic function of the composite process is obtained by multiplying the individual characteristic functions. Then, the PDF of the composite process is found by inverse Fourier transforming the characteristic function. In the end, the generic expression for the probability density function of a sine-on-random process is:

$$p_y(y) = \frac{1}{\pi}\int_0^{\infty} J_0(At)\,.\,e^{-\frac{1}{2}{\sigma_x}^2 t^2}\cos(yt)dt \qquad \text{Equation C.5}$$

This expression is identical to the one found by Rice [15, 34].

More generally, considering $N$ sine waves $s_1, s_2, \dots, s_N$, assuming their frequencies are incommensurable, the characteristic function of a sine-on-random process is given as :

$$\varphi_{sr}(k) = \prod_{i=1}^{N} J_0(2\pi k b_i)\,.\,e^{-\frac{1}{2}{\sigma_x}^2(2\pi k)^2}$$

with $b_i$ the amplitudes of the ith sine wave.

The PDF of the sine-on-random process $p_y$ is calculated by inverse Fourier transform of $\varphi_{sr}$, and after some variable substitution, is found to be:

$$p_y(y) = \frac{1}{\pi}\int_0^{\infty} \prod_{i=1}^{N} J_0(b_i t)\,.\,e^{-\frac{1}{2}{\sigma_x}^2 t^2}\cos(yt)dt \qquad \text{Equation C.6}$$

with $b_i$ the amplitudes of the ith sine wave.

Equation C.6 is the generic expression for the probability density function of a signal comprising multiple sine waves combined with a random process. This expression is also identical to the one found by Rice [15]. Both expressions in Equation C.5 and in Equation C.6 have to be evaluated numerically as no closed form solution was found.

The relative importance of the deterministic part in terms of power is indicated by the sine-to-random power ratio ${a_0}^2$, defined as [15, 34]:

$${a_0}^2 = \frac{{\sigma_s}^2}{{\sigma_x}^2} = \frac{1}{2{\sigma_x}^2}\sum_{i=1}^{N} {b_i}^2 \qquad \text{Equation C.7}$$

with $\sigma_x$ the RMS value of the random noise and $\sigma_s$ the RMS value of the combined sine waves.

Figure 82 (e) and (f) show two example PDFs obtained for two sine-to-random power ratios of ${a_0}^2 = 1$ and ${a_0}^2 = 8$ respectively. The top two graphs (a) and (b) represent the PDFs obtained from 20 seconds of a random Gaussian signal, with a flat spectrum between 50 and 250 Hz and an RMS value of 1(see the red spectrum in Figure 81). The two graphs in the middle (c) and (d) represent the PDF of two 100 Hz sine waves of amplitude $\sqrt{2}$ for (c) and an amplitude of 4 for (d). When the random signal and the sine tone are summed, the sine-on-random signal obtained possesses a sine-to-random power ratio of ${a_0}^2 = 1$ and ${a_0}^2 = 8$ respectively. The two graphs of the bottom, (e) and (f), represent the PDF of the sine-on-random process obtained, together with the theoretical distributions using dashed lines, calculated using Equation C.5.

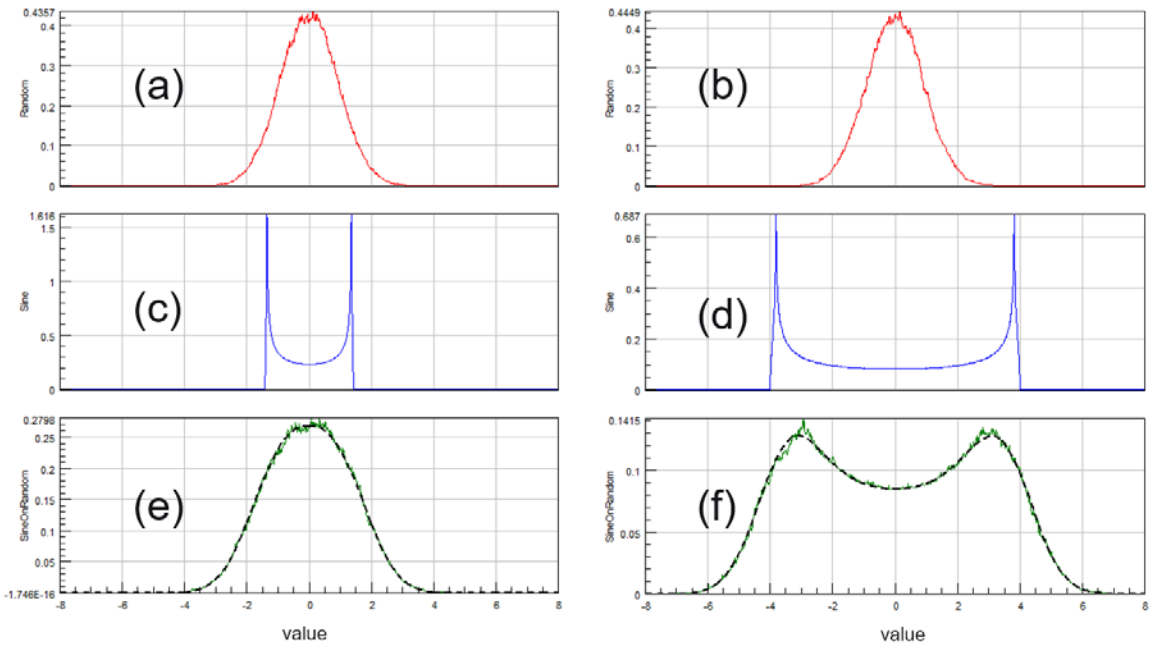


**Figure 82 : Example PDF for various sine-on-random processes with $a_0^2$=1 (left) and $a_0^2$=8 (right)**

A sine tone buried into the noise with a sufficiently high amplitude tends to make the PDF wider and for high sine-to-random power ratios, the global PDF tends to be multimodal.

The mean, variance and kurtosis for a sine-on-random process will be evaluated next. First, the global mean value is the sum of the mean value of the background noise and the mean values of the sine tones. The global mean value is therefore zero, since all mean values are considered to be zero in this thesis.

Under the assumption of independence between the sine tones and the noise, the variance of the sine-on-random process is the sum of the variances of the sine tones and the variance of the background noise. Therefore, the variance of the sine-on-random process is the quadratic sum of the variance of the sine tones and the variance of the background noise, as expressed in Equation C.8.

$$\sigma_y^2 = \sigma_x^2 + \frac{1}{2}\sum b_i^2 \qquad \text{Equation C.8}$$

For the calculation of the kurtosis and more generally for higher order statistics, the use of cumulants is required (see section 2.1.11). Note that since the random noise is assumed to be Gaussian and centred, its higher order cumulants are all zero (see section 2.1.11). So that the cumulants of a sine-on-random process equal the cumulants of the sine tones only. This illustrates an interesting use of cumulants: they allow to detect and characterizing deterministic signals buried into Gaussian noise. Statistical moments are then recovered from the cumulants using the Leonov and Shiryayev formula (see Equation 2.24).

The kurtosis $\kappa$ is defined as: $\kappa = m_4/{m_2}^2$, with $m_2$ and $m_4$ the second and fourth statistical moments.

Now, $m_2$ is the sum of all variances and $m_4$ can be written in terms of cumulants and can be expressed:

$$m_4 = c_4 + 3.{c_2}^2$$

with $c_2$ and $c_4$ the second and fourth cumulants.

Since the mean values are all zero and since $c_2 = m_2$, the kurtosis can be expressed as:

$$\kappa = \frac{(c_4 + 3.{c_2}^2)}{{c_2}^2} = \frac{c_4}{{c_2}^2} + 3.0$$

The fourth cumulant $c_4$ is calculated as the sum of the fourth cumulant of each sine wave considered. The kurtosis of a sine wave is known to be 1.5, so rearranging the equation above giving $m_4$:

$$c_4 = m_{s4} - 3.{c_{s2}}^2 = 1.5{c_{s2}}^2 - 3{c_{s2}}^2 = -1.5{c_{s2}}^2$$

where the subscript s stands for sine wave, meaning the statistics considered are those from the deterministic part of the signal only. Therefore ${c_{s2}}^2 = \sum_i (b_i^2)^2$, where $b_i$ is the amplitude of the ith sine wave.

In the end, the generic equation can be expressed as:

$$\kappa_y = 3.0 - \frac{1.5 \sum b_i^4}{(2\sigma_x^2 + \sum b_i^2)^2} \qquad \text{Equation C.9}$$

Note that the kurtosis of a sine-on-random signal cannot exceed 3.0.

Table C.1 shows an example random noise PSD, together with a sine wave, forming a sine-on-random vibration profile, similar to the one presented in Figure 81. The RMS of the random vibration signal is 1.0 g, the amplitude of the sine wave is 4 and the sine-to-random power ratio is therefore ${a_0}^2 = 8$. The global RMS of the sine-on-random signal is 3.

| Frequency (Hz) | Acceleration Spectral Density ($g^2$/Hz) |
|---|---|
| 50 | 0.005 |
| 250 | 0.005 |
| *Global RMS = 1.00 g* | |

| Frequency (Hz) | Sinusoidal peak acceleration (g) |
|---|---|
| 100 | 4 |

**Table C.1: Example sine-on-random vibration profile**

A signal of 20s sampled at 4096 points per seconds was generated. Figure 83 shows one second of the sine-on-random obtained.

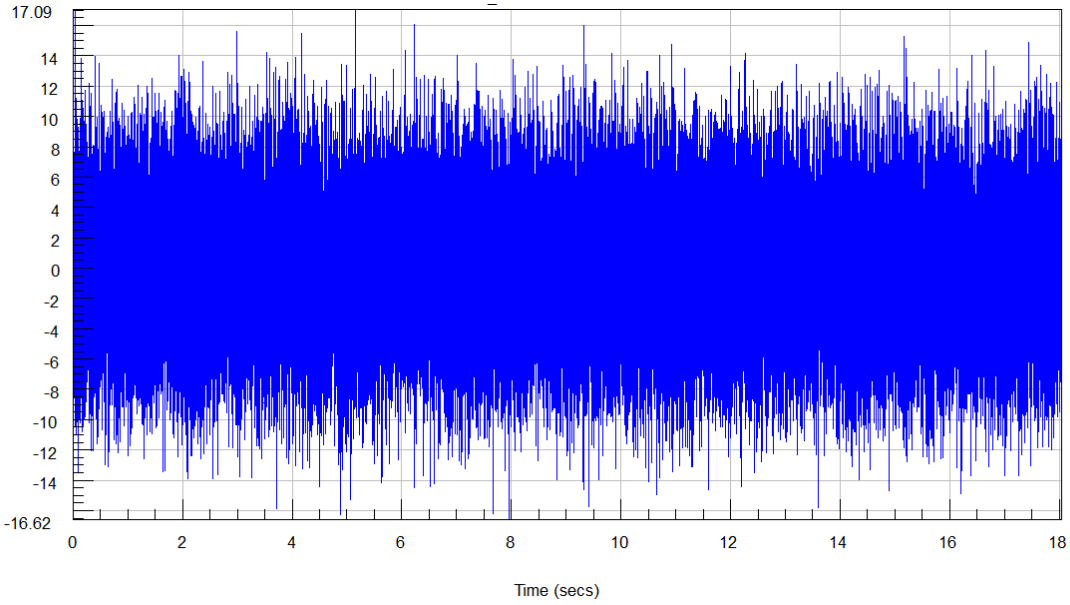


**Figure 83: Example sine-on-random signal realisation**

The PSD and the PDF of the sine-on-random signal are displayed in Figure 84. The PSD and PDF are overlaid with the theoretical PSD profile and the theoretical distribution respectively in dashed black lines. The theoretical distribution for the sine-on-random signal was calculated using Equation C.5. Note that the theoretical distribution for a Gaussian random process of RMS 3 is also displayed in Figure 84 (b) using a dotted red line.

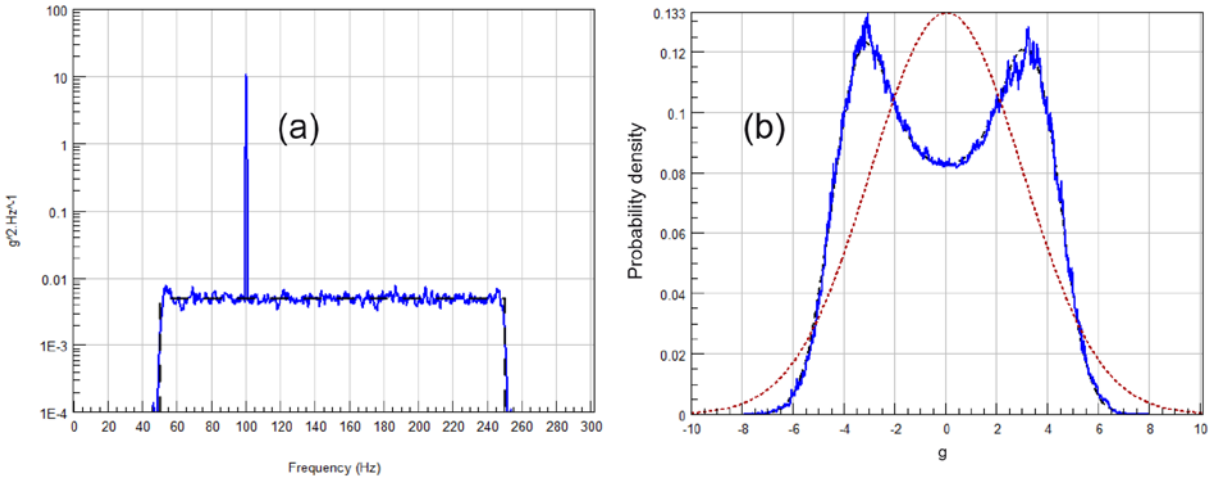


**Figure 84 : (a) PSD of the sine-on-random signal overlaid with theoretical PSD in dashed black, (b) PDF the sine-on-random signal overlaid with the theoretical solution in dashed black and the theoretical equivalent Gaussian PDF**

Note that the tails of the distribution for the sine-on-random signal are well below the tails of the theoretical distribution for a Gaussian random process of RMS 3. This illustrates the fact that the kurtosis of a sine-on-random signal is below 3.

### Output statistics from a sine on random excitation

The previous section introduces the sine-on-random excitation type and how to represent it. In this section, the statistics of the response of an LTI system to a sine-on-random excitation are predicted knowing the characteristics of both the sine-on-random excitation and the LTI system. This enables one to obtain the sine-on-random spectral representation of the stress response as well as the PDF associated with it.

The input-output relationship for linear systems presented in section 0 is applicable to a sine-on-random process: it is applied separately to the harmonic part and the random part, as in Equation C.10 (a) and (b):

$$G_{ZZ}(f) = H(f).G_{XX}(f).H^*(f) \qquad \text{Equation C.10 (a)}$$

$$Sine_Z(f) = H(f).Sine_X(f) \qquad \text{Equation C.10 (b)}$$

Equation C.10 (a) is used to calculate PSD corresponding to the random part of the response and Equation C.10 (b) is used to find the amplitudes and phases of the harmonic part of the response.

Then, Equation C.8 and Equation C.9 can be used to predict the RMS $\sigma_z$ and the kurtosis value $\kappa_z$ of the sine-on-random response.

Note that Equation C.10 (a) and (b) are applicable for cases with multiple harmonic components on random, which is typical in the case of vibrations generated by rotating machines such as engines with their multiple engine order components.

### Stress distributions from a sine-on-random excitation

The sine-on-random process is called a mixture or composite process, made of a deterministic sine wave and a (probabilistic) random process.

A statistical approach is needed to recover the cycle distribution. A new and original approach based on the distribution of peaks established by S.O. Rice is presented here. A comparison with the existing approaches in use in the industry is provided at the end of this section.

#### *Assumptions*

The random noise is assumed to be stationary, ergodic and Gaussian.

The power spectrum of the noise is assumed to be narrowband. The frequencies of the harmonic components are assumed to be within the frequency range of the noise.

Mean values of the noise and harmonics are considered to be zero in the rest of this analysis.

Another important assumption is that the sine waves frequencies are incommensurable. This means that the frequencies of the sine waves are relatively prime, i.e. they have no common factors. In other words, the sine waves frequencies must be irrational relative to each other. This means they can be considered independent and the relative phase has no importance.

Note that the main assumptions made here are useful to establish theoretical results. These assumptions are discussed at the end of this section and it will be seen that the results are still acceptable even if some of the assumptions are violated.

### *Number of peaks*

The total number of expected peaks per unit time $N_{p\_sor}$ can be derived by extending Equation 2.48. The suggested extension consists of adding the spectral moments of the sine wave to the spectral moments of the noise. $N_{p\_sor}$ is therefore expressed:

$$N_{p\_sor}=\sqrt{\frac{\sigma_{\ddot{x}}{}^2+\sum_1^N f_i{}^4 b_i{}^2/2}{\sigma_{\dot{x}}{}^2+\sum_1^N f_i{}^2 b_i{}^2/2}} \qquad \text{Equation C.11}$$

where $\sigma_{\dot{x}}{}^2$ and $\sigma_{\ddot{x}}{}^2$ are referred to as the second and fourth spectral moments of the PSD $G_{xx}$ and their expressions given in Equation 2.45 and Equation 2.49 and $f_i$ and $b_i$ are the frequency and amplitude of the $i^{\text{th}}$harmonic out of the $N$ harmonics added to the noise.

### Distribution of Peaks and Valleys

Rice [15] showed that when the power spectrum of the noise is confined to a narrow band containing the frequencies of the sine waves, the probability density of the envelope of a multi-sine-on-random signal is:

$$f_S(s)=\text{s.}\int_0^\infty x.e^{-\left(\frac{\sigma_r^2 x^2}{2}\right)}J_0(xs)\prod_{i=1}^{N}J_0(xb_i)\,dx \qquad \text{Equation C.12}$$

Theoretically, Equation C.12 is only valid when the noise is narrowband. To establish a more generic expression for sine waves on the top of noise, irrespective of its bandwidth, a similar approach as in section 2 must be adopted using the joint probability density function $p_{X,Y,Z}(x,y,z)$ of the random data $x(t)$, its derivative $y(t)=\dot{x}(t)$ and its second derivative $z(t)=\ddot{x}(t)$ and stating that a local maximum is obtained when the first derivative of the signal is equal to zero and when the second derivative is negative to obtain the marginal distribution of peaks. This approach is not straightforward due to the non-Gaussian nature of the combined data.

Equation C.12 provides a solution for the probability density of the envelope of a multi-sine-on-random signal, only when the noise is narrowband. This is similar to the Rayleigh distribution in the case of a narrowband random signal (see chapter 2.2.8, Equation 2.51Equation 2.51Equation 2.51Equation 2.51Equation 2.51Equation 2.51Equation 2.51Equation 2.50). The expression of the PDF of the peaks for a broadband random signal is somewhat more complex, as it involves the sum of a Rayleigh distribution, a Gaussian distribution and an interaction term (see chapter 2.2.8, Equation 2.54). It is interesting to note that for large positive values of the variable $x$, the distribution of peaks tends asymptotically to Rayleigh distribution multiplied by the irregularity factor (see Equation 2.55). The same

approach is proposed to match asymptotically the distribution of the peaks of large positive values. So Equation C.12 can be extended so that it provides an expression for the probability density of the envelope of a multi-sine-on-random signal, irrespective of the bandwidth of the noise. The suggested extension consists of multiplying the expression of the PDF by the irregularity factor. The probability density of the envelope of a multi-sine-on-broadrandom signal tends asymptotically to:

$$f_S(s) = \gamma s. \int_0^{\infty} x. e^{-\left(\frac{\sigma_r^2 x^2}{2}\right)} J_0(xs) \prod_{i=1}^{N} J_0(xb_i)\, dx \qquad \text{Equation C.13}$$

where $\gamma$ is the irregularity factor of the sine on random noise.

### Distribution of the Ranges

The objective of this section is to deduce the PDF of the ranges of rainflow-like cycles from the PDF of the peaks and the PDF of the valleys.

As seen in 2.6.3, the complex nature of the rainflow counting algorithm makes this exercise non-trivial, but the expression in Equation 2.87 where peaks and valleys are paired symmetrically was discussed and adopted. Equation 2.87 will be used in this section to obtain the PDF of the ranges from the peak PDF of a sine-on-random process because the assumptions adopted here make the composite process narrowband too, i.e. each peak goes with a trough of equal magnitude. Using Equation 2.87 and Equation C.12, the distribution of stress ranges is expressed as:

$$p_R(s_R) = \frac{s_R}{2}.\int_0^{\infty} \frac{x}{2}.e^{-\left(\frac{\sigma_r^2 x^2}{8}\right)} J_0\left(\frac{x s_R}{4}\right) \prod_{i=1}^{N} J_0\left(\frac{x b_i}{2}\right) dx \qquad \text{Equation C.14}$$

where $s_R$ represents the stress range.

It is suggested to call the expression in Equation C.14 “the Rician integral”.

Several particular cases are investigated next: only one harmonic added to the noise and no harmonic.

<u>Only one harmonic added to the narrowband noise:</u>

In the case of only one harmonic input with amplitude A, Equation C.14 becomes:

$$p_R(s_R) = \frac{s_R}{2}.\int_0^{\infty} \frac{x}{2}.e^{-\left(\frac{\sigma_r^2 x^2}{8}\right)} J_0\left(\frac{x s_R}{4}\right) J_0\left(\frac{x A}{2}\right) dx$$

Using entry KU 146(16)a in [109] leads to a closed-form solution:

$$p_R(s_R) = \frac{s_R}{\sigma_r^2}.\mathrm{e}^{-\left(\frac{{s_R}^2/4+4A^2}{2\sigma_r^2}\right)} I_0\left(\frac{s_R A}{2\sigma_r^2}\right) \qquad \text{Equation C.15}$$

where $I_0$ is the modified Bessel function of order zero.

The expression in Equation C.15 is a closed form solution for the distribution of stress ranges in the case where only one harmonic is added to the random signal.

The expression in Equation C.15 is called the Rician Distribution in the literature [36]. The Rician distribution is typically used in fading and multipath propagation of radio waves. The pdf of the mean square of two Gaussian processes with the same standard deviation and non-zero mean corresponds to a Rician distribution (see example 6.15 in [36]).

Narrowband noise only:

In the case where all the added harmonics have zero amplitude, then $J_0\left(\frac{xb_i}{2}\right) = 1.0$ and Equation C.14 becomes:

$$p_R(s_R) = \frac{s_R}{2}.\int_0^\infty \frac{x}{2}.e^{-\left(\frac{\sigma_r^2 x^2}{8}\right)} J_0\left(\frac{x s_R}{4}\right) dx$$

Now, using entry WA 403(4) in [109] leads to a closed-form solution:

$$p_R(s_R) = \frac{s_R}{\sigma_r^2}.\mathrm{e}^{-\left(\frac{{s_R}^2}{8\sigma_r^2}\right)}$$

which is the Rayleigh Distribution given in Equation 2.51.

Apart from those particular cases, no closed form solution was found for the general case, i.e. where more than one sine tone is added to random noise and numerical integration is required.

### Testing the assumptions

This section discusses the effects of violating the assumptions established to derive the formulation in Equation C.13.

Influence of Phase

Although the theory established by Rice and adapted here to fatigue analysis can handle the case of multiple sine waves added to random noise, the relative phase between the sine waves is not considered. The relative phase is not taken into account because the sine waves are assumed to have incommensurable frequencies, therefore the resulting wave is not periodic and there will forever be peaks moving relative to each other. This means that the phase has no importance and that the sine waves may be considered to be independent of each other. Note that an equivalent assumption is that frequencies are commensurable but with random relative phases.

This assumption is hard to satisfy in mechanisms such as rotating machines, as often frequencies are harmonics with given phases. In the case where sine waves frequencies are multiples of one another, the relative phase is important. Note however that the expressions in this paper are derived as if phase was zero, which makes the results conservative when sine waves are even harmonics.

Other observations:

- The importance of phase decreases as the harmonic's order increases: the influence of relative phase becomes negligible when the frequency rate between the harmonics exceeds 4.

- The importance of phase decreases as the noise power increases: the influence of relative phase becomes negligible when the sine-to-random power ratio $a_0{}^2$ is smaller than 1.0.

In the case where sine waves are harmonics and where the sine-to-random power ratio $a_0{}^2$ is higher than 1.0, the proposed formulation may give a conservative result in the case of even harmonics and optimistic results in the case of odd harmonics. In this case, it is suggested to use time domain simulations.

Influence of Bandwidth

The theory established by Rice and adapted here to fatigue analysis considers narrowband noise.

Often, stress responses are not truly narrowband but rather multimodal. In this case, as discussed in section 2.6.3, there are negative peaks and positive valleys. Therefore, the PDF of stress peaks and valley cross and the combination proposed in Equation 2.87, where peaks and valleys are paired symmetrically to derive the PDF of stress range, should show some probability of occurrence of negative ranges.

Therefore, applying Equation C.13 to sine tones on broadband noise will overestimate the overall histogram and therefore produce conservative results.

Simulations show that the statistical distribution of cycles provided by Equation C.13 is satisfactory when the random noise shows an irregularity factor above 0.85. It tends however to be conservative when the random noise bandwidth grows broader. For instance, an irregularity factor of 0.75 leads to more than 50% damage overestimation.

Equation C.14 is an extension to Equation C.13 that provides the theoretical PDF of stress peaks in the case of broadband noise.

Influence of the frequency of the harmonics

From a physical point of view, the presence of noise in the response is dependent on the FRF and so is the presence of a sine wave in the response. So it makes sense to limit the investigations to the case where the sine wave's frequencies are within the noise frequency range.

Three cases can be considered: the sine frequency is below, within or above the range of frequencies of the noise. Those three cases are illustrated in Figure 85: the three spectra are on the left hand side and the three corresponding range-only rainflow histograms computed from time domain simulations are on the right hand side.

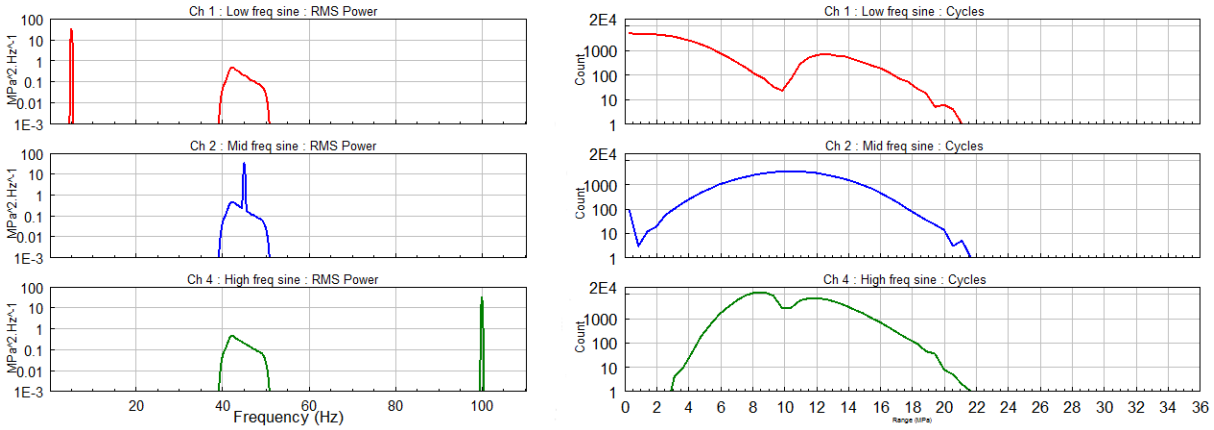


**Figure 85 : Example sine on random spectra and associated Rainflow histograms**

In the case where the sine wave's frequency is outside the noise frequency range, simulations clearly show a bimodal rainflow distribution as shown in Figure 85 (a) and (c). This is due to the fact that rainflow cycles are constructed differently. Figure 86 illustrates this with a rainflow cycle extracted from a sine-on-random signal (in green) built from a low frequency high amplitude sine wave (in red) added to a low energy random noise contained in a higher range of frequencies (in blue). The resulting cycle is not necessarily centred around zero and its range is much smaller than the range of the corresponding cycle in the noise only.

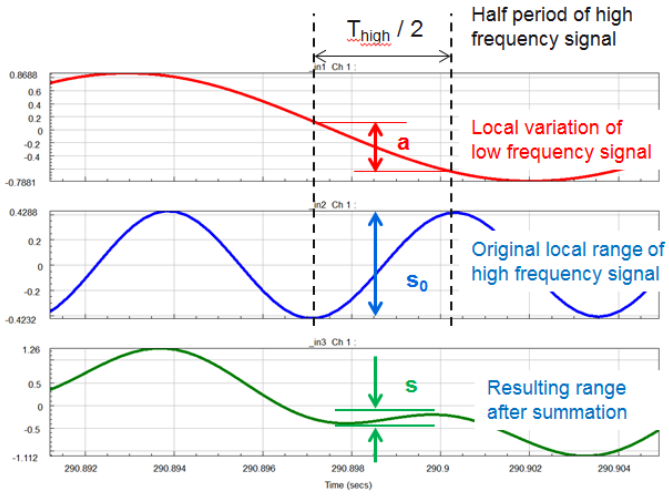


**Figure 86: Rainflow cycles obtained when a low frequency sine wave (red) is summed with a high frequency noise (blue) giving the composite signal (green)**

From a fatigue perspective, Figure 85 and Figure 86 lead to some observations:

- Cycles with non-zero mean stress values appear
- Cycles ranges are distorted
- But the maximum range will be the same in all cases (see Figure 85)

Although the proposed approach considers all the deterministic components of the composite process to be in the same frequency range as the random noise, it still gives acceptable results for fatigue applications. The higher ranges are still found and since the distortion of the cycles

is not taken into account, it is expected that the proposed approach produces conservative results when the sine wave's frequencies are far from the frequency range of the random noise.

In this case, simulations show that applying Equation C.13 will indeed overestimate the histogram in its high-range end and therefore produce conservative results. The level of conservatism goes generally up to 50% on the predicted fatigue damage.

Note that the mean stress does have an influence on fatigue life. It is often reported [73] that a tensile mean stress tends to increase the level of fatigue damage (compared to the value calculated from the stress range only), whereas a compressive mean stress tends to be beneficial to the fatigue life. The sine-on-random processes considered in this study are centred around zero. Therefore the distribution of the mean values is also centred and assumed symmetrical. This is why the influence of mean stress is assumed negligible in this study.

### Comparison with existing methods for multiple sine tones on random

There is a need in the industry to predict life of components and structures submitted to sine-on-random loadings. Fairly basic approaches are in use today. Those approaches are described and discussed here.

The simplest and most popular approach is to sum-up the damage from the sine tone and the random noise separately. This approach underestimates the damage severely as the sinusoid and random stresses combine additively to produce higher stress peaks than either random stresses or sine tones acting alone. This is equivalent to considering the sine and random loads appearing in sequence. Lambert [111] concludes that the actual damage induced by the combined sine-on-random stress can be several orders of magnitude greater than that done by the sum of each stress type acting alone.

Another approach, suggested by Halfpenny [112], consists in summing the spectral moments resulting from each sinusoidal tone and the random noise and then calculating the resultant fatigue damage treating the composite process as a random PSD. This approach is equivalent to using the energy of the harmonics to increase the overall random PSD. Although technically more elaborate, this approach does not consider the complex interactions between the sine and the random noise.

Fatigue damage from sine-on-random loadings has been treated by other authors like Lalanne [27], Lambert [111]. Both use the Ricean distribution to describe the peak distribution for a single sine-on-random process, see Equation (49). In the case of multiple harmonic inputs on top of random noise, Lalanne suggests retaining only the maximum damage from each sine calculated separately (see section 5.8 of [113]).

Figure 18 shows an overlay of various Rainflow cycles distributions obtained from the same sine-on-random spectrum but using different methods. The red histogram was obtained by Rainflow cycle counting a signal obtained by Monte-Carlo simulations. The green and the orange curves show the statistical cycles distributions obtained from the approach by Lalanne and Halfpenny respectively. Finally, the blue curve is the statistical cycles distributions obtained from the proposed approach.

As depicted in Figure 88, Halfpenny's approach tends to overestimate the fatigue damage, whereas Lalanne's tends to slightly underestimate the damage. The proposed approach seems to be the most accurate.

The sine-on-random spectrum used is displayed in Figure 87.

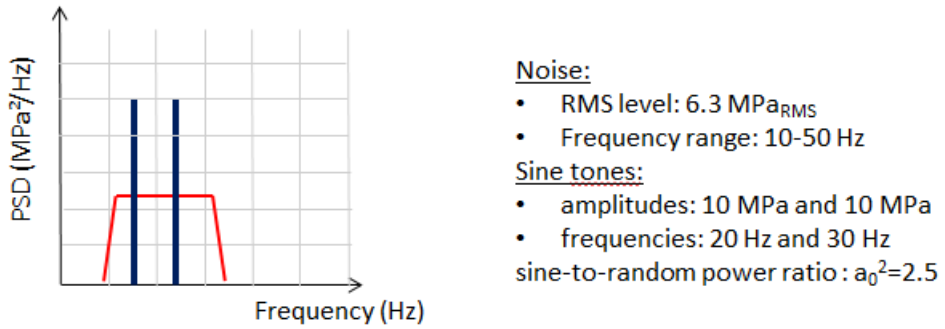


**Figure 87: Example sine-on-random spectral representation**

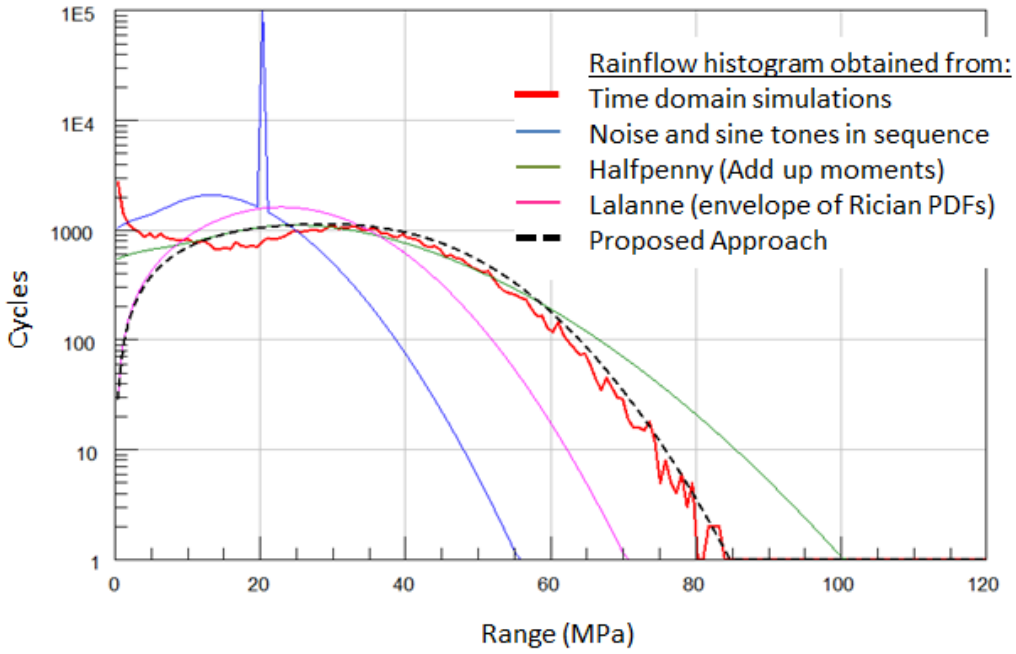


**Figure 88: Example rainflow cycle count and some model estimation results**

# APPENDIX D: Stationary non-Gaussian random signals

## Input-output kurtosis for a linear system subject to a steady non Gaussian input

The PDF of the sum of two independent variables is expressed using the convolution product of both marginal PDF, as expressed in Equation 2.14 in chapter 2.

The convolution product can be seen as a weighted sum of shifted copies of the input signal. This can be generalized by considering the sum of $N$ independent random variables:

The probability density function of their sum equals the convolution of their individual densities. Since convolution is associative, multiple convolutions of $N$ PDFs $p_1, p_2, \dots, p_N$ can be written as $p_1 * p_2 * \ \dots * p_N$ with no ambiguity.

The characteristic function is described in section 2.1.11 as the Fourier transform of the PDF. Therefore, by virtue of the convolution theorem, the convolution of $N$ pdfs becomes the product of $N$ characteristic functions [37]. The second characteristic function is described in section 2.1.11 as the logarithm of the characteristic function. Therefore, the convolution of the PDFs becomes a sum of the second characteristic functions. It becomes now clear that cumulants are additive under convolution.

Now the output signal of an LTI system is a weighted sum of independent processes. Each independent process has the same moments but is simply multiplied by a constant scalar $h_i$, the value of the impulse response function at the $i^{th}$ index. The process considered must therefore be constituted of independent and identically distributed (i.i.d) values.

If one considers a signal with statistical moments $m_n$, that is multiplied by a constant $h$. Using the fundamental definition of moments: $m_n = E[x^i]$ and the linearity of the expectation operator, the $n^{th}$ moment of the obtained signal will be $h^n m_n$.

Note: the kurtosis, like the other standardized moments, remains unchanged through multiplication.

So, if a process is multiplied by a constant coefficient $h$, then its variance will be multiplied by $h^2$. The characteristic function of $z$, the output of an LTI system with impulse response function $h(\tau)$ and a zero mean white noise input $y$ with standard deviation $\sigma_y$ is written:

$$\varphi_z(f) = \prod_{i=0}^{N-1} e^{-\frac{1}{2}{h_i}^2{\sigma_y}^2 f^2}$$

Which is :

$$\varphi_z(f) = e^{-\frac{1}{2}\left(\sum {h_i}^2{\sigma_y}^2\right) f^2}$$

The equation shows that the response $z$ will also have a Gaussian distribution of variance ${\sigma_z}^2 = \sum {h_i}^2 {\sigma_y}^2$.

Consider an i.i.d process with first four statistical moments being $\mu_1, \mu_2, \mu_3, \mu_4$. If this process is zero-mean, Equation 2.24 gives the four first cumulants in terms of the first moments:

$$c_1 = 0, \qquad c_2 = \mu_2, \qquad c_3 = \mu_3, \qquad c_4 = \mu_4 - 3{\mu_2}^2$$

Note that the cumulants up to order three match the moments. It is only at, and above, the fourth order that the distinction between moment and cumulants has an impact [38, 18].

The fact that the cumulants are additive under convolution will now be used. Once a signal $y(t)$ is filtered through a LTI system of impulse response function $h$, the output signal $z(t)$ will have the following cumulants:

$$c_{z,1} = \sum_N h_i c_{y,1}\,, \qquad c_{z,2} = \sum_N {h_i}^2 c_{y,2}\,, \qquad c_{z,3} = \sum_N {h_i}^3 c_{y,3}\,, \qquad c_{z,4} = \sum_N {h_i}^4 c_{y,4}$$

The generalisation of the expressions above to the order $k$ is Equation 4.2.

This can be expressed in terms of the moments as:

$$c_{z,1} = \mu_{y,1} \sum_N h_i$$

$$c_{z,2} = \mu_{y,2} \sum_N h_i^2$$

$$c_{z,3} = \mu_{y,3} \sum_N h_i^3$$

$$c_{z,4} = (\mu_{y,4} - 3.{\mu_{y,2}}^2) \sum_N h_i^4$$

Similarly, one can obtain the moments of a zero mean process in terms of their cumulants:

$$\mu_1 = 0, \qquad \mu_2 = c_2, \qquad \mu_3 = c_3, \qquad \mu_4 = c_4 + 3{c_2}^2$$

and the kurtosis $\kappa_z$ of the output z will be:

$$\kappa_z = \frac{\mu_{z,4}}{{\mu_{z,2}}^2} = \frac{c_{z,4}}{{c_{z,2}}^2} + 3.0$$

Developing:

$$\kappa_z = \frac{(\mu_{y,4} - 3.{\mu_{y,2}}^2)}{{\mu_{y,2}}^2} \frac{\sum h_i^4}{(\sum h_i^2)^2} + 3.0$$

And noting that $\frac{\mu_{y4}}{{\mu_{y2}}^2} = \kappa_y$, the kurtosis of the input signal, one obtains the expression giving the output kurtosis from the system's impulse response function and the input kurtosis $\kappa_y$:

$$\kappa_z = \frac{\sum h_i^4}{(\sum h_i^2)^2}\left(\kappa_y - 3.0\right) + 3.0$$

Which is the same expression as in Equation 4.5.

### Input-output higher order cumulants

Equation 4.2 was established in the previous section; it gives the expression for a $k$ order output cumulant. The Leonov and Shiryayev formula [18, 37] can be used to express the $k$ order output cumulant in terms of the statistical moments of the input signal. For example, for $k = 6$, one obtains:

$$c_{z,6} = \sum_N {h_i}^6 c_{y,6} = (\mu_{y,6} - 15\mu_{y,2}\mu_{y,4} + 30{\mu_{y,2}}^3) \sum_N h_i^6$$

Similarly for $k = 8$:

$$c_{z,8} = \sum_N {h_i}^8 c_{y,8} = (\mu_{y,8} - 28\mu_{y,2}m_{y,6} - 35{\mu_{y,4}}^2 + 420{\mu_{y,2}}^2\mu_{y,4} - 630{\mu_{y,2}}^4) \sum_N h_i^8$$

And so on for any other $k$

Ley $p_y(y)$ be the pdf of a zero-mean i.i.d. signal that can be represented by a gram-charlier series $\hat{p}_y(y)$: [18]

$$\hat{p}_y(y) = \frac{1}{\sqrt{2\pi}\sigma_y} . e^{-\frac{1}{2}\left(\frac{y}{\sigma_y}\right)^2} \left(1 + \sum_{k=4}^{N} \frac{c_{y,k}}{k!\,{\sigma_y}^k} H_k\left(\frac{x}{\sigma_y}\right)\right)$$

Where only the even orders are considered.

When going through an LTI filter of impulse response function $h$, the output pdf $\hat{p}_z(z)$ can be written:

$$\hat{p}_z(z) = \frac{1}{\sqrt{2\pi}\sigma_z} . e^{-\frac{1}{2}\left(\frac{z}{\sigma_z}\right)^2} \left(1 + \sum_{k=4}^{N} \frac{c_{z,k}}{k!\,{\sigma_z}^k} H_k\left(\frac{z}{\sigma_z}\right)\right)$$

Where ${\sigma_z}^2 = {\sigma_y}^2 . \sum h_i^2$ is the variance (or second cumulant) of the output, and more generally, $c_{zk} = c_{yk} . \sum h_i^k$. Therefore the output pdf $\hat{p}_z(z)$ can be re-written:

$$\hat{p}_z(z) = \frac{1}{\sqrt{2\pi}\sigma_z} . e^{-\frac{1}{2}\left(\frac{z}{\sigma_z}\right)^2} \left(1 + \sum_{k=4}^{N} \frac{c_{y,k}}{k!\,{\sigma_y}^k} \frac{\sum h_i^k}{(\sum h_i^2)^{k/2}} H_k\left(\frac{z}{\sigma_z}\right)\right)$$

The same term $\frac{\sum h_i^k}{\left(\sum h_i^2\right)^{k/2}}$ is found in this expression as well as in Equation 4.3 defining the input-output relationship for the standardised cumulants ($C_{z,k} = C_{y,k} \frac{\sum_i (h_i)^k}{\left(\sum_i {h_i}^2\right)^{k/2}}$)

The idea is now to study the convergence of $\frac{\sum h_i^k}{\left(\sum h_i^2\right)^{k/2}}$ with increasing values of $k$.

Dividing numerator and denominator with $h_0^k$, one obtains:

$$\frac{\sum h_i^k / h_0^k}{(\sum h_i^2)^{k/2} / h_0^k} = \frac{\sum (h_i/h_0)^k}{[\sum (h_i/h_0)^2]^{k/2}}$$

Now, since $h_i$ are the coefficients of the IRF of a linear system, it is a sum of decaying exponentials. The numerator $\sum h_i^k / h_0^k$ is a decreasing function starting at 1.0. For high values of the order $k$, $\sum h_i^k / h_0^k$ will quickly tend to 1.0, and even quicker for lightly damped systems, where the exponential decay is high.

The denominator $\sum h_i^2 / h_0^2$ will be much higher (typically >>1) as the order is only 2. When raised at the power $k/2$ its value increases even further compared to the numerator.

Therefore $\frac{\sum h_i^k / h_0^k}{\left(\sum h_i^2 / h_0^2\right)^{k/2}}$ tends quickly to 0 as the order $k$ increases.

As a corollary, one concludes that for a given impulse response function with coefficients $h_i$, the higher the order considered, the quicker $C_{z,k}$ will tend to zero. This explains why an LTI filter tends to turn any non-Gaussian input data into a Gaussian response. And this tendency will be even more pronounced for lightly damped systems.

## APPENDIX E: More example results

This appendix contains additional examples of theoretical results found for response signals resulting from a stationary, leptokurtic random excitation or from an amplitude modulated excitation. In all cases, the theoretical results match the results observed from time domain numerical simulations.

### Output kurtosis and peak response distribution in the response resulting from a stationary, leptokurtic random excitation

The first example is showing the theoretical output kurtosis and peak distribution obtained from the same input signal as in chapter 5.3 filtered through the same bimodal FRF but with a lighter damping ratio of 2%. The response signal has an irregularity factor of 0.87 so it can be considered narrowband.

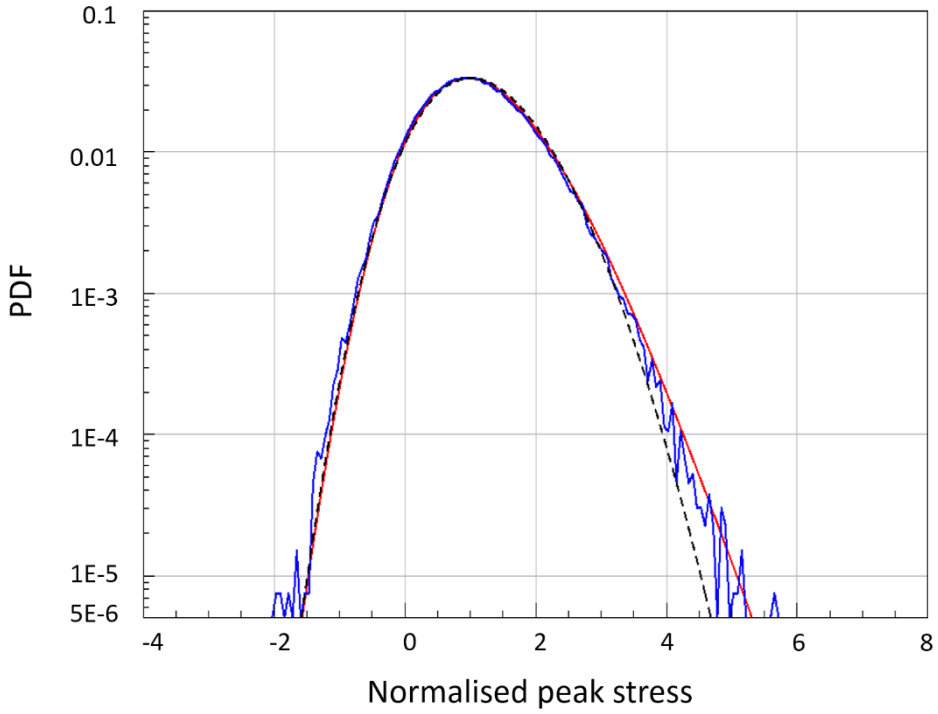


**Figure 89: The peak distributions for the leptokurtic response of the bimodal linear system (2% damping) from numerical simulations (blue), from the theoretical expression (red) and using the Gaussian assumption (dashed black).**

The next example is showing the theoretical output kurtosis and peak distribution obtained from the same input signal as in chapter 5.3 but using this time a unimodal FRF with a damping ratio of 2%. The response signal has an irregularity factor of 0.97 so it can be considered narrowband.

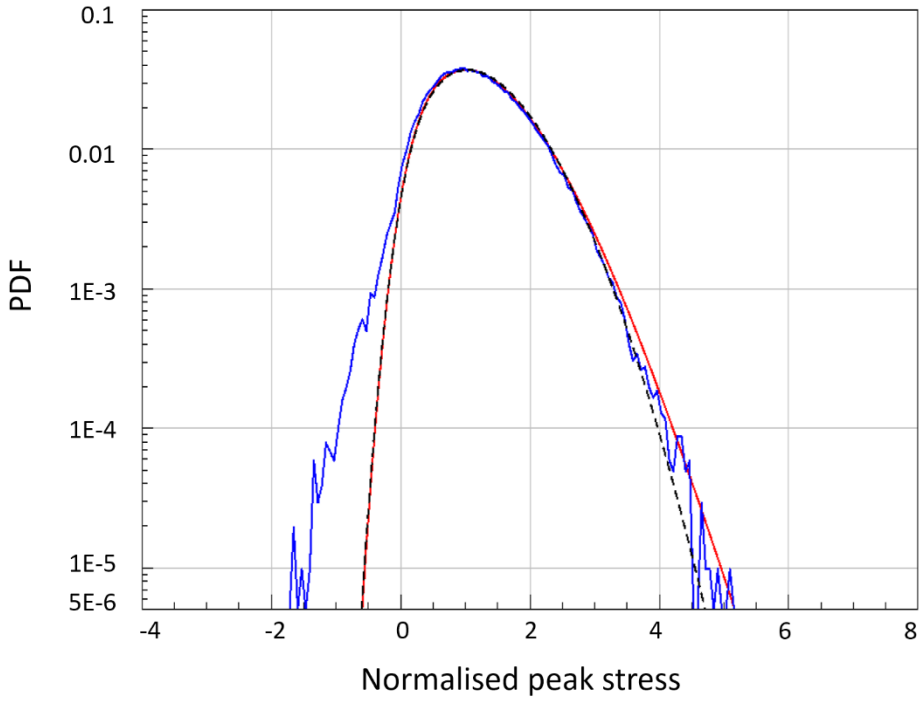


**Figure 90: The peak distributions for the leptokurtic response of the unimodal linear system (2% damping) from numerical simulations (blue), from the theoretical expression (red) and using the Gaussian assumption (dashed black).**

### Output kurtosis and peak response distribution in the response resulting from an amplitude modulated excitation

The first example is showing the theoretical output kurtosis and peak distribution obtained from the same input signal as in chapter 5.3 filtered through the same bimodal FRF but with a lighter damping ratio of 2%. The response signal has an irregularity factor of 0.87 so it can be considered narrowband.

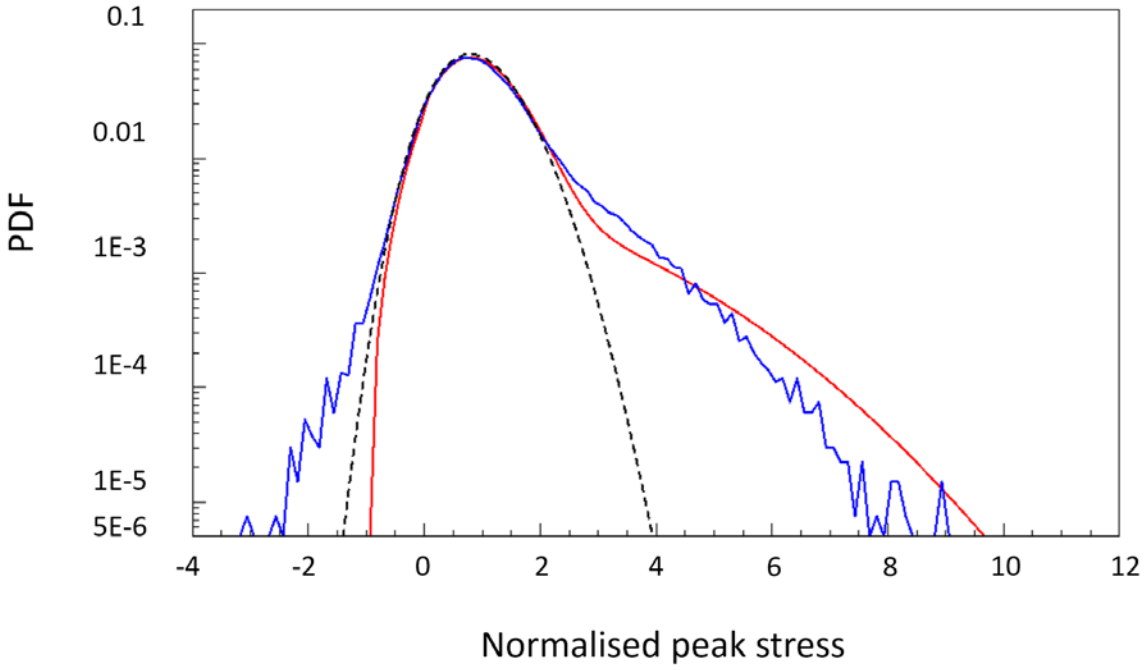


**Figure 91: The peak distributions for the leptokurtic response of the bimodal linear system (2% damping) from numerical simulations (blue), from the theoretical expression (red) and using the Gaussian assumption (dashed black)**

The next example is showing the theoretical output kurtosis and peak distribution obtained from the same input signal as in chapter 5.3 but using this time a unimodal FRF with a damping ratio of 2%. The response signal has an irregularity factor of 0.97 so it can be considered narrowband.

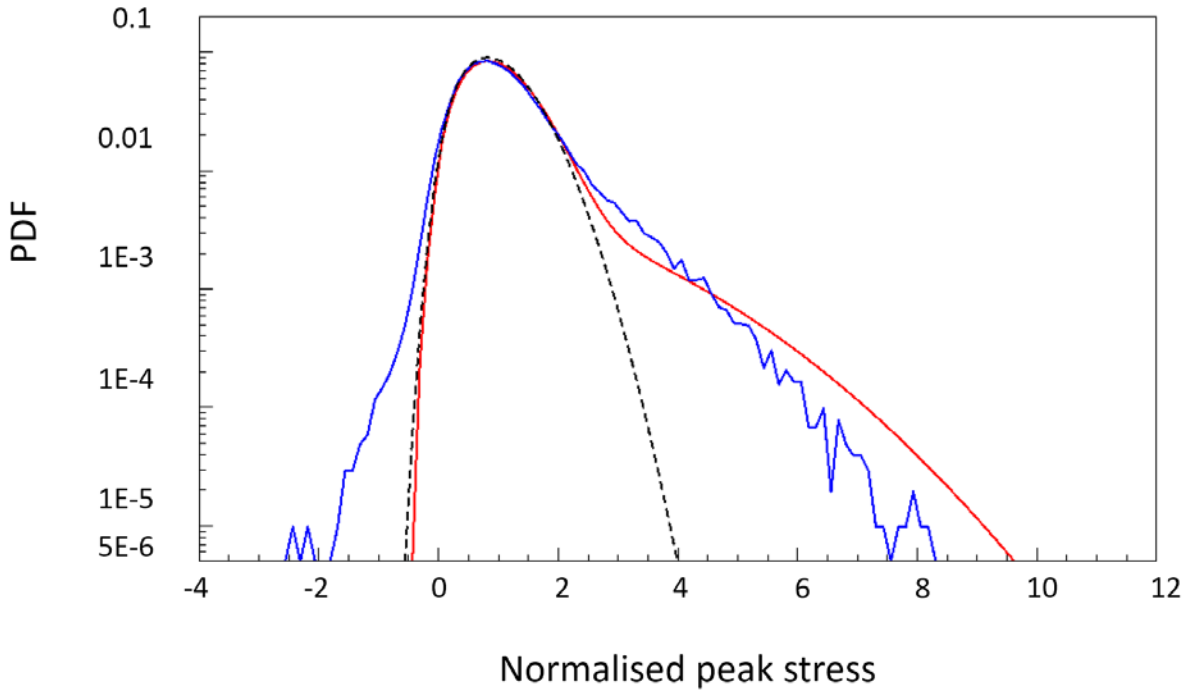


**Figure 92: The peak distributions for the leptokurtic response of the unimodal linear system (2% damping) from numerical simulations (blue), from the theoretical expression (red) and using the Gaussian assumption (dashed black)**